Dragonfly

The Electric Future of Light Trainer Aircraft

by

Bob van Dillen	**4677269**
Matthijs van Ede	**4662768**
Nwankwo Hogervorst	**4560604**
Hendrik Jan Hoogendoorn	**4651979**
Maximilian Meijkamp	**4676718**
Elias Overbosch	**4546202**
Yann Pejon	**4680340**
Florina Sîrghi	**4648579**
Casper Teirlinck	**4680723**
Ricarda Warnat	**4547306**

June 29, 2020

in partial fulfilment of the requirements for the degree of

Bachelor of Science
in Aerospace Engineering

at the Delft University of Technology,

Supervisor:	Ir. R. van Gent,	TU Delft
Coaches:	Dr. Ir. T. Michelis,	TU Delft
	Dr. Ir. D. Nardi,	TU Delft
PM/SE Teaching Assistant:	S.J. van Elsloo,	TU Delft

Version	Date	Author	Description
1.0	22-06-2020	Entire team	Final Report Draft
1.1	29-06-2020	Entire team	Final Report Final Version: - Added Chapter 14: Conclusion and Recommendations - Updated values and figures - Added sensitivity analysis - General proofreading

TU Delft Delft University of Technology

This page was intentionally left blank.

Contents

1 Introduction 1

2 Project Objectives 2

3 Sustainability development strategy 3
- 3.1 Social Sustainability . . . 3
- 3.2 Technical Sustainability . . . 3
- 3.3 Sustainability Requirements . . . 4

4 Market Analysis 5
- 4.1 Stakeholder Identification . . . 5
- 4.2 Market Segmentation . . . 5
- 4.3 Competitor Analysis . . . 5
- 4.4 Added Market Value . . . 6
- 4.5 Prediction Of Future Market . . . 7
- 4.6 SWOT Analysis of Target Market . . . 8
- 4.7 Primary Research . . . 8

5 Structures 10
- 5.1 Prioritising Subsystems . . . 10
- 5.2 Functional Analysis and Requirements . . . 11
- 5.3 Material Selection . . . 14
- 5.4 Battery Placement Trade-off . . . 17
- 5.5 Wing Design . . . 17
- 5.6 Wing Verification and Validation . . . 23
- 5.7 Fuselage Design . . . 23
- 5.8 Landing Gear Design . . . 28
- 5.9 Compliance Matrix . . . 29

6 Aerodynamics 32
- 6.1 Functional Analysis and Requirements . . . 32
- 6.2 Analysis Tooling . . . 33
- 6.3 Verification & Validation of Design Tools . . . 36
- 6.4 Wing design . . . 39
- 6.5 Empennage Aerodynamic Design . . . 42
- 6.6 Aerodynamic Performance & Efficiency . . . 44
- 6.7 Assumptions and Limitations . . . 45
- 6.8 Risks . . . 46
- 6.9 Compliance Matrix . . . 46

7 Stability and Control 47
- 7.1 Functional Analysis . . . 47
- 7.2 Requirements . . . 47
- 7.3 Horizontal Tail Sizing and Wing position . . . 48
- 7.4 Vertical Tail Sizing . . . 54
- 7.5 Control Surfaces Sizing . . . 55
- 7.6 Future Design Process . . . 60
- 7.7 Risks . . . 60
- 7.8 Compliance Matrix . . . 61

8 Power and Propulsion 62
- 8.1 Functional Analysis . . . 62
- 8.2 Requirements . . . 62
- 8.3 Battery Design . . . 63
- 8.4 Engine Design . . . 70
- 8.5 Propeller Design . . . 79
- 8.6 Compliance Matrix . . . 85

9 Training Enhancement and Cockpit Design 86
- 9.1 Market Research . . . 86
- 9.2 Functional Analysis . . . 87
- 9.3 Requirements . . . 88
- 9.4 Primary Research . . . 90
- 9.5 In-flight Segment . . . 92
- 9.6 Ground Segment . . . 101
- 9.7 Cockpit Layout Design . . . 104
- 9.8 Risk Assessment . . . 107
- 9.9 Verification and Validation . . . 108
- 9.10 Training Effectiveness Provided by the Electric Propulsion . . . 109
- 9.11 Quantifying the Training Effectiveness of the TE Package . . . 110
- 9.12 Cost-Benefit Analysis of TE . . . 114
- 9.13 Further Recommendations . . . 114

10 Final Design 116
- 10.1 Aircraft Communication . . . 116
- 10.2 Integration of the Subsystems . . . 117
- 10.3 Aircraft Parameters & Design . . . 120
- 10.4 Sustainability . . . 120
- 10.5 Verification and Validation . . . 121
- 10.6 Certifiability Issues . . . 121
- 10.7 Technical Sensitivity Analysis . . . 122

11 Business Case 123
- 11.1 Requirements . . . 123
- 11.2 Funding . . . 123
- 11.3 ELTA Company . . . 123
- 11.4 Customer . . . 125
- 11.5 Verification and Validation . . . 126
- 11.6 Risks . . . 126
- 11.7 Compliance Matrix . . . 127

12 Risk Assessment 128
- 12.1 Technical Risk Assessment . . . 128
- 12.2 Risk Map . . . 130

13 Operations, Logistics and Project Planning 131
- 13.1 Operations . . . 131
- 13.2 Production Plan . . . 132
- 13.3 Project Planning- Future Steps . . . 132

14 Conclusion and Recommendations 134

Bibliography 136

A FFD and FBS 139

Nomenclature

List of Abbreviations

ADS-B	Automatic Dependent Surveillance Broadcast
AR	Augmented Reality
CFI	Certified Flight Instructor
CRP	Contra-Rotating Propeller
DOT	Design Option Tree
DSE	Design Synthesis Exercise
EFB	Electronic Flight Bag
ELEC	Electricity
ELTA	Electric Light Trainer Aircraft
FFS	Full Flight Simulator
FTD	Flight Training Device
HR	Heart Rate
HUD	Head-up display
IFR	Instrument Flight Rules
ISA	International Standard Atmosphere
LA	Last Accessed
MAC	Mean Aerodynamic Chord
MACo	Mid-Air Collision
MFD	Multi Function Display
NOTAM	Notice to airmen
PFD	Primary Flight Display
PM	Project Management
PPL	Private pilot licence
QFD	Quality Function Deployment
RPM	Revolutions Per Minute
SEP	Single Engine Piston
TBD	To be determined
TBO	Time Between Overhaul
TCAS	Traffic Alert and Collision Avoidance System
TCR	Training Cost Ratio
TE	Training Enhancement
TER	Transfer Effectiveness Ratio
VFR	Visual Flight Rules
VR	Virtual Reality
WBS	Work Breakdown Structure
WFD	Work Flow Diagram
XR	Mixed Reality

List of Symbols

η	Efficiency
λ	Taper ratio
$\Lambda_{c/4}$	Quarter chord sweep angle
μ	Friction coefficient
ρ	Air/material density
A	Aspect ratio, cross-sectional area
b	Wing span
C_D	Drag coefficient
C_L	Lift coefficient
c_r	Root chord
c_t	Tip chord
D	Drag force
E	Modulus of elasticity
e	Oswald efficiency factor
E^*	Specific battery energy
g_0	Acceleration due to gravity at the surface
k	Power setting factor
l	Length
L/D	Lift to drag ratio
m	Mass
R	Range
S	Wing surface area
V	Velocity
W/P	Power loading
W/S	Wing loading
W_{bat}	Energy storage weight
W_{OE}	Operational Empty Weight
$W_{payload}$	Payload weight
W_{TO}	Take-off Weight

Preface

This is the final report developed by Group 06 as part of the Spring 2020 Design Synthesis Exercise, the final project in the Bachelor of Science programme at the Faculty of Aerospace Engineering at the Delft University of Technology. In the beginning of the project, our tutor, Ir. Ronald van Gent, assigned us with the task of designing an electrical light trainer aircraft with enhanced training capabilities. This report documents the steps taken towards obtaining the final design of our aircraft and offers a glimpse into the future of the project. The authors would like to express their gratitude to their tutor Ir. Ronald van Gent, coaches Dr. Ir. Theo Michelis and Dr. Ir. Davide Nardi, PM/SE teaching assistant Sam van Elsloo, as well as their external experts Matthijs de Haan and Maarten Klomp for the unconditional support and assistance throughout the project. Furthermore, we would like to thank the OSCC who made the Design Synthesis Exercise possible for us, even in these uncertain times.

Group 06

Delft, June 2020

Executive Summary

This is the final report written by Spring DSE 2020 Group 06. It is the fourth report produced in the design of an electrical light trainer aircraft, which was required to be designed by a group of 10 students in 10 weeks. The goal of this project is to encourage the use of electrical trainer aircraft in the training of student pilots, specifically PPL and IFR training, while also making flight training more financially profitable for flight schools. In this report the final phase of the DSE is presented which consists of the preliminary design of the Dragonfly. The design process is described, as well as an overview of the final design and plans for the future of the project. This executive summary will include a short description of the previous (conceptual) design phases and a more extensive overview of this preliminary design phase.

Project Objectives

For this project the mission need statement (MNS) is as follows:

Increase the usage of emission-free trainer aircraft in flight schools.

The project objective statement (POS) is as follows:

Design an emission-free trainer aircraft, establishing a justifiable business case for flight schools, by 10 students in 10 weeks.

As one can observe in the MNS and the POS, sustainability is an important factor within this project. To ensure the proper grip on this subject, it is chosen to work according to the principles of the EcoDesign Strategy Wheel. When this 'wheel' is followed, one will come up with a design that has reduced the environmental impact of the entire life cycle of the product to a minimum by analysing and improving the design on sustainability on component level, structural level and on system level.

Baseline Phase

During the baseline phase, requirements were generated from functional flow diagrams (FFD) and functional breakdown structures (FBS). In the design of the electric light trainer aircraft (ELTA), which is named the 'Dragonfly', it is important to note that the electrical engine provides many opportunities to make flight training more efficient, which would financially benefit flight students. In order to explore the competitors that the Dragonfly would face, a detailed market analysis on other trainer aircraft and electrical aircraft was performed.

Following the requirements generation and market analysis, a brainstorming session was held in which all possible design options were collected. This process identified four parts of the aircraft to be designed - the configuration, wing, propulsion and landing gear design. The options of these systems were put in a design option tree. As the training enhancement (TE) was considered a separate part of the aircraft, it was put in a separate design option tree. Based on these design option trees, five preliminary conceptual designs were created, namely: an aircraft with two ducted fans mounted on the fuselage, one with one propeller engine mounted on the nose, one with a contra-rotating propeller on the nose, one with two propeller engines mounted on the wing and one with an array of multiple engines located on the wing.

Midterm Phase

The goal of the midterm phase was to perform trade-offs for each subsystem in order to determine how good each concept is. The final product of the midterm phase was a choice of concept out of the five produced in the baseline phase. This concept turned out to be concept three and was the one to be further developed during the detailed design phase of this DSE.

The midterm report included many trade-offs, which were performed as follows. First, the quality function deployment (QFD) method was applied in order to determine the weights of each trade-off criterion. Then, the weights of each technical parameter were then used for the actual trade-off table, where the concept with the highest overall score would be deemed the winner.

Final Design Choice

After designing each aircraft subsystem and performing multiple subsystem-level trade-offs, in which all the relevant design options for the main components of the five concepts were assessed and scored, a final trade-off between the five concepts could be performed. Following the final trade-off shown in Figure 1, it was determined that the option with a contra-rotating propeller was the best option for the electric light trainer aircraft (ELTA). It received an excellent score on the training add-ons, neutral scores on both noise and flight performance (which includes endurance and weight), good scores on aircraft cost (not taking into account the cost of TE) and certifiability. It also received a good score on aircraft safety.

Design Option	Technical Performance Measurements	Added Training Effectiveness (Training Add-ons)	Noise	Flight performance	Certifiability	Aircraft Cost	Safety	Score
	Weight	25%	10%	15%	10%	20%	20%	100%
Option 1		2	4	3	1	2	2	2.25
Option 2		3	2	2	4	4	1	2.65
Option 3		4	2	2	3	3	3	3.00
Option 4		3	3	1	1	2	3	2.30
Option 5		1	4	0	2	1	4	1.85

Figure 1: Final design trade-off

The winner of the trade-off was a low-wing aircraft which uses a contra-rotating set of propellers, operating from one engine and therefore being suitable for certification under CS-VLA requirements. Its in-flight TE package includes AR glasses, an autopilot, a ballistic parachute, a fitness band for confidence and stress monitoring, a glass cockpit with integrated virtual CFI, a removable instructor seat, camera, voice and flight data recording options as well as an enhance debriefing software. Furthermore, the ground segment of the TE package will consist of a VR unit flight simulator.

Detailed Design Phase

Market Analysis

For the market analysis in this design phase, a questionnaire was performed. The questionnaire aimed to find out the price customers were willing to pay for an electrical trainer aircraft, as well as what they find important in a trainer aircraft. The results showed that the proposed price of €150,000 satisfies the willingness to pay of almost half of the participants. To pilots, added training enhancement, handling, operational cost and endurance/range are the most important aspects of a trainer aircraft.

Structures

The structures of the aircraft is what keeps everything together. Since the structure needs to be able to carry many different types of loads and connect many different components together, a lot of research is needed. The analysis for this was split up into two parts. Firstly, the wingbox was analysed in detail, sizing it for the lift distribution that was obtained from the aerodynamics department, the actual weight of the wing acting on the wing and a potential battery weight. Secondly, the fuselage was designed. As the fuselage is too big to completely design in detail in the given time frame, the design was limited to the aft portion of the fuselage, behind the cockpit bulkhead. The loads that were analysed include empennage loads, ground loads, battery weight, and emergency parachute loads. Parameters that were selected and sized include skin thicknesses, spar thicknesses, stringer numbers, number of longerons, number of frames, number of ribs, material selection, and battery position.

The analysis of the wing yielded a wing mass of 160 kg with 30 AA2024 J stringers on the upper surface and 30 AA2024 Z stringers on the bottom surface. Furthermore, the rib space was determined 200mm. The wing is over-designed at this stage due to the many conservative assumptions made, and the analysis performed will need to be refined in later stages prior to testing.

The final complete fuselage has a weight of 1229 N. The nose gear is positioned 2.00 m behind the nose, and the main landing gear is positioned 3.39 m behind the nose. These last two values followed from the c.g. position data, the requirement that the aircraft should be able to rotate while on the ground during take-off and the tail strike angle.

Aerodynamics

Aerodynamic analysis has been performed on the wing and empennage subsystems in order to design the planform parameters and assess aerodynamic performance and efficiency. The design was led by improving performance as much as possible while have safety as a driving requirement, which primarily focuses on safe stall behaviour. For the main wing, all of taper, twist and airfoils are considered as free design variables. The efficiency and stall safety characteristics are used as criteria to optimise the planform shape. This resulted in a main wing with an aspect ratio of 10.1 (set by design point), taper ration of 0.45 and twist of 5°. For the empennage, the horizontal tail was subjected to the same procedure, to optimise for safety and performance. This resulted in a horizontal tail planform with aspect ratio of 3, taper ratio of 0.7, no twist and zero trailing edge sweep. The vertical tail design was assessed by stability and control.

Stability and Control

For the assessment of the stability and control of the aircraft, the longitudinal and lateral stability have been analysed and the control surfaces have been sized. The analysis of the longitudinal stability is done by first creating the loading diagram, which resulted in a minimum centre of gravity of 2.45m and a maximum of 2.87m.

Secondly the scissor plot was created, which was used to determine the surface area of the horizontal tail, which is $3.28m^2$. The analysis was performed for different wing positions, in order to find the minimum horizontal tail surface area. This resulted in a wing position of $2.7m$ from the nose.

For the directional stability, a first estimation of the vertical tail was made, using statistical data. This resulted in a vertical tail surface area of $1.22m^2$.

The control surfaces sized are the ailerons, flaps and the elevator. The ailerons were sized based on the roll requirements, the flaps based on the required increase of lift coefficient and the elevator based on the required angular acceleration around the main gear during take-off, in order to make sure that the aircraft is able to rotate. This resulted in an aileron span of $1.34m$, a flap span of $3.58m$ and a elevator chord of $0.39m$.

Power and Propulsion

The power and propulsion subsystem consist of three main items a battery pack, an electric motor and the propeller system. These three systems have been further analysed and design in this report.

Battery. The functions that describe the battery are that the battery should be able to deliver the engine the required power, it should deliver enough power to the other systems, such as avionics, on board of the Dragonfly, and it should have enough energy storage capacity to meet the endurance and range requirements. To make sure the battery can perform these functions all phases of the flight have been analysed and it resulted in the fact that the battery should have a capacity of 59.9 kWh. The highest nominal voltage for the engine is chosen to increase efficiency, this is 400 V. Furthermore, the depth of discharge is taken as 90%. This has resulted in a total weight of 292 kg. The time to charge the battery with a high power charger is estimated to be 1.9 hours, this resulted in the requirement that the batteries should be able to be swapped out for a fully charged battery. Next to that, the cycle lifetime of the battery is estimated to be equal to 1000 cycles.

Engine. During the midterm it was decided to go for a single engine, but in this more detailed phase another trade-off was done and a twin engine with a single lever (for the pilot it feels like flying a single engine aircraft) in the cockpit turned out to be the winner. A twin configuration in which the engines are placed behind each other where the front engine propels the rear propeller and the back engine propels the front engine is chosen based on the same trade-off. From the calculations of engine parameters the Saluqi P50 twin engine turned out to be the best option. Although it delivers 10kW more power, it is lighter than the Siemens SP70D that delivers the required 70kW as maximum continuous power.

Propeller. To design the contra rotating propeller system, CROTOR was used. This program is better to be used for a single propeller design, as the counter rotating option only gives an approximation. Therefore the propeller design in this report is only preliminary. It turned out that a compromise between a high efficiency with a low number of blades and low noise by a lower RPM and smaller diameter had to be found. This resulted in a propeller system of which the forward propeller consists of 2 blades and a rear propeller of 3 blades where both propellers have a diameter of 1.8 meters. A test plan has been set up on how to test the contra rotating interaction in detail, such as flow and noise interaction. One of the test ideas is to decrease the diameter of the aft propeller in order for it to stay in the slipstream of the front propeller in order to get a higher efficiency and lower noise as the propeller tips will not go through the tip vertices of the front propeller.

Training Enhancement and Cockpit Design

After analysing the functions of the TE package and formulating the requirements, a market analysis was performed. This included several parts: performing a literature review, developing and distributing a questionnaire and conducting interviews with the Head of Training of the two biggest flight schools in the Netherlands. After the findings of the literature study and questionnaire had been analysed, the detailed design phase of the TE package occurred. During this phase, the items that will be included in the final TE package have been selected. These items are: a mixed reality headset (HTC VIVE Pro Eye VR glasses with a mounted ZED mini AR camera) which will be used for implementing the Fused Reality concept in order to turn the Dragonfly into its own in-flight simulator, the Epson Moverio BT-300 AR glasses which will be used to guide the student pilot and to display critical flight data/information right in front of their eyes, a series of items that help emulate a complex combustion engine aircraft (gear lever, propeller and mixture controls, carburettor heat control, fuel pump and fuel selector, sound system). Furthermore, a ballistic parachute and a collision avoidance system have been introduced to increase the safety of the Dragonfly. A stress monitor, voice and video recorder, electronic flight bag and debrief software have been implemented as well. Furthermore, a glass cockpit was chosen, including an autopilot and virtual certified instructor software. A removable instructor seat will be included as well, in order to help achieve a higher endurance when the student is flying solo. The ground segment of the TE package will be a VR unit simulator, as used in the US Air Force Pilot Training Next programme. Furthermore, the instructor will be offered the possibility to monitor the flight data of the students in real time, at least during take-off and landing procedures. After the items of the TE package have been established, their effectiveness was quantified

and a cost-benefit analysis was performed. It was found that the TE package will increase the effectiveness of the training by up to 30% and it will save up to 1806€ for the student from the overall PPL cost. Even though this TE package is advantageous for the student, it is not profitable for the flight schools at the moment. However, this is expected to change in the future when more and more students will be drawn to flight training on a fully electrical aircraft equipped with exciting new technology.

Final Design

The subsystems were integrated by running all analyses through an iterative loop in python. This resulted in a design with an MTOW of 884 kg. The communication of the aircraft consists of air-to-air communication, air-to-ground communication and air-to-satellite communication. The details of this are shown in a communication diagram. A hardware, software and data handling diagram of the aircraft were also generated. Additionally, it has become apparent that the aircraft will need further verification and validation in the future, in the form of both ground testing and flight testing. The aircraft also suffers from several certifiability issues. These are the take-off weight being too high to certify the aircraft within CS-VLA, the number of engines being more than one, the safety of batteries, the usage of a contra-rotating propeller, the inclusion of training enhancement practices, the ability to fly at night and IFR certification. Figure 2 shows a render of the final design of the Dragonfly.

Figure 2: Final Design Render

Business Cases

The described business cases take place in the Netherlands. The Dutch government aims to switch the entire general aviation (GA) sector from combustion engines to electric engines. Therefore subsidies will be set-up of which it is assumed the development costs of the Dragonfly will not be higher compared to the development costs of conventional aircraft in its class. To anticipate on the electrification of GA and based on production rates of current GA aircraft a production rate of 100 aircraft per year was assumed reasonable. Based on this the selling price could be €150k excluding the training enhancement package. The break-even point would then be after selling 474 aircraft. With the training enhancement the selling price will be €175,950. An option for the customer will be to lease the training enhancement package. Leasing an entire aircraft will only be possible after the break-even point has been reached. Furthermore will the direct operational costs be €22.15/hr ('fuel', engine and battery overhaul are included).

Risk Assessment

During each subsystem design specific risks were identified as well as risks for the system as a whole. These risks were analysed and mitigation strategies were created to deal with them. A significant number of risks regarding the contra-rotating propeller were identified as this is not a widely implemented system and therefore brings some uncertainties into the design. However, the most hazardous risk are some more general risks: RSK-DES-01 (MTOW exceeds the limit) and RSK-BC-01 (Lack of recharge infrastructure at airports). These risks will be reduced by aiming for a lower weight and/or adding a safety margin (for RSK-DES-01) and by making sure that current recharge technology is used (for RSK-BC-01). RSK-DES-01 is still the highest risk after mitigation, however with a lower likelihood.

Operations, Logistics and Project Planning

A flight envelope has been created in order to analyse the load factors on the Dragonfly. The maximum loads turned out to be +3.8 and -1.5 which could occur during cruise flight. For the end-of-life it is assumed the batteries and engines will get a second life in other industries. The avionics and airframe will be used to make flight simulators.

The next steps of this project will consist of start building aircraft parts and test them as the first steps for the certification process. When all ground tests have been performed, test flights will take place. After the certification process the aircraft has green light to be produced for the customers.

1
Introduction

”In the past years, several models of electrically powered general aviation (GA) aircraft have been introduced and launched on the market. The concept of using aircraft with electrical propulsion for PPL training purposes, however, is still a new one. As this type of trainer aircraft entails very low operational costs, and is a viable option from a sustainability point of view, as well as adding training effectiveness benefits, it may be argued that it represents the future of training. However, the endurance of existing electrical trainer aircraft is low, mainly due to the heavy batteries. The training capabilities that they offer are not much different from common combustion trainer aircraft. Thus, there is a need for an electrical light trainer aircraft that will determine an increase in the usage of emission-free trainer aircraft in flight schools, by means of offering higher endurance and enhanced training capabilities.”[1]

Group 06 of the 2020 spring DSE has designed an electric light trainer aircraft (Dragonfly) over the past ten weeks. The aim of this report is to document the process of the second half of this process, from the midterm until the final report. This report describes the preliminary design phase of the Dragonfly and the design of its subsystems. The final preliminary design is presented at the end of this report.

The structure of the report is as follows: Chapter 2 introduces the project objectives and describes the aim of the project. Chapter 3 explains the social and technical sustainability considerations of the group and the aircraft. Chapter 4 describes the market analysis performed and shows competitor aircraft. Furthermore, a questionnaire was performed to determine customer demands. Chapter 5 describes the structures design of the Dragonfly, including battery placement as well as wing- , landing gear-, and fuselage design. Chapter 6 elaborates upon the aerodynamic design of the Dragonfly. Chapter 7 explains the stability and control implications for the Dragonfly, and Chapter 8 describes in detail the design of the power and propulsion subsystem. Chapter 9 describes the design of the training enhancement package. Chapter 10 presents the final design achieved throughout the process of this DSE and gives an overview of the future of this project. Chapter 11 describes how the Dragonfly is beneficial to flight schools and describes various business cases. Chapter 12 shows all the risks associated with the Dragonfly’s design and aims to mitigate them. Finally, Chapter 13 describes the future of this project, such as the production, operation and distribution. The Functional Flow Diagram (FFD) and the Functional Breakdown Strcuture (FBS) are included in Appendix A.

2
Project Objectives

Over the past decades, there has been little change in the way flight schools teach student pilots how to fly. Neither students nor flight instructors seem to question whether flight training and the path to a student's PPL, instrument rating, and beyond, could be made more cost-effective, efficient, or sustainable. The DSE Group 06 would like to revolutionise the way flight training is done by designing an emission-free light trainer aircraft and a training enhancement package, which aims to improve the flight training experience.

This report describes the final phase of this project in which the chosen design option from the midterm phase is designed in detail. The designed subsystems include the structures, stability and control, propulsion, aerodynamics and the TE package. Furthermore, the business case for the Dragonfly is explored in relation to units sold, making a non-trainer version of the Dragonfly without the TE package, as well as the future planning of this project.

The mission need statement for this project has been determined as the following:

Increase the usage of emission-free trainer aircraft in flight schools.

It is important to note that this project is not only focused on making flight training more financially attractive but also to enhance the sustainability aspect [2]. In a time where global warming is a daily topic, the youth all around the world is participating in "Fridays for Future", and people face "Flight Shaming", it is ever more important to invest into the sustainable future of the aviation industry. The idea of an emission-free aircraft also includes noise emissions, as heavy noise pollution is one of the biggest criticisms towards the industry [2].

The project objective statement (POS) has thus been determined as the following:

Design an emission-free trainer aircraft, establishing a justifiable business case for flight schools, by 10 students in 10 weeks.

From an organisational standpoint, this project is divided into five main phases: project planning, project definition, concepts design, final design, and project closure. With this report, the final conceptual design phase has been completed and the previously determined best design concept [1], has been designed in more detail. Following this, the closure of the project will occur. This includes preparing a presentation for the DSE symposium, where all findings and design choices will be presented. Furthermore, a summary for the "red booklet" of the DSE will be created so that the Dragonfly design is available for future reference [2].

3
Sustainability development strategy

Sustainability is an important factor within each project and for each product. It is a broad aspect of multiple fields. This chapter covers the social sustainability in Section 3.1 and the technical sustainability in Section 3.2. The economical sustainability is discussed in Chapter 4 where the performed market research is discussed. Lastly, the sustainability requirements that followed from the EcoDesign Strategy wheel are shown in Section 3.3

3.1. Social Sustainability

A good design can only be achieved if the design team behind it is operating at their maximum potential. This was achieved by the implementation of sustainable development strategies regarding team building, communication and team well-being. These strategies were set up at the beginning of the project, in the project planning phase. The list of strategies, taken from [3], is:

- Mandatory lunch break of an hour per day;
- Use non-disposable plates/cups;
- Avoid using paper wherever possible;
- Open constructive criticism atmosphere: everyone is free to provide constructive criticism on everyone else;
- No strict coffee break times, engineers can take breaks when required;
- Trust based coffee breaks;
- Weekly evaluations regarding team dynamics and process rules.

The main idea behind all these strategies is that especially while working from home during the COVID-19 crisis, trust should be the basis of teamwork.

These rules were adhered to relatively well. This was assessed by having extensive evaluation meetings, where all the team dynamics, role division, scheduling processes, general performance and rules were evaluated. Halfway through, no significant changes were necessary and all the team members reported a high degree of satisfaction with the group and the workflow.

3.2. Technical Sustainability

For the technical part of sustainability within this project the EcoDesign Strategy Wheel [4] is used. It has eight strategies that can be categorised in different levels which are shown below. From these strategies, requirements were formed which can be seen in Section 3.3.

Global level:

1. Development of a new concept that fills a sustainability gap in the market.

This strategy is implemented by doing a market research which is described in Chapter 4.

System level:

2. Optimise the product's lifetime;
3. Optimise the system at end-of-life.

Strategy two is implemented by aiming for a lifespan that shall be at least the same as for current trainer aircraft. These current trainer aircraft last long as an age of 30 years is not uncommon. However by this time the aircraft has had all kind of revisions such as engine overhauls. With this in mind, one can think of battery replacements. One could argue that an engine overhaul may not be necessary as it consists out of fewer and less complicated parts than a conventional piston engine. To implement the third strategy an end-of-life plan is written in Section 13.1.3.

Component level:

4. Selection of materials that have a low impact on the environment;
5. Material usage reduction.

The selection of materials will be selected based on their environmental impact as well as their engineering properties. As the unit cost of the aircraft cannot exceed 150k euro compromises had to be made. For this reason, trade-offs have been performed which can be seen in Section 5.3. The fifth strategy is already implemented in every aircraft design as weight is one of the most important factors in aviation. The density of materials is an engineering property and therefore is treated in the material trade-off.

Structural level:

6. Optimise the techniques used during production;
7. Optimise the distribution system;
8. Environmental impact reduction during operation.

Bullet point six is realised by applying lean manufacturing during production. In the production plan Section 13.2 it is elaborated on this. The seventh strategy is kept as it is as it is of less importance for this project. It is about how the product will reach the customer. The very last strategy is an important one. In fact, it is already implemented in the mission need statement and the project objective statement, that state that the aircraft should be emission-free.

3.3. Sustainability Requirements

These sustainable development strategies can also be translated into requirements. The requirements flowing directly out of the sustainable development strategies are:

- **ELTA-SUS-01** - *The aircraft concept shall fill a sustainability gap in the market of current trainer aircraft for initial pilot's training.* This requirement aims to fulfil strategy 1. It also ties heavily into the mission need statement, promoting the use of emission-free trainer aircraft;
- **ELTA-SUS-02** - *The materials used for the aircraft concept shall be selected based on a trade-off between material performance, cost and environmental impact.* This requirement aims to fulfil strategy 4, 5, and 6. This requirement also ensures that each material selection process accounts for sustainability, including production as well as recycling possibilities. As a result, the environmental impact of the material selection is minimized;
- **ELTA-SUS-03** - *Lean manufacturing shall be applied during the production of the aircraft concept.* Following strategy 6, the environmental impact of the production process should be minimized. This is achieved by implementing the principles of lean manufacturing;
- **ELTA-SUS-04** - *The aircraft concept lifetime shall be at least the same as current trainer aircraft.* In general, an increase in an aircraft's lifetime means a reduction in the environmental impact of the aircraft. This is especially true for electric aircraft, as there are no operational emissions. Therefore, as a baseline, this requirement is set up to fulfil strategies 2 and 8;
- **ELTA-SUS-05** - *An end-of-life plan shall be made for the aircraft concept.* This requirement exists to fulfil strategy 3. It is important to think about the destination of the design after its useful life has depleted. This will ensure that the environmental impact of the product is reduced, especially in the long term, also after the end-of-life is reached.

4
Market Analysis

”The following chapter contains the conclusions of a market analysis performed for a zero-emission trainer aircraft. First in Section 4.1 the different stakeholders are identified. Secondly, in Section 4.2, the segmentation of the market is presented. In Section 4.3 the competitor analysis is performed. This is followed by an added value analysis in Section 4.4. Section 4.5 gives predictions of how the market will evolve over time. Thereafter a SWOT analysis is presented in Section 4.6. The chapter concludes with the performed research in the form of a questionaire to (student) pilots and instructors in Section 4.7.

4.1. Stakeholder Identification

Different stakeholders can be identified which are listed below.

- **Flight schools**: The flight schools are buying the aircraft and the TE package;
- **Student pilots**: The students will fly the aircraft and use the TE package;
- **Flight instructors**: The flight instructors will teach the students to fly on this aircraft and they will use the TE package to teach the students;
- **Aircraft manufactures**: The aircraft manufacture will build the aircraft;
- **Aviation safety agencies**: The safety agencies will certify the aircraft;
- **Airports**: The aircraft will operate at an airport;
- **Surrounding Residence of Airfields**: The people living near the airport will suffer most from aircraft noise, and therefore will be interested in noise reduction.

4.2. Market Segmentation

In the Netherlands in 2018, there were around 720 registered small aircraft flying around [1]. There is only a limiting amount of zero-emission aircraft on the market which are all powered by electricity. Aircraft that make use of other technologies (such as hydrogen) are not yet present, because the technology readiness level is still too low. The downside of electric aircraft is that they generally have a low endurance/range. Also, most of the time, the required infrastructure at airports to accommodate these aircraft is not present. These are the main reasons why there is a low demand for electric aircraft in the general aviation market. However, for the market of trainer aircraft, it might be possible to set up a viable business case for an electric aircraft. This can be done by including an enhanced training package, which increases the efficiency of the training, and which includes options that can not be implemented in conventional trainer aircraft.

In the Netherlands, there are about 23 flight schools that offer pilot training on ”regular” aircraft. In total, these flight schools own around 110 aircraft, used for training[2]. This is a market share of around 15% of the total number of small aircraft. On average half of the trainer aircraft are only VFR certified and half are also IFR certified. In Europe and the United States there are around 60,000 [5] and around 213,000 [6] small aircraft flying around respectively. If it is assumed that the market share of 15% for trainer aircraft also holds for Europe and the United States, the number of trainer aircraft in Europe is around 9,000 and in the United States around 32,000. If it is also assumed that the fractions of VFR and IFR certified can be applied to these numbers then the number of VFR (and also IFR) certified aircraft in Europe will be around 4,500 and in the United States around 16,000.

4.3. Competitor Analysis

Before starting on the design of this electric aircraft, a competitor analysis needs to be done to ensure the product will be able to compete with the status quo. This is done by analysing the current market of current zero-emission and current conventional trainer aircraft in Section 4.3.1.

4.3.1. Current Aircraft

Current Zero-Emission Aircraft

In total, three existing or near-release aircraft were found that fit the description of a light zero-emission aircraft. These can be found in Table 4.1. Note that only electric battery-powered examples have been included, as other technologies (such as hydrogen) are not yet present in state-of-the-art aircraft as of early 2020, or are in a too low technology readiness level to consider realistic.

As apparent from the table, the average endurance of a zero-emission aircraft is significantly lower than that

[1] URL https://www.cbs.nl/nl-nl/maatschappij/verkeer-en-vervoer/transport-en-mobiliteit/infra-en-vervoermiddelen/vervoermiddelen/categorie-vervoermiddelen/vliegtuigen-en-binnenschepen, LA 13-5-2020

[2] Based on the information on the websites of the flight schools

of a conventional fuel-powered aircraft. Particularly the Alpha Electro suffers from this limitation. The eFlyer series, on the other hand, features an endurance closer to that of conventional aircraft. However, these aircraft cost approximately twice as much as conventional trainer aircraft.

Table 4.1: Current Zero-Emission Aircraft

	Alpha Electro[3]	**eFlyer 2**[4]	**eFlyer 4**[4]
Endurance [h]	1	3.5	4
Range [nm]	75	-	-
Max speed [kts]	100	120	120
Weight [kg]	550	862	1225
Cost [€K]	65-87[5]	265[6]	357[6]
Operating cost [€/h]	23[7] (1 for electricity)	13 (2.76 for electricity)[8]	18
Recharge time [min]	45[9]	20[8]	-
Number built	500+[10]	1	0

Current Trainer Aircraft

Three aircraft that are commonly used by flight schools have been identified. These can be found in Table 4.2. This information shows that the average endurance of a petrol aircraft is much higher than that of electric aircraft at a relatively lower price, while also boasting slightly higher average speeds. Even though this may seem like tough competition, a significant downside to these aircraft are the much higher operating costs compared to electric aircraft. This may offset the downsides of electric aircraft. Further analysis of how this may be done can be found in Section 4.4.

Table 4.2: Current Trainer Aircraft

	Cessna 172 Skyhawk[11]	**Piper PA-28 Archer TX**[12]	**Tecnam P2002**[13]
Endurance [h]	5.1	5.5[14] [15]	5.8
Range [nm]	640	522	582
Max speed [kts]	124	128	131
Weight [kg]	1157	975	600
Cost [€K]	175	370	135 [7]
Operating cost [€/h]	90-180[16]	70[17]	150[18]
Refuel time [min]	≈ 5	≈ 5	≈ 5
Number built	43,000+[19]	32,000+[20]	≈ 330[21]

4.4. Added Market Value

This section follows up on the information from Section 4.3 to elaborate on what value the electric aircraft in question should bring to the market in order to be competitive. This is done for the aircraft itself in Section 4.4.1 and for the training in Section 4.4.2.

4.4.1. Value Over Current Aircraft

Value Over Current Electric Aircraft

Potential customers, mostly CFI's, expressed how the lack of proper infrastructure has so far withheld them from using zero-emission aircraft. In particular, flying between airports is extremely difficult with the lack of range,

[3] URL https://www.pipistrel-aircraft.com/aircraft/electric-flight/alpha-electro/#tab-id-2, LA 30-04-2020
[4] URL https://www.aerospace-technology.com/projects/sun-flyer-2-electric-aircraft/, LA 30-04-2020
[5] URL https://www.pipistrel-prices.com/alpha-trainer/, LA 30-04-2020
[6] URL https://www.ainonline.com/aviation-news/business-aviation/2018-10-18/bye-pitches-electric-aircraft-charter, LA 30-04-2020
[7] URL https://www.flyingmag.com/pipstrel-alpha-electro-coming-to-us-flight-training-market-next-year/, LA 18-05-2020
[8] URL https://byeaerospace.com/sun-flyer-2-on-the-road-to-certification/, LA 30-04-2020
[9] URL https://www.pipistrel-aircraft.com/the-alpha-electro-is-getting-established-in-switzerland/, LA 29-04-2020
[10] URL https://www.pipistrel-aircraft.com/aircraft/flight-training/alpha/, LA 14-05-2020
[11] URL https://cessna.txtav.com/en/piston/cessna-skyhawk#_model-specs, LA 30-04-2020
[12] URL https://www.piper.com/model/archer-tx/, LA 30-04-2020
[13] URL https://www.tecnam.com/aircraft/p2002-jr/, LA 30-04-2020
[14] URL https://europeanaircraftsales.com/piper-dealer/piper-archer-lx-dx/, LA 30-04-2020
[15] URL https://cutteraviation.com/cutter-piper-sales/aircraft/piper-archer-tx-trainer-pa-28-181/, LA 30-04-2020
[16] URL https://bwifly.com/cessna-172-operating-cost/, LA 30-04-2020
[17] URL https://wikiwings.com/2014/03/14/pa28-piper-archer-flight-expense-calculator/, LA 30-04-2020
[18] URL https://www.aeroclubvarese.it/en/fleet/tecnam-p2002jf-acvs/, LA 30-04-2020
[19] URL https://www.bbc.com/future/article/20170302-the-plane-so-good-its-still-in-production-after-60-years, LA 14-05-2020
[20] URL http://www.flugzeuginfo.net/acdata_php/acdata_pa28_en.php, LA 14-05-2020
[21] URL http://www.rnsa.is/media/4572/tf-ifc-air-accident-final-report.pdf, LA 14-05-2020

which adds the disadvantage of having to transport the plane by truck for maintenance, and refuelling/recharging requires infrastructure currently not present at most airports. To make the zero-emission aircraft in question feasible, the following functions can be defined.

- **ELTA-FUN-MAR-01** - *The range of the aircraft should be such that the aircraft is able to travel between airports of decent size.* This was more exactly defined as airports with a 4-digit ICAO code, within Europe. Using sample measurements of airport distances across the continent, this resulted in a required range (which is highly correlated to the endurance) of 250km. Interpolating between the endurance and cost of the Alpha Electro and the eFlyer 2, it was found that a range of 250km and a maximum cost of €150K corresponds to an endurance of 2 hours;
- **ELTA-FUN-MAR-02** - *The aircraft should be able to be refuelled/recharged on airports of decent size, using the presently available infrastructure.* If the aircraft can fly between these airports, it is also necessary to be able to refuel/recharge them. Using existing infrastructure reduces the cost and the effort needed to construct this infrastructure;
- **ELTA-FUN-MAR-03** - *The aircraft should be able to undergo maintenance at decent size airports.* This means that the aircraft should be able to undergo maintenance at conventional maintenance facilities. In this way, the aircraft can be flown to the airport where it will undergo maintenance instead of transporting the aircraft by truck (the aircraft needs to be disassembled for transport by truck);
- **ELTA-FUN-MAR-05** - *The aircraft should fly like a conventional aircraft.* When a student pilot learns to fly on a trainer aircraft, this trainer aircraft should represent a conventional aircraft. Therefore, the pilot will be able to fly on most conventional aircraft without any problems and no additional training on a conventional aircraft is needed. This makes it more feasible for flight schools to use this aircraft.

Value Over Current Conventional Trainer Aircraft

As mentioned in Section 4.3, conventional aircraft have much better endurance for a lower listing price, and due to limitations of current electric technology, this is difficult to offset. However, electric aircraft have much lower operating costs than petrol costs. This fact could be used to make zero-emission aircraft more financially feasible for customers. This resulted in the following function.

- **ELTA-FUN-MARK-04** - *The aircraft should be more financially feasible for customers.* Using a worst-case scenario analysis, it was determined that an emission-free aircraft should be able to perform 6 hours of flight training for an 8 hour day to become financially feasible for a flight school. In combination with a 2-hour endurance, this results in a required recharge time of 40 minutes. This worst-case scenario took into account a periodic propulsion replacement cost of €5,000 per 1,000 hours and a peak operating cost of €50 per hour.

4.4.2. Additional Training Value

To "Increase the usage of emission-free trainer aircraft in flight schools" [3], the aircraft needs to be more economical than existing aircraft. On top of this, the training enhancement package shall make the training more efficient, so that students can learn more in the same amount of time. For a flight school to financially profit from this, it is important to evaluate the profit that the flight school makes with every type of flight training. For example, if the flight school can charge almost the same amount of money for a flight lesson in a flight simulator, then the flight school will make a higher profit for this hour of flight training. Furthermore, if the aircraft can be used as a training aircraft without the instructor on board, then the instructor may be able to oversee several flight students from the ground and intervene in emergencies, whilst training more students at once than would be possible if he had to sit in the aircraft with the student. Furthermore, with the ability to simulate other aircraft with the TE package, it is possible to train on a more expensive to operate aircraft without actually needing that aircraft. This provides huge benefits to flight schools as they can own only one type of aircraft, but train flight students to fly several different makes and models of aircraft.

4.5. Prediction Of Future Market

As mentioned earlier, the current market for trainer aircraft is highly dominated by aircraft that use petroleum-based fuel. However, for a couple of years, some aircraft manufactures started designing aircraft with zero-emissions. The main focus is on the use of electricity and the use of hydrogen. At this moment there are already some of these designs flying around. However, the performances of these zero-emission aircraft are in most cases not comparable to the performances of conventional aircraft. For electric aircraft that are already on the market, the endurance and range are the most important limiting factors, while the design of hydrogen-powered aircraft is still in an early stage. Next to the limiting performances of the new zero-emission aircraft, the infrastructure at airports to recharge/refuel and maintain the aircraft is most of the time not present. This makes it for flight schools currently not feasible to use these zero-emission aircraft.
The innovation on these alternative sources of power, however, has not stopped. It can be expected that the performances of these zero-emission aircraft will increase. Examples of this are the eFlyer 2 and 4. Compared

to the Alpha Electro, which is already on the market, the endurance has increased significantly [22] [23]. There is also progress on the infrastructure, needed to facilitate these aircraft. For example, Groningen Airport Eelde installed a charging station for electric aircraft[24]. Taking these innovations into account, it is expected that in the future the zero-emission aircraft will slowly take over the role of the conventional aircraft.

Until the zero-emission aircraft becomes feasible for flight school based on their flight performances, flight schools should zero-emission aircraft with the current technology. Therefore these aircraft must be made feasible in a different way, for example using training enhancement. Thus this project aims to find a "temporary" solution for flight schools to make it feasible to use zero-emission aircraft until the flight performances are comparable to the flight performances of the current trainer aircraft. Of course, this does not mean that the training enhancements are not an opportunity to permanently improve the training of new pilots.

Currently, the zero-emission aircraft market is sparse. Only 3 current light airplanes were identified in the market analysis in Section 4.3. Only two of these, which are different iterations of the same aircraft, are competitive with the current fuel-based light aircraft market. However, these are not freely available to the market yet and may be costly to purchase for the average flight school. This emission-free aircraft may be able to establish a leading position in a market in affordable, financially feasible, emission-free training aircraft. Additionally, no hydrogen aircraft are as of yet available on the market.

4.6. SWOT Analysis of Target Market

The observations in this chapter have been combined into a SWOT analysis in Table 4.3."[2]

Table 4.3: Analysis of the internal (Int.) Strength & Weaknesses and external (Ext.) Opportunities & Threats.

	Strengths	**Weaknesses**
Int.	S 1. Low operating costs make the product financially attractive	W 1. Lack of infrastructure to support product
	Opportunities	**Threats**
Ext.	O 1. Low presence of competitors 2. Opportunity to be on the forefront of the sustainable aviation revolution. 3. In case of an electric aircraft: improving battery technology could make a higher capacity battery upgrade possible	T 1. Potentially conservative customer base may lack interest in new type of propulsion. 2. Technology developing at a high rate may result in the product becoming obsolete within a few years.

4.7. Primary Research

A questionnaire was performed to find out more about the views on electrical aircraft by potential customers. An extensive explanation of the questionnaire can be found in Section 9.4.

4.7.1. Questionnaire

The questionnaire contained one section on the market analysis, in which the questions were structured as follows. First, the participants were asked whats features are most important to them in a trainer aircraft. They were allowed to choose a maximum of three of the following answers, or add their own option: operational cost, noise, handling, looks, endurance/range and added training effectiveness.

Following this, partakers were asked, "If you were to buy/fly a trainer aircraft in the near future, would you consider an electrical aircraft?". Based on their answer to this question (yes or no), they were asked *why* they would or would not buy/fly an electrical aircraft. The answer options if they selected "yes" were lower operational costs, sustainability, noise emissions, added training effectiveness added by the electrical engines and other, for which they were able to specify a custom answer. If they selected that they would not consider buying or flying an electrical aircraft, the answer options were scepticism on new technology, not believing electrical aircraft are suited for flight training, low operational costs not being a priority and finally "other", for which the participants could enter a custom answer.

Furthermore, participants were asked what the maximum appropriate price for an electrical trainer aircraft would be in their opinion. The results of this will aid in determining a valid market price for the Dragonfly.

[22] URL https://www.pipistrel-aircraft.com/aircraft/electric-flight/alpha%2Delectro/#tab%2Did%2D2, LA 29-04-2020

[23] URL: https://www.aerospace-technology.com/projects/sun%2Dflyer%2D2%2Delectric%2Daircraft/, LA 29-04-2020

[24] URL https://www.groningenairport.nl/actueel/groningen%2Dairport%2Deelde%2Deerste%2Dluchthaven%2Dmet%2Delektrische%2Dlaadpaal%2Dvoor%2Dvliegtuigen, LA 29-04-2020

4.7.2. Results

The results of the market analysis questionnaire - as explained in Section 4.7.1 - are shown in this subsection. In total, 118 responses to the questionnaire were received via Google forms.

According to this study, the most important features of a trainer aircraft are by far handling and operational cost. Eighty-seven per cent of participants responded that both handling and operational cost are important to them. Thirty-nine per cent of participants considered the added training enhancement as important and twenty-three per cent considered endurance/range as important. Only 1.5% of people considered looks important. Options that were added by people (and subsequently only had one vote) included: safety, seating comfort, standardisation (similarity to other trainer aircraft) and good visibility.

When asked whether or not they would buy or fly an electrical aircraft in the near future, 64.2% of people responded with yes. Of the 76 people that would consider an electrical aircraft, 48 are interested due to low operational costs and 46 like the sustainability aspect. Twenty-nine respondents saw the benefit in the lower noise emissions, while 18 people liked the benefits of the electrical engine when considering added training effectiveness. Some custom answers that people included were reliability and maintainability of the engine, curiosity to try new technology, preparing students for the future and the simplicity of operating an electrical aircraft.

The participants that would not consider buying an electrical aircraft had the following reasoning. Most people that answered this entered custom answers, so the most important aspects that were mentioned by several people have been filtered out and summarised. Around one-third of the 42 people who selected that they would not buy an electrical aircraft are sceptical about the new technology. Several people are afraid of malfunctions during flight, others do not deem it feasible to learn on an electrical aircraft and then fly combustion engine aircraft, as there is no engine noise, only a power lever etc. Many people are also worried about charging times and the availability of chargers at airports. Furthermore, a lot of participants are afraid the technology isn't advanced enough yet but would be interested in buying an electrical aircraft as technology advances and higher endurance can be achieved.

Finally, the participants answered a question on the acceptable cost of this aircraft and the results were very spread out. The results of this can be found in Figure 4.1

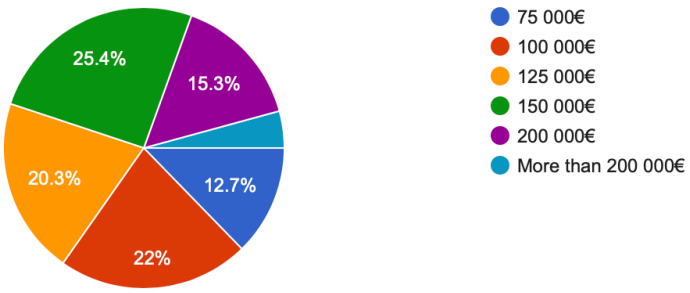

Figure 4.1:
"What is the maximum price you would consider appropriate for an electrical light trainer aircraft, certified within CS-VLA?", 118 responses

The proposed price for the Dragonfly is no higher than 150 000€, which correlates with almost half of the respondent's answers, as they responded 150 000€ or higher.

5
Structures

The structures subsystem ties everything together. It is comprised of the wing, fuselage, landing gear, empennage, control surfaces, and thrust structures. Due to the time constraints of the project, priorities had to be set about which subsystems were to be designed in detail. This is done in Section 5.1. Next, the functional analysis is done in Section 5.2. Here, also functional requirements are set up. Next, the material options are investigated in Section 5.3. Then, the battery placement is analysed in Section 5.4. After the battery, the wing is designed in Section 5.5. After the wing is designed, the fuselage will be designed. This is done in Section 5.7. Then, the landing gear is designed in Section 5.8. Finally, the compliance with the requirements is investigated in Section 5.9.

5.1. Prioritising Subsystems

Due to the restricted time of the project, not all structures of the aircraft could be analysed. This means that some subsystems needed to be prioritised. These prioritised subsystems have been analysed in as much depth as the limited time of the project allows. All other subsystems that were not considered to be a priority were sized using preliminary methods.

The subsystems that were prioritised were determined by doing a small qualitative trade-off as a selection procedure. The subsystems that were investigated were wing, fuselage, ailerons, flaps, horizontal tail (H. Tail), elevator, vertical tail (V. Tail), rudder, landing gear, and thrust structure. The trade-off was based on their impact on the following criteria flight performance, training, electrical system, control, cost, special certifiability, and RAMS. Instead of doing a numeric investigation for all these criteria, the subsystems were only scored qualitatively based on their expected impact on the criteria. This was done to prioritise the available scheduling resources on the actual design itself.

From the selection process, the subsystems with the highest impacts on average on all subsystems were deemed to be a priority. This trade-off can be seen below in Table 5.1.

Table 5.1: Subsystem priority trade-off, H = High, M = Medium, L = Low

Subsystem	Wing	Fuselage	Ailerons	Flaps	H. Tail	Elevator	V. Tail	Rudder	Gear	Thrust Struct.
Flight performance	H	M	H	H	M	H	L	M	M	L
Training	H	M	H	H	L	M	L	M	H	L
Electrical System	M	H	L	L	L	L	L	L	L	H
Control	M	L	H	M	M	H	M	H	L	M
Cost	H	H	L	L	M	L	M	L	M	M
Special certifiability	M	H	L	M	L	L	L	L	M	H
RAMS	H	H	L	L	M	L	M	L	H	M

As it may be seen from the trade-off, the subsystems that are to be prioritised are the wing and the fuselage.

In reality, all of these subsystems would be analysed in detail, but because of the time limit of the project that is not possible. Furthermore, as it may be seen from Table 5.1, the trade-off was not done quantitatively. This is once again due to the time restriction put on the project. It is clear that the wing and the fuselage have a big impact in several criteria, and substantially more than other subsystems. Hence, doing further analysis and going into numbers is highly unlikely to change the outcome of the selection. Finally, the wing and fuselage also have the highest weight of all the subsystems and are hence also very important for the performance of the complete aircraft.

5.1.1. Budgeting

All the structures have to have constraints, in order to ensure compliance with system-wide requirements, such as the maximum take-off weight. For this reason, the structural components need to have a target weight, assigned from a mass budget. After preliminary investigations, a mass budget was derived. This mass budget was tweaked throughout the design process.

The same holds for the cost budget. A preliminary cost budget was set up. After further developments and design decisions, the budget was constantly updated. Things that are included are for example a fixed cost for the motor, as an off-the-shelf motor was selected (the reasoning for this will be explained in Section 8.4).

Another point of note is that the budget for all the structures, including the power train, was merged under a single entry. This is because the method to estimate these costs combine the total material costs, manufacturing costs, labour hours etc. into one estimate.
The final budget table can be found in Table 5.2.

Subsystem	Item	Mass budget [kg]	Cost budget [kUS$]
Payload	Payload	200	0
Battery	Battery	198	30
Propulsion	Motor	30	8
	Propeller	12	6.5
	Power train	5	-
Structures	Fuselage	115	70
	H. Tail	12	-
	V. Tail	8	-
	Wing	100	-
Other	Avionics	36	10
	TE package	34	30
Subtotal	**Subtotal (excl. TE)**	**716**	**124.5**
	Insurance	-	17.25
Totals	**Total**	**716**	**141.75**
	Total incl. TE	**750**	**171.75**

Table 5.2: Aircraft mass budget

Apart from mass and cost budgets, also some design parameters were fixed after the previous phase of the project. These included the clean configuration zero lift drag coefficient, the oswald efficiency factor, and the propeller efficiency. This was done in order to meet the take-off requirement. These were set at 0.028, 0.83 and 0.88, respectively.

5.2. Functional Analysis and Requirements

In this section, the functional requirements that all the aircraft structural subsystems must comply to will be analysed. This will be done in more detail for the subsystems that are to be prioritised, namely the wing, fuselage, and landing gears. In each section, first, a brief functional analysis, following from the FFD in Appendix A, is conducted. Based on this, functional requirements were set up. These are listed after the functional analysis, together with the reasoning behind each requirement. It is important to note that only the requirements that are relevant to the structural analysis of the subsystems are included, as each subsystem has many more non-structural related requirements.

5.2.1. Wing

As previously mentioned, the wing is considered to be a priority in the structural analysis. The main function of the wing is to provide sufficient lift to the aircraft in all phases of flight. This means that sufficient lift shall be provided during take-off, cruise and landing. Furthermore, the wing shall not break under critical loading. The wing shall have the ability to house control surfaces such as ailerons and high lift devices such as flaps. The wing shall be attached to the fuselage of the aircraft. Furthermore, the wing shall be sized and positioned to permit entry into the cockpit by the pilots. Lastly, the wing shall comply with CS-VLA requirements. The requirements that the wing must adhere to are listed below, as well as the reasoning behind each requirement.

- **ELTA-W-04** - *The wing shall house the ailerons.* This requirement was set up because the ailerons are attached to the wing;
- **ELTA-W-05** - *The wing shall house the flaps.* This requirement was set up because the flaps are attached to the wing;
- **ELTA-W-06** - *The wing shall provide potential battery storage volume.* This requirement was set up because of the need of battery storage;
- **ELTA-W-07** - *The wing shall provide the lift to sustain flight in all flight conditions within the flight envelope.* This is due to the fact that the aircraft must have the ability to fly anywhere within the flight envelope. From the flight envelopes, it can be seen that the wing shall be able to sustain the loads of 4.45g and -2.45g;
- **ELTA-W-08** - *The wing shall be attached to the fuselage.* This requirement results from the fact that the wing will be attached to the fuselage;
- **ELTA-W-09** - *The wing shall not bend more than 0.1 of the wing span at maximum positive and negative loads.* This requirement stems from the fact that the bending of the wing affects the aerodynamic characteristics of the wing in a deteriorating manner. Therefore, a maximum value needs to be defined;
- **ELTA-W-10** - *The wing shall be maintainable.* The aircraft is intended to be in operation for a long

duration, and hence the wing must be maintainable should any problems arrive;

- **ELTA-W-11** - *The wing shall have two spars.* The requirement was set up because wing spars are needed within the wing;
- **ELTA-W-12** - *The wing shall allow the pilot to enter the cockpit.* The wing needs to permit entry into the cockpit by the pilots.
- **ELTA-W-18** - *The wing shall not exceed a mass of 100 kg.* This requirement flows from the engineering budget in Section 5.1.1;
- **ELTA-CS-STR-02** - *A safety factor of 1.5 shall be used for each structural component.* This requirement serves to comply with certification specifications on aircraft structures;
- **ELTA-CS-STR-03** - *The allowable stress level shall be lower than the ultimate stress of the material.* This requirement serves to comply with certification specifications on aircraft structures.

5.2.2. Fuselage

The fuselage is the second subsystem that was designed in more detail, apart from the wing. The main function of the fuselage is that it shall provide a safe, enclosed environment for its occupants. Besides that, it should transfer and carry loads coming from different components, such as the engine or the wing. Next to that, it should connect the different components together, acting as the backbone of the aircraft. Additionally, it should have enough storage space for luggage and it should be shaped aerodynamically. It is also important that the fuselage allows for sufficient space for the training enhancement package. The requirements that the fuselage must comply to structurally are listed below, as well as a brief description about the origin of each requirement.

- **ELTA-CS-FUS-01** - *The tail upsweep angle shall be such that the aircraft is able to rotate to its clean stall angle of attack.* This requirement serves to satisfy fuselage requirements in CS-VLA;
- **ELTA-CS-FUS-02** - *The cockpit width shall be 101 cm as a minimum.* This requirement serves to satisfy fuselage requirements in CS-VLA;
- **ELTA-CS-FUS-03** - *The cockpit height measured from floor to ceiling shall be 112 cm as a minimum.* This requirement serves to satisfy fueselage requirements in CS-VLA;
- **ELTA-CS-FUS-04** - *The pilot shall be able to look as a minimum 5 degrees downward over the nose of the aircraft.* This requirement serves to satisfy fuselage requirements in CS-VLA;
- **ELTA-CS-FUS-05** - *The pilot shall be able to look outside the aircraft as a minimum 135 degrees to the right and left.* This requirement serves to satisfy fuselage requirements in CS-VLA;
- **ELTA-CS-FUS-06** - *The pilot shall be able to look outside the aircraft as a minimum 30 degrees up and down using the side window.* This requirement serves to satisfy fuselage requirements in CS-VLA;
- **ELTA-FUS-01** - *The fuselage shall be designed to provide enough space for the training enhancement package.* The in-flight training enhancement package will be placed within the fuselage, and hence the fuselage should provide the required space;
- **ELTA-FUS-02** - *The fuselage shall be able to carry two passengers while flying at the maximum load factor.* The aircraft fuselage shall not break under extreme loading, as this would likely lead to fatalities;
- **ELTA-FUS-03** - *The fuselage shall provide space for the motor in the nose of the aircraft.* The motor will be placed in the nose of the aircraft, behind the propeller. Therefore, the fuselage should provide the required space in the nose;
- **ELTA-FUS-04** - *The fuselage shall be able to withstand the loads on its structure, caused by aerodynamics, ground loads, propulsion, emergency parachute, and gravity.* This once again stems from the fact that the fuselage must not break under all loads that will be encountered;
- **ELTA-FUS-05** - *The fuselage shall be designed to provide enough space for the avionics.* The avionics will be placed inside the cockpit, which is located inside the fuselage. Therefore, the fuselage shall provide enough space for these avionics;
- **ELTA-FUS-06** - *The fuselage shall connect all the primary subsystems of the aircraft together.* This requirement stems from the fact that the propeller, wing, horizontal tail and vertical tail will all be attached to the fuselage;
- **ELTA-FUS-07** - *The fuselage shall be able to carry two passengers side by side.* This requirement stems from the user requirement **ELTA-USER-PERF-02**, which states that the aircraft shall have a capacity for 2 occupants. These occupants will be located within the fuselage, and hence there must be enough space for these occupants within the fuselage. In order to assist the training procedures, the pilots shall be seated next to each other;
- **ELTA-FUS-08** - *The fuselage shall be designed to provide enough space for the batteries.* This requirement stems from the fact that the batteries will need to be located somewhere within the aircraft. The location of the batteries has not been decided upon as of this moment, if the batteries do not end up being

positioned inside the fuselage, this requirement will be scrapped;

- **ELTA-FUS-09** - *The fuselage shall not exceed a mass of 115 kg.* This requirement flows from the engineering budget in Section 5.1.1;
- **ELTA-CS-STR-02** - *A safety factor of 1.5 shall be used for each structural component.* This requirement serves to comply with structural requirements of CS-VLA;
- **ELTA-CS-STR-03** - *The allowable stress level shall be lower than the ultimate stress of the material.* This requirement serves to comply with structural requirements of CS-VLA;
- **ELTA-CS-STR-05** - *Each seat and its supporting structure shall be designed for occupants weighing at least 86 kg.* This requirement serves to comply with structural requirements of CS-VLA.

5.2.3. Landing Gear/Undercarriage

Another important subsystem is the landing gear. The primary function of the undercarriage is to support the aircraft on the ground. This extends into taxiing, take-off, and landing operations. It should make sure that the aircraft is stable on the ground. The undercarriage also provides steering capabilities, and adds braking functionality. Whilst in the air, the landing gear should produce as little drag as possible. The structural requirements that the undercarriage shall comply with are given below, with a brief description of the requirement.

- **ELTA-FLT-06** - *The main landing gear shall be positioned such that the aircraft will not tip over at its most rear centre of gravity.* This requirement was created because the aircraft shall not tip over when on the ground;
- **ELTA-FLT-07** - *The main landing gear shall be positioned such that the aircraft will be able to pitch up 15 degrees while on the ground without a tail strike.* This requirement was based on conventional values for similar aircraft [8];
- **ELTA-FLT-08** - *The line through the aft-most c.g. location and the main landing gear shall be oriented at least 5 degrees from vertical.* This requirement was based on conventional values for similar aircraft [8];
- **ELTA-FLT-09** - *The landing gear shall provide braking capabilities while the aircraft is on the ground.* The requirement stems from the fact that the aircraft will need to have a breaking system required for slowing down the aircraft when needed or rapid turns on the ground;
- **ELTA-FLT-10** - *The landing gear shall provide steering capabilities while the aircraft is on the ground.* This requirement stems from the fact that the aircraft will need to perform turns during taxi;
- **ELTA-CS-FLT-20** - *The nose wheel shall carry at least 8% of the aircraft weight with the most rear centre of gravity.* This requirement serves to comply with the CS-VLA.

5.2.4. Horizontal Tail

The horizontal tail was not prioritised for analysis, and was only looked at using preliminary methods. The horizontal tail provides the lift required to stabilise and control the aircraft. It should provide the functionality to be able to trim the aircraft. It should also have an elevator that is controllable by the pilot. It should be able to generate both negative and positive lift, while keeping the drag as low as possible at all times. It should be attached to the fuselage of the aircraft at the tail. The structural requirements that the horizontal tail shall comply with are presented below, with a brief description on the requirement.

- **ELTA-W-HT-01** - *The horizontal tail shall house the elevators.* The elavators will be placed on the horizontal tail;
- **ELTA-W-HT-02** - *The horizontal tail shall be trimmable.* It is possible that the horizontal tail will be an elevator in itself. In that case, the horizontal tail would need to be trimmable;
- **ELTA-W-HT-03** - *The horizontal tail shall provide both positive and negative lift as required.* This requirement was set up to ensure that that horizontal tail will be able to change the pitch of the aircraft;
- **ELTA-W-HT-04** - *The horizontal tail shall be able to sustain all loads imposed on it within the flight envelope.* This requirement stems from the fact that when flying under critical loading, the horizontal tail may also encounter critical loads. Therefore, the horizontal tail shall be able to carry these loads;
- **ELTA-W-HT-05** - *The horizontal tail shall be attached to the fuselage.* The requirement stems from the fact that the loads need to be transferred from the tail to the aircraft. This is done by attaching the horizontal tail to the fuselage;
- **ELTA-W-HT-07** - *The horizontal tail shall be maintainable.* This aircraft is intended to be in operation for an extended amount of time. This means that should any problems arise on the horizontal tail, it needs to be accessible for maintenance;
- **ELTA-W-HT-08** - *The horizontal tail shall have two spars.* This requirement stems from the fact that spars are needed within the horizontal tail for functionality;
- **ELTA-CS-STR-02** - *A safety factor of 1.5 shall be used for each structural component.* This requirement serves to comply with CS-VLA;

- **ELTA-CS-STR-03** - *The allowable stress level shall be lower than the ultimate stress of the material.* This requirement serves to comply with CS-VLA.

5.2.5. Vertical Tail

The last subsystem is the vertical tail. The vertical tail was also not considered to be a priority for analysis. The vertical tail functions are similar to that of the horizontal tail. It should provide a control force that is required to stabilise and control the aircraft. It should have a rudder, controllable by the pilot. It should be able to generate lift in both directions, while keeping drag low. It should be attached to the fuselage of the aircraft at the tail. The structural requirements that the vertical tail shall comply with are given below, with a brief description of the requirements.

- **ELTA-W-VT-01** - *The vertical tail shall house a rudder.* This requirement stems from the fact that the rudder shall be positioned on the vertical tail;
- **ELTA-W-VT-02** - *The vertical tail shall provide both positive and negative lift as required.* This requirement was set up to ensure that that vertical tail will be able to change the yaw of the aircraft;
- **ELTA-W-VT-03** - *The vertical tail shall be able to sustain all loads imposed on it within the flight envelope.* This requirement stems from the fact that when flying under critical loading, the vertical tail may also encounter critical loads. Therefore, the vertical tail shall be able to carry these loads;
- **ELTA-W-VT-04** - *The vertical tail shall be attached to the fuselage.* The requirement stems from the fact that the loads need to be transferred from the tail to the aircraft. This is done by attaching the vertical tail to the fuselage;
- **ELTA-W-VT-06** - *The vertical tail shall be maintainable.* This aircraft is intended to be in operation for an extended amount of time. This means that should any problems arise on the vertical tail, it needs to be accessible for maintenance;
- **ELTA-W-VT-07** - *The vertical tail shall have two spars.* This requirement stems from the fact that spars are needed within the vertical tail for functionality;
- **ELTA-CS-STR-02** - *A safety factor of 1.5 shall be used for each structural component.* This requirement serves to comply with CS-VLA;
- **ELTA-CS-STR-03** - *The allowable stress level shall be lower than the ultimate stress of the material.* This requirement serves to comply with CS-VLA.

5.3. Material Selection

A design is heavily influenced by the materials that are used. Hence, before a design can be made, the materials to be used have to be selected. For this, the method outlined by Ashby [9][10] was be used. The strategy has four steps: translation of design requirements, screening using constraints, ranking using objectives, and seeking documentation.

Translation of design requirements means expressing the functional aspects and requirements of components and subsystems as mathematical functions, constraints, objectives, and free variables as much as possible. This is done in Section 5.3.1. Screening the materials using the constraints entails eliminating unfeasible material options. The next step is ranking the materials using the objectives, which is done via a trade-off. Then, documenting the resulting materials and doing further research on them is the final step. These three steps are done in Section 5.3.2. The final step is making a final material choice. However, as the final decision is highly related to the design process itself, this was done in Section 5.5 and Section 5.7.

5.3.1. Primary Load Cases

The aircraft and its subsystems have many different components. On these components, unique loads and load cases are imposed. As a result, a single optimal material choice does not exist for the complete aircraft. Therefore, after some general remarks regarding selection criteria and translation of requirements, several components of the structures that were to be designed in detail were analysed individually.

General Considerations

All components need to be manufacturable. Due to the relatively high manufacturing costs with respect to the total aircraft unit price (48%, following the midterm report[1]), the costs of manufacture for the specific materials also need to be relatively low. Materials need to withstand wind and weather practically without corrosion, and need to be maintainable.

Furthermore, a high degree of significance is given to sustainability of the materials. This shall take into account several sustainability considerations, including, but not limited to, scarcity of materials, emissions during material processing and production, recyclability, and possible impact on communities at the source of the material.

Next to these, the most important criterion is that the weight shall be minimised, while being able to carry the loads. In order to achieve this, a high ratio of stiffness over density is favoured. However, the specific ratio

that is critical for minimising the weight depends on the specific critical load case of every component. Hence, the most important material indices for each component is identified first. The results of this can be found in Table 5.3. This table will be explained in the following subsections.

Table 5.3:
Components, critical load cases, and corresponding material indices of the fuselage and wingbox. Material indices taken from Ashby [10].

Component	Critical load case	Material index
Wing skin	Compression (plate buckling)	$E^{1/3}/\rho$
Wing spars	Bending	E/ρ
Wing ribs	Bending	E/ρ
Wing stringers	Compression (column buckling)	$E^{1/2}/\rho$
Fuselage longerons	Compression (column buckling)	$E^{1/2}/\rho$
Fuselage stringers	Compression (column buckling)	$E^{1/2}/\rho$
Fuselage frames	Bending	E/ρ
Fuselage skin	Bending	E/ρ
	Torsional shear	G/ρ
	Compression (plate buckling)	$E^{1/3}/\rho$

Stiffened Panels

The aircraft will have a semi-monocoque design, with the skin of the aircraft partially carrying the loads. However, in many cases, a skin on its own is not able to withstand the required loads while being low-weight. This is especially the case for panels in compression, where buckling is generally the critical failure mode. Hence, stiffeners, sometimes called stringers, are added. Using this configuration, the main function of the stringers is to carry compression loads, while the skin's main function is to carry the aerodynamic loads into the ribs and spars. At the underside of the wingbox, the aerodynamic loads are mainly tensile in normal flight conditions, however, in case of the minimum load factor of -2.81[1], this panel will also be in compression, while the top plate will be in tension. Hence, both failure modes were analysed.

The main objective of each component is to minimise the mass within the given constraints. This is achieved in the material selection process using material indices. The process of obtaining these is by highlighting the analysis of a column in compression, where the failure mode is buckling. Here, the mass of a constant cross-section component can be calculated using:

$$m = Al\rho \tag{5.1}$$

For a given cross-sectional shape, only the area of the cross-section is a free variable. ρ is a material property, and l is fixed, based on geometric constraints. To predict the critical buckling stress, a Johnson-Euler approximation is used, based on Megson (2014)[11]. For Euler buckling, it follows that

$$\sigma_{cr} = \frac{\pi^2 E}{(L_e/\rho_g)^2} \tag{5.2}$$

where ρ_g is the radius of gyration, defined as:

$$\rho_g^2 = I/A \tag{5.3}$$

Here, $I = A^2\phi$ where ϕ is a shape factor, in case the cross-sectional shape is already defined. Substituting Equation (5.3) into Equation (5.2), taking $\sigma_{cr} = P_{cr}/A$, and rewriting the moment of inertia, gives:

$$P_{cr} = A^2 E \frac{\pi^2 \phi}{l_e^2} \tag{5.4}$$

This implies that for a fixed P_{cr}, l_e, and geometry (ϕ), $A \propto E^{1/2}$. Substituting this result into Equation (5.1) gives that $m \propto 1/M_t = \frac{\rho}{E^{1/2}}$, which should be minimised. This fraction $M_t = \frac{E^{1/2}}{\rho}$ is called the material index, and should be maximised. It can be defined for each load case given a set of constraints. Other material indices are derived in similar fashions by and taken from Ashby [10].

A key constraint of this material index is that the cross-section of the column should be fixed in advance. To ensure this, several options of stringers were available. In aviation, usually, Z-stringers or J-stringers are used. This is because of their relatively high moments of inertia and low structural complexity, in combination with being less prone to corrosion than for example Y-stringers or hat stringers. Sometimes, extruded panels with integrated stiffening elements are also used. However, those were not selected because of the high degree of waste materials, and consequent higher costs and violation of the lean manufacturing principles from the sustainable development plan.

The main difference between Z and J stringers is that J stringers are connected with two rows of rivets instead of one. This is beneficial for delaying inter-rivet buckling, especially if the rows of rivets are staggered [12]. Due to the limited resources of the project, rivet spacing and inter-rivet buckling will not be investigated further than this. Hence, it will be assumed that inter-rivet buckling is not a critical failure mode, and will hence not be researched in more detail. However, in order to mitigate the effects of this assumptions, J stringers are selected for the top plate of the wingbox. This is because this plate is mainly in compression, which means that buckling is a failure mode with high probability to occur. For other locations on the aircraft structure where buckling is less critical, Z stringers are selected because of their more beneficial moment of inertia. For the same total cross-sectional area and ratios between the thicknesses and dimensions, the moment of inertia of a Z stringer is calculated to be roughly 37% higher.

For the plate, loaded in compression in-plane, with length and width specified and thickness as the free variable, the material index can also be taken from Ashby [10]. What should be noted here is that this dictated the order in which the wingbox would be designed. First, the spars and ribs would be positioned, after which the stiffened skin panels could be sized. This would then be iterated upon.

Wing Structural Elements

A wing's primary function is to carry the aerodynamic loads that keep the aircraft in the air. It needs to do this while being as light-weight as possible. To achieve this, the wingbox consists of several primary components. Neglecting the control surfaces, these are ribs, spars, stiffeners and a skin. The stiffeners and skin together form stiffened panels, as analysed in Section 5.3.1.

The spars are the primary elements that resist the bending loads resulting from the aerodynamics. They ensure the loads are carried to the fuselage. They can be viewed as the web plates of a beam, if the wing is idealised as a beam. Spars are mainly loaded in shear, and spars are stiffness constrained by ELTA-W-09, limiting the deflection of the beam. Their height is fixed by the airfoil shape and wing geometry, but their width (thickness of the web plate) is a free variable. Hence, the material index most relevant to spars is E/ρ.

The final primary elements are the ribs. Their function is to transfer the loads from the skin to the spars, and to maintain the wing profile. They also provide stability against panel buckling, by dividing the skin into discrete section. Finally, they provide attachment points for local loads, such as landing gear, high lift devices and control surface actuators. Ribs are mainly loaded in bending. Similar to the spar, their geometry is fixed due to the wing profile and the airfoil shape. However, the thickness is free. The governing material index is hence E/ρ.

Fuselage Structural Elements

The fuselage consists out of several distinct components, just like the wing. Primarily, there is a load-bearing skin. However, this skin is often reinforced with longerons. These are stiffening elements, much like spars and stringers. These longerons are usually complemented by stringers in certain sections of the fuselage. The stringers and skin form stiffened panels, just like in the wing, as explained in Section 5.3.1. The final major fuselage structural components are frames, sometimes in the form of bulkheads. These act as ribs in the wing, maintaining the fuselage shape, and transferring structural loads to longerons.

The skin and stringers usually carry either tension or compression, just like in the wing. However, in the fuselage, they also play a major role as web plate of the fuselage structure, taking over the role of the spars in the wing by carrying shear and bending loads. Furthermore, as the empennage and the wing impose relatively high torques on the fuselage, another load that the fuselage skin experiences is shear stress due to torsion. The fuselage shape is determined first, then the skin and other fuselage components are sized for that shape with the thickness being the free variable for the skin, after which the shape is iterated upon. Hence, the primary material indices for the fuselage skin are G/ρ (for the torsion), $E^{1/3}/\rho$ (for plate buckling), and E/ρ (bending, thickness as free variable).

5.3.2. Material Trade-off

The criteria were now translated into mathematical constraints and parameters. However, before a selection could be made, the options that were available needed to be compared. For this reason, a trade-off is done. To set this up, first, a QFD was done to determine the trade-off criteria and their weights. As explained in Section 5.3.1, the materials were graded on sustainability, cost, manufacturability, RAMS, and their effect on weight due to their material index score. The material index scores were again assessed using Ashby [9]. The final trade-off of material families can be seen in Table 5.4.

Table 5.4: Material family selection trade-off.

Design Option	Technical Performance Measurements	Weight	Sustainability	Cost	RAMS	Manufacturability	Score
	Weight	25%	15%	25%	15%	20%	100%
Foams		0	2	2	1	4	1.75
Natural materials		2	4	3	1	3	2.60
Elastomeres		0	2	4	1	3	2.05
Polymers		1	2	4	3	3	2.60
Composites		4	2	2	2	2	2.50
Non-technical ceramics		3	1	3	1	1	2.00
Technical ceramics		4	1	2	2	2	2.35
Metals		3	3	4	4	3	3.40

Three separate trade-offs were done, for different material indices. The results of these trade-offs were used to select metals and composite materials as material families of interest. In the aerospace industry, the materials that are used most often from these families are carbon fibre reinforced polymers, glass fibre reinforced polymers, and aluminium alloys. This is because they have a high strength to weight ratio, and hence score really well on the material indices. Steels are also sometimes used for a few critical components. The specific individual material selection for every subsystem was done with the subsystem design.

5.4. Battery Placement Trade-off

It is important to decide exactly where the battery will be located within the aircraft. This decision was made via a trade-off. The criteria that were deemed as relevant for the trade-off were as follows: Safety, stability, space available, accessibility, and impact on aircraft weight. The accessibility criteria refers to how accessible the battery is for procedures such as charging, replacement or maintenance. The impact on aircraft weight refers to how many structural supports need to be added to the aircraft to maintain structural integrity. This changes depending on where the battery is located within the aircraft.

In order to determine the weights of these criteria, a QFD (Quality Function Deployment) was performed. The requirements that the battery must comply to were related to each criteria. These requirements are described below:

- **ELTA-BAT-01** - *Battery placement shall not make the aircraft unstable*;
- **ELTA-BAT-02** - *Battery shall be stored in an area which has the required space and volume, providing adequate thermal control*;
- **ELTA-BAT-03** - *Battery shall be placed somewhere accessible to ensure functionality of charging and maintenance procedures*;
- **ELTA-BAT-04** - *Battery shall be placed in an area minimising the the supports required to maintain structural integrity*.

The QFD was performed, resuling in scores for five different trade-off criteria. These were:

- Safety (25%);
- Stability (10%);
- Space available (20%);
- Accessibility (15%);
- Impact on aircraft weight (30%).

Finally, the trade-off itself was performed. The option with the battery behind the cockpit, inside of the fuselage, was deemed the best option. This is because it offered a lower overall aircraft weight than if the battery was placed in the nose or the wing. These locations would result in aircraft weights of approximately 5 kg and 10 kg higher, respectively. The option was also deemed the most safe and risk-free, as fewer special considerations need to be paid to fire safety than if the battery were to be placed under the pilot seat.

5.5. Wing Design

In order to design the wing, a numerical model of the half wing was built. For analysis, only the half wing needs to be considered. This is due to the fact that the loads on both wings, under maximum load factor, will be equal. To reduce the complexity of the program, only the wingbox structure of the wing will be analysed. The program allows the user to iterate between the number of stringers required on the upper and lower skins. This allows the user to choose an optimised number of stringers, for which the material, stringer type and dimensions must be defined, such that no failure modes are encountered during maximum loading of the aircraft. Furthermore,

the program allows the user to optimise the rib spacing within the wing. Before getting to the result, many steps must be taken. This section will explain exactly how the program works as well as present the results obtained for the wing of the Dragonfly. All the equations described in this section are taken from [13].

5.5.1. Wing Geometry

The program can be separated into 3 main parts: Programming the half wing geometry in 3D and its attributes (centroids, moments of inertia and shear centers), obtaining all forces acting on the wing and finally obtaining all stresses everywhere on the wing and ensuring that none exceed critical buckling, or yield stresses of stringers or of stiffened plates. The user must input the dimensions of the stringers. These dimensions include thicknesses and lengths of all sides. Then, the wing planform parameters such as span, surface area, quarter chord sweep and airfoil used must be inserted inside the program. Lastly, the discretization that the user would like to use (how many cross sectional cuts will be made along the wing) must be inputted by the user. The latter will allow the user to increase the speed of the program by decreasing the discretization number at the cost of accuracy. Therefore, it is highly recommended that this number is set to something reasonable for the wing that needs to be analysed. From all of this, the program then generates however many cross sections that the user wanted, correcting the location and size of each cross section according to the wing planform parameters inputted by the user. Each cross section resembles the airfoil chosen by the user, with a chord sized according to the taper ratio. Before continuing further with the explanation of the program, all input parameters that the user must enter are given below in Table 5.5.

Table 5.5: Wing structural analysis program input parameters

Parameter	Unit	Description
Stringer dimensions	m	All dimensions related to stringers
Skin thickness	m	Wing skin thickness
Skin material	-	Wing skin material name
Discretization (n)	-	Number of cross sections to be made along half wing
Number of stringers on upper surface	-	-
Number of stringers in lower surface	-	-
x/c front spar location	-	-
x/c aft spar location	-	-
Spar dimensions	m	All relevant spar dimensions
Number of ribs	-	Determines rib spacing (evenly spaced along wing)
Rib dimensions	m	All relevant rib dimensions
Battery in wing (True/False)	-	Allows analysis with battery in and out of wing
Maximum load factor	-	Maximum load factor wing must be able to carry
Minimum load factor	-	Minimum load factor wing must be able to carry

Furthermore, the coordinate system is as follows: The origin is placed at the leading edge of the root chord, with the z-axis going vertically up, the y axis going along the half span of the wing and the x axis going along the length of the root-chord. The coordinate system can also be seen in Figure 5.1.

As previously mentioned, only the wingbox structure will be analyzed. What is meant by this exactly is that it will be assumed that the wingbox carries all the loads on the wing. Therefore, the next step in the program is turning these airfoil cross sections of the airfoil into cross sections of the wingbox. This means that all parts of the wing in front of the front spar and aft of the aft spar are discarded, such that only cross sections of the wingbox are left everywhere where cross sections of the airfoil were made. Each cross section of the wingbox includes front and aft spars, as well as the top and bottom parts of the skin connecting them.

The next step in the program is positioning the all stringers on the top and bottom skin. The number of stringers that are to be positioned on the top and bottom skin is precised by the user as an input. The stringers are positioned with equal spacing along the skin. Due to the fact that the wingbox structure is not symmetrical, and the fact that the top and bottom skins connecting the spars are curved, a mathematical relation must be found in order to position the stringers along the length of the skin. This derivation will be omitted because it is quite long. But by doing this, the stringers can be positioned evenly along the top and bottom skins, depending on the number of stringer precised by the user. The out put of this function will then be the x and z positions of all stringers for every cross sections made.

Next, the height of the front and aft spars are calculated for every cross section. This is easily done for the top by taking the z-coordinate of the top skin at the minimum x-coordinate of the top skin and subtracting that from the z-coordinate of the minimum x-coordinate of the top skin. For the aft spar, instead of looking at the minimum x-coordinates of the top and bottom skin, the z-coordinates at the maximum x-coordinate must be used.

For all further calculations, to simplify the analysis, structural idealisations will be made. This means that all

stringers will be converted to booms, with point areas equal to their actual cross sectional area. The next step of the program is to calculate the centroid location for every cross section generated by the program. Using structural idealisations, and assuming zero thickness for the wing skin thickness, the centroid of a single cross sections can be estimated by using Equation (5.5) and Equation (5.6) below. Furthermore, the impact of this assumption needs to be evaluated. Due to the assumption made, the centroid location obtained will not be exact. This is due to the fact that when assuming the skin has zero thickness, it also means that it has zero area, and therefore the skin is not taken into account when determining the centroid location. However, the results obtained do not deviate too much from the real location as the stringers follow the shape of the skin, and the main contributions to centroid location are the stringers and spars. The higher the number of stringers along the skin, the more accurate the centroid location is. The equations used to determine the centroid for an arbitrary cross section are given below in Equation (5.5) and Equation (5.6).

$$\bar{x} = \frac{\Sigma_{i=1}^{n} \tilde{x_i} A_i}{\Sigma_{i=1}^{n} A_i} \tag{5.5}$$

$$\bar{z} = \frac{\Sigma_{i=1}^{n} \tilde{z_i} A_i}{\Sigma_{i=1}^{n} A_i} \tag{5.6}$$

Where $\bar{x}$ is the x-coordinate of the centroid of the cross sections, $\bar{z}$ is the z-coordinate of the centroid, $\tilde{x_i}$ is the centroid location of the ith area and A_i is the ith Area. This is done taking into account all stringers and both spars, and repeated for all cross sections generated by the program. The cross sections along with the position of the centroid of an arbitrary cross section can be seen clearly below in Figure 5.1.

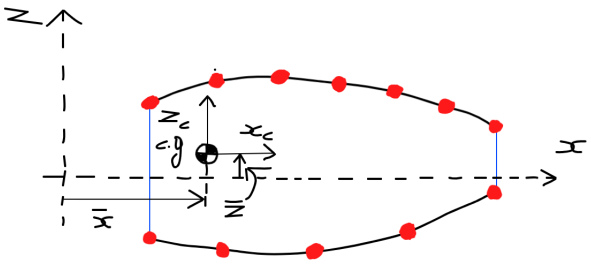

Figure 5.1: Arbitrary cross section

In Figure 5.1, the blue segments on the left and right are the front and rear spar, respectively, the red point areas are the stringers, the black curves connecting the spars are the upper and lower skins. Next, the moments of inertia of every discretized cross section must be determined. Once again, structural idealizations are made to make this process less complex. Furthermore, this leads to the skin being neglected when calculating the moment of inertia of a cross section. In turn, this means that for every cross section, the moment of inertia is under-estimated, which will later mean an over-estimation of the stresses calculated. This means that this assumption is conservative. Furthermore, thin walled assumption is used, and higher order terms of the thickness in the spars are neglected and assumed to be approximately zero. Once again, this assumption is conservative.

The moment of inertia is calculated about the axes x_c and z_c, which are axes for which the orientation is the same as the original reference axes previously described in . However, its origin is located at the centroid of the cross section. This is done for every cross section. This can be seen more clearly in Figure 5.1. The moments of inertia about the axes just described, $I_{z_c z_c}$ and $I_{x_c x_c}$, are calculated using the steiner theorem. This is presented below in Equation (5.7), Equation (5.8) and Equation (5.9):

$$I_{z_c z_c} = I_{z'z'} + A d_x^2 \tag{5.7}$$

$$I_{x_c x_c} = I_{x'x'} + A d_z^2 \tag{5.8}$$

$$I_{x_c z_c} = I_{x'z'} + A d_x d_z \tag{5.9}$$

This theorem is used for every individual element that is taken into account, namely the two spars and all stringers. The axes x' and z' are the axes about the centroid of each individual element. The variables d_x and d_z are the x and z distances, respectively, from the cross sections centroid to the centroid of a certain object. As the stringers are assumed as booms with point areas, and therefore $I_{z'z'}$ and $I_{x'x'}$ are assumed to be zero for those booms. This equation is applied to every object within the cross section, and all are summed up to come up with the moment of inertia about both axes about the centroid of the cross section. This process is then repeated for every cross section.

The last part of building the geometry of the wing and obtaining all relevant geometrical properties of the wing consists of obtaining the shear center location for every cross section generated by the program. In the following paragraphs, the process as to how the shear center was derived will be explained.

Due to the section not being symmetrical, the shear center may not be directly determined by inspection and must instead be calculated. When a shear force in the positive z direction V_z is applied about the shear center of the section, it generates a moment about the centroid of the cross section. The location of the shear center

is assumed to be at a distance ξ in the positive x direction. Assuming counter-clockwise positive moments as positive, this means that the shear force applied at the shear center creates a torque equal to $V_z\xi$. Furthermore, the shear force applied at an arbitrary gets diffused with the structure such that the shear flow $q = \tau * t$, where τ is the shear stress and t is thickness, integrated over the whole section is equal to the shear force being applied at the section. This means that the torque generated from the shear force around the centroid of the cross section is equal to the torque created by the shear flow distribution around the section. Therefore, one may say that for a closed section such as the wingbox, Equation (5.10).

$$V_z\xi = 2A_m q_{s_0} + \oint \rho q_b ds \tag{5.10}$$

Where A_m is the enclosed area of the section, q_{s_0} is a constant shear flow, ρ is the perpendicular distance from the centroid of the section to the segment of the section ds and q_b is the basic shear flow. The values of q_{s_0} and q_b are given by Equation (5.11) and Equation (5.12) below.

$$q_{s_0} = \frac{\oint (q_b/Gt) ds}{\oint ds/Gt} \tag{5.11}$$

$$q_{b_2} - q_{b_1} = -\frac{V_z I_{z_c z_c} - V_x I_{x_c z_c}}{I_{x_c x_c} I_{z_c z_c} - I_{x_c z_c}^2} \int tz ds - \frac{V_x I_{x_c x_c} - V_z I_{x_c z_c}}{I_{x_c x_c} I_{z_c z_c} - I_{x_c z_c}^2} \int tx ds \tag{5.12}$$

Where G is the shear modulus of the material, q_{b_2} is the shear flow at a section 2 and q_{b_1} is the shear flow at a section 1. As it may be seen from equation Equation (5.12), the basic shear flow can only be obtained at an arbitrary point along the section if and only if it is already know at one point along the section. That is why a cut is made on the section to create a free surface, where the shear flow is known to be zero, and from that the varying basic shear flow can be estimated all over the cross section. The constant factor q_{s_0} is there to correct for this assumption and close the section once again.

Once again, to simplify the analysis, the structure is idealised by turning the stringers into booms and assuming zero thickness all around, this time including the spars. Using this assumption results in constant shear flow along the sheet in between two booms, however the shear varies across a boom. The change in basic shear across a boom is given by Equation (5.13) below.

$$q_{b_2} - q_{b_1} = -\frac{V_z I_{z_c z_c} - V_x I_{x_c z_c}}{I_{x_c x_c} I_{z_c z_c} - I_{x_c z_c}^2} B_r z - \frac{V_x I_{x_c x_c} - V_z I_{x_c z_c}}{I_{x_c x_c} I_{z_c z_c} - I_{x_c z_c}^2} B_r x \tag{5.13}$$

Where B_r is the area of the boom and x and z are the coordinates of the boom w.r.t the axes about the centroid of the section.

Making a cut in the section anywhere between two booms means that the shear flow in between these two booms is zero. This means that the basic shear flow q_b may be found all across the section by using Equation (5.13).

Now, going back to Equation (5.10), a function must be written within the program to estimate ρ in order to find the perpendicular distance to the sheets between two booms. This can be done by using trigonometric relations for every sheet inside the cross section.

Now that every term in Equation (5.10) is know, x position of the shear center w.r.t. may be estimated by simply applying unit shear $V_z = 1N$. This procedure is then repeated for every cross section generated by the program. The z location of the shear center was not calculated because the drag is assumed to act along it. In reality it doesn't exactly, but it is usually acting very close to it. This means that very little torque will result from the drag force.

5.5.2. Moments, Torque, Shear and Normal Forces Acting on the Wing

The next step in the program is to come up with the moment, torque, shear and normal force diagrams for the wing. For that, it is first imperative to determine all loads acting on the wing. There will be 3 different loads acting on the wing: The distributed lift over the wing, the distributed drag, and finally all reaction forces at the connection to the fuselage. These reaction forces would need to be examined in more detail to ensure that they do not cause the fuselage to fail. However, due to the restricted time of this project, this has not been analyzed into more detail, only magnitude of forces and moments acting on the fuselage will be known.

The lift and drag is obtained from the Aerodynamics department. However, what is given is the lift coefficient distribution along the span. However, this is not a force. Therefore, the lift coefficient along the span must be corrected to a lift force such that the integral of the lift force along the half span is equal to the maximum (or minimum) load factor that must be carried by the divided by two (due to analysis only applied to half wing).

This is given below in Equation (5.14).

$$\int_0^{b/2} L(y)dy = \frac{n_{max} \cdot m \cdot g_0}{2} \tag{5.14}$$

Where b is the wing span, $L(y)$ is the lift as a function of y in N/m, n_{max} is the maximum load factor, m is the aircraft mass in kg and g_0 is the acceleration due to gravity at sea level (9.80665 m/s^2). This then leads to Equation (5.15) below.

$$\frac{1}{2}\rho_0 v^2 S \int_0^{b/2} c_L(y)dy = \frac{n_{max} \cdot m \cdot g_0}{2} \tag{5.15}$$

With ρ_0 being the air density at sea level, v is the local velocity required to achieve the required lift (the scaling factor), S is the wing surface area, and $c_L(y)$ is the lift coefficient as a function of y. In this equation, the only unknown within this equation is the local velocity v. This can be solved by rearranging Equation (5.15) above. Once this velocity is solved for, every value of c_L given by the aerodynamics department can be multiplied by the factor $0.5\rho_0 v^2 S$ to scale the distributed lift coefficient to a distributed lift force. To verify that this procedure is correct, the distributed lift force obtained needs to be integrated along the half span and the relation given in Equation (5.14) needs to be satisfied. In this case it was satisfied. Furthermore, the lift force distribution needs to be plotted next to the c_L distribution. These were shown to have the same general shape, and therefore the procedure used to determine the lift distribution along the wing is correct. Furthermore, the drag coefficient c_D also needs to be multiplied by the same factor of $0.5\rho_0 v^2 S$ to scale it to a drag force.

Furthermore it is important to note that these forces act at the center of pressure for which the location of it along the chord is known. Because the center of pressure and the shear center rarely coincide, the lift force will generate a torque on the wing. As previously mentioned, the torque resulting from drag is present but however will be ignored because it is assumed to act along the shear center. Furthermore, the z location of the center of pressure is unknown, and therefore could not be analyzed either way. It is very important to know this as this means that the internal torques calculated at every cross section is under estimated. The center of pressure, lift force and drag forces distributions can then be interpolated for all cross sections.

From this, all reaction forces and moments at the root of the wing can be calculated. The results obtained for the aircraft under maximum loading (4.45g) and minimum loading (-2.45g) are given below in Table 5.6 and Table 5.7.

Table 5.6: Wing root reaction forces under maximum g loading with no battery inside wing

Forces	Value [N]	Moments	Value [Nm]
R_z	-17106.3	M_z	1407.7
R_x	554.1	M_x	49913.1
R_y	0	T_y	-5439.8

Table 5.7: Wing root reaction forces under minimum g loading with no battery inside wing

Forces	Value [N]	Moments	Value [Nm]
R_z	9215.0	M_z	268.0
R_x	105.5	M_x	-32988.4
R_y	0	T_y	2930.3

This process was then repeated for the wing with the battery inside. The results for the scenario in which the battery is included within the wing are given below in Table 5.8 for the maximum loading and Table 5.9 for the minimum g loading case.

Table 5.8: Wing root reaction forces under maximum g loading with battery inside wing

Forces	Value [N]	Moments	Value [Nm]
R_z	-16187.0	M_z	1407.7
R_x	554.1	M_x	49693.9
R_y	0	T_y	-5696.4

Table 5.9: Wing root reaction forces under minimum g loading with battery inside wing

Forces	Value [N]	Moments	Value [Nm]
R_z	10134.4	M_z	268.0
R_x	105.5	M_x	-33207.6
R_y	0	T_y	2673.6

Lastly, shear, moment and torque diagrams can be derived. Due to the space restriction, these diagrams are only displayed for the maximum g condition with no battery inside the wing. Figure 5.2 represents the variation of the internal moment around the z axis along the span, Figure 5.3 represents the variation of the internal moment around the x axis along the span, Figure 5.4 represents the internal torque variation along the span, Figure 5.5 represents the variation of the internal shear in the z direction along the span and finally, Figure 5.6 represents the variation of the internal shear in the x direction along the span.

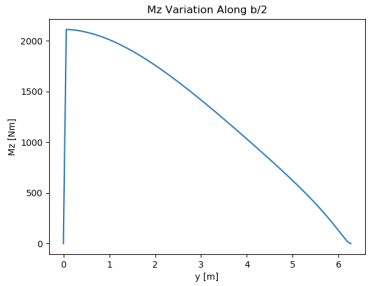

Figure 5.2: Torque vs y

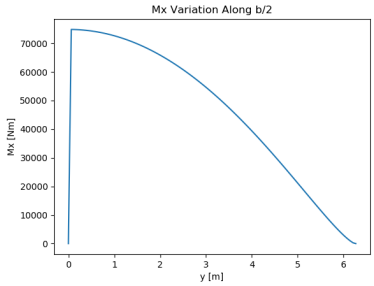

Figure 5.3: Mx vs y

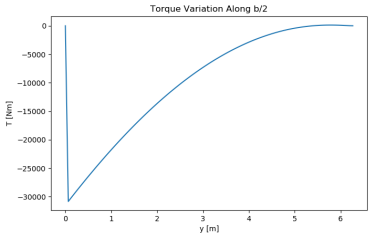

Figure 5.4: Torque (T) vs y

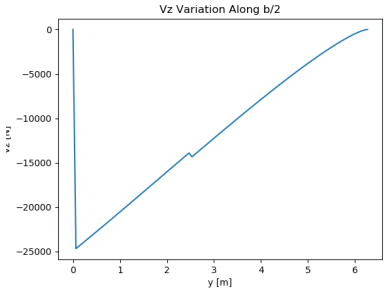

Figure 5.5: Vz vs y

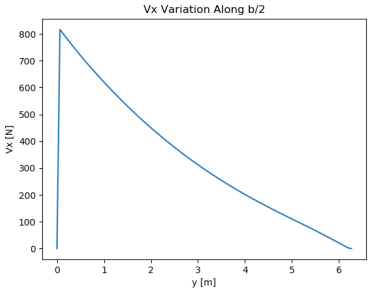

Figure 5.6: Vx vs y

5.5.3. Stress analysis, Tip Deflection and Results

Once the internal loading throughout the span of the wing is determined, it is possible to determine all normal stresses and shear stresses acting along the span of the wing. The normal stresses may be determined at any point on all cross sections by using Equation (5.16) which is given below.

$$\sigma_y = \frac{(M_x I_{zz} - M_z I_{xz})z + (M_z I_{xx} - M_x I_{xz})x}{I_{xx} I_{zz} - I_{xz}^2} \quad (5.16) \qquad q_T = \frac{T}{2A_m} \quad (5.17) \qquad \tau = \frac{q_{tot}}{t} \quad (5.18)$$

Where M_x is the bending moment around the x-axis, M_z is the bending moment around the z-axis and finally, I_{xx}, I_{zz} and Ixz are the moments of inertia of the cross section about the x- and z- axis of the cross section, which are located at the centroid of the cross section. Furthermore, it is important that shear within the cross sections occurs due to both internal shear force, and internal torque. First, the shear flow components all around an arbitrary section must be determined, and then from this the shear stresses. The shear flow due to torque is constant around the cross section in a single cell closed section. This shear flow due to torque q_T is given by Equation (5.17).

Where T is the internal torque at that cross section, and A_m is the enclose area of that section. The shear flow due to shear can then be calculated by using Equation (5.11) and Equation (5.13). The procedure for using these equations is the same as the one presented in the section where the shear center is derived. Then, all of these shear flows calculated can be added together all around the section to obtain the total shear flow everywhere in the section. Furthermore, the shear stress may be calculated by using Equation (5.18).

Where q_{tot} is the total shear flow and t is the thickness at a point on the section. This can be repeated everywhere along a single cross section, and for every cross section generated by the program. Finally, the wingbox can be sized such that no critical buckling stresses of the stiffened panels on the wing and stringers are not exceeded, and no material yield stresses are exceeded.

Lastly, the tip deflection of the wing can be calculated by using the Equation (5.19). If the deflection is below the requirement of 10% of the span (**ELTA-W-09**). This requirement is incorporated inside the sizing loop, where if it is exceeded, stringers are added to ensure compliance. The results are presented below in Table 5.10

Table 5.10: Final output values of the wing design

Parameter	Value	Unit
Number of ribs on upper surface	30	-
Number of ribs on upper surface	30	-
Rib spacing	300	mm
Total wing mass	160	kg

5.6. Wing Verification and Validation

Verification was done at every step of the program. The first step in the program is generating the cross sections. These were verified by plotting these cross sections and ensuring that the correct wing planform geometry and airfoil is obtained. Next, the position of stringers and wingbox geometries were also verified via inspection of the plots. This was also done for the position of the spars. The centroid location, shear center, and moments of inertia were verified by doing the calculations by hand and comparing to those obtained numerically. These were proven to be the same for both the first and last cross sections, and therefore the process followed is correct. The lift and drag distribution method were verified by the fact that if integrated over the half span, the wanted lift load shall be obtained, which in this case is 4.45W or -2.45W, where W is the aircraft weight. Furthermore, the lift load distribution should look similar to the lift coefficient plot along the half span of the wing, this is verified by plotting the two next to each other and comparing. This lift load is then interpolated so that it is obtained at every cross section generated. This is also done for the center of pressure and drag. The interpolation is done using a verified python function. The internal loading diagrams are verified by first of all ensuring that the results obtained are realistic. Then, the calculations are done in a simplified manner and compared to the results obtained numerically. If these are approximately equal, then the process used is correct and the code functions as intended. Finally, the stresses were verified by comparing the values obtained numerically with values obtained by hand for the first and last cross sections. If the results are equal, then the code works as intended.

There are two main methods of validation for this analysis. The first one is by entering inputting the wing of another aircraft into the program and comparing the results obtained from the program with the actual aircraft wing. However, this data is very hard to obtain, and therefore the validation of the analysis would need to be done via scale testing. This would include mostly failure tests and buckling tests, to see whether the wing can actually withstand the current load it is sized for, and if so how much more load can it carry, or how over designed is the wing. However, before getting to this stage, the analysis needs to be refined such that no money is wasted in testing, this is because as of right now, it is known that the wing is over-designed.

5.6.1. Wing Risk and Certifiability Analysis

The design of the wing was performed by considering mainly the mass of the wing structure. The main risks of the wing are as follows: The wing is overweight, the wing is overpriced, the wing is under-designed, the wing is not certifiable. It is likely that as of right now, the wing is a little bit over-designed due to the many conservative assumptions made to perform the structural analysis of the wing. However, the program could be refined to obtain more accurate results. The actual cost of the wing was not looked at within this section. This means that it is probable that the cost of the wing exceeds the budget. If that is the case, then the materials of the structural components will need to be looked at, and probably changed. This will in turn change the mass of the wing and lead to a possibly over-weight wing. Therefore more research needs to be done within this sector. The third risk is that the wing is under-designed. This is highly unlikely due to all the conservative assumptions made in the analysis. This however would have a very high impact if this risk came out to be true. The wing failing in flight will inevitably lead to a catastrophe, possibly fatal. This is why the assumptions made must be conservative. Furthermore, a safety factor of 1.5 was applied on the maximum and minimum load factors, which serves to comply with CS-VLA. As a safety factor of 1.5 was applied, and all stresses are under the material ultimate stress, the wing is certifiable under CS-VLA.

5.7. Fuselage Design

The fuselage was designed similar to the wing. Designing the fuselage was an iterative process, as the mass needed to be minimized at every stage. The fuselage design process is visualized in Figure 5.7.

First, it was decided that the fuselage aerodynamics would not be investigated. This was chosen because it was deemed too complicated and time-intensive for the resources available. However, the aerodynamic shape was taken into account. Following Gudmundsson [14], the choice was made for a tadpole shaped fuselage design, because it reduces the C_{D0} by almost 30%. While a frustrum shaped fuselage would be easier to design, every single bit of performance was necessary in order to meet the requirements.

The fuselage was then sized around the other aircraft components. The preliminary tail and wing positions and sizing parameters were plotted using CATIA, together with the motor and propeller disk. Finally, the cockpit

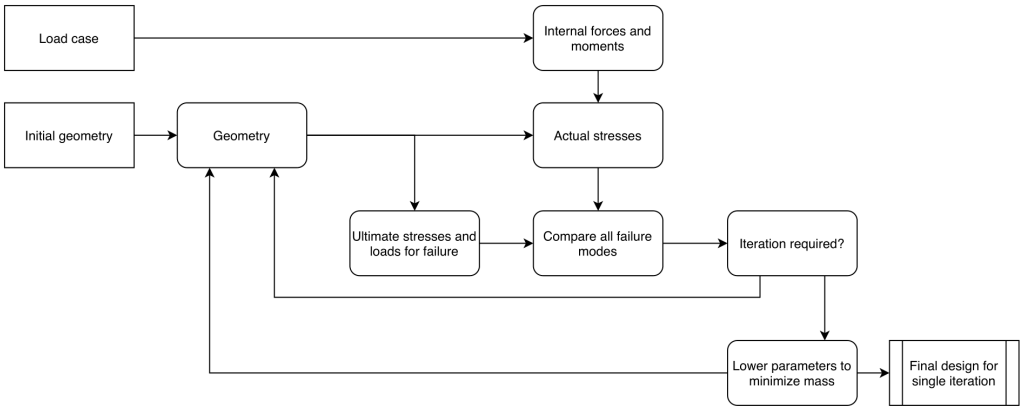

Figure 5.7: Work flow diagram of the fuselage design

was drawn using the minimal dimensions from the requirements. Next, a tadpole shape was drawn around these components, such that everything would fit inside of the fuselage. This shape was extruded into 3D, where some final touch-ups followed to make the fuselage more streamlined and reduce the wetted surface area. The results of this can be seen in Figure 5.8.

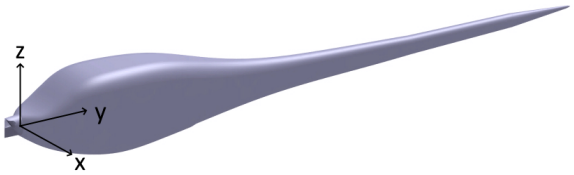

Figure 5.8: Rendering of the preliminary fuselage, indlucing the coordinate system that was used.

Next, the method of analysis was determined. The fuselage shape is quite predictable in the aft section of the fuselage, compared to the front section. In the front of the fuselage, there were a number of features that made the fuselage too difficult to design for in the limited resources that were available. These features include mounting points for the engine and propeller, the avionics and flight instruments, the seating and stick of the pilot, and the doors to the main fuselage. As a higher degree of certainty could be obtained for designing the aft fuselage, it was chosen to only design this section of the fuselage in more detail.

The aft fuselage was also designed to have two halves. Near the tail, the fuselage geometry is almost circular. It was hence chosen to use carbon fibre in this section of the fuselage, as circular shapes are among the cheapest geometries to produce with carbon fibre. Nearer to the front of the aircraft, the section is not circular anymore, which makes that section significantly more expensive to produce with carbon fibre. Hence, here, an aluminium alloy is used for the skin. The specific alloy chosen is 7075, as it offers high strength and toughness, as well as excellent corrosion resistance, while having a manageable density, all in comparison to other aluminium alloys. It is less workable than a 2024 aluminium alloy, however, the properties like corrosion resistance are more important for the skin of the aircraft. The stringers will be made from 2024, because of its workability and its lower price when compared to other alloys. The longerons will be made from carbon fibre, as its high strength is very important for these primary components. With these material choices made, the fuselage can be analysed.

An important assumption that was done is that the fuselage was discretized into several sections. These sections run from frame to frame, and have a constant cross-section over their length. This was done in order to simplify the analysis. To mitigate the effects of this assumption, this assumption was applied in a conservative manner. For example, the cross-sectional area and geometry that was used for every section was the smallest cross-section between the two frames, so the smallest moment of inertia is used, which results in higher stresses, which makes the estimate conservative. Also, having a smaller moment of inertia results in a smaller critical buckling stress, making the assumption even more conservative. The sections were positioned such that the cross-sectional centroids of the sections all lie on the y-axis. The model of Figure 5.8 was then used to obtain cross-sectional areas, widths, heights, and radii of the corners for every location along the length of the fuselage, and these were interpolated to the locations of the frames.

The frame locations were determined based on the number of frames. The frames were spaced equally apart

from each other, along the length of the fuselage. The number of frames was based on minimising the mass, while still being able to fulfil the requirements. The mass of the frames was estimated based on the enclosed area of a cross-section, multiplied by 0.25, the skin thickness for that section, and the material density for that section.

The final discrete sections, in combination with the material properties, then result in a variable Young's modulus E based on the component materials. Additionally, for every section, the centroid, using Equation (5.5) and Equation (5.6), and mass are calculated, as well as the critical buckling stress, ultimate tensile stress, and a cost estimation is done. Finally, the moments of inertia I_{xx}, I_{zz}, and I_{xz} are calculated. These parameters could then be used in the load calculations.

In order to analyse the loads, linearized beam theory was used, based on Megson's book [11]. This was considered valid, as the fuselage does not undergo extreme deflections, and the loads are relatively simple. The basis for this method is the differential equation for the deflection:

$$EI\frac{d^2v}{dy^2} = -M \tag{5.19}$$

This method can be integrated to obtain angles and deflections of the beam at every longitudinal location. This is done for deflection in the x and z directions, for every longitudinal position y. In order to be able to solve this equation for arbitrary external loads and moments, equilibrium should be assured. This is done by calculating the reaction forces and moments in the cantilever support. A cantilever support is assumed to exist in the cockpit bulkhead of the aircraft, right behind the cockpit, as the forces and moment should be in equilibrium around any point in straight, steady flight. Furthermore, this is where the aft section of the fuselage is attached to the rest of the aircraft, and where the load transfer between the two parts takes place. In reality, there is no support here, and what is modelled as reaction forces are actually forces caused by other components of the aircraft, such as the front section of the fuselage and the wing. The cockpit bulkhead, being a cantilever support in the model, as a result also becomes the location of the boundary conditions that are necessary to solve the equations. It is assumed that both the deflection and the angle of the beam at the cockpit is 0, in all directions. This system is verified and validated in Section 5.7.1.

Now that a solver is available, the stresses can be calculated. This is done by calculating the internal shear force, normal force, and moment, across the fuselage, in all directions. Given the centroid of the cross section and the geometry of a cross-section, the normal stress due to bending and internal normal force respectively can be evaluated at any arbitrary point using the stress equations:

$$\sigma_y = \frac{(M_x I_{zz} - M_z I_{xz})z + (MzI_{xx} - M_x I_{xz})x}{I_{xx}I_{zz} - I_{xz}^2} \quad \text{and} \quad \sigma_y = \frac{N_y}{A_{\text{cs}}} \tag{5.20}$$

Here, x and z are the locations distance to the centroid. M_x and M_z come from the load calculations and are the internal bending moments. After the normal stress was calculated, the shear stress was next. The shear stress is slightly more difficult to calculate. First, there is a torsion component. This results directly in a shear stress in the skin of the fuselage, provided the structure is thin-walled:

$$\tau = \frac{T}{2tA_m} \tag{5.21}$$

where A_m is the area enclosed by the thin-walled structure, not the cross-sectional area of the components themselves. Next to the torsion, also the internal shear force causes shear stresses. For this, it is crucial to know the shear centre. However, given the many components of the fuselage, this is very difficult to calculate precisely. In contrary to the wing, the fuselage is symmetric around its middle (the z axis). Therefore, the shear centre lies on the y-z plane of the fuselage, with the reference coordinate system being shown in Figure 5.8. As the section is closed and not far from being symmetric around the x axis as well, the shear centre is assumed to be located at the centroid. Next to the shear centre, also the effects of the stringers and longerons should be taken into account. As the number of stringers can differ a lot for every section, the stiffened panels (combination of plate and stringers) are each idealized. To calculate the shear, every panel is modelled as three separate booms. These booms are positioned at the two ends of a plate cross-section, as well as in the middle of the cross-section. Each boom gets a third of the area of the plate itself. Then, the areas of the stringers are added to the booms that are closest to each stringer. This process is visualised in Figure 5.9

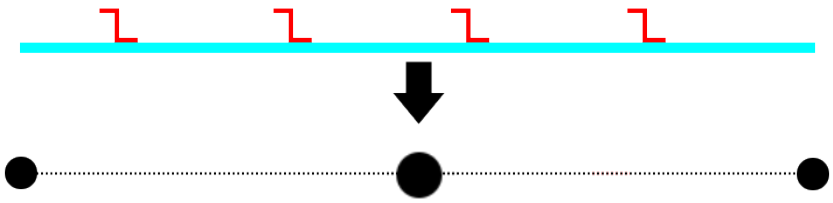

Figure 5.9: Idealization of a stiffened panel with four equally spaced stringers.

For a panel with a width of 0.5 m and a skin thickness of 2 mm, and four equally spaced stringers as in Figure 5.9 of 0.000012 m^2 each, the areas of the three booms become $3.45 \cdot 10^{-5}$, $3.57 \cdot 10^{-5}$, and $3.45 \cdot 10^{-5}$ m^2 from left to right. Next, the equation for shear flow of an idealized section is used:

$$q_s = -\frac{(V_z I_{zz} - V_x I_{xz})}{I_{xx} I_{zz} - I_{xz}^2}\left[\sum_{r=1}^{n} B_r z\right] - \frac{(V_x I_{xx} - V_z I_{xz})}{I_{xx} I_{zz} - I_{xz}^2}\left[\sum_{r=1}^{n} B_r x\right] + q_{s0} \tag{5.22}$$

where B_r is the area of a single boom element, and x and z its distance to the shear centre. V_x and V_z are the internal shear forces. The only unknown here is q_{s0}. This shearflow is required for 'closing' the cross-section, as this equation is only valid for a closed section that has been 'cut' open for the analysis. This parameter is calculated by multiplying the shearflow with the skin thickness in order to calculate the shear stress. This shear stress is then multiplied with the length of the segment, resulting in a 2D vector force. Next, the cross-product is taken with the vector distance from the shear centre. This is done for every segment of the cross-section, resulting in a resultant moment due to the internal shear force. Because the system should be in equilibrium, the parameter q_{s0} is adjusted such that the resultant moment is exactly 0. The total shear stress of any point on the section can then be calculated.

After all the stresses were calculated, the critical load cases from Table 5.3 in combination with additional possible failure modes like von Mises stress, shear failure, and ultimate tensile stress were all analysed for every point in every cross-section. If the structure exceeded any of the stresses that would make it fail, the input parameters were adjusted automatically to decrease the stress or to distribute the stresses better. These input parameters included number of stringers, number of longerons, stringer dimensions, longeron dimensions, number of frames, skin thickness, battery position, and material selection. The choice of which parameter to change was unique to each failure mode and section of the fuselage, in order to achieve the most optimal combination of final parameters. Additionally, after all the failure modes were nullified, the parameters were tweaked further, in order to achieve the lowest weight possible. After each change, the structure was checked for compliance with the requirements and the load case.

This complete process was iterative, and was ran until convergence in combination with other subsystems of the aircraft. An example is the battery weight, which has direct influence on the fuselage structure as the battery is located in the fuselage. Another example of iterated parameters is the total fuselage length, and the ultimate tail loads that the fuselage was sized for. The final shear forces and moments can be found in Figure 5.10.

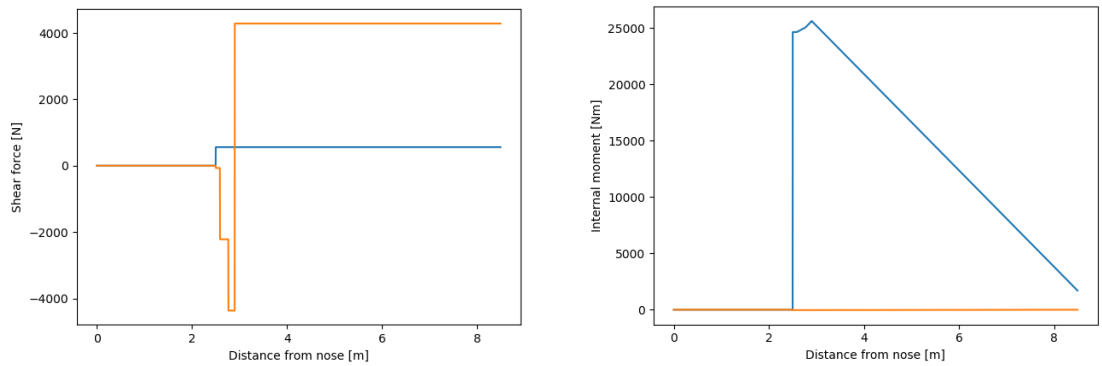

(a) Internal shear force in the x and z directions

(b) Internal moment in the x and z directions

Figure 5.10: Internal shear forces and moments.

The final normal force and normal stress for the middle top of the fuselage can be found in Figure 5.11. The jump

that can be seen in Figure 5.10a just after 2m (the cockpit bulkhead is located at 2.2m, no forces are applied before that) is due to the battery weight.

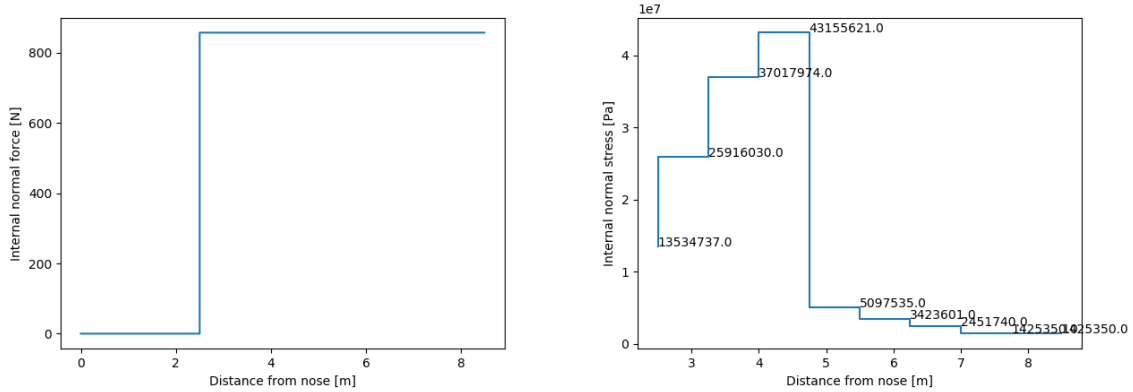

(a) Internal shear force in the x and z directions

(b) Normal stress at the middle top of the fuselage for every section.

Figure 5.11: Normal force and stress in the aft fuselage.

The input parameters for the final iteration for the fuselage design can be found in Table 5.11. The final output values can be found in Table 5.12.

Table 5.11: Final input values of the aft fuselage design

Parameter	Value	Unit
MTOW	8671	N
Horizontal tail force	-4282	N
Vertical tail force	558	N
Battery weight	2864	N
Emergency parachute force	8671	N
Cockpit bulkhead position	2.5	m

Table 5.12: Final output values of the aft fuselage design

Parameter	Value	Unit
Aft fuselage weight	72.3	kg
Total fuselage weight	105	kg
Amount of frames	8	-
Frames material	AA2024	-
Amount of longerons	4	-
Longeron plate thickness	2.2	mm
Longeron height	4.5	cm
Longeron width	4.5	cm
Longeron stringer type	J-stringer	-
Longeron material	CFRP	-
Skin thickness cockpit	3.3	mm
Skin material cockpit	AA7075	-
Skin thickness tail	2.2	mm
Skin material tail	CFRP	-
Amount of stringers tail	19	-
Amount of stringers cockpit	0	-
Stringer plate thickness	0.6	mm
Stringer height	1.2	cm
Stringer width	1.2	cm
Stringer type	Z-stringer	-
Stringer material	AA2024	-
Battery position	2.59&2.77	m
Parachute position	2.9	m

5.7.1. Fuselage Verification and Validation

The calculations that are done to size the fuselage are quite complex. In order to provide a degree of certainty to the calculations, the load solver was extensively verified. This was done both by hand and by using an external tool. First, a solution was calculated by hand for the deflection of a beam of 1 meter long. A load is applied to the end of the beam, with a magnitude of 1 N in both the x and z directions. Additionally, a moment is applied with a magnitude of 3 Nm, also in both the x and z directions, also at the end of the beam. The beam is fixed with a cantilever support at the other end of the beam. This results in a reaction force vector with the same magnitude as the applied load, but opposite direction. This load case also results in a reaction moment, with a magnitude of -4 Nm in the x direction, and -2 Nm in the z direction. The internal moment M of Equation (5.20) then becomes:

$$M = -\begin{bmatrix}-4\\0\\-2\end{bmatrix}\langle z-0\rangle^0 + \begin{bmatrix}-1\\0\\-1\end{bmatrix}\langle z-0\rangle^1 - \begin{bmatrix}3\\0\\3\end{bmatrix}\langle z-1\rangle^0 + \begin{bmatrix}1\\0\\1\end{bmatrix}\langle z-1\rangle^1 \tag{5.23}$$

Here, $\langle\cdot\rangle$ indicates a Macauley step function, which is 0 if the argument is below 0, else it is its argument. This equation can be plugged into Equation (5.20). The product of I and E in equation Equation (5.20) is assumed to be constant along the cross-section, with an arbitrary magnitude of 7.34. Now, the equation can be integrated. After solving for the fixed boundary conditions, the deflection in the x-direction is:

$$v = \frac{Py^2}{6EI}(3L - y) - \frac{My^2}{2EI} \tag{5.24}$$

where P is the applied force in the x-direction (positive value is in the positive x-direction), and M is the moment applied in the z-direction (positive along the z axis), and L is the length of the beam. Comparing this equation to the output of the script at several points, verified that the integrator, boundary condition solver and load calculator worked properly.

The next part that was verified was the internal shear force and moment calculator. This was done by comparing the output internal shears and internal moments of a complex load case of three vector forces and two vector moments with the output of an online accessible calculator [1]. Furthermore, it was tested whether the output internal shears and moments were beyond either edge of the beam. These tests also all corresponded exactly, and the calculator is hence also considered verified.

Validating the tool is not possible at this stage. Hence, the final fuselage design should be validated before it can be assembled into the complete aircraft. While this is not possible during this phase of this project, it is taken into account in the project planning for the next phase of the project.

Validation of the fuselage will be done by further simulations, prototyping, and testing. Once the system aerodynamics has been analysed to a higher degree, the precise loads of the tail can be identified more precisely. The fuselage can be modelled in CAD, after which a finite element method can be used to simulate the entire fuselage much more precisely under the given loads. If the model passes these tests, a prototype of the fuselage or of a set of subsystems of the fuselage can then be constructed. This test article can then be put under the precise critical loads it is designed for. Using strain gauges, the stress and stress distribution in several components can be measured, after which the structure can be tested until failure. If the structure does not fail before it is designed to, the structure is validated.

5.7.2. Fuselage Risk Management

The fuselage has been designed with cost and weight in mind. However, there exists a risk that the fuselage either costs more than anticipated, or that the fuselage weighs more than expected. The cost issue can be mitigated by thorough checks of the budgets and costs throughout the rest of the design process. The weight issue can be mitigated by redesigning the panel or using more advanced design and estimation techniques. Also, using known materials and production methods, as is the plan, also helps with estimating the weight.

Another risk is the battery placement. Currently, the battery is placed right behind the bulkhead behind the cockpit. This is done so that the battery is easily accessible during maintenance, and so that it can easily be swapped on the ground. However, should the battery catch fire, this could pose a risk to the pilots. This risk is to be minimised by doing extensive testing on the battery. The cockpit aft bulkhead will also be made fireproof, to protect the pilot from a possible fire. The emergency parachute will be shielded from the fire as well, and attached to the cockpit. Hence, in case of a big battery fire, the pilot can pull the emergency parachute. The option of dropping the batteries in case of a fire was investigated, but deemed unfeasible. This is due to the extra structural mass this would add, the reliability of the dropping system would be hard to achieve, and due to the fact that dropping a burning 292 kg battery from the sky is not a good idea.

The risk of having misidentified loads also exist. This risk is minimised by doing extensive flight testing, while monitoring the loads on the aircraft. It can also be reduced by doing further engineering reviews. Currently, this risk exists in the form of not extensively modelling the weight of the fuselage itself as a load that the fuselage has to carry.

5.8. Landing Gear Design

5.8.1. Landing Gear Sizing and Positioning

As previously mentioned, the landing gear design was not be prioritised for analysis. Therefore, only a preliminary sizing was performed on it. The trade-off concerning which type of landing gear configuration will be used was previously done in the Midterm report [1]. The configuration that will be used will be the tricycle configuration. The landing gear is an essential aircraft subsystem. It ensures stability on the ground, enables taxiing, and provides landing, steering, and breaking capabilities for the aircraft.

The steering and braking capabilities were combined into one function. Namely, the undercarriage incorporates differential braking as steering method. Differential braking was chosen in order to provide the functionality

[1] URL: `https://clearcalcs.com/freetools/beam-analysis/au` Last accessed: 22-06-2020

required by ELTA-FLT-09 and ELTA-FLT-10, while still keeping the costs and complexity low. Due to the lesser on-ground stability properties of incorporating differential braking, a contingency management safety margin of 5% was imposed on the tip-over angles of the gear design.

The aircraft landing gear is positioned such that the aircraft does not tip over backwards or forwards, that no tail strike occurs during take-off, and such that the nose wheel carries enough weight to ensure steering capabilities. This is ensured by drawing two lines on the aircraft. One of these lines goes through the aircraft aft c.g., at an angle of 5.25°(requirement ELTA-FLT-08, plus a safety margin of 5%) to the left of the vertical. The other line is drawn from the tail of the aircraft and has an angle of 15.75°from the horizontal (ELTA-FLT-07 plus 5%). This is shown clearly below in Section 5.8.1.

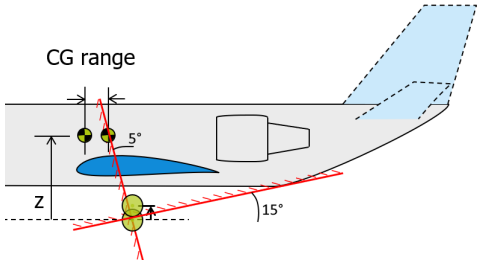

Figure 5.12: Tip-over constraints for the main gear of an aircraft [8]

Once the intersection of these two lines is found, the gear can be positioned anywhere below the 15°line and to the right of the 5°line. Furthermore, the nose gear can be positioned by using moment equilibrium about the cg of the aircraft. The aircrafts nose landing gear must carry at least 8% of the aircrafts MTOW to ensure good steering capabilities. Using safety factor of 1.5, this value will be increased to 12%. By doing so, Equation (5.25) below may be used.

$$x_{NG} = \frac{(1-f)}{f} x_{MG} \tag{5.25}$$

Where f is the fraction of weight the nose gear (NG) must carry (0.12 in this case), x_{NG} is the location of the nose gear to the left of the aft cg, and x_{MG} is the location of the main gear to the right of the aft cg. The main landing gear is to be positioned 12cm aft of the c.g. and the nose landing gear shall be placed 90cm forward of the cg.

5.8.2. Landing Gear Risk Analysis

Once the sizing is performed, it is imperative to identify all risks associated with the design. One risk can be that the breaking system is not functioning, this is quite hazardous and hence an emergency break system will be implemented. Next to that, it might be the case that the tyre pressure is too high or too low, this should be checked during maintenance. Furthermore, the gear positioning might not be done properly, this should be avoided by iterating the position in the stability analysis. However, an option could be added to shift landing gear location once built, this can also aid in ensuring that the weight on the front gear is within the allowable range. Finally, the landing gear should ensure enough ground clearance for the propeller and during landing the gear should be able to take critical impact by means of gear suspension.

5.8.3. Landing Gear Certifiability

Lastly, it is important to determine whether the current landing gear design conforms to the required certification specification standards, namely CS-VLA. The only requirement stemming from the certification specifications that is relevant to the landing gear is **ELTA-CS-FLT-20**, stating that the nose wheel shall carry at least 8% of the aircraft weight with the most rear centre of gravity. As it can be seen from Section 5.8.1, a safety factor of 1.5 was applied on this factor in order to ensure that the aircraft will be able to carry at least 8% of the aircraft weight at the aft-most centre of gravity. As long as this requirement is met, the landing gear should not cause any problems when it comes to certifiability.

5.9. Compliance Matrix

The wing compliance matrix can be found in Table 5.13, the fuselage compliance matrix can be found in Table 5.14 and finally, the landing gear compliance matrix can be found in Table 5.15.

Table 5.13: Compliance Matrix Wing

Identifier	Requirement	Obtained value	Requirement met?
ELTA-W-04	The wing shall house the ailerons	*	✓

ELTA-W-05	The wing shall house the flaps	*	✓
ELTA-W-06	The wing shall provide potential battery storage volume	*	✓
ELTA-W-07	The wing shall provide lift to sustain flight in all flight conditions within the flight envelope	*	✓
ELTA-W-08	The wing shall be attached to the fuselage	*	✓
ELTA-W-09	The wing shall not bend more than 0.1 of the wing span at maximum positive and negative loads	0.06	✓
ELTA-W-10	The wing shall be maintainable	*	✓
ELTA-W-11	The wing shall have two spars	*	✓
ELTA-W-12	The wing shall allow the pilot to enter the cockpit	*	✓
ELTA-W-18	The wing shall not exceed a mass of 100kg	160kg	✗
ELTA-CS-STR-02	A safety factor of 1.5 shall be used for each structural component	*	✓
ELTA-CS-STR-03	The allowable stress level shall be lower than the ultimate stress of the material	*	✓

Table 5.14: Compliance Matrix Fuselage

Identifier	Requirement	Obtained value	Requirement met?
ELTA-CS-FUS-01	The tail upsweep angle shall be such that the aircraft is able to rotate to its clean stall angle of attack.	15.75°	✓
ELTA-CS-FUS-02	The cockpit width shall be 101 cm as a minimum.	1.06 m	✓
ELTA-CS-FUS-03	The cockpit height measured from floor to ceiling shall be 112 cm as a minimum.	1.21 m	✓
ELTA-CS-FUS-04	The pilot shall be able to look as a minimum 5 degrees downward over the nose of the aircraft.	11°	✓
ELTA-CS-FUS-05	The pilot shall be able to look outside the aircraft as a minimum 135 degrees to the right and left.	135°	✓
ELTA-CS-FUS-06	The pilot shall be able to look outside the aircraft as a minimum 30 degrees up and down using the side window.	>60 °	✓
ELTA-FUS-01	The fuselage shall be designed to provide enough space for the training enhancement package.	*	✓
ELTA-FUS-02	The fuselage shall be able to carry two passengers while flying at the maximum load factor.	*	✓
ELTA-FUS-03	The fuselage shall provide space for the motor in the nose of the aircraft.	*	✓
ELTA-FUS-04	The fuselage shall be able to withstand the loads on its structure, caused by aerodynamics, ground loads, propulsion, emergency parachute, and gravity.	*	✓
ELTA-FUS-05	The fuselage shall be designed to provide enough space for the avionics.	*	✓
ELTA-FUS-06	The fuselage shall connect all the primary subsystems of the aircraft together.	*	✓
ELTA-FUS-07	The fuselage shall be able to carry two passengers side by side.	*	✓
ELTA-FUS-08	The fuselage shall be designed to provide enough space for the batteries.	150L	✓
ELTA-FUS-09	The fuselage shall not exceed a mass of 115 kg.	121 kg	✗
ELTA-CS-STR-02	A safety factor of 1.5 shall be used for each structural component.	1.5	✓
ELTA-CS-STR-03	The allowable stress level shall be lower than the ultimate stress of the material.	*	✓
ELTA-CS-STR-05	Each seat and its supporting structure shall be designed for occupants weighing at least 86 kg.	100 kg times ultimate load factor	✓

Table 5.15: Compliance Matrix Landing Gear

Identifier	Requirement	Obtained value	Requirement met?
ELTA-FLT-06	The main landing gear shall be positioned such that the aircraft will not tip over at its most rear centre of gravity.	*	✓
ELTA-FLT-07	The main landing gear shall be positioned such that the aircraft will be able to pitch up 15 degrees while on the ground without a tail strike.	15.75°	✓

ELTA-FLT-08	The line through the aft-most c.g. location and the main landing gear shall be oriented at least 5 degrees from vertical.	5.25°	✓
ELTA-FLT-09	The landing gear shall provide braking capabilities while the aircraft is on the ground.	Brakes on main wheels	✓
ELTA-FLT-10	The landing gear shall provide steering capabilities while the aircraft is on the ground.	Differential braking	✓
ELTA-CS-FLT-20	The nose wheel shall carry at least 8% of the aircraft weight with the most rear centre of gravity.	12%	✓

The compliance matrices for the horizontal and vertical tail have been excluded from this report, as these still have to be designed in detail. Hence, only a few requirements can be assured to have been met at this stage of the design. It should be noted that no design decision has been made that would restrict compliance with any of their requirements. Hence, the structural design is still on track to be compliant with all its requirements.

6
Aerodynamics

This chapter goes over the aerodynamic analysis and aerodynamics driven design of several subsystems. These subsystems include the wing and the empennage. Fuselage contributions are taken into account in this chapter, however, the fuselage design is discussed in Chapter 5. First, Section 6.1 summarises all functions and requirements applicable to the wing and empennage aerodynamics. Then, Section 6.2 describes all the tools researched and developed in order to execute the aerodynamic design. This includes an evaluation of the assumptions made for these tools. After this, Section 6.3 contains verification and validation of the tools that are used. In Section 6.4, the design of the wing planform is performed. This includes airfoil selection. Next, Section 6.5 outlines the empennage aerodynamic planform design, also including airfoil selection. After the initial planform is designed, an analysis on the drag and Oswald efficiency is performed in order to provide valuable output used in the evaluation of requirement compliance and other subsystem design. Note that on aerodynamic analysis, a priority had to be made on the development of the tools due to time constraints. The priority has been placed on the wing analysis over the empennage, as the main wing generally has a bigger impact on overall aerodynamic performance. This results in the use of more empirical tools for the empennage.

6.1. Functional Analysis and Requirements

This section includes all functions and requirements that are relevant to the aerodynamic design procedure. This includes the wing and empennage subsystems. The functions are derived as a flow down of the functional flow diagram presented in the baseline report [2]. Note that only the requirements that are relevant to the aerodynamic design are included per subsystem.

6.1.1. Wing Subsystem Functional Analysis

Considering aerodynamic analysis and design, the wing is the primary subsystem, thus is analysed in detail for the functions and requirements. The following functions are taken or derived from the midterm report [1]. These flow down from the functions **D.4, D.5, D.6** in the functional flow diagram, see Appendix A.

- **ELTA-FUN-W-01** - *Generate lift, such that the aircraft can fly*;
- **ELTA-FUN-W-02** - *Provide roll control to the aircraft*.

6.1.2. Wing Subsystem Requirement Analysis

The following requirements are set in order for the wing to adequately perform the above mentioned functions. These requirements were taken or derived from the midterm report [1]. Note that also requirements concerning the airfoil are included in the wing subsystem.

- **ELTA-W-01** - *The aircraft shall have a maximum lift coefficient of 1.4 in a clean configuration.* This requirement serves to comply with **ELTA-FUN-W-01** and the value for the lift coefficient is determined in the design point for the limiting configuration;
- **ELTA-W-02** - *The aircraft shall have an maximum lift coefficient of at least 1.8 in a take-off configuration.* This requirement serves to comply with **ELTA-FUN-W-01** with the design point for the limiting configuration in consideration;
- **ELTA-W-03** - *The aircraft shall have an maximum lift coefficient of at least 2 in a landing configuration.* This requirement serves to comply with **ELTA-FUN-W-01**;
- **ELTA-W-04** - *The wing shall house the ailerons.* This requirement was set up, because the ailerons are attached to the wing;
- **ELTA-W-05** - *The wing shall house the flaps.* This requirement was set up, because the flaps are attached to the wing;
- **ELTA-W-06** - *The wing shall provide potential battery storage volume.* This requirement was set up, because of the need of battery storage;
- **ELTA-W-13** - *The wing shall have a safe stall behaviour.* This requirement serves to comply with the need for safety in flight training scenarios;
- **ELTA-W-14** - *The aircraft shall have a clean zero-lift drag coefficient of CD0 = 0.028.* This requirement serves to comply with the design point [1];
- **ELTA-W-15** - *The aircraft shall have a take-off zero-lift drag coefficient of CD0 = 0.038.* This requirement serves to comply with the design point [1];
- **ELTA-W-16** - *The aircraft shall have an Oswald efficiency factor of 0.83.* This requirement serves to comply with the design point [1];

- **ELTA-W-17** - *The wing root shall stall before the wing tip.* This requirement serves to comply with **ELTA-W-13**;
- **ELTA-W-AF-01** - *The airfoil shall provide a maximum lift coefficient of 1.55 during cruise conditions.* This requirements serves to comply with **ELTA-W-01**;
- **ELTA-W-AF-02** - *The airfoil shall have a thickness to chord ratio allowing potential battery storage.* This requirement serves to comply with **ELTA-W-06**;
- **ELTA-W-AF-03** - *The airfoil lift curve shall have a gradual stall behaviour.* This requirement serves to comply with **ELTA-W-13**.

6.1.3. Empennage Subsystem Functional Analysis

Next to the aerodynamic analysis and design of the wing, also the empennage, i.e. the horizontal and vertical tail, should be aerodynamically analysed and sized. Therefore, a functional analysis and a requirement analysis for the empennage was performed as well. The functions of the empennage follow from the stability & control functional analysis. These functions are listed below.

- **ELTA-FUN-SC-01** - *The aircraft empennage should provide stability*;
- **ELTA-FUN-SC-02** - *The aircraft configuration should provide the pilot with the ability to control the aircraft.*

6.1.4. Empennage Subsystem Requirement Analysis

- **ELTA-W-HT-03** - *The horizontal tail shall provide both positive and negative lift as required*;
- **ELTA-W-VT-02** - *The vertical tail shall provide both positive and negative lift as required.*

6.2. Analysis Tooling

In order to perform aerodynamic analysis, an adequate set of tools need to be selected. This section goes over the different tools considered and selected for this process. Both analytical empirical and semi-empirical formulas are considered, as well as numerical simulation tools. Both will be used in the actual design process as well as to verify and validate each other.

6.2.1. Empirical & semi-empirical methods

Empirical and semi-empirical methods are used for efficiency and drag estimations. This is due to the lack of analytical solutions and/or available accurate numerical tools. The (semi)empirical are employed due to the capability to include interaction effects between wing, fuselage and empennage into the drag and efficiency calculations. This was deemed preferable over using more complex numerical tools for these purposes as it would provide results with adequate accuracy for this phase of the project.

Zero lift drag estimation

Drag can be split up in two components: parasitic (zero-lift) and lift-induced drag. Note that the induced drag is able to be calculated numerically using the numerical tool-set described later, since viscous effects can be neglected for induced drag. The zero-lift drag of the aircraft is a factor that is highly dependent on viscous effects of the airflow, however. Available tools are extremely limited in their ability to provide a good estimate of zero-lift drag, thus only a semi-empirical method is used to calculate this drag. The following method is based on the component drag build-up method. All formulas and statistical values used for the zero lift drag estimation are based on [15]. The total zero lift drag of the aircraft is estimated by Equation (6.1) as the sum of the aircraft components (c). The components considered for this drag calculation are: wing, empennage and fuselage, with the landing gear and flaps as miscellaneous components. Here the S is reference surface area (wing surface area), C_f is flat plate skin friction coefficient, FF the component form factor and IF the Interference factor. The interference factors IF are derived from statistics for every component.

$$C_{D_0} = \frac{1}{S}\sum_c \cdot C_{f_c} \cdot FF_c \cdot IF_c \cdot S_{wet_c} + \sum C_{D_{misc}} \tag{6.1}$$

The skin friction coefficient C_f depends on boundary layer type and Reynolds number. The ratio of turbulent and laminar flow is determined on statistics per aircraft component. This depends on the component type and the material chosen, but due to the presence of a nose-mounted propeller, the $C_{turbulent}$ of the fuselage is assumed to be 1. The total C_f is then given by Equation (6.2) with $C_{turbulent}$ being the fraction of turbulent boundary layer. Equation (6.3) gives the friction coefficient for laminar boundary layer, and Equation (6.4) for turbulent boundary layer, simplified for subsonic speeds. For this, Equation (6.5) is used for all Reynolds number calculations.

$$C_f = C_{turbulent} \cdot C_{f_{turbulent}} + (1 - C_{turbulent}) \cdot C_{f_{laminar}} \tag{6.2}$$

$$C_{f_{laminar}} = \frac{1.328}{\sqrt{Re}} \quad (6.3) \qquad C_{f_{turbulent}} = \frac{0.445}{\log_{10} Re^{2.58}} \quad (6.4)$$

$$Re = \frac{\rho V l_{Re}}{\mu} \quad (6.5)$$

The form factor FF is calculated differently for the different components. For the wing and empennage Equation (6.6) is used, simplified for subsonic speeds. This equation requires additional airfoil characteristics which are: $\left(\frac{x}{c}\right)_{max}$ location of maximum thickness, and $\frac{t}{c}$ for thickness over chord ratio.

$$FF_{wing,emp} = 1 + \frac{0.6}{(x/c)_{max}} \frac{t}{c} + 100\left(\frac{t}{c}\right)^4 \quad (6.6)$$

The form factor of the fuselage is calculated with Equation (6.7). Here $A_{max_{fus}}$ is the maximum cross section of the fuselage and l_{fus} the fuselage length.

$$FF_{fus} = 1 + \frac{60}{f^3} + \frac{f}{400} \text{ width } f = \frac{l_{fus}}{\sqrt{(4/\pi) A_{max_{fus}}}} \quad (6.7)$$

For miscellaneous drag, the landing gear and flaps are considered. For the landing gear Equation (6.8) is used to determine an additional drag component to C_{D_0}. Here S_s is the landing gear reference area defined as the frontal area.

$$\Delta C_{D_{LG}} = \Delta C_{D_s} \frac{S_s}{S} \quad (6.8)$$

An additional drag contribution from the flaps is determined by Equation (6.9) simplified for plain flaps. Here $\frac{c_f}{c}$ is the flap chord length as percentage of wing chord. $\frac{S_{flap}}{S}$ is the wing area affected by the flap and δ_{flap} is the flap deflection.

$$\Delta C_{D_{flaps}} = 0.0144 \frac{c_f}{c} \frac{S_{flap}}{S} (\delta_{flap} - 10) \quad (6.9)$$

All input values used to calculate an eventual C_{D_0} using Equation (6.1) are presented in Table 6.8. The Oswald efficiency factor calculation depends on this value of the zero lift drag together with the span efficiency factor obtained from the wing analysis tool. All results are presented in the appropriate section on wing or empennage design.

Oswald efficiency factor

Oswald efficiency is a major factor in the overall efficiency of the aircraft. Optimising the aerodynamic design for the Oswald efficiency is a driving factor in the optimisation of the wing, as it affects the take-off weight achievable significantly. This is demonstrated by the sensitivity analysis performed in the midterm phase [1]. The span efficiency factor, belonging to the wing alone, can be calculated numerically using the developed tool described in Section 6.2.2. However the Oswald efficiency factor includes viscous effects and interaction effects, thus a (semi)-empirical tool is used. The formulas used are a combination of methods as described in [16].

The Oswald efficiency factor e is calculated using Equation (6.10), simplified for subsonic speeds, thus neglecting compressibility effects. This equation includes a correction factor for the potential contribution of winglets $k_{e,WL}$. The necessity of these will be investigated in Chapter 10. Furthermore, the Oswald factor depends on an inviscid part Q, a viscous part P, and the wing aspect ratio A. Q is given by Equation (6.11). This includes the theoretical Oswald factor e_{theo} and a fuselage factor $k_{e,F}$. P is given by Equation (6.12), where $K = 0.38$[16] is a correction factor to the zero-lift drag C_{D_0}, which is calculated using the method described in the previous subsection.

$$e = \frac{1}{Q + P\pi A} \cdot k_{e,WL} \quad (6.10) \qquad Q = \frac{1}{e_{\text{theo}} \cdot k_{e,F}} \quad (6.11) \qquad P = K C_{D,0} \quad (6.12)$$

The theoretical factor e_{theo} is assumed equivalent to the span efficiency factor of the wing calculated by the wing analysis tool. $k_{e,F}$ is given by Equation (6.13) and uses d_F as the fuselage width and b as the wingspan.

$$k_{e,F} = 1 - 2\left(\frac{d_F}{b}\right)^2 \quad (6.13)$$

Furthermore, the winglet factor $k_{e,WL}$ is calculated by Equation (6.14). The depends on the winglet height h_{WL}, the winglet effectiveness factor k_{WL} and the wingspan b. The value of $k_{e,WL}$ has to be taken from statistics, the value used is shown in Table 6.9.

$$k_{e,WL} = \left(1 + \frac{2}{k_{WL}} \frac{h_{WL}}{b}\right)^2 \tag{6.14}$$

6.2.2. Numerical methods

For 3D finite wing aerodynamic analysis, a numerical approach can be of great value. Also, during the detailed airfoil selection analysis, a numerical result from e.g. the Vortex Panel Method is convenient to use alongside experimental data.

Tools applicable to and considered for 2D airfoil analysis are XFoil [1] and Javafoil [2]. Both use panel methods to evaluate he potential flow, and have similar benefits and drawbacks. Thus the tool used is selected on the basis of the 3D analysis tool.

For 3D analysis, the tools considered are Xflr5 [3] and AVL [4]. AVL makes use of the Vortex Lattice Method (VLM), just like Xflr5. However, Xflr5 also supports 3D panel methods and lifting line theory. The selection was made based on ease of use and further options, thus, Xflr5 will be used for further numerical analysis. This decision is also supported by Xflr5 including XFoil by default, as well as using a more friendly user interface compared to the command-line only interface of AVL.

Furthermore, a custom tool is developed for lift and drag analysis of the 3D wing. This is done in order to easily iterate on the wing planform design and gain insight in the design factors. This tool is described in the following section.

Custom Wing Planform Analysis Tool

In order to effectively iterate on design parameters, a custom tool was developed that calculates primarily the lift distribution and other aerodynamic parameters, including the C_{L_α}, C_{D_i} and $C_{L_{max}}$, as well as the span efficiency factor. This tool is based on a numerical solution of the lifting line theory, constructed using [17] and [18].

The method is based around solving for N unknown coefficients $A_1, ..., A_N$ which form a truncated series. The expression stating the equation to be satisfied for the coefficients can be seen in Equation (6.15)[18]. Here, θ is the spanwise coordinate from $0 < \theta < \pi$, which maps to the normal spanwise coordinate $\frac{-b}{2} < y < \frac{b}{2}$ with b the wingspan. Furthermore, a_0 is the local lift curve slope, c the local chord and $\alpha_{L=0}$ the local zero lift angle of attack. Note that the solution of the coefficients is a function of angle of attack α.

$$\frac{4b}{a_0 c} \sum_{n=1}^{N} A_n \sin(n\theta) + \sum_{n=1}^{N} n A_n \frac{\sin n\theta}{\sin\theta} = \alpha - \alpha_{L=0} \tag{6.15}$$

With the coefficients known, this enables the lifting line theory to calculate the circulation distribution along the span which can be seen in Equation (6.16)[18]. Here V_∞ is the free stream velocity. The circulation can be converted to local lift coefficient and thus a lift distribution with the use of Equation (6.17)[18]. Note that this formula is used within the tool, thus, the free stream velocity cancels out and is not a required input of the lift analysis. Furthermore Equation (6.18)[18] makes use of the dominant first coefficient to calculate the total lift coefficient of the wing, with A the aspect ratio of the wing.

$$\Gamma(\theta) = 2bV_\infty \sum_{n=1}^{N} A_N \sin n\theta \tag{6.16}$$

$$c_l = \frac{2\Gamma(y)}{V_\infty c(y)} \tag{6.17}$$

$$C_L = A_1 \pi A \tag{6.18}$$

The theory also allows for the calculation of the induced drag as can be seen in Equation (6.20)[18], with δ from Equation (6.19). This is a function of C_L, which is in turn a function of alpha, as is δ. Alongside the induced drag, the span efficiency factor can be calculated as well using Equation (6.21)[18], also using δ. The results of the induced drag is to be evaluated with the addition of viscous effects, which are not included in the tool analysis due to lack of realistically implementable and accurate methods for viscous analysis, and are addressed by (semi)empirical methods as outlined in Section 6.2.1. The span efficiency factor can be used to evaluate the Oswald efficiency factor of the whole aircraft by the same way of addition of (semi-)empirical methods.

$$\delta = \sum_{n=2}^{N} n \left(\frac{A_n}{A_1}\right)^2 \tag{6.19}$$

$$C_{D_i} = \frac{C_L^2}{\pi A}(1 + \delta) \tag{6.20}$$

$$e = \frac{1}{1 + \delta} \tag{6.21}$$

[1] https://web.mit.edu/drela/Public/web/xfoil/, Last Accessed 03-06-2020
[2] https://www.mh-aerotools.de/airfoils/javafoil.htm, Last Accessed 03-06-2020
[3] http://www.xflr5.tech/xflr5.htm, Last Accessed 03-06-2020
[4] http://web.mit.edu/drela/Public/web/avl/, Last Accessed 03-06-2020

The number of coefficients N to solve for requires N sample control points along the span to solve for the coefficients, which then results in a NxN matrix to solve. In Equation (6.15), $\alpha_{L=0}$, a_0 and c are all a function of the control points and thus of the spanwise location. In order to use the formulas stated above, a transformation has to happen between the y-coordinate and θ, seen in Equation (6.22)[18].

$$y = -\frac{b}{2}\cos\theta \tag{6.22}$$

The coordinate mapping can be used in the following equations in order to obtain functions for the variable properties in the coefficient calculation in terms of the span location. Derived directly from unswept and tapered wing geometry, Equation (6.23) describes a relation for tip (c_t) and root chord (c_r) in terms of wing area (S), wing span (b) and taper ratio (λ). Also derived directly from the unswept wing geometry, Equation (6.24) describes the chord length along the span as a function of span.

$$S = \frac{(c_r + c_t)b}{2} \Leftrightarrow c_r = \frac{2S}{b(1+\lambda)} \text{ with } c_t = \lambda c_r \tag{6.23}$$

$$c(y) = \frac{2(c_t - c_r)}{b}|y| + c_r \tag{6.24}$$

The lift curve slope also is dependent on the control point location and can be linearly interpolated between the known values of the root airfoil lift curve slope ($C_{L_{\alpha,r}}$) and the tip airfoil lift curve slope ($C_{L_{\alpha,t}}$) using formula Equation (6.25)

$$C_{L_\alpha}(y) = \frac{2}{b}(C_{L_{\alpha,t}} - C_{L_{\alpha,r}})|y| + C_{L_{\alpha,r}} \tag{6.25}$$

Furthermore, the local twist has to expressed in function of y as well. This equation was derived as a linear interpolation over the span

$$\tau(y) = \tau\frac{1-|y|}{b} \tag{6.26}$$

Finally the zero lift angle of attack has a relation to the spanwise location described in Equation (6.27). This is also a linear interpolation over the span with $\alpha_{L=0,t}$ for the tip and $\alpha_{L=0,r}$ for the root being known parameters. Note the addition of the local twist $\tau(y)$.

$$\alpha_{L=0}(y) = \frac{1}{b}(\alpha_{L=0,t} - \alpha_{L=0,r})|y| + \alpha_{L=0,r} - \tau(y) \tag{6.27}$$

The equations above describe all parameters used in the determination of the lift distribution. The control points are sampled linearly over θ N times, and is then solved using a matrix solver. Following the verification of this tool, it will be used to judge the design parameters of the wing planform. Note that the lift distribution used as input for the structural analysis will be taken from the analysis in Xflr, with the planform parameters the design tool has optimised. Thus the purpose of the development of this custom tool becomes clear as an optimisation tool.

6.3. Verification & Validation of Design Tools

Te following section discusses the verification and validation that was done to ensure reliable results from the tools used. First, Xflr5 is validated on its 2D implementation with experimental data from NACA [19].

6.3.1. Numerical Tool Validation

The Xflr5 tool includes 2D (Xfoil) and finite wing analysis, which in the best case are both to be validated using experimental data.

XFoil 2D Validation

A number of airfoil polars are compared to experimental data to assess the validity of the Xfoil results. For this, the NACA series are used, since the experimental polars have been reliably documented. The simulation will be run using Reynolds numbers available in the experimental data. First, the minimum and maximum Reynolds numbers that are applicable are determined based on the operating conditions of the aircraft. These can be seen in Table 6.1 and are determined with the mean aerodynamic chord from the midterm report [1]. Since the NACA experimental data provides polars for $Re = 3.0e6$ and $Re = 6.0e6$, these are close enough to the determined values and will be used for comparison. The results are compared with 2 airfoils: the NACA4415, and NACA65(2)-415. The first is chosen as it is the base airfoil chosen in the midterm phase, while the latter airfoil is used since the 6-series was deemed a possible option as well in the midterm report, because of the high lift and drag performance [1]. The experimental data of these airfoils is retrieved from [19].

$$RMSD = \sqrt{\frac{\sum_{n=1}^{N}(\hat{y}_n - y_n)^2}{N}} \qquad NRMSD = \frac{RMSD}{y_{max} - y_{min}} \tag{6.28}$$

Table 6.1: Reynolds Number Range

	MAC [m] [1]	ν **[m2/]**	V **[kts] [1]**	Re
Min Reynolds number	1.45	13.28e-6 @ 0C	45	2527673
Max Reynolds number	1.45	15.52e-6 @ 25C	120	5767611

Figure 6.1 shows the polar comparison of the 4415 for $Re = 3e6$., and Figure 6.2 shows the polar comparison of the 65(2)-415 for $Re = 6e6$, between the XFoil results and the experimental data. The analysis has been performed for both $Re = 3e6$ and $Re = 6e6$ for both airfoils, and the resulting error can be seen in Table 6.2. For this, the normalised root-mean-square deviation (NRMSD) Equation (6.28) [5] was used as a metric, in order to extract percentage contingency margins out of the results. Here, $\hat{y}_n$ is the predicted value, and y_n the validation data for N samples. The errors in Table 6.2 are evaluated for the full range provided by the experimental data, and a limited range, since it is known that the panel methods are not always accurate close to Clmax. The limited range for $C_l - \alpha$ is taken to be [-10, 8] and for $C_l - C_d$ [-0.8, 1.2] is used. This demonstrates higher accuracy of the numerical tools at lower angle of attack. The NRMSD peaks at 18% for the drag polar NACA4415. This value can be decreased when staying in the lower AoA. All other errors are lower, thus the airfoil analysis in Xflr5 is deemed accurate enough for this design phase.

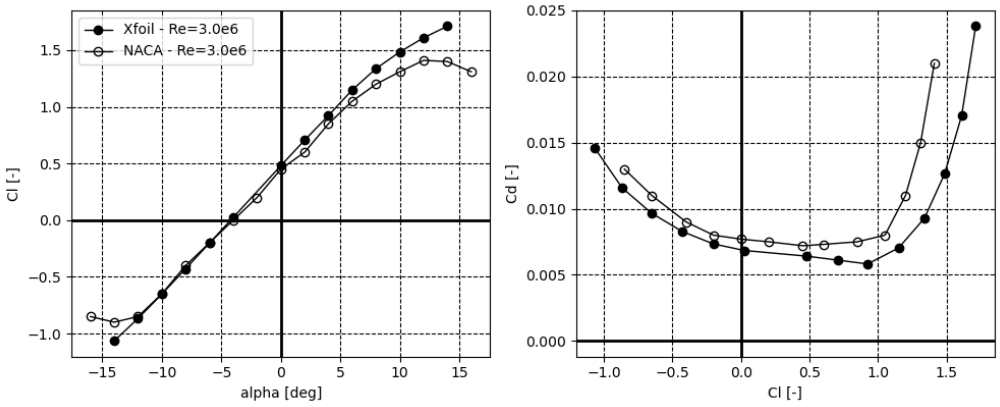

Figure 6.1: NACA 4415 Result Comparison

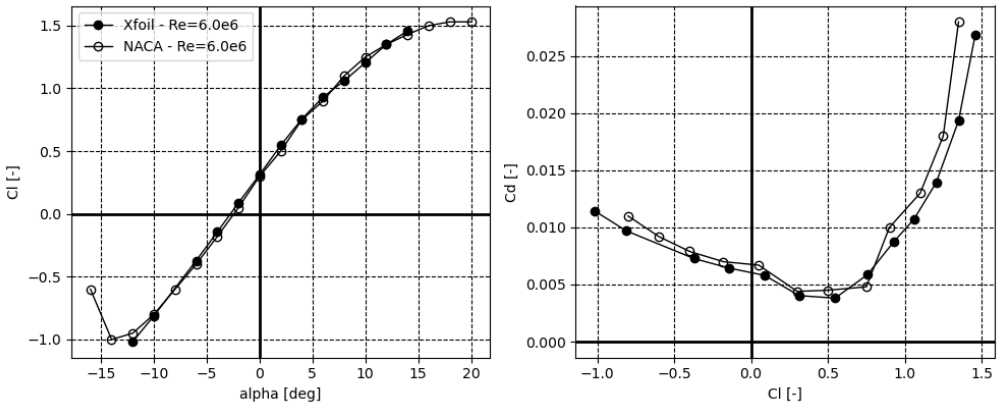

Figure 6.2: NACA 65(2)-415 Result Comparison

[5] https://www.marinedatascience.co/blog/2019/01/07/normalizing-the-rmse/ Last accessed on 05/06/2020

Table 6.2: XFoil validation errors

Airfoil	NRMSD $C_l - \alpha$ $Re = 3e6$	NRMSD $C_l - C_d$ $Re = 3e6$	NRMSD $C_l - \alpha$ $Re = 6e6$	NRMSD $C_l - C_d$ $Re = 6e6$
	Full range:			
NACA 4415	4.6%	16.4%	3.9%	18.0%
NACA 65(2)-415	1.7%	8.3%	1.2%	6.5%
	Limited range:			
NACA 4415	2.7%	8.7%	2.8%	9.8%
NACA 65(2)-415	1.2%	8.3%	1.0%	3.6%

XFlr5 Finite Wing Validation

No experimental data usable for finite wing analysis could be found or analysed in the given time frame. Instead is it assumed that due to the validity of the 2D analysis demonstrated in the section above, the 3D analysis using Xflr5 is deemed satisfactory for the design needs. This decision is based on the fact that the viscous analysis will not be used numerically, and will instead be addressed by (semi)-emperical methods, and this removes part of the inaccuracy in the 3D analysis that will be used due to the nature viscous analysis is implemented in Xflr5 [6].

6.3.2. Analytical Model Verification

The wing planform model developed in Section 6.2 has to be verified before trusting the results in the design process. The Xflr5 3D analysis will be used for this, as the validity of this tool has been partially demonstrated in Section 6.3.1. The verification is performed on a model of wing planform with similar dimensions that is to be expected from the actual design based on the conceptual design results [1]. The parameters used for the wing model can be seen in Table 6.3. The output from the model analysis and Xflr analysis are compared and errors are presented in Table 6.3. For the distribution error, the NRMSD is used again to quantify the difference in lift distribution. This analysis is performed on 3 angles of attack from 2° to 10°. The lift distribution, total lift, lift curve slope and induced drag are compared. As can be seen from the table, the values for all parameters are very close within acceptable margin of error. The actual lift distributions are plotted in Figure 6.3 and the NRMSD relate to those distributions. Looking at the results minimal error's can be seen, thus the aerodynamic tool will be used further in the design process.

Table 6.3: Wing planform Model Verification

A	**S [m2]**	**V [m/s]**	**taper**	**twist [deg]**	**tip airfoil**	**root airfoil**	**CL - alpha**	
10	15	50	0.9	2	NACA4415	NACA65(2)415	Model C_{L_α} [/deg]	0.082
							Xflr C_{L_α} [/deg]	0.083
							diff C_{L_α}	1.2%

Alpha [deg]	**Model CL**	**Xflr CL**	**diff CL**	**Cl NRMSD**	**Model CDi**	**Xflr CDi**	**diff CDi**
2	0.54	0.58	6.9%	5.1%	0.010	0.009	11.1%
6	0.87	0.88	1.1%	5.7%	0.025	0.025	0.0%
10	1.20	1.21	0.8%	6.0%	0.048	0.047	2.1%

6.3.3. Future Validation & Verification

As written above, the verification procedure of the custom wing analysis tool, as well as the final used results of lift and (induced) drag distributions are performed and obtained from the Xflr5 3D analysis. As already mentioned in Section 6.3.1, the full 3D validation of Xflr5 could not be performed within the given time frame. To ensure the quality of the design parameters that come out of the iteration tool, and the distributions, a full validation of the 3D results of Xflr5 has to be performed. For this, wind tunnel data of finite wing models has to be available. This can then be compared with Xflr5 results analogous to what has been done for the custom tool verification in Section 6.3.2.

[6] `http://www.xflr5.tech/xflr5.htm`, Last Accessed 03-06-2020

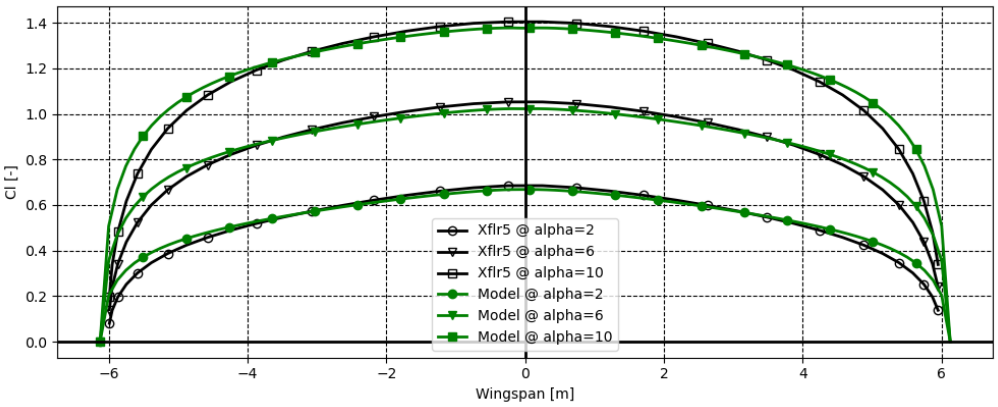

Figure 6.3: Model Lift distribution vs Xflr5

6.4. Wing design

The following section will describe the design process for the wing. The main wing of the aircraft will be designed based on the outcome of the midterm design report [1]. Several considerations were made, however, before this detail design was initiated. The sensitivity analysis in the midterm report [1] shows that the aerodynamic design has a predominant influence on the take-off weight. Thus, considerations in this chapter were always made in favour of aerodynamic performance. However, safety should be prioritised over performance, particularly in the case of a trainer aircraft. The design will thus first be considered in terms of safety, and only then is performance optimised. Naturally, both will be optimised if possible. Section 6.2.2 describes the tool that is used to evaluate the planform design. Note that sweep is not considered to the main wing. This is due to the strictly subsonic and relatively slow speeds of the aircraft. Hence, sweep will generally decrease aerodynamic performance and increase structural complexity. This decision is reinforced by the fact that low speed general aviation aircraft generally do not have quarter chord sweep applied.

6.4.1. Design for safety

The safety aspect of the aerodynamic design of the aircraft particularly concerns the stall properties of the wing. The scope of this is encompassed by requirement **ELTA-W-13** and, more specifically, its sub-requirements, **ELTA-W-17** and **ELTA-W-AF-03**. This can be achieved by selecting the right airfoil, and by designing the wing planform accordingly.

Airfoil selection

The airfoil, as per requirement **ELTA-W-AF-03**, should have gradual stall behaviour. In accordance with this requirement, the decision was made to limit the scope of possible airfoils to the NACA 4-series, which are known for their benign stall characteristics [14]. In a semi-qualitative trade-off procedure, the airfoils within this family were scored on lift, drag and structural depth (more detail found in the midterm report of this project [1]). The winning airfoil was the NACA 4415. Data shows that this airfoil has very smooth stall characteristics [20], while at the same time having decent lift, drag and structural characteristics. Its geometry is shown in Figure 6.4. The experimental airfoil properties are shown in Table 6.4 (values taken for $Re = 6 \cdot 10^6$) [19]. Additionally, the airfoil data shows no evidence of the presence of laminar separation bubbles at these Reynolds number, which is beneficial for the lift curve slope and the stall characteristics of the profile. Note that even though the analysis tools are able to analyse variable airfoils, the advantages are marginal, and the increased complexity on manufacturing is deemed a large enough disadvantage to not consider variable airfoil for the final design.

Initial wing planform considerations

In order for the full wing to have safe stall characteristics, as dictated by requirement **ELTA-W-13**, the wing should also have smooth stall progression. An additional consideration is that the ailerons need to remain operational despite partial stall of the wing. Associated with this requirement is that the onset of wing stall should occur at the inboard location of the span [21], as already determined in requirement **ELTA-W-17**. As a limitation, it was chosen to use a maximum in-board stall position of $\frac{|y|}{b/2} = 0.4$. Additionally, another limitation is that the difference of stall angle between the angle of the initial stall position and the stall angle at $\frac{|y|}{b/2} = 0.75$ is at least 1 degree, as the ailerons are likely to be located more outboard than 0.75% of the wing. Both of these measures should achieve a sufficient contingency margin for safe stall characteristics. To achieve this, a geometric twist is applied from the tip chord to the root chord of the wing, thus increasing the effective angle of attack of the root chord and, consequently, moving the stall location inboard without having to sacrifice aerodynamic performance due to tuning of other wing planform

parameters. A downside to twist is that it increases manufacturing complexity, and therefore, the cost of the wing.

In order to evaluate the stall onset location and progression over the span, the custom design tool determines the intersection of local $C_{l_{max}}$ of the lift distribution with the local $C_{l_{max}}$ of the airfoil distribution [22]. This is iterated to generate a stall progression plot, the result of which can be seen in Figure 6.6. This procedure includes the method of determining the $C_{L_{max}}$ of the wing, as this fist point of contact with lift distribution and airfoil maximum lift limit is taken as fist stall onset, from which the total wing C_L can be calculated using the lift distribution at that point, as described in Equation (6.18). The same holds for stall onset location, as it directly flows out of the fist stall onset determined by the tool.

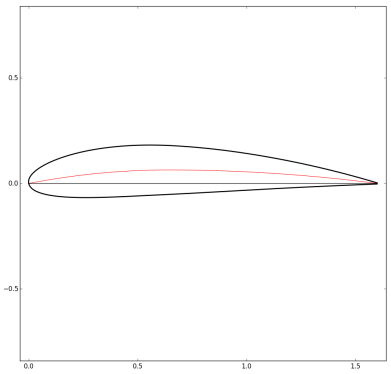

Figure 6.4: NACA 4415 airfoil geometry (root chord)

Parameter	Value	Unit
Maximum section lift coefficient $C_{l,max}$	1.6	$[-]$
Lift curve slope C_{l_α}	5.73	$[1/rad]$
Zero lift angle of attack $\alpha_{L=0}$	-0.007	$[rad]$

Table 6.4: Properties of the NACA 4415 airfoil @$Re = 6 \cdot 10^6$

6.4.2. Design for performance

To make electric flight feasible, the aerodynamic performance of the airplane during cruise should be optimised as far as possible. For the clean configuration wing, this concerns requirement **ELTA-W-01**, **ELTA-W-14** and **ELTA-W-16**. These parameters were analysed using the tools described in Section 6.2.1 and Section 6.2.2. These were achieved by adjusting the taper ratio of the wing to obtain the best possible lift distribution. Preferably, the Oswald efficiency is maximised beyond the requirement of 0.83, as this parameter in particular has a large influence on the take-off weight of the aircraft as demonstrated by the sensitivity analysis [1]. Due to the limitations of these tools, the fuselage influence on the wing lift distribution cannot be straightforwardly determined. Thus, as a contingency margin, the design maximum lift coefficient shall be increased by a margin of $\frac{b}{b-w_{fus}}$, to account for the effective "shortening" of the wing by adding a fuselage to the span. Note that the determination of the maximum lift coefficient has already been described in Section 6.4.1.

Results of the analysis are shown in Figure 6.5, which visualise how the maximum lift coefficient and the span efficiency factor behave for different twist and taper ratios. The first conclusion that can be drawn from these figures is that the optimum is created by a combination of twist and taper. Additionally, the optimum taper ratio always tends to lie between 0.3 and 0.6. Within this range, a discrete number of design options were selected. Those that did not meet the required maximum lift coefficient or the additional stall safety limits set in Section 6.4.1, were excluded, and the design with the largest span efficiency factor was found. The resulting wing design is presented in Section 6.4.3.

6.4.3. Wing Design Results

As already mentioned previously, the design tool was iterated to provide a discrete number of ranked options of twist and taper. The effect of twist and taper ratio combinations was evaluated on the basis of $C_{L_{max}}$, span efficiency factor e_{span}, and the spanwise stall onset position. The maximum lift coefficient (in clean configuration) had to adhere to the minimum required given by **ELTA-W-01**. The same held for the initial stall location. The final chosen design parameters presented in Table 6.5 were deemed the most acceptable combination as they adhere to the lift and efficiency requirements within margin without having excessive twist in favour of structures.

From the aforementioned analyses, the final wing parameters were determined, that can be found in Table 6.5. A visualisation of the wing planform is shown in Figure 6.7. Table 6.5 shows the parameters that define the wing, including airfoils.

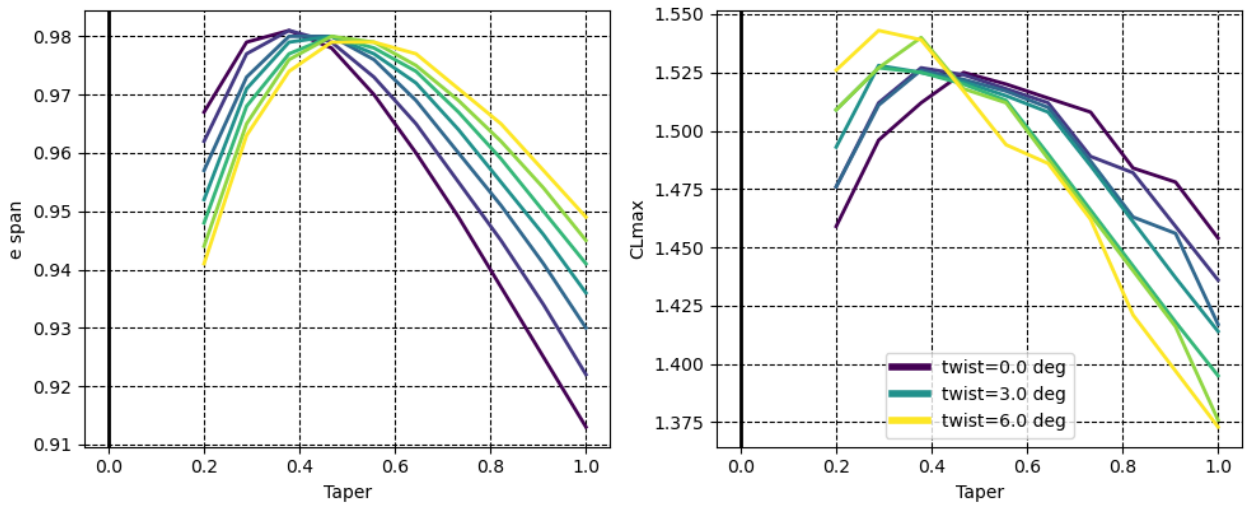

Figure 6.5: Wing planform Design Parameters Iteration

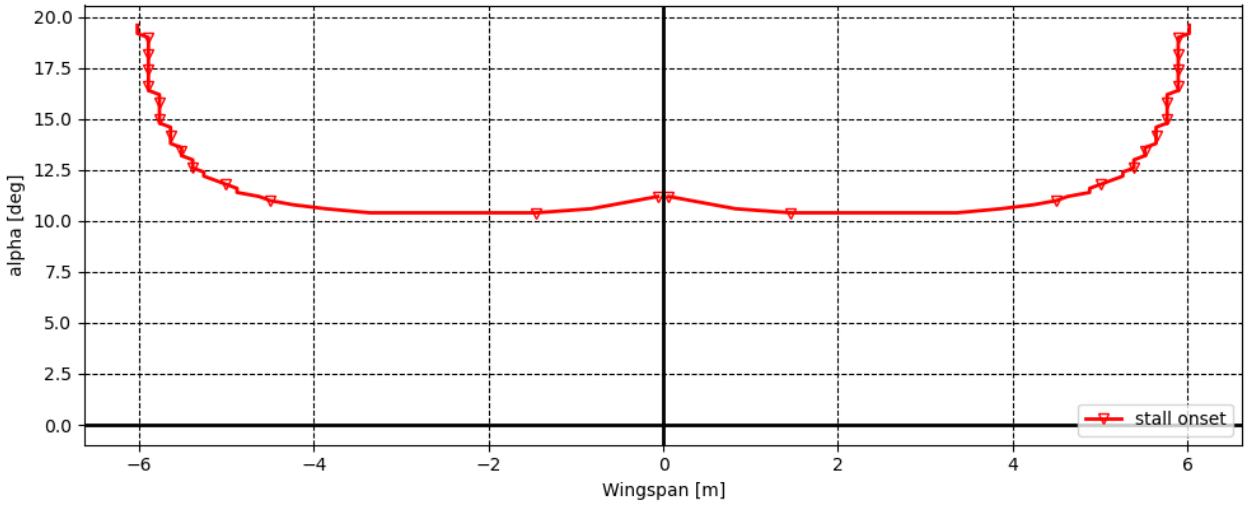

Figure 6.6: Main Wing Stall Onset Progression

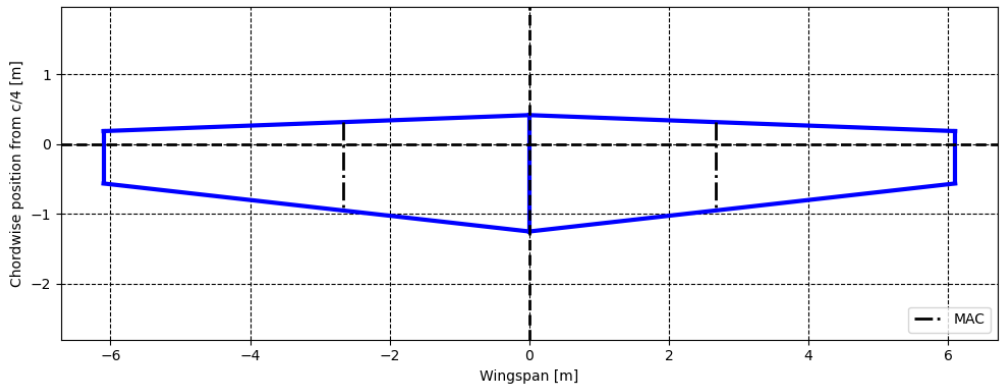

Figure 6.7: Wing Planform

Table 6.5: Wing Planform Design Results

Parameter	Symbol	Value	Unit
Design point			
Aspect ratio	A	10.1	-
Wing surface area	S	14.7	m2
Wing span	b	12.2	m
Airfoils (NACA4415)			
Clmax root	$C_{L_{max},r}$	1.6	-
Clmax tip	$C_{L_{max},t}$	1.6	-
Lift curve slope root	$C_{L_\alpha,r}$	0.1	1/deg
Lift curve slope tip	$C_{L_\alpha,t}$	0.1	1/deg
Zero lift angle of attack root	$\alpha_{L=0,r}$	-4	deg
Zero lift angle of attack tip	$\alpha_{L=0,t}$	-4	deg
Design parameters			
taper ratio	λ	0.45	-
twist (tip - root)	τ	5	deg

6.5. Empennage Aerodynamic Design

This section goes over the aerodynamic design process of the empennage. This includes both the horizontal and vertical stabilisers. Chapter 7 assesses stability and control and designs for the surface area of the horizontal and vertical tail. With the surface areas as given input, a planform shape of the empennage surfaces can be designed, based on mainly aerodynamic considerations.

6.5.1. Airfoil Selection

Airfoil selection for the empennage is more limited than for the wing. In general, symmetrical airfoils are used for this. The focus while choosing an empennage airfoil should be on minimising the trim drag. Also stability and control requires a certain lift coefficient to be generated from the horizontal tail surface. With this, also structural considerations are important as thinner airfoils pose an extra challenge for structural design and are able to increase the weight.

The horizontal tail airfoil selection is based on the criteria of the lift curve slope, structural thickness and stall safety. The lift curve slope of the horizontal tail should be as high as possible [23], as this has an advantageous effect on the stability curve as describes by Equation (7.3). From this can be derived that the airfoil c_l as well should be as high as possible.

When evaluating reference aircraft, symmetrical airfoils are widely used for the horizontal stabiliser. The advantage of using a cambered airfoil in this area is to delay the lower surface stall [23]. This option will not be designed with in order to reduce structural complexity and drag in this area. Also, since the Dragonfly is not an aerobatic aircraft, no particular requirement is set on the maximum lift coefficient of the tailplane, thus the use of simple symmetrical airfoils is deemed acceptable.

To narrow down the options, the conventional choice of NACA0009 and NACA0012 are considered for the horizontal and vertical stabiliser based on literature [23]. When looking at both these airfoils, the lift curve slope and maximum lift coefficient are compared. The NACA0009 has $C_{l_\alpha} = 6.30/rad$ and NACA00012 has $C_{l_\alpha} = 6.45/rad$ [19]. Both airfoils have similar ranges of angles of attack, but the NACA0012 has the advantage in structural depth because of the large thickness ratio, and has the larger lift curve slope. The advantage of the thinner 0009 is slightly lower drag polar, however, the advantages of the 0012 make it the choice of airfoil for both the horizontal an vertical stabiliser.

6.5.2. Planform Design

For the stabilisers, an aspect ratio, taper and sweep is chosen based on statistical and empirical methods.

Horizontal Stabiliser

The aspect ratio of the horizontal stabiliser has both significant aerodynamic and structural effects that need to be taken into account. Higher aspect ratios generally increase the aerodynamic effectiveness of the tailplane, which in turn is advantageous for control and stability. Disadvantages of high aspect ratio for the horizontal tailplane include the reduction of the stall angle of attack and increase in structural weight [24]. The aspect ratio for subsonic aircraft lies in the range of $3 < A_h < 5$ [8]. To limit the range, only $3 < A_h < 4$ is considered as aspect ratio of 5 is deemed too high in the interest of structural weight.

Even tough the custom wing design tool is not suitable for low aspect ratios, the results of the design parameter iteration seen in Figure 6.5 illustrate an optimum taper ratio over no taper at all for an increase in aerodynamic

performance and efficiency. For the horizontal tailplane, a slight taper is considered for an advantage in the aerodynamic performance, while also reducing structural weight. The range of possible tapers in similar aircraft is between $0.3 < \lambda_h < 1$[8]. High taper ratios increase the chance of tip stall [25], thus the range of possible taper ratios will be limited to $0.6 < \lambda_h < 1$.

For low speed aircraft like the Dragonfly, no sweep is required for coping with shock waves and high mach phenomena. However, a number of other effects can be seen from applying sweep to the horizontal tailplane. An increase in sweep increases the moment arm of the horizontal tailplane, thus, technically increasing the controllability and stability effectiveness of the horizontal tail. Furthermore, an increase in sweep has an advantageous effect on stall delay. Hence, sweep is considered for the sake of stall safety. Also, an increase in sweep angle decreases the lift curve slope, which has a negative effect on the stability curve. However, this is partially compensated by the accompanying increase in moment arm from the perspective of control and stability. This is supported by Torenbeek [23], as up to 25 degrees sweep, an advantage can be seen. For the sake of structural simplicity, a sweep that yields a straight trailing edge is used, which significantly reduces structural considerations for the elevator.

To decide on an aspect ratio and taper, the maximum angle of attack is evaluated using DATCOM method for low aspect ratio wings [17]. As the maximum angle of attack increases the stall safety of the empennage, maximising this angle was a driving factor, while staying inside the statistical feasibility ranges. Figure 6.8, Figure 6.9 and Figure 6.10 were used to determine the $\left(\alpha_{C_{L_{max}}}\right)_{base}$ and $\Delta\alpha_{C_{L_{max}}}$ which added together formed an estimate for the stall angle. For this, no compressibility correction was used due to low speed critical cases. Furthermore, Λ_{LE} was determined on the basis of the zero angle trailing edge sweep. From geometry, Equation (6.29) is derived with λ the taper ratio and A aspect ratio.

$$\Lambda_{LE} = \arctan\frac{4}{A}\frac{1-\lambda}{1+\lambda} \tag{6.29}$$

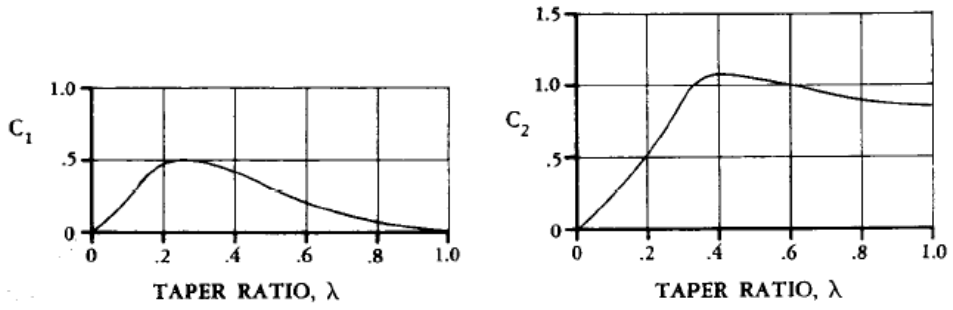

Figure 6.8: DATCOM Alpha stall low aspect ratio coefficients [17]

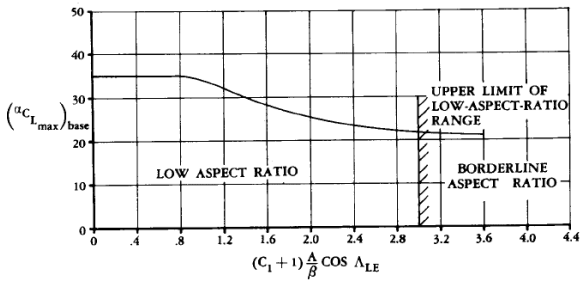

Figure 6.9: DATCOM Alpha stall low aspect ratio base [17]

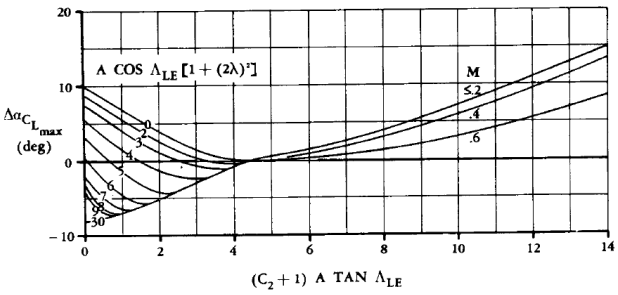

Figure 6.10: DATCOM Alpha stall low aspect ratio delta [17]

This estimation is run for a number of different aspect ratio's and taper ratio's. Note that with $A = 4$, the maximum taper ratio allowed by the DATCOM method is 0.7, since otherwise, Figure 6.9 overshoots the range for low aspect ratio. Due to a limited amount of tools, this dictates the taper ratio range considered as well to $0.7 < \lambda < 1$. Table 6.6 shows the DATCOM results of stall angle of attack for different taper and aspect ratio's. As can be seen from the table, the best combination for stall would be for no taper with aspect ratio 3. Some taper is desirable for other reasons outlined in the paragraphs above, so the second best option of $\lambda = 0.4$ and $A = 3$ is chosen as planform for the horizontal tail, see Figure 6.11.

Table 6.6: Horizontal stabiliser planform stall estimation

Taper	Aspect ratio	$\left(\alpha_{C_{L_{max}}}\right)_{base}$ [deg]	$\Delta\alpha_{C_{L_{max}}}$ [deg]	α_{max} [deg]
0.7	3	21.0	-6.5	14.5
0.8	3	21.1	-7.5	13.6
0.9	3	21.4	-7.5	13.9
1.0	3	21.4	-6.5	14.9
0.7	4	20.5	-6.5	14.0
0.8	4	20.4	-7.0	13.4
0.9	4	20.5	-7.5	13.0
1.0	4	20.5	-7.5	13.0

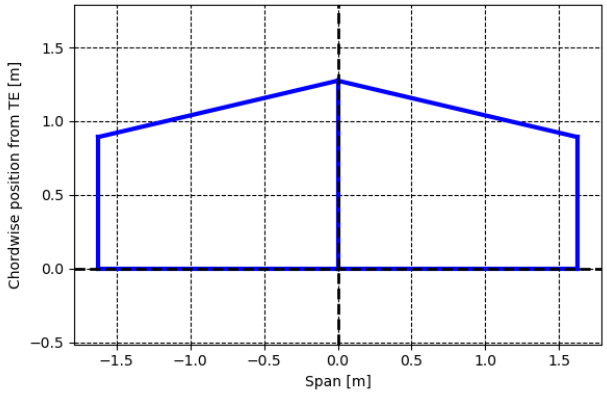

Figure 6.11: Horizontal Stabiliser Planform

Table 6.7: Empennage Planform Parameters

	Horizontal stabiliser
Area S_h [m2] Chapter 7	3.83
Airfoil	NACA0012
Aspect ratio A_h	3
Taper λ_h	0.7
Sweep TE Λ_{TE_h} [deg]	0
Sweep LE Λ_{LE_h} [deg]	13.2

Vertical Stabiliser

For the discussion regarding the design of the vertical tail plane please refer to Chapter 7.

6.6. Aerodynamic Performance & Efficiency

Now that the wing and empennage have been defined, an analysis on the drag and efficiency can be done. For this, the C_{D_0} and thus Oswald efficiency factor are to be determined with the tools explained in the previous sections. The zero-lift drag calculation requires a set of inputs, given in Table 6.8. These are organised per drag component analysed, thus wing, empennage and fuselage, together with miscellaneous inputs. The leakage contingency margin is applied to the total value of C_{D_0}. The other aerodynamics output parameters of the defined planform are given in Table 6.9.

The values for the wetted area for the components are calculated as follows. For the fuselage, this was derived from CAD geometry. For the wing wetted area, the wing area is taken minus the fuselage covered part. This area is then multiplied by 2.06 (derived from airfoil geometry) to obtain the wetted area from surface area. For empennage, the horizontal and vertical tail areas are multiplied by 2.04 (derived from airfoil geometry) to get wetted area.

Note that values for winglet sizing are implemented here as well. This is set to a 0.3m height in order to increase the Oswald efficiency factor, while not oversizing the winglets and adding more weight than the aerodynamic improvements.

Table 6.8: Zero lift drag estimation inputs

	Wing	Empennage	Fuselage
S_{wet} [m2]	26.93	9.55	17.51
$C_{turbulent}$	0.65	0.65	1
l_{Re} [m]	$MAC = 1.27$	$MAC = 1.5$	l_{fus}
l_{fus} [m]	N/A	N/A	9.42
$A_{max_{fus}}$ [m2]	N/A	N/A	1.218
t/c	0.15	0.12	N/A
$(x/c)_{max}$	0.3	0.3	N/A
IF [15]	1.25	1.05	1
Miscellaneous			
S_s [m2]	0.14		
ΔC_{D_s}	0.15		

δ_{flap} [deg]	40		
$\frac{c_f}{c}$	0.8		
$\frac{S_{flap}}{S}$	0.623		
Other			
V [m/s]	23.15		
ρ [kg/m3]	1.12		
μ [Pa s]	1.8e-5		
leakage contingency margin	5%		

Table 6.9: Aerodynamic Performance Results

Parameter	Symbol	Value	Unit
Wing lift curve slope	C_{L_α}	0.08	1/deg
Wing CLmax	$C_{L_{max}}$	1.52	-
Wing alpha max	α_{max}	10.2	deg
Span efficiency factor	e_{span}		-
Zero lift drag clean	$C_{D_0,clean}$	0.0176	-
Zero lift drag with flaps	$C_{D_0,flaps}$	0.0331	-
Oswald efficiency factor clean	e	0.816	-
Winglet height	h_{WL}	0.3	m
Winglet effectiveness factor	k_{WL}	2.1	-

6.7. Assumptions and Limitations

A number of assumptions have been made during the design and development of the aerodynamic planforms. These are documented in this section to be as complete as possible, along with the limitations these assumptions bring.

6.7.1. Validation & Verification

- *XFlr5 3D method not validated, assumed to be accurate enough based on the 2D validation.* This was assumed due to lack of available validation data and time constraints;
- *The span efficiency factor calculation done by the custom wing analysis too was assumed to be accurate.* Following the verification of the lift distribution of this tool, the coefficients the tool uses were deemed accurate, thus, since the calculation of the efficiency factor uses the same coefficients as the lift distribution calculation, it was assumed accurate as well. The efficiency factor out of XFlr5 was not used to verify this, since this results of the panel method used by XFlr5 is known to be overestimated [7].

6.7.2. Assumptions and simplifications

- *All compressibility effect were neglected.* Due to the low speed nature of the aircraft, compressibility does not have significant impact on the aerodynamic behaviour. However completely neglecting this always introduces discrepancies in comparison to the real world;
- $C_{L_{max}}$ *calculation model has no strong theoretical basis.* The source for this method states that, "Though this estimate has no strong theoretical justification it is also given as the preferred method by DATCOM" [22]. The accuracy of this method therefore may be limited to an unknown degree. Its employment in the determination of the stall progression should also be put under scrutiny;
- *Oswald efficiency factor does not include empennage contribution.* Since the low-aspect ratio wing planform was more difficult to analyse within the short time span of this project, the empennage contribution to the total oswald efficiency factor has been redacted. This results in an underestimation of this factor;
- *Winglet contribution only models effect on oswald efficiency.* The addition of winglet contribution is only integrated into the calculation of the total oswald efficiency of the aircraft. It does not take into account the effect on zero-lift drag, wing moment coefficient, structural characteristics of the wing and manufacturability.

6.7.3. XFlr5 Theoretical Limitations

Xflr5 uses VLM and 3d panel methods as mentioned in the sections above. These methods contain some drawbacks due to the assumptions made in the algorithms. The 3 main drawbacks of the Xflr5 implementation are: [8]

- *3D geometry is entirely composed of flat quad panels:* Real wing geometry is not manufacturable that

[7] https://engineering.purdue.edu/~aerodyn/AAE333/FALL10/HOMEWORKS/HW13/XFLR5_v6.01_Beta_Win32%282%29/Release/Guidelines.pdf Last Accessed 19/06/2020

[8] http://www.xflr5.tech/docs/Part%20IV:%20Limitations.pdf Last Accessed 03-06-2020

way, thus a discrepancy in geometry is always present. This introduces numerical errors, however these are expected to be small with high enough panel density and appropriate distribution;

- *The viscous drag analysis is merely an interpolation of viscous drag from local 2D wing lift:* This leads to underestimation of the total drag;
- *Lack of interactive boundary layer feedback loop in 3D panel method:* This leads to no valid results for high angles of attack or low Reynolds numbers in 3D wing evaluation.

6.8. Risks

A high impact risk for aerodynamic design is the possibility to not meet the performance requirements. Verification and compliance analysis of the resulting wing design has a risk of not meeting $C_{L_{max}}$, efficiency or safe stall characteristics. Chances of this are low, since these are the driving requirements that guide the aerodynamic design. However, testing has to be planned to evaluate the actual lift, drag, and efficiency of the aircraft, during which over estimations of performance in this design chapter can arise.

Another risk is the effect of the aerodynamic design parameters on structural complexity and thus weight. Therefore there is a risk of the wing and/or empennage weights being higher than expected which reduces the endurance and range performance. Tying into this, the manufacturability of the wing structures can be affected by the planform design which has a risk of posing extra challenges and costs which are higher than expected. These risks can be reduced by making aerodynamics and structures work together closely and plan evaluation meetings together with the systems engineer to make sure no complications arise.

Noise has not been analysed for the main wing and empennage, for which aerodynamic noise is the main contributor, There is a risk of the noise from these sources being higher than expected, which results in a decreased market appeal. These components will be windtunnel tested where they will be analysed for noise.

Further integration of the planform affected subsystems with the rest of the aircraft has a chance of showing incompatibilities which were not anticipated. This poses a risk which can result in an unfeasible design. It is the job of the systems engineer and the team as a whole to make sure this does not happen and integration of all components guaranteed.

6.9. Compliance Matrix

Empennage compliance is presented in Chapter 7. Table 6.10 Shows the compliance matrix of the wing aerodynamic requirements presented in Section 6.1. Requirements **ELTA-W-02** and **ELTA-W-03** are treated in Section 7.8.

Table 6.10: Compliance matrix Wing aerodynamics

Identifier	Requirement	Value	Req. met?
ELTA-W-01	The aircraft shall have a maximum lift coefficient of 1.4 in a clean configuration.	1.52	✓
ELTA-W-04	The wing shall house the ailerons.	*	✓
ELTA-W-05	The wing shall house the flaps.	*	✓
ELTA-W-06	The wing shall provide potential battery storage volume.	not relevant anymore	
ELTA-W-13	The wing shall have a safe stall behaviour.	*	✓
ELTA-W-14	The aircraft shall have a clean zero-lift drag coefficient of CD0 = 0.028.	0.0176	✓
ELTA-W-15	The aircraft shall have a take-off zero-lift drag coefficient of CD0 = 0.038.	0.0331	✓
ELTA-W-16	The aircraft shall have an Oswald efficiency factor of 0.83.	0.844	✓
ELTA-W-17	The wing root shall stall before the wing tip.	*	✓
ELTA-W-AF-01	The airfoil shall provide a maximum lift coefficient of 1.55 during cruise conditions.	1.6	✓
ELTA-W-AF-02	The airfoil shall have a thickness to chord ratio allowing potential battery storage.	not relevant anymore	
ELTA-W-AF-03	The airfoil lift curve shall have a gradual stall behaviour.	*	✓

7
Stability and Control

This chapter discusses the assessment of the stability and control of the aircraft. In Sections 7.1 and 7.2 the functional and requirements analysis is performed respectively. The sizing of the horizontal tail and the determination of the optimal wing position is described in Section 7.3. In Section 7.4 the sizing of the vertical is described. The sizing of the control surfaces is then described in Section 7.5. The risk assessment that has been performed will be touched upon in Section 7.7. Lastly, in Section 7.8, the compliance matrix is shown.

7.1. Functional Analysis

There are multiple functions which are related to stability and control. These flow down from the functions **D.4**, **D.5** and **D.6** in the functional flow diagram. A top level function is that the aircraft should be safe to operate. Therefore, the aircraft should be first of all stable. Next to this, the aircraft should also be controllable. This is related to the three rotational movements, roll, yaw and, pitch, but it is also related to the ability to take-off and land, i.e. the ability to operate with crosswind and the use of flaps. This resulted in several functions, which are listed below.

- **ELTA-FUN-SC-01** - *The aircraft empennage should provide passive stability*;
- **ELTA-FUN-SC-02** - *The aircraft configuration should provide the pilot with the ability to control the aircraft*;
- **ELTA-FUN-SC-03** - *The aircraft should provide safe take-off and landing*.

Next to the specific stability and control functions two other relevant function is applicable.

- **ELTA-FUN-MAR-05** - *The aircraft should fly like a conventional aircraft*;
- **ELTA-FUN-W-02** - *The wing should provide roll control to the aircraft.*

7.2. Requirements

Based on the functional analysis, requirements related to stability and control were defined. These are listed below.

- **ELTA-SC-01** - *At a 45 degree angle of attack at least one-third of the rudder shall remain outside the wake of the horizontal stabiliser.* This requirement serves to comply with **ELTA-FUN-SC-02**, because this requirement is set up to be able to exit a spin, which is therefore related to controllability;
- **ELTA-SC-02** - *The aircraft shall have a take-off pitch angular acceleration of 12* deg/s^2. This requirement serves to comply with **ELTA-FUN-SC-03**. During the take-off roll, the aircraft should be able to pitch in order to take-off. The value for the pitch angular acceleration was based on common values for this type of aircraft;
- **ELTA-SC-03** - *The aircraft shall have a conventional tail.* This requirement serves to comply with **ELTA-MAR-09**.

Other relevant requirements are listed below.

- **ELTA-MAR-09** - *The system shall be able to educate a student to pilot a range of other aircraft.* This requirement serves to comply with **ELTA-FUN-MAR-05**;
- **ELTA-CS-FLT-03** - *During take-off conditions at sea level it shall be possible, using a favourable combination of controls, to roll the aeroplane from zero degrees of bank to an angle of 60 degrees within 5 seconds from initiation of roll.* Origin: CS-VLA;
- **ELTA-CS-FLT-04** - *During landing conditions at sea level it shall be possible, using favourable combination of controls, to roll the aeroplane from zero degrees of bank to an angle of 60 degrees within 4 seconds from initiation of roll.* Origin: CS-VLA;
- **ELTA-CS-FLT-05** - *The short period oscillation shall be heavily damped in stick free position.* Origin: CS-VLA;
- **ELTA-CS-FLT-06** - *The short period oscillation shall be heavily damped in stick fixed position.* Origin: CS-VLA;
- **ELTA-CS-FLT-07** - *The Dutch roll shall be damped to 1/10 amplitude in 7 cycles in stick free position.* Origin: CS-VLA;
- **ELTA-CS-FLT-08** - *The Dutch roll shall be damped to 1/10 amplitude in 7 cycles in stick fixed position.* Origin: CS-VLA;
- **ELTA-CS-FLT-10** - *The aircraft shall be controllable on the ground up until a maximum cross wind of 10 kts from a 90 degree angle.* Origin: CS-VLA;
- **ELTA-CS-FLT-12** - *The elevator shall support maximum upward/downward deflection at speed VA.* Origin: CS-VLA;

- **ELTA-CS-FLT-13** - *The elevator shall support one-third maximum upward/downward deflection at speed VD.* Origin: CS-VLA;
- **ELTA-CS-FLT-19** - *The aircraft shall be longitudinally, laterally and directionally stable*;
- **ELTA-W-02** - *The aircraft shall have an maximum lift coefficient of at least 1.8 in a take-off configuration.* This requirement serves to comply with **ELTA-FUN-W-01**, which can be found in Section 6.1.1, with the design point for limiting configuration considered;
- **ELTA-W-03** - *The aircraft shall have an maximum lift coefficient of at least 2 in a landing configuration.* This requirement serves to comply with **ELTA-FUN-W-01**, which can be found in Section 6.1.1;
- **ELTA-W-CONT-01** - *The ailerons shall provide the aircraft with the ability to roll.* This requirement stems from the function **ELTA-FUN-W-02**;
- **ELTA-W-CONT-02** - *The high lift devices shall provide the ability to increase the $C_{L_{max}}$ of the wing.* This requirement stems from **ELTA-FUN-W-01**, which can be found in Section 6.1.1.

7.3. Horizontal Tail Sizing and Wing position

This section explains the procedure for sizing the horizontal tail surface area and determining the optimal wing position for stability and control.

First, the type of horizontal tail had to be determined. There are three types of horizontal tails: a full moving tail, an adjustable tail and a fixed tail. The full moving tail was deemed to be unfeasible, because of its structural complexity and therefore the relative high weight. In the end an adjustable tail was chosen, since this will result in a lower horizontal tail surface compared to the fixed tail, which will be discussed in Section 7.3.2. This means the horizontal tail will be adjusted to trim the aircraft, and that the elevator will be used to pitch the aircraft.

7.3.1. Loading Diagram

To be able to assess the stability and controllability of the aircraft, it is needed to determine the centre of gravity range. This is done by creating the loading diagram. The starting point of the loading diagram is the operational empty weight (OEW) and the corresponding centre of gravity (cg). To calculate this, the aircraft is split up into two parts, the fuselage group (f) and the wing group (w). The cg at the OEW is then calculated using Equation (7.1). It should be noted that x coordinates indicate the distance from the nose of the aircraft.

$$x_{cg,OEW} = \frac{W_f \cdot x_{cg,f} + W_w \cdot x_{cg,w}}{W_{OE}} \tag{7.1}$$

Next, two loading procedures are considered, first the battery loading and then the payload loading (two pilots or one pilot and one additional battery) or first the payload loading and then the battery loading. However only the first loading procedure will influence the stability during flight, since the aircraft will only be able to fly when the batteries inserted in the aircraft. The second loading procedure is only relevant for ground stability. The centres of gravity are calculated using the general equation for the centre of gravity, Equation (7.2).

$$x_{cg} = \frac{\sum W_i \cdot x_{cg,i}}{\sum W_i} \tag{7.2}$$

These centres of gravity were then normalized by dividing them by the mean aerodynamic chord.

The loading diagram was constructed using the values listed in Table 7.1. From the loading diagram, shown in Figure 7.1, the minimum and maximum $\bar{x}_{cg}$ could be obtained. The second loading procedure is indicated with dashed lines. For contingency management a 5%MAC margin is added to the centre of gravity range.

Table 7.1: Loading diagram input parameters

Parameter	Symbol	Value	Unit	Assumption
Fuselage group weight	W_f	265.2	kg	-
Fuselage group centre of gravity	$x_{cg,f}$	2.73	m	-
Wing weight	W_w	127.0	kg	-
Wing centre of gravity	$x_{cg,w}$	3.07	m	-
Battery weight	W_{bat}	292.0	kg	-
Battery centre of gravity	$x_{cg,bat}$	2.68	m	-
Payload weight	W_{PL}	200	kg	-
Payload centre of gravity	$x_{cg,PL}$	1.5	m	-

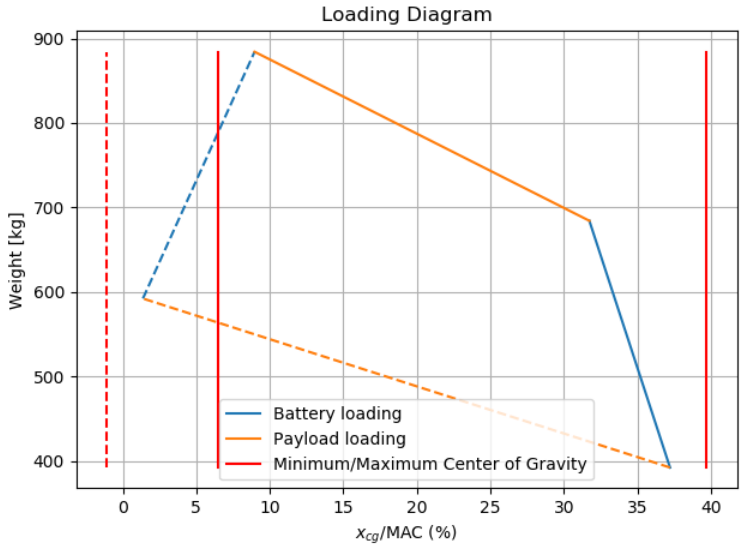

Figure 7.1: Loading diagram

7.3.2. Scissor Plot

Next, the scissor plot had to be created to be able to determine the required horizontal tail surface area. It contains two curves, the stability- and controllability curve. The stability curve describes the maximum centre of gravity allowed (i.e. the neutral point (x_{np})), to provide stability. The controllability curve describes the minimum centre of gravity allowed to be able to trim the aircraft. The functions that describe the curves will be explained below. Based on a centre of gravity range, a minimum required horizontal tail surface area could be determined using the scissor plot. On page 52 Table 7.2 can be found, which presents all the input parameters for the formulas used for the scissor plot. The scissor plot itself is presented in Figure 7.6.

Stability

For stability, Equation (7.3) [23] describes the maximum position of the centre of gravity by adding a stability margin ($S.M.$) to the equation that expresses the stick-fixed neutral point as function of the horizontal tail size. The bar above the x-locations indicates that it is normalised by dividing by the mean aerodynamic chord (MAC). The parameters in Equation (7.3) will be explained below.

$$\bar{x}_{cg} = \bar{x}_{ac} + \frac{C_{L\alpha_h}}{C_{L\alpha_{A-h}}}\left(1 - \frac{d\varepsilon}{d\alpha}\right)\frac{S_h l_h}{S\bar{c}}\left(\frac{V_h}{V}\right)^2 - S.M. \tag{7.3}$$

Aerodynamic centre

The aerodynamic centre of the aircraft less tail is described by Equation (7.4) [24].

$$\bar{x}_{ac} = (\bar{x}_{ac})_{wf} + (\bar{x}_{ac})_n = \left[(\bar{x}_{ac})_w + (\bar{x}_{ac})_{f1} + (\bar{x}_{ac})_{f2}\right] + (\bar{x}_{ac})_n \tag{7.4}$$

The location for the wing aerodynamic centre ($(\bar{x}_{ac})_w$) is assumed to be at 25% of the MAC. The fuselage contribution consists of two parts. The first fuselage contribution to the location of the aerodynamic centre ($(\bar{x}_{ac})_{f1}$) is described by Equation (7.5) [23]. Furthermore, there is no second fuselage contribution ($(\bar{x}_{ac})_{f2}$), because $\Lambda_{c/4} = 0$ (therefore $(\bar{x}_{ac})_{f2} = 0$) [23]. Finally, the aircraft has no nacelles, therefore $(\bar{x}_{ac})_n = 0$.

$$(\bar{x}_{ac})_{f1} = -\frac{1.8}{C_{L\alpha_{A-h}}}\frac{b_f h_f l_{f_n}}{S\bar{c}} \tag{7.5}$$

Lift rate coefficients

The tail lift rate coefficient is described by Equation (7.6) [15]. The airfoil efficiency coefficient (η) can be assumed constant and equal to 0.95. β can be calculated using Equations (7.7) to (7.9).

$$C_{L\alpha_h} = \frac{2\pi A_h}{2 + \sqrt{4 + \left(\frac{A_h \beta}{\eta}\right)^2\left(1 + \frac{\tan^2 \Lambda_{0.5c_h}}{\beta^2}\right)}} \tag{7.6}$$

$$V_h = \frac{V_h}{V} V \quad (7.7) \qquad M_h = \frac{V_h}{a} \quad (7.8) \qquad \beta = \sqrt{1 - M_h^2} \quad (7.9)$$

The lift rate coefficient of the aircraft less tail is described in Equation (7.10) [24]. $C_{L_{\alpha_w}}$ is the wing lift rate coefficient and S_{net} is S minus the projection of the central wing part inside the fuselage.

$$C_{L_{\alpha_{A-h}}} = C_{L_{\alpha_w}} \left(1 + 2.15 \frac{b_f}{b}\right) \frac{S_{net}}{S} + \frac{\pi}{2} \frac{b_f^2}{S} \quad (7.10)$$

Downwash

The downwash gradient effect of the wing on the tail is described in Equation (7.11) [24]. Here, the K_ε terms account for the wing sweep angle (Λ), which is evaluated at quarter chord ($\Lambda_{0.25c}$) and which can be seen in Equations (7.12) and (7.13) [24]. Furthermore, $r = 2l_h/b$ and m_{tv} is the distance between the horizontal tail and the vortex shed plane (which can be approximated with the plane from the wing root chord) divided by $b/2$. See Figure 7.2 for a visualisation of these parameters.

$$\frac{d\varepsilon}{d\alpha} = \frac{K_{\varepsilon_\Lambda}}{K_{\varepsilon_{\Lambda=0}}} \left(\frac{r}{r^2 + m_{tv}^2} \frac{0.4876}{\sqrt{r^2 + 0.6319 + m_{tv}^2}} + \left[1 + \left(\frac{r^2}{r^2 + 0.7915 + 5.0734 m_{tv}^2}\right)^{0.3113}\right] \left\{1 - \sqrt{\frac{m_{tv}^2}{1 + m_{tv}^2}}\right\} \right) \frac{C_{L_{a_w}}}{\pi A} \quad (7.11)$$

$$K_{\varepsilon_\Lambda} = \frac{0.1124 + 0.1265\Lambda + 0.1766\Lambda^2}{r^2} + \frac{0.1024}{r} + 2 \quad (7.12)$$

$$K_{\varepsilon_{\Lambda=0}} = \frac{0.1124}{r^2} + \frac{0.1024}{r} + 2 \quad (7.13)$$

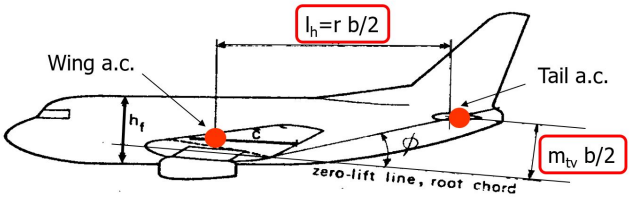

Figure 7.2: Visual representation of the parameters used for the determination of wing downwash gradient effect. [24]

Other considerations

The tail-wing speed ratio ($(V_h/V)^2$) is 0.85 for fuselage mounted stabilisers. Furthermore, it is assumed that l_h can be calculated using Equation (7.14) [24].

$$l_h = x_{tail} - x_{np} \quad (7.14)$$

Finally, the stability margin had to be determined. Since the aircraft will have reversible commands, the stick-free stability is more limiting than the stick-fixed stability. As stated in [26], the stick-free stability neutral point (maximum centre of gravity) is 2-5% ahead of the stick-fixed neutral point. Therefore, the stick-free maximum centre of gravity could be calculated using Equation (7.15). In addition the stability margin is set to 5%MAC, to account for minimum control force limits.

$$\bar{x}_{cg_{free}} = 0.95 \bar{x}_{cg_{fixed}} - S.M. \quad (7.15)$$

Controllability

For controllability the trim equation is used as described in Equation (7.16) [24]. The parameters in this equation will be explained below.

$$\bar{x}_{cg} = \bar{x}_{ac} - \frac{C_{m_{ac}}}{C_{L_{A-h}}} + \frac{C_{L_h}}{C_{L_{A-h}}} \frac{S_h l_h}{S\bar{c}} \left(\frac{V_h}{V}\right)^2 \quad (7.16)$$

Pitching moment

The zero lift pitching moment coefficient of the aircraft without tail is given by Equation (7.17) [23]. The contributions of the wing, flaps and fuselage are described by Equations (7.18), (7.19) and (7.22), respectively. Again, the aircraft has no nacelles therefore the corresponding term will equal zero.

$$C_{m_{\mathrm{ac}}} = C_{m_{\mathrm{ac_w}}} + \Delta_f C_{m_{\mathrm{ac}}} + \Delta_{fus} C_{m_{\mathrm{ac}}} + \Delta_{\mathrm{nac}} C_{m_{\mathrm{ac}}} \tag{7.17}$$

In Equation (7.18), $C_{m_{0,airfoil}}$ is the airfoil's zero lift pitching moment coefficient.

$$C_{m_{\mathrm{ac_w}}} \approx C_{m_{0,\mathrm{airfoil}}} \left(\mathrm{A}\cos^2\Lambda / (\mathrm{A} + 2\cos\Lambda)\right) \tag{7.18}$$

In Equation (7.19), the flap coefficients (μ_i) are determined with Figures 7.3 to 7.5. The aircraft will have plain flaps, which have an deflection angle of $40°$ and have an flap to wing chord ratio of 0.2. Since plain flaps are considered, it is assumed that the chord extension due to flap deployment is relatively small and therefore $c' = c$. This was then used to determine μ_1. For the determination of μ_2 and μ_3, it was found that the flap to wing span ratio will vary between 0.25 and 0.35. This range was found by calculating the flap span for different wing surfaces area (and therefore different wing chord and span), ranging from $7m^2$ to $15m^2$. Given the taper ratio of 0.45, a linear interpolation for μ_1 and μ_2 was done. This resulted in Equations (7.20) and (7.21). When the final value of b_{fl}/b is known, it will be checked whether this assumption was valid.

Next, C_L is the wing lift coefficient at landing when all flaps are deployed and $\Delta C_{l_{\max}}$ is the airfoil lift coefficient increase due to flap extension at landing condition (Approach lift coefficient minus airfoil maximum lift coefficient), which is explained in Section 7.5.2.

$$\Delta_f C_{m_{\mathrm{ac}}} = \mu_2 \left\{ -\mu_1 \Delta C_{l_{\max}} \frac{c'}{c} - \left[C_L + \Delta C_{l_{\max}} \left(1 - \frac{S_{wf}}{S}\right)\right] \frac{1}{8} \frac{c'}{c} \left(\frac{c'}{c} - 1 \right) \right\} + 0.7 \frac{A}{1 + 2/A} \mu_3 \Delta C_{l_{\max}} \tan\Lambda_{1/4} \tag{7.19}$$

$$\mu_2 = 1.2 \frac{b_{fl}}{b} + 0.13 \tag{7.20}$$

$$\mu_3 = 0.06 \frac{b_{fl}}{b} + 0.0335 \tag{7.21}$$

Finally, in Equation (7.22), b_f, h_f and l_f are the fuselage width, height, and length, respectively. C_{L_0} is the flapped lift coefficient at zero lift angle of attack and $C_{L_{\alpha_{A-h}}}$ is computed using Equation (7.10) using approach speed.

$$\Delta_{fus} C_{m_{\mathrm{ac}}} = -1.8 \left(1 - \frac{2.5 b_f}{l_f}\right) \frac{\pi b_f h_f l_f}{4 S \bar{c}} \frac{C_{L_0}}{C_{L_{\alpha_{A-h}}}} \tag{7.22}$$

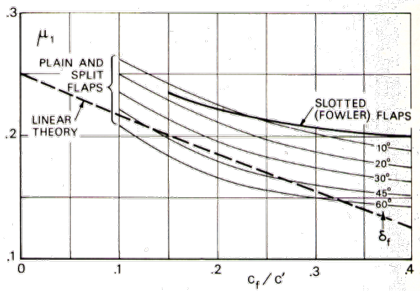

Figure 7.3: μ_1 determination graph. [23]

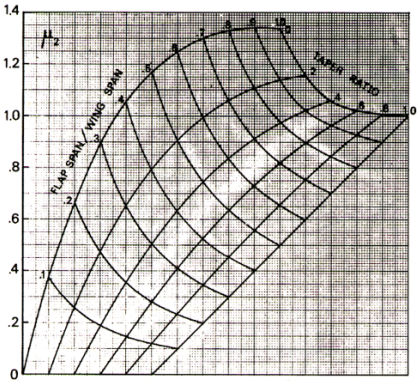

Figure 7.4: μ_2 determination graph. [23]

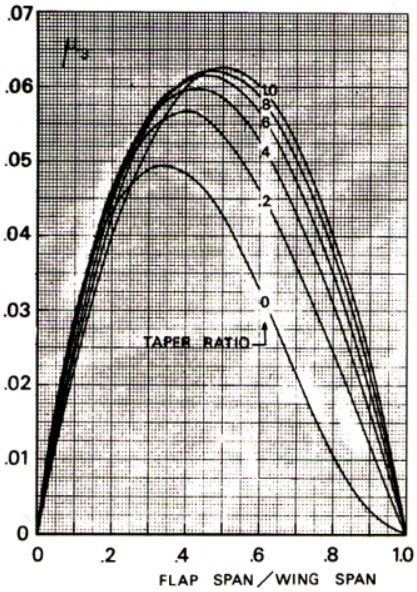

Figure 7.5: μ_3 determination graph. [23]

Lift coefficients

The lift coefficients need to be evaluated during landing conditions [24]. The lift coefficient of the horizontal tail depends on the type of the horizontal tail. A lower C_{L_h} results in a higher control curve slope (less negative) and

therefore a smaller horizontal tail surface. Since an adjustable tail is considered C_{L_h} will have a value of -0.8 [24]. The value for the lift coefficient of the aircraft less tail is assumed to be equal to the maximum required lift coefficient, as stated in **ELTA-W-03**. This is the lift coefficient when the flaps are fully deployed, which is the case during landing conditions.

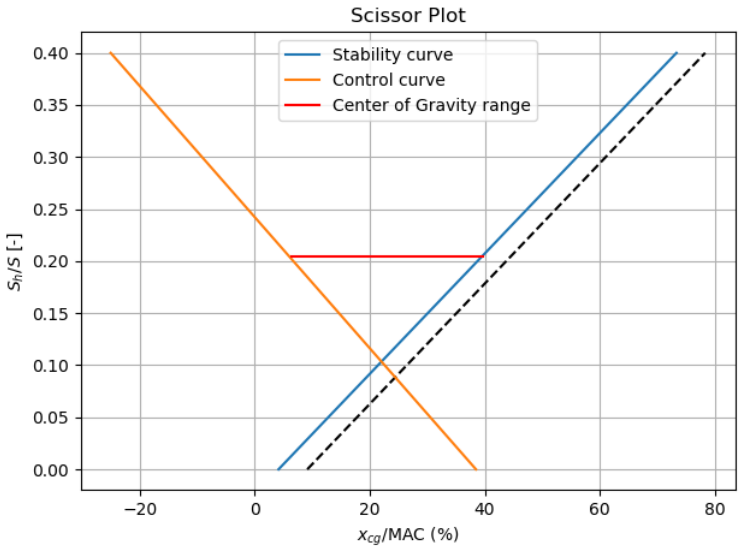

Figure 7.6: Scissor plot

Table 7.2: Scissor plot input parameters

Parameter	Symbol	Value	Unit	Assumption
Mean aerodynamic chord	$\bar{c}$; MAC	1.26	m	-
Distance nose - leading edge mean aerodynamic chord	x_{lemac}	2.37	m	-
Aerodynamic centre wing	$(\bar{x}_{ac})_w$	25	$\%MAC$	$(\bar{x}_{ac})_w$ is assumed to be at 25%MAC
Mean diameter (or width) fuselage	b_f	1.05	m	-
Height fuselage	h_f	1.21	m	-
Distance nose - leading edge wing at the fuselage end	l_{fn}	2.29	m	-
Wing surface area	S	14.7	m^2	-
Aspect ratio horizontal tail	A_h	3	$-$	-
Tail-wing speed ratio	$(V_h/V)^2$	0.85	$-$	Fuselage mounted stabilisers
Cruise speed	V	50	m/s	-
Cruise speed of sound	a	336.8	m/s	-
Airfoil efficiency coefficient	η	0.95	$-$	Assumed constant and equal to 0.95
Half chord sweep angle horizontal tail	$\Lambda_{0.5c_h}$	6.70	deg	-
Aspect ratio wing	A	10.1	$-$	-
Wing lift rate coefficient	$C_{L_{\alpha_w}}$	4.80	$1/rad$	-
Wing span	b	12.2	m	-
Net wing area	S_{net}	12.9	m^2	-
Quarter chord sweep angle wing	$\Lambda_{0.25c}$	0	deg	-
Distance horizontal tail - vortex shed plane	m_{tv}	0.18	$-$	-
Tail arm	l_h	5.90	m	Assumed to be $x_{tail} - x_{np}$
Stability margin	$S.M.$	0.05	$-$	To account for minimum control force limits
Airfoil zero lift moment coefficient	$C_{m_{0,\text{airfoil}}}$	-0.1	$-$	-
Flap coefficient 1	μ_1	0.3	$-$	$c' = c$
Flap span	b_{fl}	3.48	m	-

Airfoil lift coefficient increase at landing	$\Delta C_{l_{\max}}$	1.2	–	Explained in Section 7.5.2
Chord ratio (extended flap/clean)	c'/c	1	–	$c' = c$
Reference wing flapped surface area	S_{wf}	9.14	m^2	-
Fuselage length	l_f	9.24	m	-
Flapped wing lift coefficient at zero AoA	C_{L_0}	1.0	–	-
Aircraft less tail lift coefficient at landing	$C_{L_{A-h}}$	2.0	–	Maximum lift coefficient

7.3.3. Results

To determine the the lowest possible horizontal surface area, the loading diagram was made for different longitudinal positions of the wing. This resulted in different most forward and most aft centre of gravity for the different wing positions, which is shown in Figure 7.7.

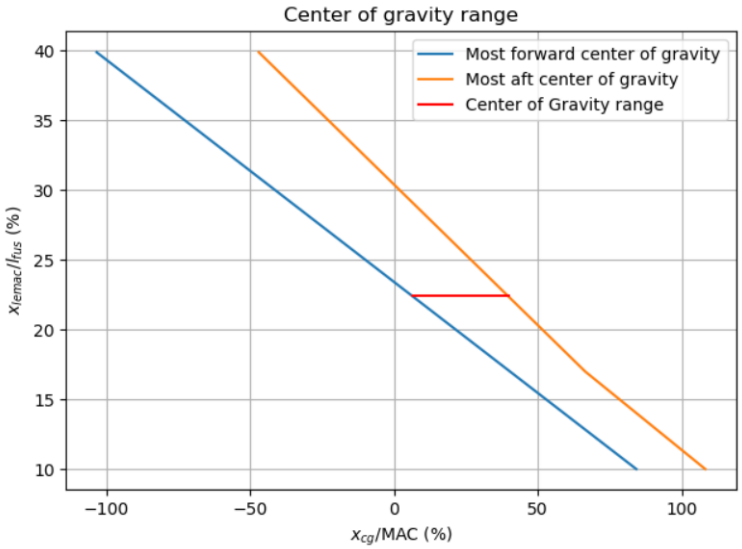

Figure 7.7: Centre of gravity range for different wing positions

For every wing position the horizontal surface area was determined using the scissor plot, while taking into account an updated tail arm. This resulted is a minimum horizontal surface area with a corresponding wing position, shown in Table 7.3.

Table 7.3: Results horizontal tail sizing and wing position

Parameter	Symbol	Value	Unit
Wing position	x_{wing}	2.70	m
Most forward centre of gravity	$x_{cg,min}$	2.45	m
Most aft centre of gravity	$x_{cg,max}$	2.87	m
Horizontal tail surface area	S_h	3.28	m^2

7.3.4. Verification & Validation

Verification

As a first step in the verification process unit tests are performed on the loading diagram and scissor plot tools. For the loading diagram tool, the minimum and maximum centre of gravity were calculated using both the tool and an excel file, for the same set of input parameters. These outcomes were then compared and since the results were the same, the unit test was successful. For the scissor plot tool, the minimum horizontal tail surface required was calculated using both the tool and an excel file, for a certain centre of gravity range and the same set of input parameters. These outcomes were then compared and since the results were the same, also this unit test was successful.

An integration test was performed on the calculation of the minimum horizontal tail surface determination, since this is done by integrating both the loading diagram and scissor plot tool. First the results of the integrated tool,

for a certain set of input parameters, where used as input for both the loading diagram and scissor plot tool, to check whether this would result in the same outputs. For the loading diagram tool, this means that the resulting wing position was put into the tool and it was checked whether this would indeed result in the right minimum and maximum centre of gravity. This was indeed the case. For the scissor plot tool, the resulting maximum and minimum centre of gravity where used as input. It was checked whether this resulted in the right minimum horizontal surface required. This was indeed the case. Secondly, the loading diagram plot, scissor plot and wing shift plot were created. It was checked whether these plots indeed indicate the right centre of gravity range (for all plots) and whether the horizontal tail surface is indeed the lowest possible (using the scissor plot). This was indeed the case for the different plots. Therefore it was concluded that the integration test was successful.

Validation

The validation of this tool will be done using simulation software and eventually during a flight test. This process is however part of the next phase, which is post-DSE. This will be explaned in Section 7.6.

7.4. Vertical Tail Sizing

7.4.1. Method

Vertical tail sizing can be done by using Figure 7.8, with on the x-axis the weathervane stability (C_{n_β}), split up in a fuselage (f), wing configuration (i), and propeller (p) component. These stability considerations are driving the vertical tail sizing for a tractor aircraft.

$C_{n_{\beta f}}$ could be calculated using Equation (7.23) [23]. This equation is valid for aircraft where $l_f/h_{f_{max}} > 3.5$, which is the case for this aircraft. k_β could be calculated using Equation (7.24) [23]. The dimensions used in these formulae are visualised in Figure 7.9.

$$C_{n_{\beta f}} = -k_\beta \frac{S_{fs} l_f}{Sb} \left(\frac{h_{f_1}}{h_{f_2}}\right)^{1/2} \left(\frac{b_{f_2}}{b_{f_1}}\right)^{1/3} \tag{7.23}$$

$$k_\beta = 0.3\frac{l_{cg}}{l_f} + 0.75\frac{h_{f_{\max}}}{l_f} - 0.105 \tag{7.24}$$

$C_{n_{\beta i}}$ is 0.024 for low wing aircraft. And finally $C_{n_{\beta p}}$ could be calculated using Equation (7.25). In this equation, B_p is the number of blades per propeller, l_p is the distance between the propeller plane and the aircraft centre of gravity, which could be calculated using Equation (7.26), and D_p is the propeller disk diameter. The term within the summation had to be evaluated for every propeller.

$$C_{n_{\beta p}} = -0.053 B_p \sum \frac{l_p D_p^2}{Sb} \tag{7.25}$$

$$l_p = x_{cg} - x_p \tag{7.26}$$

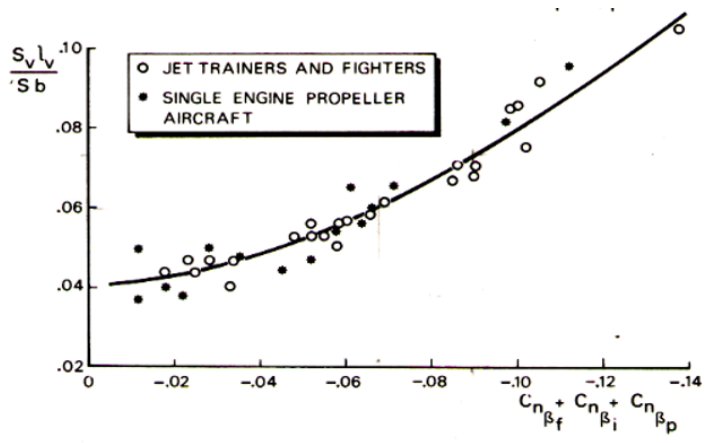

Figure 7.8: Vertical tail sizing graph for directional stability of fuselage mounted engine aircraft. [23]

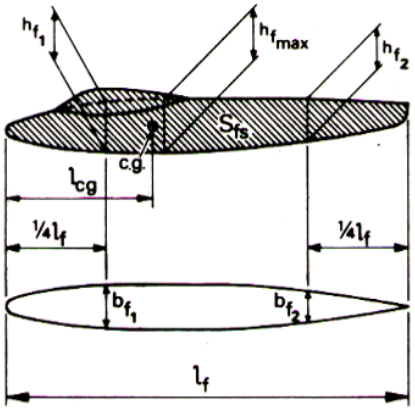

Figure 7.9: Fuselage dimensions. [23]

7.4.2. Results

The input parameters can be found in Table 7.4. These parameters are used to determine the vertical tail surface area.

Table 7.4: Vertical tail sizing input parameters.

Parameter	Symbol	Value	Unit	Assumption
Distance nose to cg	l_{cg}	2.20	m	-
Fuselage length	l_f	9.24	m	Estimated using CAD drawing
Maximum height fuselage	$h_{f_{\max}}$	1.21	m	Estimated using CAD drawing
Lateral surface area fuselage	S_{fs}	5.26	m^2	Estimated using CAD drawing
Fuselage nose height	h_{f_1}	1.15	m	Estimated using CAD drawing
Fuselage tail height	h_{f_2}	0.31	m	Estimated using CAD drawing
Fuselage nose width	b_{f_1}	0.96	m	Estimated using CAD drawing
Fuselage nose width	b_{f_2}	0.24	m	Estimated using CAD drawing
Number of blades per propeller	B_p	2.5	-	The average of the two propellers
First propeller disk diameter	D_{p_1}	1.8	m	-
Second propeller disk diameter	D_{p_2}	1.8	m	-
First propeller plane location	x_{p_1}	0.15	m	Estimated using CAD drawing, assumed to be the same for both propellers
Second propeller plane location	x_{p_2}	0.15	m	Estimated using CAD drawing, assumed to be the same for both propellers
Wing surface area	S	14.65	m^2	-
Wing span	b	12.16	m	-
Wing configuration stability component	$C_{n_{\beta i}}$	0.024	-	Low wing configuration
Vertical tail arm	l_v	5.95	m	$l_v = x_{tail} - x_{cg}$, where for x_{cg}, the maximum is taken, since this will result in the highest area, and therefore an extra margin is implemented

This resulted in a vertical tail surface area (S_v) of 1.22 m^2 and a C_{n_β} of -0.011.

7.4.3. Verification & Validation

Verification

First a unit test on the tool that calculates the C_{n_β} was done. The output of the tool was compared with the output of an excel sheet. Since the outputs were the same, it was concluded that the unit test was successful.

Next, the output of the tool should be negative and should be in the range of the horizontal axis of Figure 7.8.

Validation

The validation of this tool will be done using simulation software and eventually during a flight test. This process is however part of the next phase, which is post-DSE. This will be explaned in Section 7.6.

7.5. Control Surfaces Sizing

This sections explains the procedure for sizing the control surfaces, which are the aileron, flaps, elevator and the rudder. The layout of the wing planform with the control surfaces and the relevant parameters can be seen in Figure 7.10.

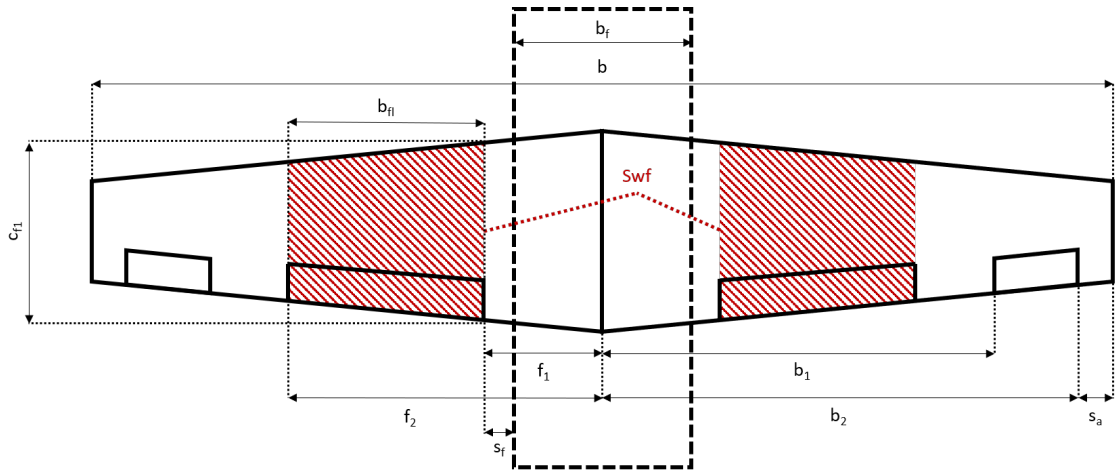

Figure 7.10: Wing Layout

7.5.1. Aileron Sizing

The ailerons are used to roll an aircraft as required by **ELTA-W-CONT-01**. Therefore, the sizing of the ailerons is driven by requirement **ELTA-CS-FLT-03** and **ELTA-CS-FLT-04**. These roll requirements could be transformed into a required roll rate, using Equation (7.27) [14]. For contingency management a margin of 10% was added to this value.

$$p_{req} = \frac{\Delta\phi}{\Delta t} \tag{7.27}$$

The ailerons should be sized such, that this roll rate can be achieved. The roll rate generated by the ailerons could be calculated using Equation (7.28) [14], where $C_{l_{\delta_a}}$ is the roll authority, C_{l_p} the roll damping coefficient, δ_a the aileron deflection angle, V the airspeed and b the wing span.

$$p = -\frac{C_{l_{\delta_a}}}{C_{l_p}} \delta_a \left(\frac{2V}{b}\right) \tag{7.28}$$

Since the aircraft has a straight tapered wing, the roll damping coefficient could be calculated using Equation (7.29) [14], where c_{l_α}, c_{d0} is the wing lift curve slope, c_{d0} the wing zero lift drag, C_R the wing root chord, S the wing surface area and λ the wing taper ratio.

$$C_{l_p} = -\frac{\left(c_{l_\alpha} + c_{d0}\right) \cdot C_R b}{24S} [1 + 3\lambda] \tag{7.29}$$

The roll authority could be calculated using Equation (7.30) [14], where $c_{l_{\delta_a}}$ is the change in the airfoil's lift coefficient with aileron deflection, b_1 the starting point of the aileron and b_2 is the end point of the aileron, as indicated in Figure 7.10.

$$C_{l_{\delta_a}} = \frac{c_{l_{\delta_a}} C_R}{Sb} \left[\left(b_2^2 - b_1^2\right) + \frac{4(\lambda - 1)}{3b} \left(b_2^3 - b_1^3\right) \right] \tag{7.30}$$

The aileron will be most effective when it is located as far as possible from the centre line of the aircraft, which will result in a smaller aileron. Therefore, the aileron end (b_2) will be located at the wing tip, taking into account a small spacing, indicated as s_a in Figure 7.10. As starting point of the sizing, a first estimation of b_1 was made. With these values, the roll rate was calculated. When the roll rate was to low, the aileron size was increased (decreasing b_1) and vice versa, until the size of the aileron converged.
The input values used are listed in Table 7.5.

Table 7.5: Aileron sizing input parameters

Parameter	Symbol	Value	Unit	Assumption
Take-off bank angle	$\Delta\phi_{TO}$	60	deg	-
Take-off roll time	Δt_{TO}	5	s	-
Landing bank angle	$\Delta\phi_{L}$	60	deg	-
Landing roll time	Δt_{L}	4	s	-
Aileron deflection angle	δ_a	20	deg	Based on literature [14]
Wing lift rate coefficient	c_{l_α}	4.80	$1/rad$	-
Wing take-off zero lift drag	$c_{d0_{TO}}$	0.018	$-$	-
Wing landing zero lift drag	$c_{d0_{L}}$	0.04	$-$	-
Wing root chord	C_R	1.66	m	-
Wing span	b	12.16	m	-
Wing surface area	S	14.65	m^2	-
Wing taper ratio	λ	0.45	$-$	-
Change in airfoil's lift coefficient with aileron deflection	$c_{l_{\delta_a}}$	2.7	$1/rad$	Estimated using Xfoil [27]
Aileron start	b_1	4.9	m	-
Aileron end	b_2	5.88	m	-

7.5.2. Flap Sizing

The flaps should increase the maximum lift coefficient ($C_{L_{max}}$) as required by **ELTA-W-CONT-02**. For this aircraft plain flaps will be used, which will have a maximum deflection angle of 40° [1]. The required increase in maximum lift coefficient could be calculated using Equation (7.31), where $C_{L_{max,req}}$ is the required maximum lift coefficient (**ELTA-W-03**) and $C_{L_{max,wing}}$ is the maximum lift coefficient of the clean wing (**ELTA-W-01**, Section 6.1.2). A margin of 10% is added for contingency management.

$$\Delta C_{L_{max}} = C_{L_{max,req}} - C_{L_{max,wing}} \tag{7.31}$$

The required flapped surface area could then be calculated using Equation (7.32) [15], where Λ_{hinge_line} is the sweep angle at the hinge line and $\Delta C_{l_{max}}$ is the airfoil maximum lift coefficient increase with flap deflection. The value for $\Delta C_{l_{max}}$ was taken from the $C_L - \alpha$ curve of the NACA 4415 airfoil with a split flap [28]. However, this aircraft has an plain flap. Based on data from [29] is was concluded that a plain flap will have a 4% lower $\Delta C_{l_{max}}$ compared to a split flap.

$$\frac{S_{wf}}{S} = \frac{\Delta C_{L_{max}}}{0.9\Delta C_{l_{max}} \cos\Lambda_{hinge\_line}} \tag{7.32}$$

Since the chord of the wing at the root is larger than the chord at the wing tip, the flaps will be more effective when they are positioned closer to the root (larger S_{wf}, for the same flap span), which will result in a smaller flap. Therefore it was assumed that the flap will start at the end of the fuselage, taking into account a small spacing, indicated with s_f in Figure 7.10. The span of one the flaps (b_{fl}) could then be calculated by solving Equation (7.33), where Λ_{LE} and Λ_{TE} are the leading edge and trailing edge sweep angles, respectively. The other parameters can be found in Figure 7.10.

$$\frac{Swf}{2} = c_{f_1} b_{fl} - \frac{1}{2} b_{fl}^2 tan\Lambda_{LE} + \frac{1}{2} b_{fl}^2 tan\Lambda_{TE} \tag{7.33}$$

The end of the flap could then be calculated using Equation (7.34).

$$f_2 = f_1 + b_{fl} \tag{7.34}$$

Next to the increase in maximum lift coefficient, the zero lift angle of attack will change as well. This change could be calculated using Equation (7.35), where $(\Delta\alpha_{0l})_{airfoil}$ depends on the type of flap and deflection angle. It was determined using the $C_L - \alpha$ curve of the NACA 4415 airfoil [28].

$$\Delta\alpha_{0L} = (\Delta\alpha_{0l})_{airfoil} \frac{Swf}{S} \cos\Lambda_{hinge\_line} \tag{7.35}$$

The input values used are listed in Table 7.6.

Table 7.6: Flap sizing input parameters

Parameter	Symbol	Value	Unit	Assumption
Required maximum lift coefficient	$C_{L_{max,req}}$	2.0	–	-
Clean wing maximum lift coefficient	$C_{L_{max,wing}}$	1.39	–	-
Airfoil lift coefficient increase with flap deflection	$\Delta C_{l_{max}}$	1.2	–	Based on the $C_L - \alpha$ curve of the NACA 4415 [28] and taking into account a correction of 4% for the plain flap [29]
Hinge line sweep	Λ_{hinge_line}	-3.6	deg	-
Leading edge sweep	Λ_{LE}	1.6	deg	-
Trailing edge sweep	Λ_{TE}	-4.9	deg	-
Flap start	f_1	0.58	m	-
Chord length at flap start	c_{f_1}	1.57	m	-
Change in airfoil's zero lift angle of attack with flap deflection	$(\Delta\alpha_{0l})_{airfoil}$	-15	deg	Based on the $C_L - \alpha$ curve of the NACA 4415 [28]

7.5.3. Elevator Sizing

The elevator provides the aircraft the ability to pitch. First of all, the aircraft should be able to rotate during take-off, with a rotational acceleration described in **ELTA-SC-02**. It is assumed that the span of the elevator is equal to the span of the horizontal tail.

First the lift produced by the wing and fuselage, the drag and the moment around the aerodynamic centre during take-off condition had to be calculated. This is done using Equations (7.36) to (7.38) [30]. $C_{m_{ac_{wf}}}$ was calculated using Equation (7.17) and the parameters listed in Table 7.2. The value of $\Delta C_{l_{max}}$ is however slightly lower, since the flaps are not fully deployed during take-off conditions. Since the total wing $\Delta C_{L_{max}}$ is 10% lower, it is assumed that the value for the airfoil is 10% lower as well.

$$L_{wf} \cong \frac{1}{2}\rho_{TO} V_{TO}^2 C_{L_{TO}} S_{ref} \tag{7.36}$$

$$D_{TO} = \frac{1}{2}\rho_{TO} V_{TO}^2 C_{D_{TO}} S_{ref} \tag{7.37}$$

$$M_{ac_{wf}} = \frac{1}{2}\rho_{TO} V_{TO}^2 C_{m_{ac_{wf}}} S_{ref} \bar{C} \tag{7.38}$$

Next, the linear acceleration during take-off was calculated using Equation (7.40) [30]. In this equation N is calculated using Equation (7.39) [30].

$$N = W - L_{TO} \approx W - L_{wf} \tag{7.39}$$

$$ma = T - D - \mu N \tag{7.40}$$

The following step was to calculate the pitching moments during the take-off around the main landing gear (mg). These are the weight pitching moment, Equation (7.41) [30], the drag pitching moment, Equation (7.42) [30], the thrust pitching moment, Equation (7.43) [30], the wing and fuselage lift pitching moment, Equation (7.44) [30], and finally the linear acceleration pitching moment, Equation (7.45) [30].

$$M_W = W_{TO}\left(x_{mg} - x_{cg}\right) \tag{7.41}$$

$$M_D = D\left(z_D - z_{mg}\right) \tag{7.42}$$

$$M_T = T\left(z_T - z_{mg}\right) \tag{7.43}$$

$$M_{L_{wf}} = L_{wf}\left(x_{mg} - x_{ac_{wf}}\right) \tag{7.44}$$

$$M_a = ma\left(z_{cg} - z_{mg}\right) \tag{7.45}$$

Using the calculated pitching moments, the required lift produced by the horizontal tail could be calculated using Equation (7.46) [30]. In this equation I_{yymg} is the moment of inertia around the pitching axis evaluated around the main landing gear. The value of I_{yymg} is estimated using an estimation of the radius of gyration, which was calculated using Equation (7.47) [31]. In this equation, l_a is the aircraft length and C is a constant which depends on the type of aircraft. The moment of inertia is then calculated using Equation (7.48). Finally the moment of inertia should be evaluated around the main gear, which is done using Equation (7.49).

$$L_h = \frac{M_{L_{wf}} + M_{ac_{wf}} + M_a - M_W + M_D - M_T - I_{yymg}\ddot{\theta}}{x_{ac_h} - x_{mg}} \tag{7.46}$$

$$k_y = Cl_a \quad (7.47) \qquad I_{yy} = k_y^2 W_{TO}/g \quad (7.48) \qquad I_{yymg} = I_{yy} + \left(z_{cg} - z_{mg}\right)^2 W_{TO}/g \quad (7.49)$$

The required horizontal tail lift coefficient at take-off conditions was then calculated using Equation (7.50) [30].

$$C_{L_h} = \frac{2L_h}{\rho_{TO} V_{TO}^2 S_h} \quad (7.50)$$

The elevator angle of attack effectiveness was then calculated using Equation (7.52) [30], where α_h could be calculated using Equation (7.51) (at take-off, the $\alpha = 0$). This value needed to be less than 1, since there exists no elevator which can satisfy the take-off rotation acceleration requirement [30].

$$\alpha_h = \alpha + i_h - \epsilon = i_h - \alpha_0 \frac{d\epsilon}{d\alpha} \quad (7.51) \qquad \tau_e = \frac{\left(C_{L_h}/C_{L_{\alpha_h}}\right) - \alpha_h}{\delta_E} \quad (7.52)$$

Using tau_e, the chord of the elevator could be determined using Figure 7.11 and using Equation (7.53). It was chosen to use the root chord of the horizontal tail, since this will lead to the larges elevator and therefore an extra safety margin is built in. The input parameters can be found in Table 7.7.

$$c_e = \frac{c_e}{c_h} c_{r_h} \quad (7.53)$$

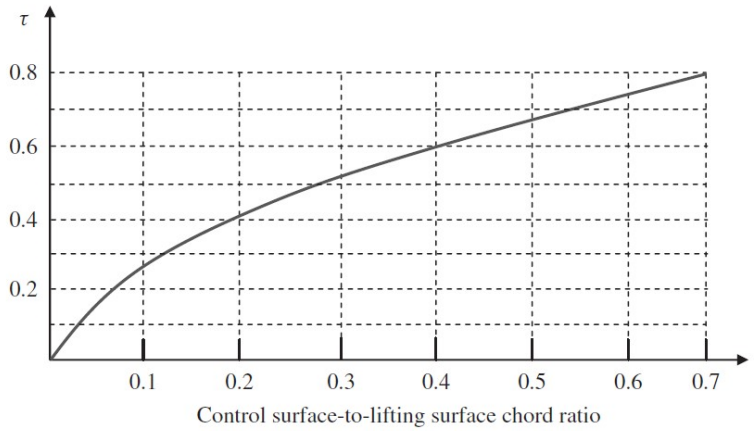

Figure 7.11: c_e/c_h determination graph [30]

Table 7.7: Elevator sizing input parameters

Parameter	Symbol	Value	Unit	Assumption
Take-off air density	ρ_{TO}	1.04	kg/m^3	-
Take-off velocity	V_{TO}	26.46	m/s	-
Take-off lift coefficient	$C_{L_{TO}}$	1.8	–	Based on **ELTA-W-02**
Take-off drag coefficient	$C_{D_{TO}}$	0.15	–	-
Airfoil lift coefficient increase at take-off	$\Delta C_{l_{max}}$	1.08	–	10% lower compared to landing
Mean aerodynamic chord	$\bar{C}$	1.26	m	-
Take-off weight	W_{TO}	8671	N	-
Take-off thrust	T_{TO}	546	N	-
Friction coefficient	μ	0.05	–	-
Centre of gravity location	x_{cg}	2.45	m	-
Centre of gravity location	z_{cg}	1.41	m	-
Main gear location	x_{mg}	2.99	m	-
Main gear location	z_{mg}	0	m	-
Drag vector location	z_D	1.41	m	Assumed to be halfway the fuselage height
Thrust vector location	z_T	1.41	m	Estimated using CAD drawing

Wing/Fuselage aerodynamic centre location	$x_{ac_{wf}}$	2.69	m	Assumed to be at 25% of the MAC
Horizontal tail aerodynamic centre location	x_{ac_h}	8.82	m	-
Take-off pitch angular acceleration	$\ddot{\theta}$	12	deg/s^2	-
Moment of inertia constant	C	0.176	$-$	Value for 1 piston engine aircraft
Aircraft length	l_a	9.54	m	-
Horizontal tail surface area	S_h	3.28	m^2	-
Take-off horizontal tail incidence angle	i_h	0	deg	Assumed to be 0 during take-off
Wing zero lift angle of attack	α_0	-7.4	deg	-
Horizontal tail lift rate coefficient	$C_{L_{\alpha_h}}$	3.29	$1/rad$	-
Minimum elevator deflection angle	$\delta_{e_{min}}$	-25	deg	Based on literature [30]
Maximum elevator deflection angle	$\delta_{e_{max}}$	20	deg	Based on literature [30]
Horizontal tail root chord	c_{r_h}	1.23	m	-

7.5.4. Results

The results of the control surface sizing are presented in Table 7.8.

Table 7.8: Elevator sizing input parameters

Parameter	Symbol	Value	Unit
Aileron start	b_1	4.54	m
Aileron end	b_2	5.88	m
Aileron span	b_a	1.34	m
Flap start	f_1	0.58	m
Flap end	f_2	4.05	m
Flap span	b_{fl}	3.58	m
Flapped area	S_{wf}	9.14	m^2
Elevator span	b_e	3.14	m
Elevator chord	c_e	0.39	m

7.5.5. Verification & Validation

Verification

As first step in the verification process, unit tests are performed on the aileron sizing, flap sizing and elevator sizing tool. The outputs of these tools were compared to the calculated values using Excel. Since these values were the same, it was concluded that the unit tests were successful.

Next, it was checked if the control surfaces would fit on the aerodynamic surfaces, i.e. that the control surfaces were not too large.

Validation

The validation of this tool will be done using simulation software and eventually during a flight test. This process is however part of the next phase, which is post-DSE. This will be explaned in Section 7.6.

7.6. Future Design Process

The assessment of the stability and control will be finalised during the next phases, which are post-DSE. The first step is a more detailed analysis of the lateral stability, in order to optimise the design of the vertical tail. This includes determining the aspect ratio, taper, span and root/tip chord. Once the vertical tail has been designed in more detail, the rudder can be sized as well.

The next step is choosing the software for the stability analysis. A trade-off has to be done on the different software tools available, to be able to determine most suitable tool. The software should then be verified and validated. Using this software, the tools described before can be validated. Also, the eigenmotions of the aircraft can be analysed using the software. In this way, it can be checked whether requirements **ELTA-CS-05** until **ELTA-CS-08** are met. If this is not the case, or the aircraft is heavily over-designed, the design of the aircraft should be adjusted.

The last step is the flight test. During this test, it will be checked whether the requirements are actually met. Therefore, this is also the last step in the validation process of tools used.

7.7. Risks

The risk with the highest impact regarding stability and control is that the aircraft will not be longitudinally and laterally stable and that it is not controllable. This risk was reduced by implementing safety margins. Also good

verification and validation procedures for the tools used, and tools that will be used, will reduce the risk.

7.8. Compliance Matrix

The compliance matrix for the stability and control requirements is shown in Table 7.9.

Table 7.9: Compliance matrix stability and control.

Identifier	Requirement	Obtained value	Requirement met?
ELTA-SC-01	At a 45 degree angle of attack at least one-third of the rudder shall remain outside the wake of the horizontal stabiliser.	*	TBD
ELTA-SC-02	The aircraft shall have a take-off pitch angular acceleration of 12 deg/s^2.	$12 deg/s^2$	✓
ELTA-SC-03	The aircraft shall have a conventional tail.	*	✓
ELTA-MAR-09	The system shall be able to educate a student to pilot a range of other aircraft.	*	TBD
ELTA-CS-FLT-03	During take-off conditions at sea level it shall be possible, using a favourable combination of controls, to roll the aeroplane from zero degrees of bank to an angle of 60 degrees within 5 seconds from initiation of roll.	60° in 2.4s	✓
ELTA-CS-FLT-04	During landing conditions at sea level it shall be possible, using favourable combination of controls, to roll the aeroplane from zero degrees of bank to an angle of 60 degrees within 4 seconds from initiation of roll.	60° in 2.3s	✓
ELTA-CS-FLT-05	The short period oscillation shall be heavily damped in stick free position.	*	TBD
ELTA-CS-FLT-06	The short period oscillation shall be heavily damped in stick fixed position.	*	TBD
ELTA-CS-FLT-07	The Dutch roll shall be damped to 1/10 amplitude in 7 cycles in stick free position.	TBD	TBD
ELTA-CS-FLT-08	The Dutch roll shall be damped to 1/10 amplitude in 7 cycles in stick fixed position.	TBD	TBD
ELTA-CS-FLT-10	The aircraft shall be controllable on the ground up until a maximum cross wind of 10 kts from a 90 degree angle.	TBD	TBD
ELTA-CS-FLT-12	The elevator shall support maximum upward/downward deflection at speed VA.	*	TBD
ELTA-CS-FLT-13	The elevator shall support one-third maximum upward/downward deflection at speed VD.	*	TBD
ELTA-CS-FLT-19	The aircraft shall be longitudinally, laterally and directionally stable.	*	TBD
ELTA-W-02	The aircraft shall have an maximum lift coefficient of at least 1.8 in a take-off configuration.	1.8	✓
ELTA-W-03	The aircraft shall have an maximum lift coefficient of at least 2 in a landing configuration.	2.0	✓
ELTA-W-CONT-01	The ailerons shall provide the aircraft with the ability to roll.	TBD	TBD
ELTA-W-CONT-02	The high lift devices shall provide the ability to increase the $C_{L_{max}}$ of the wing.	0.6	✓

8
Power and Propulsion

This chapter will focus on one of the aspects that differentiates the Dragonfly trainer aircraft from others, namely the contra-rotating propeller (CRP). First of all, in Section 8.1, the functional analysis for the power and propulsion subsystem will be performed. The corresponding requirements are discussed in Section 8.2. The power and propulsion subsystem consists of the detailed battery, motor and propeller design. Section 8.3 discusses the detailed design of the battery, the motor is discussed in Section 8.4 and, Section 8.5 discusses the detailed propeller design. Finally in Section 8.6 the compliance with the requirements is checked.

8.1. Functional Analysis

The first step in the detailed design of the power and propulsion subsystem is to identify the functions associated with this subsystem. These functions are described below. Behind each function description the link to upper-level function in the functional flow diagram discussed in Appendix A is displayed.

- **ELTA-FUN-PRO-01** - *Generate thrust in order to overcome the total drag force in the flight profile.* This function can be linked to function D.3 up to and including D.7;
- **ELTA-FUN-PRO-02** - *Provide maximum required power dictated by the design point.* This function can be linked to function D.3 up to and including D.7, and is important for the design of the electric motor;
- **ELTA-FUN-PRO-03** - *Provide enough energy to comply with the range and/or endurance requirements as well as to power all the onboard systems.* This function can be linked to function D.3 up to and including D.7;
- **ELTA-FUN-PRO-04** - *Operate each propeller on a different rotational speed.* This function can be linked to function D.3 up to and including D.7 as well as function B.4.1;
- **ELTA-FUN-PRO-05** - *Operate as an alternator to trade potential energy for electrical energy.* This function can be linked to function D.9.4;
- **ELTA-FUN-PRO-06** - *Recharge the battery system.* This function can be linked to function D.9.4;
- **ELTA-FUN-PRO-07** - *Operate safely.* This function can be linked to the entire operations flow described by flow D.

8.2. Requirements

In order to make sure the power and propulsion system is designed within the constraints of the design space the requirements will have to be setup. Below the requirements for the propulsion subsystem, these requirements flow down from the functional analysis, the market analysis and the VLA certification requirements.

- **ELTA-CS-PRO-01** - *Any electric energy storage device providing electric energy to an electric engine(s), shall be designed and constructed so as to provide the required energy for the electric engine(s) of the Electric/Hybrid propulsion system at all times during the flight in order to provide the rated powers that ensure safe operations*;
- **ELTA-PRO-02** - *The motor shall be able to provide the maximum power loading of 0.121 N/W.* This requirement is set up in order to make sure the motor design is in compliance with the design point specified in the midterm report [1];
- **ELTA-PRO-03** - *The battery and engine temperatures shall be displayed.* A temperature gauge can indicate the potential hazard of an engine or battery fire;
- **ELTA-PRO-04** - *The engine computer shall calculate the current reserve on board.* This requirement will increase the safety as the pilot will know how much power/flight time is left;
- **ELTA-BAT-05** - *The battery shall not exceed the maximum current and voltage levels specified by the manufacturer.* In order to prevent the batteries from catching fire or damaging the batteries it is important that this requirement is met;
- **ELTA-BAT-06** - *The battery cell type for the battery pack shall be rechargeable*;
- **ELTA-MAR-12** - *The endurance of the aircraft shall be 2 hours, when flying with maximum payload.* The energy supply must provide enough energy in order to reach the 2 hours of endurance;
- **ELTA-MAR-14** - *The recharge time of the aircraft shall be 40 minutes.* In order to make the business case attractive this is an important requirement to be met;
- **ELTA-MAR-17-01** - *The aircraft range shall be 250 km, when flying solo.* The energy supply must provide enough energy in order to reach the 250 km of range;
- **ELTA-MAR-20** - *The aircraft shall be rechargeable with currently available technology.* Once again, in order to make the business case attractive this is an important requirement to be met;

✈ **ELTA-MAR-21** - *30 minutes of flight time endurance shall be added to the endurance of the aircraft as reserve.* Once again the energy supply shall have enough energy to provide this reserve.

8.3. Battery Design

The first component in the chain of the power and propulsion subsystem design is the battery. In the midterm phase, it was concluded that a Lithium-ion battery will be used for the aircraft design due to its good energy density and popularity in electrical vehicles. Next to that, it was estimated in the midterm phase that the battery mass is equal to approximately 26% of the maximum take-off weight of the aircraft. In this section a more detailed design is performed for the battery pack. The battery pack design starts off by the creation of an electrical block diagram in Section 8.3.1. After this, an estimation has to be made on the energy required by the aircraft. This is described in Section 8.3.2. With this information the mass, volume and battery composition are determined in Section 8.3.3. The time to charge the battery and the battery lifetime estimation is performed in Sections 8.3.4 and 8.3.5 respectively. Finally, the battery design tools are verified and validated in Section 8.3.6 and the involved risks are analysed in Section 8.3.7.

8.3.1. Electrical Block Diagram

As described above, the first step in the battery pack design is to acknowledge all the components that are connected to the battery. These components are displayed in an electrical block diagram, see Figure 8.1. One should note that the AC motor includes a DC AC inverter, this will be further explained in Section 8.4.2. Next to that, the battery pack is composed of multiple smaller modules, which will therefore add redundancy in case one of the modules or battery cells fails.

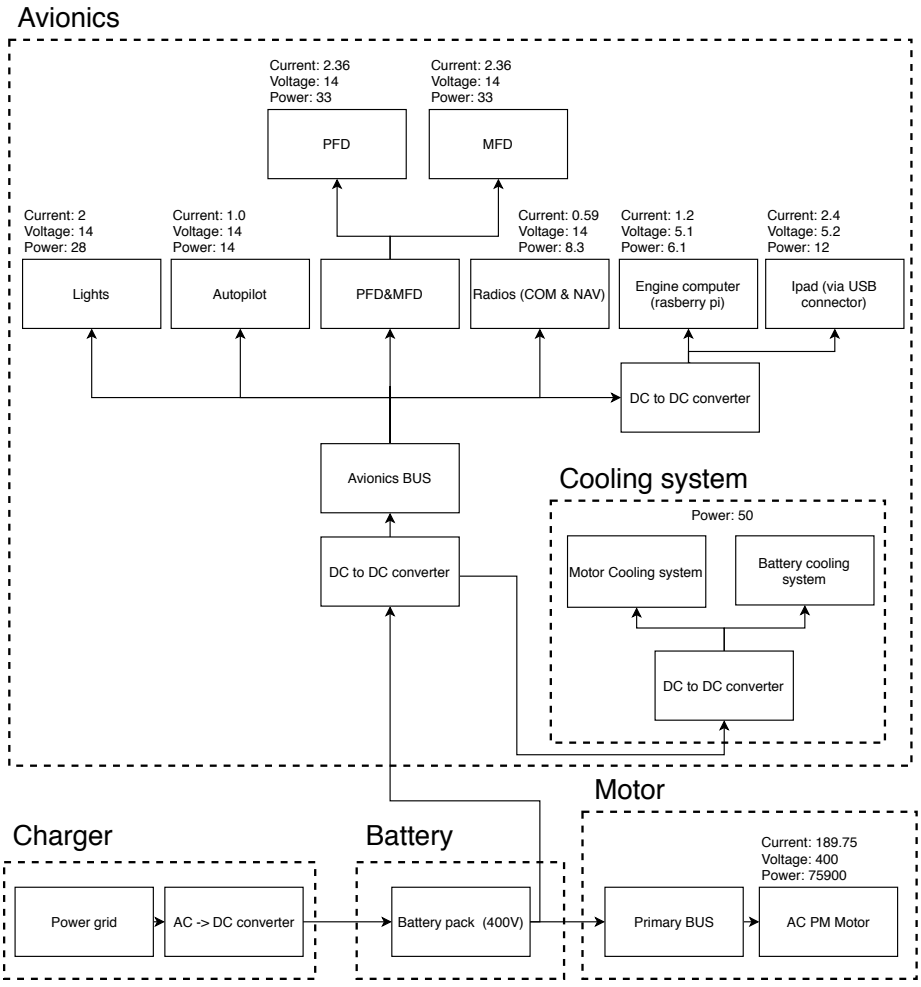

Figure 8.1: Electrical block diagram

8.3.2. Energy Determination

The next step, after identifying all the electrical components, is to determine how much energy each component requires from the battery, in order to determine the required battery capacity. To calculate this capacity, and thus

the battery mass in the end, the energy required is split up into two categories; motor and avionics.

Motor

First of all, the required energy for the electrical motor is determined. This energy is calculated for two different flight profiles, see Figure 8.2. The first one is the flight profile to fulfil the range requirement of 250 km (**ELTA-MAR-17-01**), which can be seen in Figure 8.2a. The second one is the flight profile to fulfil the endurance requirement (**ELTA-MAR-12** and **ELTA-MAR-21**), see Figure 8.2b.

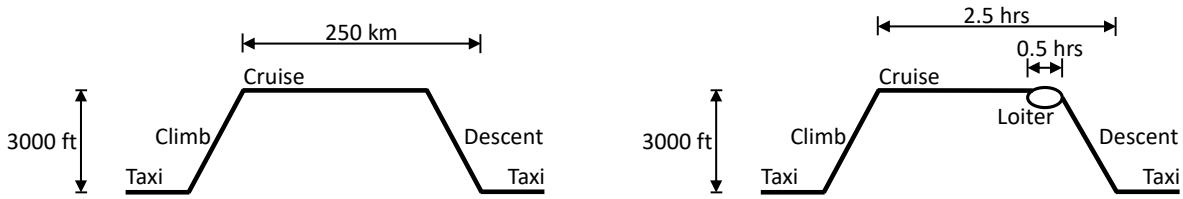

(a) Range (b) Endurance

Figure 8.2: Flight profiles for the different requirements (not to scale).

Both flight profiles can be combined into one equation in order to calculate the energy required for the electric engine, see Equation (8.1). In which E describes the energy required per flight phase and η_{total} describes the total propulsive efficiency from battery to propeller.

$$E_{motor} = \frac{1}{\eta_{total}}\left(2E_{taxi} + E_{climb} + max\left(E_{range}, E_{endurance}\right)\right) \tag{8.1}$$

Taxi and Climb

The energy required for the taxi and climb phase can be calculated using Equations (8.2) and (8.3) respectively. In these equations P_{max} equals the maximum power in Watt delivered by the electric motor, which will be determined in Section 8.4. k equals the power setting, ranging from 0.0 to 1.0, to control the amount of power required for the certain phase. Lastly t equals the time to perform that specific flight phase in seconds.

To determine the energy required for the taxi phase a power setting of 0.05 was assumed as well as a time to taxi of 5.5 minutes.

$$E_{taxi} = P_{max} k_{taxi} t_{taxi} \tag{8.2}$$

To determine the energy required for the climb phase, a power setting of 1.0 was assumed. To determine the time to climb Equation (8.4) was used. In this equation the cruise altitude (3000 ft) h_{cruise} in meters is divided by the climb speed requirement V_y of 2 m/s (**ELTA-CS-FLT-16**). To ensure there is enough energy for the climb phase, a safety margin (t_{extra}) of 30 seconds is added.

$$E_{climb} = P_{max} k_{climb} t_{climb} \tag{8.3}$$

$$t_{climb} = h_{cruise}/V_y + t_{extra} \tag{8.4}$$

Range

In order to calculate the energy required for the cruise and descent phase based on the range requirement, Equation (8.5) [1] was used. In this equation R is the required range in meters and W is the take-off weight of the aircraft. It should be noted that this is for flying solo as described by **ELTA-MAR-17-01**. Lastly, C_D and C_L describe the total drag and lift coefficients of the aircraft.

$$E_{range} = RW\frac{C_D}{C_L} \tag{8.5}$$

The lift and drag coefficients required for Equation (8.5) can be estimated using Equation (8.6) [8]. This equation estimates the optimal value for C_L and C_D in order to achieve maximum range.

$$C_L = \sqrt{\pi A e C_{D0}} \quad \text{and} \quad C_D = 2C_{D0} \tag{8.6}$$

[1] URL: https://lochief.wordpress.com/2015/08/04/how-the-musk-electric-jet-works/ LA: 17-06-2020

This is not the full story however, as in the proposed design the range requirement is when flying solo, meaning that the payload mass of the second pilot can be replaced with a battery pack of equivalent mass, which is 100 kg. In order to make sure that Equation (8.1) works correctly the E_{range} should be corrected for this so that the stationary battery pack is sized correctly. Thus E_{range} will be described as in Equation (8.7) and the quantity of energy a 100 kg battery contains will be described in Section 8.3.3. Using this method will keep the take-off weight equal for both the range and endurance requirements, while still calculating the energy required for the most critical case.

$$E_{range} = E_{range} - E_{100\,\text{kg battery pack}} \tag{8.7}$$

Endurance

In order to calculate the energy required for the cruise and descent phase based on the endurance requirement, Equation (8.8) [32] was used. In this equation the power required is calculated by multiplying the endurance speed (V) by the total drag of the aircraft (D), ρ equals the air density at sea level in kg/m^3 and S the wing surface area in m^2.

$$E_{endurance} = t_{endurance} P_{req} = t_{endurance} VD = t_{endurance} \frac{1}{2} C_D \rho V^3 S \tag{8.8}$$

The total lift and drag coefficients for the aircraft optimised for maximum endurance can be estimated with Equations (8.9) and (8.10) [8].

$$C_L = \sqrt{3\pi A e C_{D0}} \tag{8.9}$$

$$C_D = 4C_{D0} \tag{8.10}$$

The endurance speed required for Equation (8.8) can be calculated with Equation (8.11) using the lift coefficient from Equation (8.9).

$$V = \sqrt{\frac{W}{S} \frac{2}{\rho} \frac{1}{C_L}} \tag{8.11}$$

Avionics

Secondly, in order to calculate the energy required by all the avionics Equation (8.12) was used. In this equation the power required in Watt of all components of the avionics group (P_i) are summed and multiplied by the time these avionics are required (t). In this case, t is equal to the 2.5 hrs of endurance plus twice the time to taxi plus the time to climb, in total this equals 10147.2 seconds ($\approx$ 2.8 hrs). Next to that, the efficiency of the battery ($\eta_{battery}$) should be taken into account as well in order to properly determine the required energy.

$$E_{avionics} = \frac{1}{\eta_{battery}} \sum P_i t \tag{8.12}$$

The power required for each avionics component is listed in Table 8.1. These only include the avionics that require electrical power. For a full overview of the avionics please refer to Section 9.7.

Table 8.1: List of avionics power consumption.

Name	**Power** (P_i) [W]
PFD & MFD[2]	66
autopilot[3]	14
radios[4]	8.3
IPad[5]	12
Engine computer[6]	6.1
Exterior lights[7]	28
Cooling pump[8]	50

From Table 8.1 it can be concluded that the total amount of energy required for the avionics equals 184.4 [W].

[2] http://static.garmin.com/pumac/GDU104X_GDU104XInstallationManual.pdf LA: 17-06-2020
[3] http://www.peter-ftp.co.uk/aviation/kap140/KAP140-im.pdf LA: 17-06-2020
[4] https://www.seam-avionic.com/pdf/a9hdjzromj.pdf LA: 17-06-2020
[5] https://support.apple.com/en-us/HT210133 LA: 17-06-2020
[6] https://www.pidramble.com/wiki/benchmarks/power-consumption LA: 17-06-2020
[7] https://www.whelen.com/pb/Aviation/Catalog%20Price%20Lists%20and%20Manuals/Orion_Series.pdf LA: 17-06-2020
[8] Estimated to be 50 W

Total Energy Result

After the energy for both categories is calculated, the total energy required from the battery system can be determined with Equation (8.13).

$$E_{total} = E_{avionics} + E_{motor} \tag{8.13}$$

By the use of the input parameters described in Table 8.2, it was concluded that the battery should be sized to deliver a total energy of 59.9 kWh. Next to that, for this energy required the endurance requirement was limiting. Namely, with this energy, a total range of 310 km for two pilots or 460 km for a solo pilot with a 100 kg battery pack could be achieved.

Table 8.2: Input parameters energy determination.

Parameter	value
R [km]	250
$t_{endurance}$ [hrs]	2.5
e	0.815
S [m^2]	14.73
A	10.1
W [N]	8725.0
P_{max} [kW]	72.2
C_{D0}	0.018
$\eta_{battery}$	0.95
η_{total}	0.836

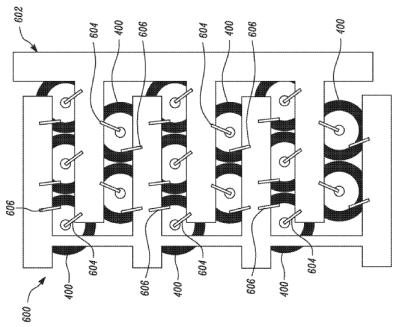

Figure 8.3: Battery architecture example, adapted from [9]

8.3.3. Battery Characteristics

The next step, after determining the energy required from the battery, is to determine the battery composition, mass and volume. For the battery composition of this aircraft, it is chosen to go with an architecture in which multiple cylindrical battery cells are connected in series and/or parallel. To illustrate this design see Figure 8.3 [9]. In order to cool this battery pack, a heat pipe will be in contact with all battery cells through which a coolant fluid is pumped which will absorb the heat from the battery cells. This heated up coolant fluid will then be cooled by flowing through a radiator that is exposed to airflow from the aircraft.

Battery Cell Data

In order to calculate the number of battery cells, first the specific battery cell data must be known. For the design of the battery pack three different cells were compared, which can be found in Table 8.3.

Table 8.3: Battery cell data.

Name	INR21700-50E[10]	INR21700-40T[11]	NCR-18650B[12]
Manufacturer	Samsung	Samsung	Panasonic
Diameter [m]	0.0211	0.0211	0.0185
Length [m]	0.0707	0.0704	0.0653
Mass [kg]	0.0687	0.0669	0.0475
Nominal Voltage [V]	3.6	3.6	3.6
Max. discharge current [A]	9.8	35	4.87
Capacity [Ah]	5.0	4.0	3.35

Amount of Battery Cells

With the specific cell data known the amount of cells required in series and parallel can be calculated. The amount of cells in series (N_S) is calculated using Equation (8.14) [33], as the voltage of cells add up when connected in series. In this equation $V_{req.}$ is equal to the required voltage level of the entire electrical subsystem in volts, V_{nom} is equal to the nominal voltage of a battery cell in volts. When observing Figure 8.1 it can be concluded that the highest voltage required equals 400 V. $V_{req.}$ is thus equal to 400 V as all systems in the electrical block diagram (Figure 8.1) are connected in parallel.

$$N_S = \frac{V_{req.}}{V_{nom}} \tag{8.14}$$

[9] https://patentscope.wipo.int/search/en/detail.jsf?docId=US254721855&tab=DRAWINGS, LA 18-06-2020
[10] https://www.imrbatteries.com/content/samsung_50E.pdf, LA 18-06-2020
[11] https://www.imrbatteries.com/content/samsung_40T.pdf, LA 18-06-2020
[12] https://www.imrbatteries.com/content/panasonic_ncr18650b-2.pdf, LA 18-06-2020

Equation (8.15) [33] is used to calculate the amount of battery cells required in parallel (N_P). In this equation $C_{req.}$ equals the required battery capacity in Ah and C_{cell} equals the capacity of a single battery cell.

$$N_P = \frac{C_{req.}}{C_{cell}} \tag{8.15}$$

The required capacity ($C_{req.}$) is calculated using Equation (8.16) [33], in which E_{total} is the total energy required in Wh, discussed in Section 8.3.2. η_{total} is the total efficiency between battery and load, however, as the efficiency is already incorporated in the energy determination, Section 8.3.2, it is set to 1.0 in this equation. V_{load}, the load voltage of the battery, as described above in the determination of the amount of cells in series V_{load} is equal to 400 V. Lastly DoD is the depth of discharge of the battery.

$$C_{req.} = \frac{E_{total}}{\eta_{total} V_{load} DoD} \tag{8.16}$$

Finally, the total amount of cells (N) can then be calculated using Equation (8.17). It should be noted that N_S and N_P are rounded up to the smallest integer value greater than N_S or N_P, this to make sure that the voltage and capacity requirements are met.

$$N = N_S \cdot N_P \tag{8.17}$$

Battery Mass and Volume

With the number of battery cells calculated the mass of the battery can be determined by just multiplying N with the mass of a single cell. However, this does not include the weight of the connectors between the cells, the cooling heat pipes between the cells, the housing to keep the cells in place, etc. Do note that the aforementioned housing does not include the structural protective housing of the battery pack, since this is part of the aircraft structural design. The mass of all the battery cells is multiplied by a factor of 1.15 in order to account for the extra mass added to the battery cells. The total estimated mass of the battery pack (m_{batt}) in kg can then be calculated using Equation (8.18), in which m_{cell} equals the mass of an individual battery cell in kg and N equals the total amount of battery cells required, see Equation (8.17).

$$m_{batt} = 1.15 \cdot N \cdot m_{cell} \tag{8.18}$$

The factor of 1.15 is based upon data from the Pipistrel Alpha Electro[13] [34] a GA aircraft similar to the Dragonfly, for which it was assumed to use the NCR-18650B battery cells.

The volume of the battery (v_{batt}) is estimated in m^3 using Equation (8.19), in which d_{cell} and l_{cell} are the diameter and the length of the battery cell in meters. This equation assumes that all the battery cells are fitted into a rectangle box.

$$v_{batt} = (N_S \cdot d_{cell}) \cdot (N_P \cdot d_{cell}) \cdot l_{cell} \tag{8.19}$$

Battery Sizing Results

The sizing method described above to size the battery pack is used for all three cells described in Table 8.3. From this it was concluded that the Samsung INR21700-50E is the best out of these three for the battery design, as both the resulting mass and volume are minimal, which is important for the design of an aircraft as both the available volume and mass are limited. The input data for sizing the battery pack can be found in Table 8.4, respectively the results can be found in Table 8.5. Note that due to the power density of the batteries not being high enough the mass budget for the batteries, described in Section 5.1.1, could not be achieved.

Table 8.4: Input values for the sizing of the battery pack.

Parameter	Value
E_{total} [kWh]	59.9
Battery cell	Samsung INR21700-50E
$V_{req.}$, V_{load} [V]	400
DoD	90%

Table 8.5: Results of sizing the battery pack

Parameter	Value
N_S	112
N_P	33
N	3696
m_{batt} [kg]	291.9
v_{batt} [m^3]	116.34

[13] https://www.pipistrel-aircraft.com/aircraft/electric-flight/alpha-electro/, LA: 18-06-2020

8.3.4. Battery Charging

As specified by **ELTA-MAR-14**, the recharge time of the battery shall be 40 minutes. In order to confirm whether this requirement can be met the charging time of the battery should be calculated. The time to charge the battery can be estimated by dividing the capacity of the battery in Wh by the power output of the AC DC converter multiplying it with a loss factor which is estimated to be 1.2[14]. The AC DC converter can be seen in Figure 8.1 and will not be onboard the aircraft, to save weight. This will thus require airports to have the charger available.

The battery manufacturer Samsung specifies that the INR21700-50E battery cell should be charged with a current of 2.450 A and a voltage of 4.2 V[15]. As the battery design consists of 3 cells in parallel and 112 cells in series this will equal a maximum charge current of 80.85 A with a voltage equal to 470.4 V. This is equivalent to a maximum charge power of 38.0 kW. One should not exceed this charging power to ensure the battery lifetime, discussed in Section 8.3.5, which is also closely related to requirement **ELTA-BAT-05** which specifies that the battery shall not exceed the maximum current and voltage levels specified by the manufacturer.

If a standard charger would be used, which will be plugged into the normal available power grid, it can produce approximately an output of 3 kW [34]. This would result in a charging time of $(59.9 \cdot 1.2)/3 = 24hrs$. This charge time exceeds the specified requirement of 40 minutes. The maximum charge power of 38.0 kW, calculated above, could be achieved with for example a supercharger. An example of this is the Telsa supercharger which can deliver direct current power outputs up to 120 kW[16]. Thus, using a supercharger with a power output of 38.0 kW would result in a charge time of $(59.9 \cdot 1.2)/38.0 = 1.9hrs$. This is unfortunately still above the required 40 minutes, therefore the aircraft design requires a battery that can be swapped with a fully charged battery. As the charge time with a supercharger equals 1 hrs and 54 minutes, only two battery packs are required as the empty battery pack can be recharged within the flight time of 2 hrs (**ELTA-MAR-12**).

8.3.5. Battery Lifetime

In order to determine the business case for the aircraft, it is important to know what the battery life is. More specifically how many charge-discharge cycles the battery can do before becoming unusable. In most literature, such as [35], it is assumed that the end of life of a battery is achieved once the capacity of a battery has dropped below 80% of its original capacity.

The loss of capacity over time or use (capacity fade) is due to multiple occurrences and circumstances such as the loss of lithium-ion and active material within the battery cell over time, the atmosphere in which the battery is stored as well as the load to which the battery is applied.

The advertised cycle life of the Samsung INR21700-50E is 500 cycles[17]. After these 500 cycles the capacity has faded to 80% of its original capacity. This is, however, measured for a depth of discharge of 100%. As described by [36] the battery cycle life can be enlarged by decreasing the depth of discharge at which the battery is operated. Next to that, it can be seen that for the electric cars of Tesla the battery packs still have 93% of their original capacity left after 1000 cycles- this data is based on a survey conducted among Tesla car owners[18]. This data can be useful for the proposed aircraft design in this report as the battery cells used in the battery modules of Tesla are similar to the ones used for the battery design proposed in this report[19]. The battery having a cycle life above 1000 cycles is supported by H. Popp et al. [37], a paper in which the cycle life of the Samsung INR21700-50E battery cell was tested for different C-rates and DoD's. From this research it can be concluded the Samsung INR21700-50E battery cell has a cycle life of 1500 cycles for a DoD of 80% .

Therefore it is estimated that the battery life cycle of the battery design proposed in this report, consisting of the aforementioned Samsung INR21700-50E battery cells, for a depth of discharge of 90% equals 1000 cycles, as the depth of discharge is slightly higher in comparison to [37].

8.3.6. Verification and Validation

This section describes the verification and validation of the methods described in Section 8.3. First, the verification tests are described, then the validation tests, and lastly a future plan for validation will be proposed.

Verification

In order to verify both the energy determination method and the battery composition method, small unit tests were used. First of all, for the energy determination, a test was performed in which the required endurance and range were both set to 0, this should result in the motor energy calculated for only the climb and taxi phases. Calculation by hand may be easily performed for these phases. This unit test was performed successfully.

[14] http://www.csgnetwork.com/batterychg2calc.html, LA: 21-06-2020
[15] https://www.imrbatteries.com/content/samsung_50E.pdf, LA: 21-06-2020
[16] https://www.tesla.com/nl_NL/support/home-charging-installation, LA: 29-06-2020
[17] https://www.imrbatteries.com/content/samsung_50E.pdf, LA 18-06-2020
[18] https://maartensteinbuch.com/2015/01/24/tesla-model-s-battery-degradation-data/, LA: 19-06-2020
[19] https://electrek.co/2017/08/24/tesla-model-3-exclusive-battery-pack-architecture/, LA: 19-06-2020

Secondly, a unit test was performed on the battery composition method. One example of this was to hand calculate the number of cells required in series. This test was successful. Next to that, it was checked if the depth of discharge (DoD) decreases the capacity required and thus the number of cells in parallel should increase. This was tested successfully.

Validation

In order to validate the energy determination method, for the battery composition method and the charging time estimation real-life examples were used. For the energy determination and charging time estimation the Pipistrel Alpha Electro was used for comparison. For the validation of the battery composition a battery module of a Tesla Model S was used as an example.

First of all fot the energy determination method (Section 8.3.2), as described above, the case of the Pipistrel Alpha Electro was used. The Alpha Electro has a battery pack of 21 kWh for an endurance of 1.5 hrs[20], including reserve time. For the input of the method the technical data[20] and estimated values for the efficiencies and C_{D0} [8] were used. This resulted in an energy required of 25.8 kWh. Thus a difference of 4.8 kWh of energy is present, one could argue that this difference of 22.8% is quite significant, however, as already described above the C_{D0} as well as the efficiencies (Oswald efficiency, battery efficiency and propeller efficiency) had to be estimated, this brings some uncertainty in the validation process. Overall this validation is concluded as a success, as although it is not highly accurate, it does come close and overshoots the energy required a little bit. In this case an overshoot is a better result than producing an underestimation as this will make sure the endurance requirement will be met. Next to that, in the energy determination method C_L and C_D are estimated therefore a little inaccuracy can be expected.

Secondly, to validate the method to determine the battery composition required a battery module from the Tesla Model S was used. This battery module is composed of 6 cells in series and 74 cells in parallel for a nominal voltage of 22.2 V and a capacity of 5.2 kWh[21]. The type of cell is similar to the Panasonic NCR-18650B. Using the values described above for a DoD of 100% results in a composition of 7 cells in series and 70 in parallel. By decreasing the DoD to 95% results in a battery composition of 7 cells in series and 74 parallel, which is almost equal to the original composition of the Tesla battery[21]. Therefore the validation is concluded as a success. Multiplying the 444 cells (6×74) with the factor of 1.15 and the individual cell mass, see Equation (8.18), results in a battery mass of 24.25 kg, this is slightly lower compared to the 26.3 kg described on [21]. This is most likely due to the fact that for the automotive industry cheaper, less exotic materials are used in comparison to the aircraft industry (materials as Kevlar or carbon fibre), which therefore results in the estimated mass to be slightly lower.

Lastly to validate the battery charging time estimation described in Section 8.3.4 the case of the Pipistrel Alpha Electro was used. In [34] it is specified that the charge time of the 21 kW battery is equal to 2 hours and 30 minutes for a charger output power of 10 kW and 1 hour and 10 minutes for a charger output power of 20 kW. The results of the relation described in Section 8.3.4 are a charge time of 2.52 hrs (2 hours and 31 minutes) and a charge time of 1.26 hrs (1 hour and 15 minutes) respectively. Which is almost identical to the test case and therefore the validation test is successful.

Future Validation

Of course validating the sizing methods does not cover the whole validation process. It is therefore recommended to, once the battery is built, test the capacity of the battery by connecting it to a load similar to the flight profile. In this way it can be validated whether the battery contains enough energy and can provide enough power for the full flight profile. Next to that, it can also be tested on the time to fully charge the battery as well as what the cycle life of the battery is. The latter is however quite expensive as you need to run the battery for more than 500 cycles, therefore it might be a better solution to computationally model the cycle life.

8.3.7. Risks

The first risk that was identified is the fact that in the energy determination method the values for C_L and C_D are estimated and thus might not be the exact real numbers. A way to mitigate this risk is to check the value for C_L and C_D during the subsystem integration process, and check whether these values are within the limit for a general aviation aircraft.

Next to that, another risk that was identified is whether the factor of 1.15 to calculate the battery mass is not realistic, which will result in an unachievable or over-designed battery weight. This risk can be mitigated by making sure the percentage of battery weight of the maximum take-off weight is similar to other GA aircraft.

One should also keep in mind the risk of one battery cell being faulty, as for the battery composition method it is assumed that all battery cells are working properly. To mitigate this risk the composition should be slightly over-designed, by adding for example an extra cell to the series or parallel rows, which already happens as the number of cells are rounded up to the nearest integer.

[20] https://www.pipistrel-aircraft.com/aircraft/electric-flight/alpha-electro/#tab-id-2, LA: 18-06-2020
[21] https://hsrmotors.com/products/battery_modules, LA: 18-06-2020

Another risk is that the estimation of the battery charging time is not accurate enough and that for example the charging losses are greater or smaller than expected. To mitigate this risk a battery storage design should be used in which the battery can be swapped for a fully charged battery.

8.4. Engine Design

In this section all the necessary steps will be taken to design the engine of the aircraft. To do this, the required engine parameters are first calculated in Section 8.4.1. Based on these parameters, a market research will be performed in Section 8.4.2. Thereafter, the propulsion configuration will be determined in Section 8.4.3. With that in mind, the propeller shaft can be designed in Section 8.4.4. Then verification & validation is done in Section 8.4.5. After that, the layout of the engine computer is described in Section 8.4.6. Lastly the risks will be touched upon in Section 8.4.7.

8.4.1. Engine parameters

This section explains the calculations or reasoning for the engine parameters. With these parameters in mind one can have a look at the current market to find an electric engine that best suits the requirements. This is discussed in Section 8.4.2.

RPM Range

Most single engine piston (SEP) trainer aircraft, like the Cessna 172, in use today have a maximum RPM of 2700. The Alpha Electro, however, has a maximum of 2500 RPM and aircraft equipped with a Thielert TAE engine have a maximum RPM of 2300 RPM[22]. Due to the fact there are two propellers in the Dragonfly-aircraft, the RPM can be kept lower compared to conventional aircraft. The exact RPM will flow out the propeller analysis, but for the market analysis a maximum RPM of 2300 will be chosen based on the lowest RPM from conventional GA aircraft.

Maximum Continuous Power

To calculate the maximum continuous power needed from the engines, three cases were studied: power needed during the take-off run, power needed for cruise climb at sea level and power needed for cruise climb at ceiling.

Power needed during take-off

For the power calculation during take-off it was assumed there is no ground effect. Furthermore, the calculation is for sea level ISA conditions with zero wind. Also, the calculation is based on average parameters, as will become clear with the following formulas which are based on [14].

First the average acceleration was calculated during the take-off run with Equation (8.20), where V_{lof} is the lift-off speed which is $1.05 \cdot V_{stall}$ and s is the take-off run. A take-off run of 250 meters is assumed. That leaves another 250 meters to climb to 50 feet/15 meters which satisfies **ELTA-CS-FLT-15**.

$$\overline{a} = \frac{V_{lof}^2}{2s} \tag{8.20}$$

Next, the average velocity was calculated with Equation (8.21). After that, the average drag was calculated with Equation (8.22). The only tricky parameter was $C_{D_{to}}$ which is the drag coefficient during the take-off run. On the internet not much information was given on this parameter. Therefore, examples were used from the book [14]. In these examples a value of 0.0414 (from a Cirrus SR22) was the highest and was used for safety reasons. For the average lift the same equation is used as for the drag, but the coefficient $C_{L_{to}}$ is used instead. Using examples from [14] it was found this coefficient was 34% of the $C_{L_{max}}$ during take-off.

$$\overline{V} = \frac{V_{lof}}{\sqrt{2}} \tag{8.21}$$

$$\overline{D} = \frac{1}{2}\rho \overline{V}^2 S C_{D_{to}} \tag{8.22}$$

Now Equation (8.23) can be rewritten to find $\overline{T}$ which is the only unknown. g is namely the gravitational acceleration, W the aircraft weight and μ the friction coefficient which for GA aircraft is 0.03-0.05. For safety reasons 0.05 is chosen.

$$\overline{a} = \frac{g}{W}(\overline{T} - \overline{D} - \mu(W - \overline{L})) \tag{8.23}$$

The last step is to multiply the founded thrust with the highest speed that is reached on the runway, which is V_{lof} as power is thrust times velocity. The drawback of this method is that the average thrust is calculated. It turned out, however, that the power during take-off was not limiting as can be seen in Section 8.4.1.

Power needed during cruise climb at sea level

Requirement **ELTA-CS-FLT-16** states that the climb rate shall be at least 2 m/s. However, for this calculation a rate of climb of 2.54 m/s is used. This is based on IFR regulations that state single engine aircraft shall have a minimum rate of climb of 500 ft/min.

[22] All mentioned RPMs are from the respective pilot's operating handbook

Equation (8.24) is used for the power calculation. ROC is the rate of climb, W is the aircraft weight, DV is the drag multiplied with the speed which is the required power and TV is the thrust multiplied with the speed which is the power available. For the drag Equation (8.22) is used with the parameters tuned for sea level ISA conditions. For the speed the cruise speed is taken. In this equation it is assumed the lift equals drag. For the actual values please refer to Section 8.4.1. When Equation (8.24) is rewritten to Equation (8.25) one can calculate the power the engine needs to deliver.

$$ROC = \frac{TV - DV}{W} \tag{8.24}$$

$$P_{avail} = ROC \cdot W + DV \tag{8.25}$$

Power needed for cruise climb at ceiling

The climb requirement of 500 feet/minute has to be met at the service ceiling as well. For this the same method is used as for the climb rate at sea level with the difference the ρ within the drag equation is changed to the value at the ceiling altitude and the cruising speed is converted to true airspeed according to Equation (8.26). In this equation it is assumed V_{cruise} is the equivalent airspeed. ρ_0 is the air density at sea level and $\rho_{ceiling}$ the air density at ceiling altitude.

$$V_{TAS} = V_{cruise} \sqrt{\frac{\rho_0}{\rho_{ceiling}}} \tag{8.26}$$

Engine Weight and Volume

Using off the shelf PM motors the power density is 3.5-4 kW/kg. Then, the required inverter will be 8 kW/kg which means the combined power density is 2.5 kW/kg. At this moment Saluqi Motors is developing a motor with an integrated inverter which results in a power density of over 3 kW/kg. For the calculations of the engine for the Dragonfly the 2.5 kW/kg will be taken into account to have a margin. For the motor volume a power density of 9 kW/liter is taken [23]. Lastly the efficiency of an AC PM motor is around 0.95.

Engine Voltage and Current

It is beneficial to have a voltage as high as possible, because then the efficiency goes up and one needs less thick power cables. For engines between 75-200 kW, voltage levels between 250-400 V are optimal according to Saluqi Motors. Going for the highest possible efficiency a voltage of 400 V is chosen. For this more batteries should be connected in series instead of parallel, but this was no issue as can be seen in Section 8.3. To calculate the amount of current one can use Equation (8.27) where P_{in} is the amount of power that is delivered to the motor.

$$I = \frac{P_{in}}{V} \tag{8.27}$$

Engine Torque

The torque delivered by the engine can be calculated by dividing the amount of output power by the angular velocity which can be seen in Equation (8.28), where ω is the angular velocity which can be related to RPM by Equation (8.29).

$$T = \frac{P_{out}}{\omega} \tag{8.28}$$

$$\omega = RPM \cdot 2\pi/60 \tag{8.29}$$

Results

In Table 8.6 the input parameters and their values can be seen for the power calculations. Then in Table 8.7 the power results are shown. Finally in Table 8.8 all the required engine parameters are shown.

Table 8.6: Input parameters for the maximum power calculations

Parameter	Power calculation for: Take-off run	Cruise climb at sea level	Cruise climb at ceiling	Unit
s	250	-	-	m
V_{lof}	24.31	-	-	m/s
V_{cruise}	-	50.0	50.0	m/s
ρ	1.225	1.225	0.849137 (at 12000FT)	kg/m^3
C_D	0.0414	0.0341	0.0341	–
C_L	0.628	-	-	–
μ	0.05	-	-	–
W	8671	8671	8671	N
S	-	14.73	14.73	m^2
ROC	-	2.54	2.54	m/s
η_{engine}	0.95	0.95	0.95	–

[23] Saluqi Motors

Table 8.7: Power calculation output

Parameter	Power calculation for Take-off run	Cruise climb at sea level	Cruise climb at ceiling	Unit
$P_{out_{max}}$	36.5	60.3	68.0	kW
$P_{in_{max}}$	38.5	63.5	71.6	kW

Table 8.8: Required engine parameters

Parameter	Value	Unit
RPM	2300	-/min
$P_{out_{max}}$	68.0	kW
$P_{in_{max}}$	71.6	kW
W_{engine}	297.8	N
V	$8.9{\cdot}10^{-3}$	m^3
U	400	V
I	200	A
T	282.4	Nm

Sensitivity Analysis on Calculations

For the power calculations several assumptions were made in the calculations which implies that the results are not true to life. To start with the calculation for the take-off run power required, an average acceleration is used for this. In reality the acceleration will decrease during the take-roll due to the increase of the drag force. Also for the lift and drag forces averages are taken which are based on examples in [14]. As a result the calculated thrust is also an average. Furthermore the ground effect is neglected in the performed calculation. In reality this ground effect will reduce the tire friction because the lift force will become stronger due to the downwash of the wings that will 'push' the aircraft from the ground. Furthermore ISA circumstances were assumed. As the take-off run requirement is based on ISA as well, this will not result in a problem. In the end the required power for the take-off run is half the value compared to the climb rate required power and it was concluded the take-off run is not the limiting factor and it was deemed unrealistic that without the taken assumptions the outcome would result in an increase of 50% to become critical compared to the other power results.

For the climb rate required power, it is assumed the lift equals the weight due to the small angle approximation. In reality this is of course not the case as the lift force will be larger. With this simplification the rate of climb would be larger in reality which is beneficial compared to the other way around. TU Delft did a calculation on the climb rate with the full set of equations of motion and the simplified ones. It turned out that the climb rate with the full equations of motion was 0.52% higher. [24] Furthermore a rate of climb of 500 ft/min or 2.54 m/s is taken instead of 2.0 m/s which is a CS-VLA requirement. With this it can be concluded the required power that resulted from the calculations is realistic and has a safety margin in it.

8.4.2. Market Research on Existing Engines

Currently, several companies produce PM engines. For the aerospace industry Siemens is developing permanent magnet motors. In Table 8.9 data for these engines is shown [25]. Saluqi motors also has developed a suitable engine, namely the P50 engine. When this engine is used in a twin configuration the parameters do exactly match with the parameters of Table 8.8. That is why it is included although it is a twin engine instead of a single engine. Both engines could be positioned next to each other and drive a single axis for the propellers which can be seen in Figure 8.4 where the propeller axis would be connected to the wheel on the top.[26] Another possibility is that both engines drive a propeller individually. It should be noted that the engine weight of the Siemens engines is without engine inverters of 8-10 kg. For the Saluqi this is included as the engine has its inverter integrated within the engine.

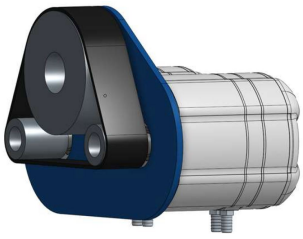

Figure 8.4: Saluqi P50 twin

From the data in Table 8.9 it can be concluded that the calculated parameters for the engine of the Dragonfly are realistic and it will be possible to find a suitable engine. It is difficult however to find prices for these engines. Fortunately Saluqi had price data, namely that a PM engine plus inverter for aviation purposes cost around 100€/kW.

[24] Lecture 12 on climb and decent performance of the AE2230-I course at the TU Delft

[25] https://www.ie-net.be/sites/default/files/Siemens%20eAircraft%20-%20Disrupting%20Aircraft%20Propulsion%20-%20OO%20JH%20THO%20-%2020180427.cleaned.pdf and https://www.bbaa.de/fileadmin/user_upload/02-preis/02-02-preistraeger/newsletter-2019/02-2019-09/02_Siemens_Anton.pdf

[26] From datasheet Saluqi P50 twin - 100 kW

Table 8.9: Engine data of current engines on the market

	SP45D	SP55D	SP70D	SP200D	SP260D-A	Saluqi P50 twin
Continuous Power (kW)	45	55	70	200	260	80
Peak Power (kW)	60	72	92	204	-	100
Max RPM	2500	3000	2600	1300	2500	1600-2500
Weight (kg)	28	27	26	49	44	30
max Torque (Nm)	324	180	340	1500	977	380-600
Voltage (nominal) (V)	300-450	350-450	350-450	450-850	580	300-400

8.4.3. Propulsion Configuration

During the midterm phase of this project [1], it was decided to go for a single engine design with two contra-rotating propellers (CRPs). In this more detailed design phase, there was a more thorough look in the different possibilities on how to activate the propellers. Current aircraft (projects) use for example one electric engine per propeller [27] due to the small size of an electric motor in combination with the low weight [28]. There are more possibilities however, for example one engine with a gearbox attached. This gearbox could be fixed or adjustable to get different RPM ratios between the two propellers.

To find out what type of configuration was most suitable for this project a trade-off was performed. It started with a QFD which can be seen in Figure 8.5. The customer importance rating for the aircraft cost was chosen to be 4 and not 5 because €150 000 is relatively cheap for an aircraft when compared to conventional trainer aircraft like the Cessna 172 or the Piper Archer. On the other hand, it was a customer requirement that the aircraft's price shall be at maximum €150 000. The 'CS-VLA certifiable' requirement is marked with a 4 instead of a 5, because the ultimate goal is to certify it for CS-23. As the student pilots who are going to use the aircraft will be trained for other conventional aircraft the 'fly like a conventional aircraft' is marked with a 5. For the next criterion a score of 3 was assigned as some sort of autopilot is good to have, but it is not highly necessary. The last criterion is marked with a 5 as this whole project is about the enhancement of the pilot's training. The technical performance measurements speak for themselves. For the conventionality it was chosen to link it to a SEP aircraft as these aircraft are mostly used initial flight training.

Customer importance rating	Customer Requirements/ Customer Demands (What)	Functional Requirements/ Technical Performance Measurements (How)	Cost	Complexity	System Weight	Fly like a conventional single engine aircraft	Added TE	Certifiability	Total
4	Aircraft cost max 150k		9	6	3	6	3	6	132
4	CS-VLA certifiable		1	1	9	6		9	104
5	Fly like a conventional aircraft		3	3		9	6	6	135
3	Autonomous flight (AP)		6	6	6	1	6	3	84
5	Added value in training		3		1	3	9	3	95
	Technical Importance Score		88	61	71	111	105	114	550
	Criteria Importance		16.00%	11.09%	12.91%	20.18%	19.09%	20.73%	100.00%
	Criteria Weight		**15%**	**10%**	**15%**	**20%**	**20%**	**20%**	**100%**

Figure 8.5: QFD on engine configuration

Propulsion Configuration Trade-Off

To propel the CRPs five concepts were created and were traded off, which will be discussed in this section. Furthermore each design refers to Figure 8.6 where the trade-off on the propulsion configuration is shown.

Two engines, single lever

This concept consists of two engines behind each other, where the front engine propels the rear propeller and the rear engine the front propeller. A visualisation of this can be seen in Figure 8.7. To give the pilot a feeling as they are flying a single engine aircraft, they have only one lever in the cockpit. An engine computer will then convert the lever inputs into power inputs for the two engines. Furthermore this computer should deal with failures itself such as an engine malfunction as the pilot cannot do it (he only has a single lever). A first thought was that such a computer would be very complex, but Tesla uses a similar principle where the driver has only one gas paddle and a computer regulates the power to the different engines. Furthermore, in drone applications the different propellers are driven by different engines although the user does not steer those motors individually and directly. Additionally, the operational costs will be low as there are not many mechanical parts that need to be inspected during maintenance. For this reasons the cost and complexity are both marked with a 3. As there are not many mechanical parts and as according to Table 8.9 the engines combined weigh not much more than a single engine,

[27] Contra Electric Propulsion Ltd. and Electroflight
[28] According to Electroflight the two motors weigh approximately 50kg whereas with piston engines it would be 150/200kg (≈ 300 HP)

the system weight is marked with a 4. Because there is only one lever in the cockpit it handles like a normal SEP aircraft. It is marked with a 3 and not a 4 as there should be information present in the cockpit about the state of the engines. This information is about two engines and not about a single engine. Going to the training effectiveness, this is marked with a 4 due to the engine computer. This computer could adjust the amount of power to the engines to simulate different weight and weather conditions which is beneficial for the student pilot to train for. The certifiability is marked with a 1, because VLA certification can only be done with single engine. It was chosen not to award a score of 0, as the end-goal is to certify the aircraft under CS-23 and there one can have multiple engines.

Two engines, multi lever

This concept uses the same layout as the previous concept with the exception that it has a lever in the cockpit for each engine. Therefore, there is no need for an engine computer. This resulted in a score of 4 for both the 'cost' and 'complexity'. The system weight is marked with a 4 for the same reasons as the previous concept. As the pilot is now flying a multi-engine aircraft it scores a 1 on the SEP criterion. It was chosen not to mark it with a 0 due to the fact that there are no extra mixture levers for both engines and the two engines are mounted in the front. This will not result in a strong torque, which would be the case when there are two wing-mounted engines. The added training effectiveness is neutral. The pilot can train for multi engine aircraft, but there is no computer in between that regulates the amount of power to the engines which can be used for simulating different weight and weather conditions. Therefore this criterion is marked neutral with a 2. For the certifiability the same reasoning as for concept 1 applies.

Single engine with fixed gearbox

A single engine is used for this concept. In order to propel two propellers, a gearbox is used. In this design this is a fixed gearbox which means the RPM ratio between the propellers is fixed. Due to this fixed property the system will not be that complex and the costs will not be that high. Therefore these criteria are marked with a 3. Due to the added weight of the gearbox the system weight is marked with a 3. As there is only one engine and one lever in the cockpit it feels for the pilot as a SEP and therefore it is ranked as a 4. The training effectiveness is marked neutral because there is no engine computer in between that can simulate different weight and weather conditions. The certifiability is scored with a 3 because it fulfils the VLA requirements. Due to the CRPs however, it is not marked with a 4.

Single engine with variable gearbox with extra lever

This concept is the same as the previous concept, but instead of a fixed gearbox it used a variable gearbox which means the pilot can regulate the RPM ratio between the two propellers by means of a second lever in the cockpit. One could see this extra lever as a sort of governor lever. The gearbox will be more complex compared to the previous concept and will also be heavier. The complexity is therefore marked with a 1 as well as the system weight. The cost is marked neutral as it is a well-known concept when one looks at the car industry for example. On the other hand, it is still expensive due to the complex gearbox. When the extra lever in the cockpit is seen as a governor the aircraft acts like a 'complex' aircraft used for CPL training. For beginning students it can be hard at first, therefore it is marked a 3 and not a 4. Also the training effectiveness is marked a 3 due to the extra lever. The certifiability is marked as a 2 due to the possible extra issues certifying the gearbox.

Single engine with variable gearbox computer steered

The only difference with regards to the previous concept is that the gearbox is now not controlled by a lever in the cockpit, but by the engine computer. Due to the added costs of the engine computer the cost criterion is marked with a 1. The complexity is 1 just like the manual gearbox variant. The system weight however is chosen to be 2 due to the fact that there are more mechanical parts as the gearing is done manually. Because there is only one lever in the cockpit it flies like a SEP aircraft and therefore scores a 4. The training effectiveness is marked a 4 as well due to the fact that the computer can change the amount of input power to the engine and the gearing to simulate different aircraft weight and weather conditions. The certifiability is scored with a 2, for the same reasons as the last concept plus the fact that the engine computer needs to be certified as well.

Design Option	Technical Performance Measurements	Cost	Complexity	System weight	Fly like a conventional SEP aircraft	Added Training Effectiveness	Certifiability (VLA)	Score
	Weight	15%	10%	15%	20%	20%	20%	100%
two engines, single lever		3	3	4	3	4	1	2.95
two engines, multi lever		4	4	4	1	2	1	2.40
Single engine with fixed gearbox		3	3	3	4	2	3	3.00
Single engine with variable gearbox with extra lever (governor lever)		2	1	1	3	3	2	2.15
Single engine with variable gearbox computer steered		1	1	2	4	4	2	2.55

Figure 8.6: Trade-off on engine configuration

When looking at the scoring, 'the two engines, single lever' and 'single engine with fixed gearbox' score the best and are close to each other. As the difference is so small one cannot just say that the single engine concept will win. After a brainstorm with the entire team it was decided to value the added training effectiveness more and the certifiability less as the aircraft's final goal is to be certified within CS-23. With this in mind the two engines with a single lever in the cockpit will win the trade-off. During the sensitivity analysis it furthermore turned out that if the added TE was increased with only 3% or the certifiability decreased with 3% the two engine concept with single lever would win.

8.4.4. Engine Shaft Design

As the Saluqi P50 twin engine configuration fulfils all calculated required engine parameters it was decided to go for this engine. The only problem was the engine configuration, as in the given datasheet the motors were positioned next to each other instead of behind each other. After having contact with Saluqi, it was no problem changing to this configuration. The cost would still be the same (100€/kW). The diameter would increase with 5-10 cm due to the shaft going through the front engine. The engines plus inverters could however be 5 cm shorter due to this configuration. Placing the engines after each other has the advantage of using a direct shaft, which means they will directly propel their respective propeller without any belting or gearing in between. During gliding flight when the engines do not have to produce thrust they will become automatically generators that recharge the battery. A downside is that the engines will operate at relatively low RPMs which affects their efficiency, but it was deemed the advantages overcome this downside as there is no need for a freewheel bearing for recharging the battery and no gearing or belting is needed which would result in extra weight.

To have the configuration visualised, please see Figure 8.7. The back engine propels the front propeller and the front engine the back propeller. For visualisation purposes the engines are drawn with an exaggerated space between each other. In reality they will lie exactly behind each other with no gap in between. For the calculation of the shaft's shear stress, twist and bending will be evaluated. In the exaggerated Figure 8.7 one can see that bending is an important factor as the shaft of the back engine has to go all the way to the front propeller, acting as a 'cantilever beam'.

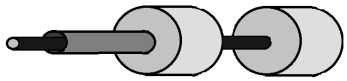

Figure 8.7: Twin engine configuration

Material Selection

The propeller shaft will be loaded in torsion which will result in shear stresses and a twist angle. Normal stresses are created due to the thrust force of the propellers and lastly bending will take place as the shaft can be seen as a cantilever beam which is fixed at one end (at the engine) and is free at the other end with a weight on it (the propeller). Fatigue will play an important role as the shaft will be continuously rotating during the aircraft's operation [38]. With this in mind one should select a material with isentropic properties. Metals fulfil these requirements. Composites too if they are produced with several fibre layers such that they are not unidirectional anymore. For the scope of this project a metal is chosen as it is easier to perform calculations on it. Several metals (alloys) exist, but in aerospace weight is an important factor. For this reason, Aluminium 2024 is chosen.

Bending

For the bending calculations it is assumed the bending will occur symmetrically, being influenced only by the gravity force of the propeller. In reality there will be more bending due to the changing angle of attack of the propeller blades when going up with respect of going down in climbing or descending flight.

Calculating the bending of a cantilever beam can be done with Equation (8.30) [13] where P is the force exerted on the end of the beam which is the propeller weight, l is the length of the beam, E is the Young's modulus of the material and I is the moment of inertia. As an exact value for the maximum deflection of the shaft could not be found in regulations, a deflection of 0.5 mm was taken. Next, Equation (8.30) was rewritten to find the moment of inertia. This moment of inertia equals Equation (8.31) [13] where a thin walled assumption is applied. t equals the thickness of the shaft and d_m equals the middle diameter. This equation was then rewritten in order to find the diameter. t was also unknown, so an iteration took place in order to find a thickness that was at least 10 times smaller than the diameter in order to legally apply the thin walled assumption.

$$\delta_{max} = \frac{Pl^3}{3EI} \tag{8.30}$$

$$I = \frac{\pi}{8} t \cdot d_m^3 \tag{8.31}$$

The limiting case for bending is the shaft that originates from the back engine and goes all the way to the front propeller, as it will have the smallest diameter and is the longest shaft. For the shaft originating from the front

engine and going to the back propeller the only constraint was that the inner diameter should be larger than the outer diameter of the inner shaft plus a margin such that the two shafts will not touch each other. This safety margin was taken as 1 cm on the radius. As the maximum deflection allowed is only 0.5 mm, no touching will occur.

Shear Stress

For the calculation of the shear stress also a thin walled assumption was applied. First the shear flow was calculated using Equation (8.32) [13] where T_{max} is the maximum torque and A is the enclosed area. In Section 8.4.1 it was calculated that the maximum torque of the engine needs to be 293 Nm. The Saluqi P50 however can produce 400 Nm of torque. Furthermore the propeller will introduce additional torque due to the drag of the propeller blades. This torque was assumed to be 100 Nm. The total torque will therefore be assumed as 500 Nm. Lastly the maximum shear stress is calculated with Equation (8.33) where t is the thickness of the shaft.

$$q_{max} = \frac{T_{max}}{2A} \tag{8.32}$$

$$\tau = \frac{q_{max}}{t} \tag{8.33}$$

Twist

The twist should be as low as possible for fatigue reasons and for the fact that one does not want the propeller to lack behind the power setting of the engine. First, one should calculate the twist angle θ per unit length z with Equation (8.34) [13], where T is the torque, A the enclosed area, G the shear modulus of the material and t is the thickness of the shaft. The integral can be simplified to πd_m using the thin walled assumption. Integrating Equation (8.34) is simply multiplying the equation with the length of the shaft as the torque is constant along the shaft.

$$\frac{d\theta}{dz} = \frac{T}{4A^2} \oint \frac{ds}{Gt} \tag{8.34}$$

Normal Stress

Thrust is provided by the propellers. This means that the propellers are 'pulling' the aircraft forward. This force will go through the shafts and hence they should be able to withstand these forces. The normal stress σ is calculated using Equation (8.35) where F is the exerted force and A the area. Note that it is not the enclosed area, but the area of the material itself which can be calculated by subtracting the radius minus half the material thickness from the radius plus half the material thickness. The question is what force F to use. For this Section 8.4.1 is used where the required power is calculated. Then $P = TV$ is used where P equals the power, T the thrust and V the velocity. Comparing the powers from Table 8.7 with their corresponding velocities which can be seen in Table 8.6 it was found the cruise climb at sea level required the highest thrust which was 1500 N. This is the total thrust provided by both propellers. Per propeller this should be divided by two. For safety margins, this division was not done.

$$\sigma = \frac{F}{A} = \frac{F}{\pi((r+t/2)^2 - (r-t/2)^2)} \tag{8.35}$$

Results

In Table 8.10 all the input parameters for the shaft design are shown. For the maximum twist angle and maximum deflection 0.1°and 0.5 mm is used respectively. Exact constraints for these parameters have not been found, but in a normal engine one can assume there are by far more vibrations compared to an electrical engine, so the mentioned values are considered reasonable.

The results are shown in Table 8.11. In this table, it can be seen that all the constraints are met. Furthermore the calculated stresses are below the maximum stresses of Aluminium 2024. This is including a safety factor of 1.5 that is applied to the calculated stresses. With this safety factor applied the formulas described in the previous section were reverse engineered to find the new diameter and thickness. To have a valid thin walled assumption the thickness was taken as 10% of the diameter of the long shaft which is the limit for the thin walled assumption.

The only thing that does not result from this table is the fatigue. According to [29] (where all the Aluminium 2024 was collected from) the fatigue strength of Aluminium 2024 is 138 MPa with 500 million cycles. The calculated stresses are the maximum stresses that will only occur if the propeller goes from standing still to its highest RPM. Besides, from engine tests on the ground, this will only occur during take-off. Furthermore the calculated maximum stress is an order of 10 smaller than the fatigue strength. Therefore it is deemed to be on the safe side.

[29] http://asm.matweb.com/search/SpecificMaterial.asp?bassnum=MA2024T4

Table 8.10: Input parameters for shaft design

Parameter	Value	Unit
Thrust, max	1500	N
Torque, max	500	Nm
Young's modulus of aluminum 2024	$73*10^9$	Pa
Shear modulus of aluminum 2024	$28*10^9$	Pa
density aluminum 2024	$2.78*10^{-3}$	kg/m^3
Propeller weight	49	N
length long shaft	0.5	m
length short shaft	0.15	m
max deflection constrain at the tip of the long shaft	0.0005	m
max twist angle constrain at the tip of the long shaft	0.1	deg

Table 8.11: Calculated shaft properties

Parameter	Long shaft	Short shaft	Aluminum 2024 property	Unit
Middle diameter	0.080	0.100	-	m
Thickness	0.008	0.008	-	m
Max shear stress	$9.33*10^6$	$2.33*10^6$	$283*10^6$	Pa
Max normal stress	$1.12*10^6$	$0.560*10^6$	$324*10^6$	Pa
Max twist angle	0.04	$2.4*10^{-4}$	-	deg
Deflection at tip	$7.0*10^{-5}$	$1.07*10^{-5}$	-	m
Mass	2.80	1.68	-	kg

8.4.5. Verification & Validation

Power Calculation

For the required power calculation equations were used from [14]. These equations were then put into a Python script where they were verified by inserting sample exercises out of the book. The validation was done by comparing the obtained values with existing aircraft. For this the Pipistrel Alpha Electro was chosen. From the POH the wingspan, climb speed, max ceiling, rate of climb and the MTOW was taken. The only assumption made was the drag coefficient during cruise. This was kept the same as for the calculations on the Dragonfly. It turned out the limiting power case was cruise climb at ceiling where the required power according to the Python script was 55 kW. With an engine efficiency of 95% this results in an engine input power of 58 kW. The Alpha Electro is fitted with a 60 kW engine, so the code is validated.

Shaft Design

The equations used are taken from [39]. The same holds as for the power calculations: the equations were put in a Python script and verified with examples from the book. The reverse engineered equations due to safety factors were verified by setting the safety factor to 1 and assessing if the results are the same with the non-reversed equations. The calculations were validated by comparing the found diameter for the Dragonfly with a real aircraft propeller shaft. For this a propeller shaft of a Cessna 172 was taken. After measuring this diameter on a real aircraft it turned out to be 5.7 cm This is smaller than the founded diameter of the Python script. This is due to the fact the shaft of the Dragonfly is longer and hence it is subjected to more forces. As the order of magnitude is the same, the script passed the validation.

8.4.6. Hardware Diagram

In Figure 8.8 the hardware diagram the propulsion system is shown. The engine computer is powered by the battery pack through the DC-DC converter. It also uses this input to calculate the remaining battery capacity. Furthermore, the engine computer gets input from the throttle lever, namely its position in percentages of the total power available. Then the engine computer will divide the amount of power to each engine based on this throttle position. The front propeller, for example, should be powered up first as it has a smaller angle of attack and hence is easier to spin up. Then the rear propeller can be spun up easily due to the increased incoming velocity. The TE is also connected to the engine computer. If one wants to simulate different weight or weather conditions, the engine computer will adjust the power that is sent to the engine's respective Electronic Control Unit (ECU) A (or B in case of an ECU A failure). These control units then create set-points about the required RPM which are sent to

the inverter of the motors. The inverters then ensure these set-points are realised by the motors. The ECUs also receive engine temperature and torque from the motor's inverter. Based on this information the set-points can be adjusted. Furthermore, this data is continuously sent back to the engine computer and from there it is redirected to the cockpit instruments. The ECUs are powered from the DC-DC converter as well. The motor inverters are powered by their respective motor directly as they are integrated within each other. Lastly, one can see there is a two-sided arrow going from the battery pack to the motors. This is because the engines can function as a generator in gliding flight. In this case the battery will be recharged.

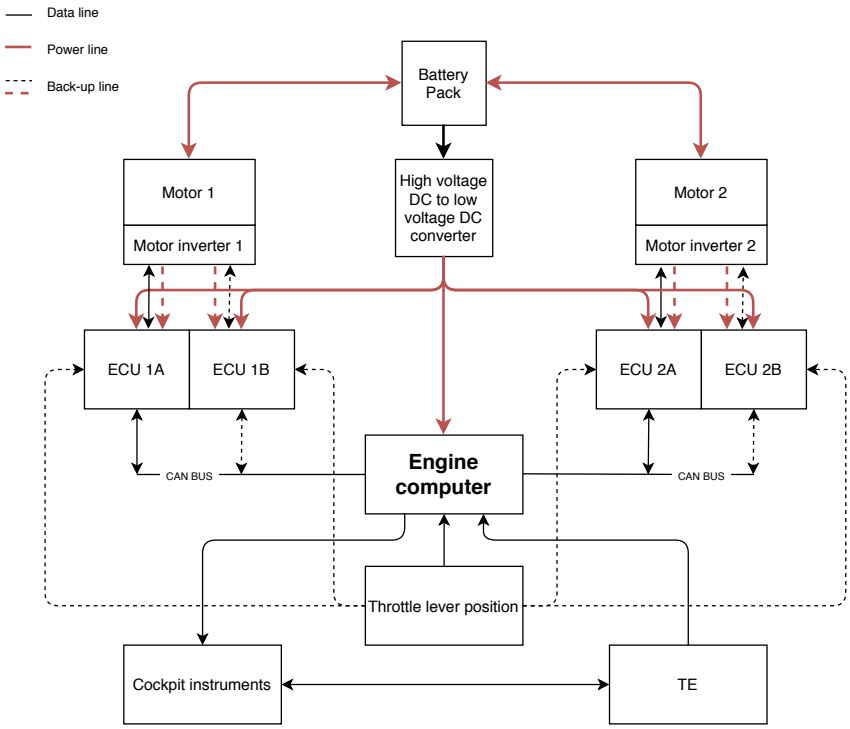

Figure 8.8: Lay-out of propulsion's electrical system

8.4.7. Risks

During the design of the engine several risks were thought of. To begin with the power of the engine, the limiting case was cruise climb at service ceiling. The required power for this was two times as high as the power required for the take-off run. Hence, the engine is overpowered during take-off. The risk is that students are overwhelmed by this additional power. To minimise this risk, the throttle could have a maximum position which will not result in 100% power. In emergency situations or on very short runways the lever then could be positioned in TOGA-mode (Take-Off, Go-Around) similar to Airbus aircraft.

Going to the propeller shaft, a risk is that the calculated stresses are lower than they will be in reality. To minimise this risk a safety factor of 1.5 is applied to the stresses. With these new stresses the required area of the shaft was recalculated.

Then there is still the electrical system which is shown in Figure 8.8. The engine computer may fail. In this case, the throttle lever position is directly sent to the respective ECU. This means that the propulsion efficiency will go down as the exact amount of thrust that should be generated by each engine will not be known. Furthermore, it is not possible in this scenario to simulate different weight and or weather conditions as there is no direct connection between the TE and the ECUs. As one can see, there is no direct connection between the ECUs and the flight instruments. This is done to save wiring and complexity. Hence, if the engine computer fails the pilot does not receive the engine temperature and RPM. Therefore they should land as soon as possible.

An ECU may also fail. For this reason each engine has a back-up, namely ECU B. If this failure is due to a malfunction of the DC-DC converter the ECUs will be powered by the motor inverter as a back-up. As the engine computer will fail in this scenario the ECUs will directly receive the throttle input data.

If a total battery failure occurs, the engines will stop working. In this case the pilot should trim for best glide speed and prepare for an emergency landing.

What is not yet mentioned is the risk of an engine failure in general which is not caused by a failure of the battery

pack. In this case the aircraft is still flyable. When using maximum power on the remaining engine the aircraft is still able to climb although it is only 60 feet/minute at sea level.

8.5. Propeller Design

This section presents the design and set-up of the propellers. During the literature study it became clear that little literature is available about the design of a contra-rotating propeller (CRP). For this reason. only a basic analysis could be performed with no detailed design. To compensate for this and to be able to achieve a final design in the future, a test plan is generated in Section 8.5.6.

8.5.1. Literature Study

As mentioned before it was decided during the midterm phase of this project to go for a CRP system. Research into this is not new, however little is explored and there are a lot of grey areas. CRPs have high potential due to the increase in efficiency and a cancellation of torque caused by the propeller [40]. Furthermore, the diameter of the propellers can be made smaller and/or the RPM can go down. For a single propeller, this would imply a noise reduction, for a CRP this is not a one-to-one relation as the rear propeller will go through the tip vortices of the front propeller if the diameters are kept the same. Despite the advantages of a CRP, it is not widely used. This is due to the added complexity which results in higher maintenance costs and a less reliable system when looking at conventional engines. With electric engines it is a different story. These engines are smaller, have less moving parts and hence are less complex and more reliable. Besides, their weight is less than conventional piston engines. With all of this in mind the concept of CRPs does not add much complexity as one can see in Figure 8.7.

In the literature study the focus was on propeller noise and the interaction between two propellers behind each other in contra-rotating configuration. It was difficult to find information on these subjects, especially on the combination of the two. Currently research on CRPs in combination with electric engines is performed - for example by Contra Electric Propulsion Ltd [30], however findings are not (yet) published.

For noise produced by a single propeller more information was found e.g. in a report by NASA [40]. This paper explains that increasing the number of blades of a propeller will result in a reduction of noise produced. Going from two to three propellers would result in a decrease of 4 dB and going from three to four blades 4.5 dB. This has to be done in combination with decreasing the RPM. Furthermore, it will result in a heavier propeller and the costs will go up. Next to that, it is said that the climb performance of an aircraft will go down with an increasing number of propeller blades according to Rathgeber and Sipes. Salikudding is also mentioned in the NASA report. He investigated how much of a reduction in noise was possible by sending a sinusoidal sound from a speaker placed on the fuselage of an aircraft. It turned out the decrease could be in the order of 8-14 dB when sending a signal between 200 and 1000 Hz. This reduction of noise was however not unidirectional. Weiblen, also states in his research that a noise reduction of 2-3 dB is observed per 100 RPM propeller speed decrease. The same holds for a decrease in propeller diameter per 10 cm. However, the propeller diameter cannot be decreased too much as then the propeller slipstream velocity will increase which results in more drag, which then should be solved by increasing the thrust.

For the CRP the slipstream of the front propeller needs to be analysed. This slipstream is affected by the induced velocity (which is created by the thrust and the contraction of the slipstream), the change of total pressure across the slipstream and the tangential velocity and swirl introduced by the propeller torque [41]. From a noise perspective the rear propeller should be located within the slipstream of the front propeller, therefore the rear diameter should be made smaller. If the diameters would be the same the propeller tips would smash into the tip vortices of the front propeller. An optimum has to be found as the contraction of the slipstream is stronger at low speeds with full thrusts (due to the high ΔV) compared to cruising conditions. Furthermore, the angle of attack of the rear propeller should be made larger due to the increased velocity with respect to the free stream velocity in the slipstream. Once again, no literature was found that investigated this in detail and hence a test plan is set up in Section 8.5.6.

8.5.2. Single Propeller Analysis

In order to design and size the propellers for the final stage of aircraft design in this project, first an analysis had to be performed to understand what influence the propeller design parameters (number of blades, diameter, geometry, power and rotation speed) have on the performance of a propeller system. Although the final aircraft design will feature a CRP setup, it was decided to first analyse the influence of the design parameters for a single propeller. This was done in order to get an understanding of the basic propeller phenomena. In order to perform this analysis, the tool CROTOR [42] was used. The principle behind CROTOR will be discussed in Section 8.5.4.

For the analysis it was decided to use an equivalent of a fixed pitch Hercules propeller, which is already tested for a CRP setup, because of its simplicity (consequently low cost and low maintenance) and good efficiency, see Figure 8.9 [30] [31] [43]. This propeller is thus used for analysis. However, the final selection procedure of the propeller is described in Section 8.5.6. It should be noted that this analysis was performed mainly to explore the differences in

[30] URL: https://www.contraelectric.com/, LA 19-06-2020
[31] URL: https://www.hercprops.com/, LA 19-06-2020

propeller configuration. Alongside the geometry, the aerodynamic parameters of a Clark Y airfoil are used. This airfoil is widely used as a blade airfoil and known for its high efficiency and improved aerodynamic characteristics [44]. The aerodynamic parameters of this airfoil are approximated using JavaFoil [45]. JavaFoil is an already validated[32] aerodynamic tool which can be used to approximate airfoil characteristics. The diameter of the propeller was set to 2 meters. The atmospheric conditions were set to the ISA-standard atmosphere at an altitude of 1000 meters and the Reynolds number was set to $1 \cdot 10^5$. The flight velocity [m/s], input power [W] and the number of blades are kept as variables. Using these input values for CROTOR Figure 8.10, Figure 8.11 and Figure 8.12 were obtained.

Figure 8.9: Propeller blade used for analysis [43]

An important parameter in the performance of a propeller is the propeller efficiency. This defines how much power from the engine is translated into thrust. Therefore it is preferred to have the propeller efficiency as close to 1.0 as possible, especially since the efficiency is one of the parameters with the most impact on MTOW, because of its close relation to the battery weight. Figure 8.10 displays the propeller efficiency with respect to the advance ratio. The advance ratio J is described by Equation (8.36) [26] in which V equals the aircraft flight velocity or true airspeed in meters per second, n equals the rotational speed of the propeller in rotations per second and D equals the diameter of the propeller in meters, which is in this case equal to 2.

$$J = V/(nD) \tag{8.36}$$

From Figure 8.10a, which describes the propeller efficiency of a 2 bladed propeller for different power settings, it can be concluded that the efficiency curve will not vary with varying power settings. It should be noted that the x-values of both curves in this figure do not line up due to the fact that a fixed pitch propeller is used. This means that the rotation speed n will vary with different power settings, as a propeller with a higher power setting can produce more torque and thus can rotate the propeller at a higher rotation speed. That is why the efficiency is plotted as a function of J. This will make the efficiency curve independent of the rotation velocity and the flight velocity.

The propeller design (geometry and number of blades) influences the efficiency curve, as can be seen in Figure 8.10b, in which the efficiency curve is displayed for different blade configurations at a power setting of 40 kW. From this curve, it can be concluded that adding more blades to the propeller will decrease the overall efficiency. In conclusion, the less propeller blades the better the propeller efficiency.

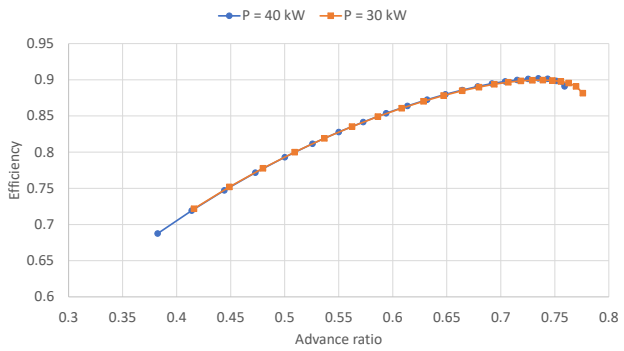

(a) Number of blades = 2

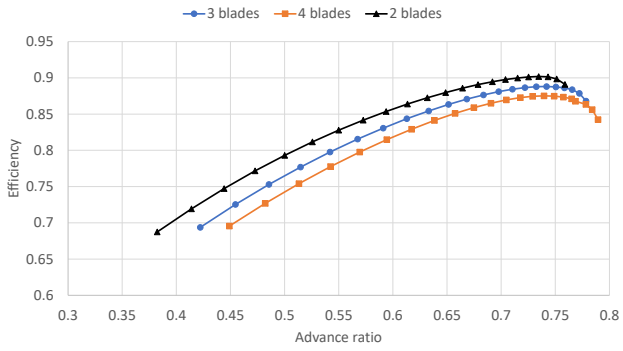

(b) Power = 40 kW

Figure 8.10: Efficiency versus advance ratio.

The advantage of having more than two blades can, however, be seen in Figure 8.11, in which the rotational velocity of the propeller in revolutions per minute (RPM) and the thrust generated by the propeller are displayed as a function of the flight velocity with a fixed power setting of 40 kW. In these two figures it can be seen that for example a 3 blade propeller can generate the same amount of thrust at a lower rotational speed in comparison to a propeller with 2 blades. This is beneficial for the reduction of noise emission, as a lower rotational speed will result in a lower helical tip Mach number, as the diameter is kept constant, which will reduce the produced noise as discussed in the previously mentioned NASA paper [40].

[32] https://www.mh-aerotools.de/airfoils/javafoil.htm LA: 16-06-2020

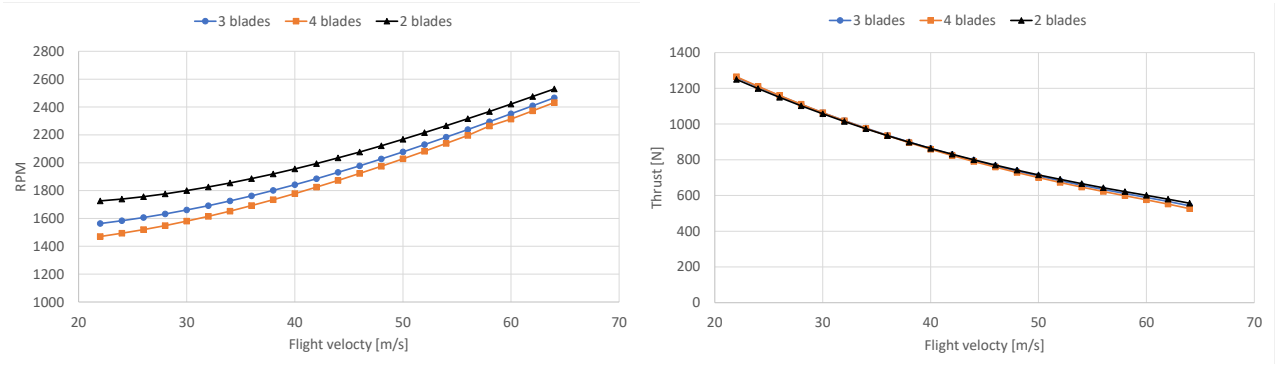

(a) (b)

Figure 8.11: Rotational velocity and thrust versus flight velocity.

The final design parameter to be discussed is the propeller diameter. Figure 8.12 shows the efficiency and rotational speed for different propeller diameters. These plots were created for a two-bladed propeller for a constant power of 40 kW and a flight velocity of 46 m/s. From these figures it can be concluded that the propeller efficiency remains constant for diameters larger than 2 meters, however, once the diameter is smaller than 2 meters the efficiency will decrease rapidly. This is most likely due to the fact that for these smaller diameters the rotation speed increases very rapidly, Figure 8.12b, therefore the tip of the propeller is approaching Mach 1.0 resulting in the efficiency to decrease very rapidly as the Clark Y airfoil is not suited for high Mach numbers. For a diameter larger than 2 meters the relation between RPM and diameter is almost linear, which will result in a constant advance ration, which in turn will result in a constant efficiency.

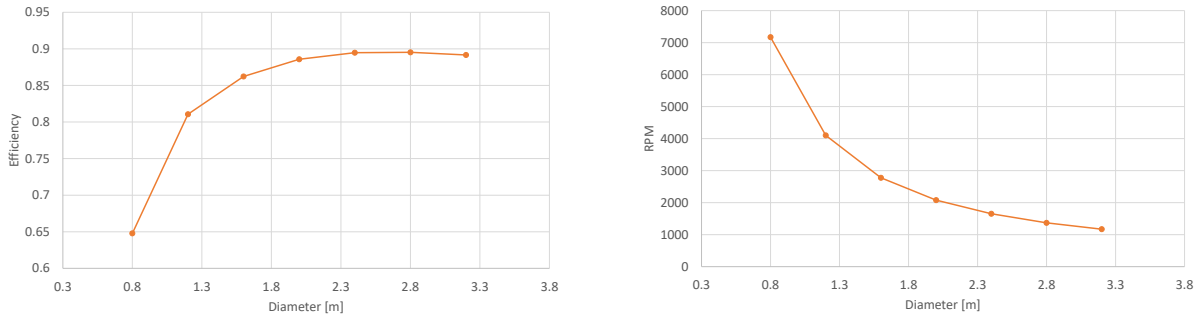

(a) (b)

Figure 8.12: Efficiency and rotational velocity versus propeller diameter (2 blades, Power = 40 kW, Flight velocity = 46 m/s).

So, overall, in the decision on the configuration of the propeller one should account for the influences of the design parameters described above. This single propeller analysis can now be used for the CRP setup.

8.5.3. Contra-Rotating Propeller Analysis

The actual design of the aircraft will feature a CRP. Therefore it should be investigated whether the propeller design parameters will have the same influence on a CRP as on a single propeller as described in Section 8.5.2. The analysis for the CRP setup was also performed in CROTOR. This tool is able to approximate the effects of a contra-rotating propeller by first analysing the forward propeller and calculating its far-downstream slipstream velocity components. These components are then added to the free-stream velocity and used as an input for the aft propeller. The slipstream output from the aft propeller can then be used again as an input for the forward propeller. This process is iterated until a certain threshold is approached.

The CPR analysis was performed on a setup with two fixed pitch propellers as described in Section 8.5.2. However, the number of blades per propeller could vary. The diameter of both propellers is equal and set to 2 meters. The atmospheric conditions were set to the ISA-standard atmosphere at an altitude of 1000 meters and the Reynolds number was set to $1 \cdot 10^5$. The flight velocity [m/s] and input power [W] are kept as variables. Next to that the rotational velocities of the propellers were not synced for noise considerations, this will be further explained in Section 8.5.6.

The influence of the number of blades for the forward and aft propeller can be seen in Figure 8.13a, which displays the efficiency with respect to the advance ratio of the average rotational speed of both propellers for a total power of 80 kW. This efficiency curve is created for three propeller setups displayed in the legend above the figure, as an

example: 3 Aft 3 Fwd describes a CRP setup of a 3 blade aft propeller and a 3 blade forward propeller. The same relation as for a single propeller can be concluded, namely that increasing the number of blades will decrease the efficiency.
From Figure 8.13b, which displays the efficiency curves of the aft and forward propeller for a 2x2 setup at a power setting of 80 kW, it can be concluded that due to the extra rotation of the flow coming into the aft propeller it will have a slightly higher overall efficiency. Next to that the rotational velocity of the aft propeller is slightly lower, which can be seen in the fact that the x-values (advance ratio) do not line up.

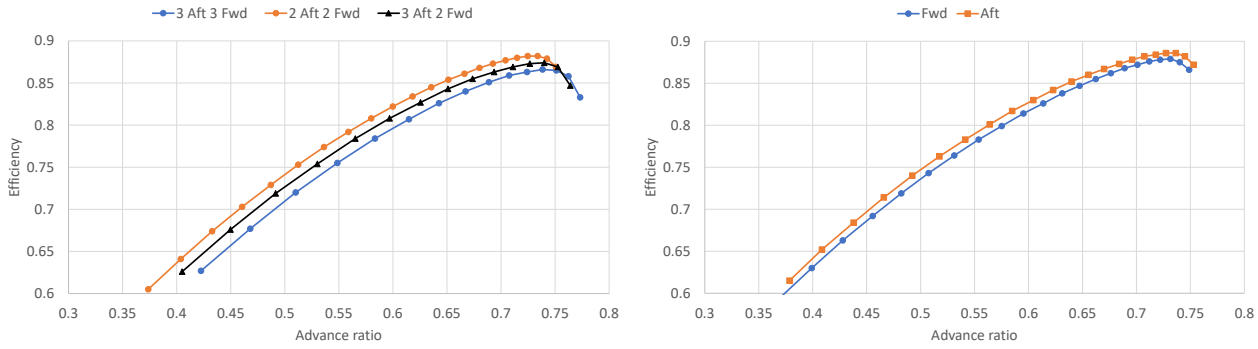

(a) Contra-rotating system efficiency

(b) Seperate propeller efficiency

Figure 8.13: Efficiency versus advance ratio (Power = 80 kW).

Regarding the rotational velocity, the same principle holds for a CRP setup with respect to a single propeller. Figure 8.14a displays the rotational speed of the aft propeller for a total power setting of 80 kW. From this figure it can again be noticed that the rotational speed of a 3x3 configuration is lower compared to a 2x2 configuration while maintaining the same thrust, see Figure 8.14b. Which is beneficial for the noise of a single propeller, however, the interaction between the two propellers should also be investigated as the turbulent flow coming from the forward propeller will most likely be amplified by the back propeller. More on this will be discussed in Section 8.5.6.

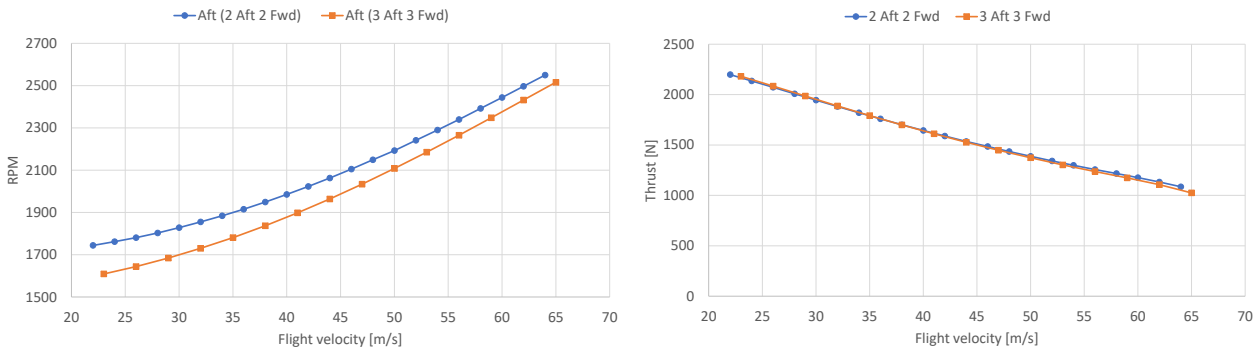

(a)

(b)

Figure 8.14: Rotational velocity and thrust versus flight velocity (Power = 80 kW).

So all in all it can be concluded that the same design parameter influence is present for a CRP setup in comparison to a single propeller setup. And that thus a compromise in the number of blades, desired RPM and diameter should be made.

8.5.4. Limitations CROTOR

For then analyses performed in the above sections CROTOR v755es1.3 was used. CROTOR is an extension based on XROTOR v7.55c [46], CROTOR namely automates the process of extracting and inputting for the velocity fields of the aft and forward propellers in a CRP setup. Next to that it adds an input interface for designing CRP setups.
As CROTOR is based on XROTOR, basically the functionalities of XROTOR were used for the single propeller analysis, described above in Section 8.5.2. XROTOR uses a propeller lifting line theory to calculate the performance parameters of the propeller. To calculate the induced velocities and induced losses the graded-momentum method was used for the analysis described above. This method is applicable for advance ratios, J, up to 0.5π [47]. As can be seen in for example Figure 8.10 the advance ratio is well below this threshold.

For the contra-rotating propeller calculation it should be noted that CROTOR makes an approximation, as for the analysis the far-downstream velocity field of the forward propeller is taken as an input for the aft propeller. This will introduce a significant error as the aft propeller is most likely very close to the forward propeller, so not in the far-downstream velocity field. To correct for this XROTOR (and CROTOR) uses standard velocity weights, however, these weights will only correct slightly as the weights will most likely differ per propeller type. Therefore experiments will have to be conducted to find these weights.

A noticeable shortcoming of CROTOR in the analysis of a CRP was observed, in this analysis it was noticed that the efficiency of a CRP compared to a single propeller was slightly lower. However, literature [48] shows that the efficiency of the same propeller should increase when converting from a single propeller to a CRP, hence the decision of using a CRP in the Dragonfly.

In the end, it can be concluded that CROTOR is very useful for the initial estimation of the propeller parameters, however, more research is required to fully improve the design of contra-rotating propellers. As CROTOR is only able to approximate the interactions between the two propellers in a CRP.

8.5.5. Final Propeller Design Conclusion

As mentioned before a compromise has to be found between high efficiency by a low number of blades and low noise by a lower RPM and smaller diameter (which will lead to a higher number of blades). Therefore, the conclusion from the CROTOR analysis is that the Dragonfly trainer aircraft will fly with a 2x3 CRP (2 blade front propeller and 3 blade rear propeller), this will make it easier to play with RPM setting and diameter during testing as a 3 blade propeller can have a smaller diameter than a 2 blade propeller for an equal amount of thrust and therefore there will be a larger range in which the rear propeller will lay inside the slipstream of the front propeller. This configuration is, however, subject to change after testing described in the next section.

With this configuration the propeller diameter could be determined, for now it is assumed that both propellers will feature the same diameter, which is an assumption as most likely the aft propeller will feature a smaller diameter to stay in the slipstream of the front propeller more on this in Section 8.5.6. The diameter was calculated based on the critical required thrust, which is calculated by dividing the required power, calculated in Section 8.4.1, by the true airspeed. It was concluded that the critical thrust would be equal to 1.5 kN at an altitude of 1700 m (highest airport from which the aircraft should be able to take-off) for an airspeed of 26.46 m/s, which is equal to the take-off speed at that altitude. As specified in Section 8.4.1 the available take-off power is equal to 67 kW, using this as an input variable for Crotor will result in a required diameter of 1.4 m for the 1500 N of thrust. However, the rotational velocity of the propellers will in that case be equal to approximately 3000 RPM. As the noise produced by the propeller should be taken into account a solution was found by increasing the diameter to 1.8 meters which would result in a rotational velocity of only 1850 RMP for both propellers with a required input power of 56 kW, which is below the available power thus this design is viable. The relatively low RPM value will result in the noise produced by each individual propeller to be low, however, the interaction between the propellers will have to be investigated as well, which will be described in Section 8.5.6. For the total weight calculations of the complete aircraft it was assumed that the propeller mass is equal to 12 kg, based on data from [33].

8.5.6. Test Plan on Fixing Propeller Parameters

This section describes the way the propeller set-up and layout will be finalised during testing post-DSE. First tests will be performed for scaled models in simulated take-off, climb and cruise conditions. These results will be taken as a starting point for tests on a 1:1 scale testing programme. The configuration of the number of blades is already determined for each propeller: the front propeller has two blades and the rear propeller three blades. To limit the scope of testing and keep the development costs low, the propellers will be off-the-shelf, in these tests one wants to determine the distance between the two propellers, the RPM ratios and the diameter & pitch of the rear propeller to maximise efficiency and minimise noise.

Scaled Testing Set-Up

The scaled testing will take place in a wind tunnel. Here the front propeller will be fixed pitch as this propeller will receive free-stream air velocity. In the tests however the influence of the suction of the rear propeller on the front propeller will be examined, if this turns out to have a noticeable influence the pitch might need to change. In that case the propeller will be substituted with a variable pitch propeller in the end of the testing sequence described below. The rear propeller will be variable pitch during the entire duration of the tests as the incoming air velocity depends on the distance from the front propeller and the RPM of the front propeller. To properly scale the propellers for testing the advance ratio should be kept constant with respect to the full-scale propellers. During all tests the noise will be measured in weighted decibels, in addition the frequency spectrum will be measured as noise spread out over a larger frequency spectrum will result in lower experienced noise. Furthermore the RPM, power input and thrust output will be measured for each propeller where the thrust measurement at the back of

[33] https://whirlwindpropellers.com/aircraft/product/propellers-for-ul260350-engines/, LA: 22-06-2020

the rear propeller is the thrust generated by the entire propulsion system.

The first scenario tested will be a simulated take-off condition where the free-stream velocity equals zero. The propellers are both rotating at their maximum RPM and are placed as close as possible to each other where the pitch of the rear propeller is full fine and both propellers have the same diameter. Then the pitch of the rear propeller will be increased such that the thrust will remain the same while the RPM is decreased. Then the rear propeller will be swapped with a new one with the pitch fixed at the position found in the previous test, the same RPM will be used and the diameter will be halved. This is done to ensure the aft propeller is in the slipstream of the forward propeller. The distance between the propellers will be increased, by doing this the distance can be found where the noise is minimised (the noise caused by smaller pressure waves in the slipstream that will be amplified by the rear propeller) whilst keeping the thrust constant. If and when such a distance is found and it is realistic (in the order of centimetres) the rear propeller will be replaced again, now by a propeller with a diameter as large as possible, still keeping it in the slipstream of the front propeller. To find the diameter one can use a smoke system to see where the boundary of the slipstream is. With this increased diameter one has to examine if the thrust requirement is still met. If it is underpowered the rear propeller has to be placed closer to the front propeller with an increased diameter that still is in the slipstream. When it is overpowered one can adjust the RPMs of both propellers to find an RPM ratio where the thrust requirement is met and where the noise is minimised. Now it is time to look to the influence of the rear propeller on the front propeller. The efficiency of the front propeller is measured with and without the rear propeller, if there is a noticeable difference the front propeller pitch could be changed to compensate for the influence of the rear propeller.

After this first series of tests, one repeats it at least three times, this time with a frontal velocity which simulates cruising conditions (simulate both cruise at cruise power and cruise climb with maximum power) and maximum speed conditions. The results of these tests will lead to different diameters of the rear propeller if the distance between the propellers would be the same as in the first test series, as the slipstream contraction depends on the velocity difference of the slipstream with respect to the free stream velocity as one can see in Figure 8.15. This figure is based on a report by NASA [41]. As there was no visualisation of the slipstream contraction, the formulas were inserted into python to make Figure 8.15. At all flight velocities shown, take-off power is used. Furthermore, the RPM ratio differences between the simulated cruise flight and the climb performance might be large as one can differ the RPMs more during cruise flight, for example let the RPM of the rear propeller be as high as possible whilst keeping the RPM of the front propeller as low as possible.

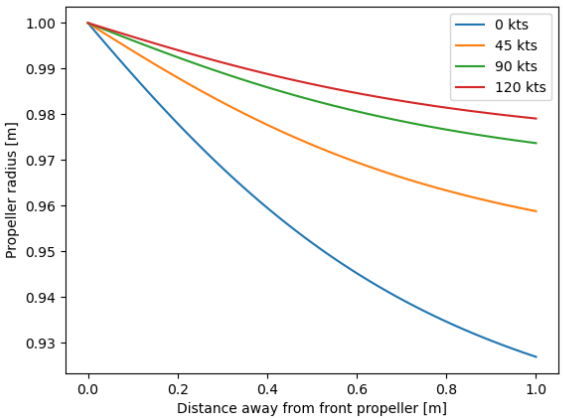

Figure 8.15: Slip stream contraction at different flight velocities

At the end of these test series, one has to determine what to do with respect to efficiency and noise. As shown in Figure 8.15 the slipstream contraction is different for different flight phases. Most of the time the aircraft will fly in cruising conditions. To maximise the efficiency the diameter of the rear propeller will have to be larger than the best performing diameter for take-off conditions, if this is done, the noise at take-off would go up as the rear propeller will go through the tip vortices of the front propeller. Preferably this issue will be solved before going to the 1:1 scale testing as it is more expensive to build propellers at full-scale as you would need multiple with different diameters.

Full Scale Testing

The results from the scaled testing will be the starting point for full-scale testing. As a wind tunnel would be too expensive, two alternatives come into play. The first one is to mount a set-up on a car and drive with this car at different speeds on a straight track such as a runway. The other way is to mount the set-up onto an existing

aircraft. This is mostly done for high performance engine testing (jet engines or turboprop engines), therefore the first option is most suitable, also due to costs.

To reduce costs it should be aimed for to fix the rear propeller diameter before starting the full-scale tests. Hence, the diameter should be based on the scaled tests. During the full-scale test series the distance between the two propellers can then be adjusted such that the diameter still fits within the slipstream. This distance should be a compromise as the slipstream contraction is different for each different flight phase. During these tests the discovered RPM ratios of the scaled tests should be validated and if necessary adjusted.

The final step would be to test it on the real aircraft during its test flights.

8.5.7. Verification & Validation

For verification of CROTOR some tests were performed. First, it was checked if the Mach number increases from root to tip like expected, which it does. Then it was investigated if the rear propeller is actually influenced by the front propeller by running analysis on the rear propeller alone and see if there is a difference (increase in efficiency etc.), this is the case as can be seen in e.g. Figure 8.13b. Furthermore, if a smaller diameter is inputted and power is kept constant one would expect the RPM to go up. This is proven in Figure 8.12.

Validation of CROTOR will be performed during testing described in Section 8.5.6.

8.5.8. Risks

One of the most hazardous risks is that the noise pollution of the CRP is higher than expected. To reduce the risk the test plan must be strictly followed to analyse the CRP in more detail and reported on to help in further research and implementation of CRPs in general aviation. During testing, anti-phasing of the two propellers will be examined, this will be done by finding the RPM ratio at which the sound is minimised.

Another risk is that testing might become expensive as there is little known about CRPs. By analysing the best options only and preparing the tests in high detail, unexpected and high costs will be avoided.

Furthermore, during testing it might turn out that the CRP is not fully suitable for the Dragonfly design e.g. because of noise. In that case the engines could be positioned next to each other propelling the propeller shaft by means of a belt which can be seen in Figure 8.4, this will add the option of removing a propeller and flying with only one.

8.6. Compliance Matrix

Below in Table 8.12 the requirements compliance matrix for the Power & Propulsion requirements can be found.

Table 8.12: Compliance matrix for the propulsion system.

Identifier	Requirement	Obtained value	Requirement met?
ELTA-CS-PRO-01	Any electric energy storage device providing electric energy to an electric engine(s), shall be designed and constructed so as to provide the required energy for the electric engine(s) of the Electric/Hybrid propulsion system at all times during the flight in order to provide the rated powers that ensure safe operations.	*	✓
ELTA-PRO-02	The motor shall be able to provide the maximum power loading of 0.121 N/W.	0.121 N/W	✓
ELTA-PRO-03	The battery and engine temperatures shall be displayed.	*	✓
ELTA-PRO-04	The engine computer shall calculate the current reserve on board.	*	✓
ELTA-BAT-05	The battery shall not exceed the maximum current and voltage levels specified by the manufacturer.	400 V	✓
ELTA-BAT-06	The battery cell type for the battery pack shall be rechargeable.	*	✓
ELTA-MAR-12	The endurance of the aircraft shall be 2 hours, when flying with maximum payload.	2.5 hrs.	✓
ELTA-MAR-14	The recharge time of the aircraft shall be 40 minutes.	1.9 hrs.	✗
ELTA-MAR-17-01	The aircraft range shall be 250 km, when flying solo.	310 km	✓
ELTA-MAR-20	The aircraft shall be rechargeable with currently available technology.	*	✓
ELTA-MAR-21	30 minutes of flight time endurance shall be added to the endurance of the aircraft, as reserve	30 min.	✓

9
Training Enhancement and Cockpit Design

This chapter describes the design of the training enhancement package, as well as the cockpit layout. It begins with the performed market analysis in Section 9.1 to find out what the current training capabilities are. Thereafter, a functional analysis is performed in Section 9.3 and the requirements that followed from this analysis are listed in Section 9.3. The primary research that was conducted is discussed in Section 9.4. Next, the design of the in-flight segment (Section 9.5) and the ground segment (Section 9.6) of the TE package is explained. With this in mind, the cockpit layout was generated, as shown in Section 9.7. After this, the risks and verification and validation strategies are described in Section 9.8 and Section 9.9 respectively. Thereafter the benefits of having electric propulsion for the training enhancement are given in Section 9.10. Nearing the end of the chapter the training effectiveness is quantified in Section 9.11 and the cost benefits are given in Section 9.12. The chapter concludes with further recommendations in Section 9.13.

9.1. Market Research

Before any research on the TE items could be performed, it was vital to perform a market research in order to determine the current training capabilities of both the in-aircraft segment as well as the flight simulators on the ground.

9.1.1. In-Aircraft Segment

In order to ease piloting, many devices exist which could potentially be used for training enhancement. For example a portable HUD can be used in order to display altitude, a virtual horizon and other items with the use of an iPad and app onto the windshield. At a cost of around $2,000 and a mass of around 1kg [1], it is a reasonable addition to the cockpit. More expensive options also exist, which have more features such as enhanced runway vision and are not simply a mirror of a smartphone or tablet screen. However, at a cost upwards of $25,000, these are not considered for the Dragonfly TE package.

Adding a primary flight display (PFD) adds a digital screen on which navigation, traffic and other items can be displayed. Their sizes and prices vary from single-instrument-slot PFD's for around $3,000 to larger PFD's such as the Garmin G1000, which costs up to $425,000 to retrofit [2].

The market analysis shows that even though at the moment a significant amount of GA aircraft are equipped with an autopilot, the pilots still struggle with operating it, either in the sense that they rely too much on this technology and sequentially their manual flying skills deteriorate or in the sense that they are reluctant to use it, ending up just ignoring it [49]. It is important to have an autopilot on-board and a training procedure that allows gaining the necessary skill to operate the autopilot safely and efficiently, as this can reduce the workload during critical phases of flight significantly [50].

A critical part of the training consists of debriefing the performed flight. The majority of the light GA aircraft are not required to carry a flight data recorder [51] which could have an added value to this debriefing. Several types of debriefing software such as CloudAhoy[3], and CEFA AMS[4] have been newly introduced on the market however and can be used in conjunction with flight data retrieving technology for immediate after-flight debriefing procedures.

Regarding the training of extreme/emergency situations, this is usually performed using scenario based training (SBT). Some scenarios may be trained in the aircraft under the close supervision of the instructor (stall recovery, engine failure, cross-wind landing etc.) but the training of most extreme situations is preferably performed in a safe environment: the flight simulator. However, it is apparent that certain situations, such as a near-miss, are insufficiently trained with a simulator alone, as the level of realism of the actual situation may not be entirely mimicked and the pilots do not feel the same level of risk/adrenaline as in reality. As a solution for this, NASA has recently introduced on the market the Fused Reality concept[5]. This is however not widely used for training in GA at the moment. Furthermore, the use of a VR headset during flight implies that an instructor needs to be present on board as at least one flight crew member should have visuals with the outside during VFR flight training.

[1] URL https://epicoptix.com/epic-eagle/, LA 11-05-2020
[2] URL https://www.flyingmag.com/avionics-retrofits/, LA 11-05-2020
[3] URL https://www.cloudahoy.com/, LA 11-05-2020
[4] URL https://www.cefa-aviation.com/ams/, LA 11-05-2020
[5] URL https://www.nasa.gov/centers/armstrong/features/fused_reality.html, LA 11-05-2020

9.1.2. Ground Segment

Currently flight schools use varying levels of flight simulators for training, which sparks debates on which one is suited for which level of training. While some people argue that a motion base is not required for ab initio training, others value the added training effectiveness [52]. Prices for flight simulators can range from around $1,500 for a simple at-home simulator, to upwards of $20 million for a full flight simulator (FFS), certified at level D. Most larger flight schools that do operate flight simulators operate either reconfigurable training devices (RTD), for around $50,000 or an (entry-level) advanced aviation training device for as low as $90,000 [53].

A new type of flight simulator was introduced by the US Air Force in April 2019, through the Pilot Training Next program. This simulator consists of a VR headset in conjunction with artificial intelligence and advanced biometrics [54]. Even though it is not used on a large scale on the market at the moment, this compact simulator has a lot of business potential due to its relatively low price (around $8,000-$10,000 per unit [55] [6]) and high level of realism that would allow for more efficient and affordable training for the GA pilots.

According to [56], in 2002, 87% of pilots receiving their PPL had never been trained in a simulator. Even though the percentage of pilots being trained on simulators ought to be higher today, there is still a large gap in the use of flight simulators to not only enhance training effectiveness, but make flight training more financially viable.

9.2. Functional Analysis

In order to extract the TE package requirements, first, a market analysis into current training capabilities has been performed, researching the technology/methods currently used to train pilots in very light aircraft. After this, the main functions from the FFD found in Appendix A related to the training enhancement have been identified, namely:

- Setup training routine;
- Perform flight training routine;
- Perform flight training program checklist;
- Perform training manoeuvres;
- Perform take-off/train take-off;
- Perform landing/train landing;
- Receive flight training feedback.

Then, specific functions of the TE package have been derived. The identifier of each function mentioned inside the round brackets corresponds to the identifier used in the FBS [1]. It is important to note that the following items, starting with **ELTA-FUN** are not requirements, but are functions. First, the top level function:

- **ELTA-FUN-TE-01** (A.3) - *Enhance training effectiveness*.

Followed by additional functions:

- **ELTA-FUN-TE-02** (A.3.1) - *Improve accessibility to the daily training routine.* This function comes from the need of improving the efficiency of presenting the student with the training routine. As of now, students usually have the training routine written on paper. The training experience will be enhanced by decreasing the amount of time needed for the student to be informed about the training routine, as well as improving focus as the student will not have to carry and search through a thick training syllabus. Furthermore, this will be favourable for the flight school in terms of sustainability as well as cost effectiveness, eliminating the need to use paper and ink;
- **ELTA-FUN-TE-03** (A.3.2) - *Improve checklist procedures.* As of now, checklist procedures may be time consuming. In addition to this, paper checklist are currently used. By digitising the checklist procedure, the training experience will be improved by decreasing the time needed to complete the checklists, as well as the reliability of the procedure. Furthermore, it is positive from a sustainability and cost effectiveness perspective, as paper and ink will not be needed for this task;
- **ELTA-FUN-TE-04** (A.3.3) - *Improve manoeuvre training.* The effectiveness of the training procedure of the different manoeuvres performed both on ground and in-flight needs to be increased by the addition of the TE systems on-board the aircraft;
- **ELTA-FUN-TE-05** (A.3.4) - *Improve the assistance given to the students during flight, by means of autonomous flying technology*. As of now, autonomous flying technology is usually not implemented in very light trainer aircraft. The addition of various levels of autonomous flying technology will improve the training experience, by increasing the overall safety of the process and providing the student with the possibility to raise or lower the level of difficulty of the training. Furthermore, this is profitable for the flight schools because it may allow the instructor to remain or ground and train multiple students at the same time;
- **ELTA-FUN-TE-06** (A.3.5) - *Improve debriefing procedure*. One of the crucial parts of the training routine is the debriefing procedure. By improving the complexity and the quality of the feedback received by

[6] URL https://www.airforcemag.com/usaf-brings-pilot-training-next-to-regular-training-in-experimental-curriculum/

the students, the training process is enhanced, as the students/instructor may observe and correct certain mistakes faster;

- **ELTA-FUN-TE-07** (A.3.6) - *Improve training possibilities on the ground, outside of the aircraft*. The part of training that occurs outside of the aircraft may be further improved, by offering the students means of gaining more realistic and cost effective experience compared to the standard practise. Furthermore, by limiting the amount of hours needed on board the aircraft to complete training, the flight school may train more student at the same time;
- **ELTA-FUN-TE-08** (A.3.7) - *Improve the procedure of training emergency situations.* Some extreme situations, such as near-miss, are usually difficult to train in such a way that it would provide the student with the necessary set of skills and level of experience to be able to handle them. The TE package aims to provide solutions for this problem;
- **ELTA-FUN-TE-09** (A.3.8) -*Improve visualisation of instantaneous flight information.* One of the goals of the TE package is to make flight information easily available to the pilot, for example by displaying relevant information right in front of their eyes, without distracting them. This will improve the effectiveness of training in terms of decreasing the amount of time needed for the pilot to identify the relevant information on the many different instruments inside the cockpit.

9.3. Requirements

Having identified the main functions that have to be fulfilled by the TE package, the functional requirements could be extracted. Some of the very detailed requirements have been omitted from this section but can be found in [2]. First, the top level functional requirement:

- ***ELTA-TE-01*** *The TE package shall increase the training effectiveness of the system in comparison to existing training solutions.* Related to ELTA-FUN-TE-01. This is the main purpose of the TE package. In the following weeks, a method of measuring (the increase in) effectiveness will be developed.

Followed by additional functional requirements:

- **ELTA-TE-01-01** - *The TE package shall provide the option of simulating different weight, wind and weather conditions during flight*. Related to **ELTA-FUN-TE-01**. With an electrical power source, it is easy to control the amount of power delivered at all times. This enables the possibility of simulating a different weight, wind and weather condition so that the student may benefit from gaining experience in a larger range of situations;
- **ELTA-TE-01-02** - *The TE package shall provide means of tracking the student's stress level*. Related to **ELTA-FUN-TE-01**. The level of stress of the student is related to the level of confidence of the student in a certain manoeuvre/skill. Monitoring the stress level could provide useful insights into the skill level of the student, and can also be used to notify the instructor when the students is too overwhelmed to perform a certain manoeuvre/recover from a dangerous situation;
- **ELTA-TE-01-03** - *The TE package shall provide the possibility of simulating a different aircraft than the one the student is flying in, during flight*. Related to **ELTA-FUN-TE-01**. The student will benefit from gaining experience with regards to flying a different, bigger aircraft by inputting design parameters of said aircraft. Furthermore, this is attractive for the flight schools as it eliminates the need of purchasing multiple models of aircraft;
- **ELTA-TE-01-04** - *The TE package shall provide the option to switch off all the enhanced training technology*. Related to **ELTA-FUN-TE-01**. It is important for the pilot to be able to switch off all the TE systems if any of the system is impeding his training experience, if a fault in the system was observed or simply if the pilot wants to fly the aircraft fully manually;
- **ELTA-TE-02** - *The TE package shall improve accessibility to the daily training routine*. Related to **ELTA-FUN-TE-02**. This will increase the effectiveness of the training process in the sense that all the information needed for the student about the training routine will be easily accessible to them, as opposed to the student having to manually prepare and keep track of the flight routine;
- **ELTA-TE-02-01** - *The TE package shall display the lesson's learning objectives and schedule on a screen inside the cockpit*. Related to **ELTA-FUN-TE-02**. In this way, the student will be provided with a clear overview of the lesson at the beginning of it, knowing exactly what their goals are for the day, which may help in better mentally preparing the student for the session;
- **ELTA-TE-03** - *The TE package shall improve checklist procedures*. Related to ELTA-FUN-TE-03. The existent checklist procedures may be time consuming and due to the human factor they may sometimes be unreliable, thus they need to be improved;
- **ELTA-TE-03-01** - *The TE package shall include a digital version of all checklists*. Related to **ELTA-FUN-TE-03**. Having a digital version of each checklist will make the checklist procedure more efficient in the sense

that, the student won't need to manually check off each action on a piece of paper, costing time and money for the flight school. Instead, the student could for example easily check each task by touching a screen or by focusing on the task and just vocally inform the on-board computer that the action has been completed;

- **ELTA-TE-04** - *The TE package shall improve manoeuvre training*. Related to **ELTA-FUN-TE-04**. An important part of flight training consists of learning how to perform certain manoeuvres. Thus, the TE package shall offer ways of improving this process;
- **ELTA-TE-04-01** - *The TE package shall announce the next manoeuvre to be performed by the student*. Related to **ELTA-FUN-TE-04**. The student will benefit from having the next manoeuvre announced to them by not needing to check the training routine manually each time a manoeuvre is scheduled. This would improve effectiveness by saving time and also avoiding the loss of focus;
- **ELTA-TE-04-02** - *The TE package shall display the steps of the manoeuvre that is being performed*. Related to **ELTA-FUN-TE-04**. By having the steps of the manoeuvre displayed right in front of the student, their level of confidence to perform the certain manoeuvre would be improved. Furthermore, seeing the steps multiple times would help in memorising them and in building a habit of correctly performing the manoeuvre in the future;
- **ELTA-TE-04-03** - *The TE package shall warn the student when they make a mistake*. Related to **ELTA-FUN-TE-04**. It is highly important for the student (as well as the instructor) to be notified when a mistake has been made in performing a certain action. By receiving a warning when this happens, the student will learn to avoid the mistake in the future, while the instructor will be able to easily identify the weak points in the student's training routine and thus guide them more efficiently;
- **ELTA-TE-05** - *The TE package shall provide assistance to the students, by means of autonomous flying technology*. Related to **ELTA-FUN-TE-05**. Especially in the beginning of the training process, it is beneficial for the students to have assistance, in terms of having the autopilot/instructor perform some of the tasks/instruct how to correctly perform certain tasks;
- **ELTA-TE-05-01** - *The TE package shall provide flexible levels of autonomy*. Related to **ELTA-FUN-TE-05**. The student will have the possibility to decrease the level of autonomy of the aircraft in order to raise the level of difficulty and to aid in solidifying their skills;
- **ELTA-TE-06** - *The TE package shall improve debriefing procedure*. Related to **ELTA-FUN-TE-06**. Improving the debriefing procedure will enhance the post-flight learning experience of the student;
- **ELTA-TE-06-01** - *The TE package shall provide the possibility to record audio/video/flight data*. Related to **ELTA-FUN-TE-06**. In order to improve the learning effectiveness, it is important that the student has the possibility to review their flight, and video and audio recordings are good means of doing this, as the student has the opportunity to comprehend their exact mistakes;
- **ELTA-TE-07** - *The TE package shall improve training possibilities on the ground, outside of the aircraft*. Related to **ELTA-FUN-TE-07**. By limiting the time spent in the air in a real plane, the business case is improved for a flight school, as they can charge similar rates for training in a simulator but without the cost of operating the aircraft;
- **ELTA-TE-07-01** - *The TE package shall include a flight simulator capable of simulating the aircraft, including the TE systems on board*. Related to **ELTA-FUN-TE-07**. A flight simulator allows the training effectiveness to be enhanced greatly, as certain manoeuvres such as crosswind landings can be trained at a higher frequency than in a real aircraft and it is relatively cheap to operate;
- **ELTA-TE-08** - *The TE package shall improve the procedure of training emergency situations*. Related to **ELTA-FUN-TE-08**. The importance of training emergency situations is obvious. The more routine a pilot has when reacting to an emergency situation, the better they will handle the situation, possibly saving lives in the process;
- **ELTA-TE-08-01** - *The TE package shall provide the possibility to train stall-recovering manoeuvres*. Related to **ELTA-FUN-TE-08**. Training stall recovery, both in the plane and the simulator, is crucial for training the pilot's response to this incident;
- **ELTA-TE-08-02** - *The TE package shall provide the possibility to train flying/landing with inoperative power source, in flight*. Related to **ELTA-FUN-TE-08**. It is important for a pilot to have experience in operating and landing a plane even when there is no power available, so that the pilot is prepared in the case that this emergency occurs;
- **ELTA-TE-08-03** - *The TE package shall provide the possibility to train a near-miss of another aircraft, in flight*. Related to **ELTA-FUN-TE-08**. Perhaps in the simulator or with VR technology, it shall be possible for the pilot to experience a near-miss, so that the they can learn how to react in this situation and potentially save lives in the future;
- **ELTA-TE-09** - *The TE package shall improve visualisation of instantaneous flight information*. Related to

ELTA-FUN-TE-09. The flight visualisation can be improved by means of a glass cockpit, or in addition a HUD to display the flight information in front of the pilot's eyes instead of lower down in the cockpit;

- **ELTA-TE-09-01** - *The TE package shall provide the student with near-instantaneous flight information on the TE systems*. Related to **ELTA-FUN-TE-09**. If the TE systems are in use, it is important to ensure that the flight information displayed on them is near-instantaneous, in order to ensure the safety of the pilot and passengers.

Lastly, from various constraints, non-functional requirements have been formulated:

- **ELTA-TE-NF-01** - *The TE package shall not limit the view of the pilot when not in use*. This requirement results from a space constraint in the cockpit, as well as a constraint on the quality of the training experience, from the pilot's perspective: the TE package mounted on-board should not limit the training experience;
- **ELTA-TE-NF-02** - *The on-board TE package shall fit within the aircraft's structure*. This is a structural constraint. The TE systems on board need to be placed inside the aircraft in such a way that they do not negatively affect the performance of other subsystems;
- **ELTA-TE-NF-03** - *The TE package shall have access to all the aircraft's flight data*. This results from an operational constraint of the TE systems. These systems need to have access to the real flight data in order to be able to display it, process it, give the pilot the option to change certain flight parameters;
- **ELTA-TE-NF-04** - *The TE package shall draw power from no other source than the main power source of the aircraft*. This results from a constraint related to power. The TE package needs to receive power directly from the power source of the aircraft, in order to be utilised;
- **ELTA-TE-NF-05** - *The TE package shall be developed by 10 students in 10 weeks*. This results from a time, scheduling and human resources constraint.

9.4. Primary Research

In order to gather primary data on the TE package as well as the electrical aircraft, a questionnaire was created. The goal of this questionnaire was to determine what (student) pilots think could be improved about flight training and to find out about the acceptance of electrical aircraft.

9.4.1. Questionnaire

The questionnaire was distributed to the aerospace BSc students of the TU Delft, in the team member's personal surroundings as well as in several pilot forums for VFR and IFR pilots. In total, 118 responses were submitted through the Google form.

The questionnaire was set up as follows. The first section analysed the demographics of the participants, including their age, the type of pilot's license they have received, how long they have had their certification and finally how many hours they fly per month. This allows for an analysis of the opinions of different age groups or different pilot license types, for example whether airline transport pilots have different opinions than private pilots.

The following section included an open question on whether and if so, how flight training could be improved. It was made an open question in order to get all the ideas from the pilots before they were pre-occupied with the ideas of the TE package.

Subsequently, opinions on the usefulness of TE items were gathered. The participants could select on a scale from 1 (not useful at all) to 5 (very useful) their view on AR glasses, autopilot, debrief software, ballistic parachute, fitness band, virtual CFI, modular cockpits and the use of simulators. Parts of these results of these will be explained in detail in Section 9.5.

In the next section, a simple selection question was added, asking which type of flight simulator participants thought were the most useful for initial flight training, when taking into account both cost per hour and perceived training effectiveness. The options were the VR simulator at 35$/hr, a fixed base FTD at 75$/hr and finally the Redbird MCX with 3 axis motion at 100$/hr.

The final part of the questionnaire was used for market research. First, participants were asked what is most important to them regarding a trainer aircraft, followed by the question whether they would buy/fly an electrical aircraft in the near future. Finally, based on their answer to this question, they were asked why they answered with yes or no in order to gather information on the acceptance of electrical aircraft and the perceived downsides to potential customers.

9.4.2. Results

The demographics of the participants are as follows. Of the 118 partakers, 52% were PPL and IFR pilots (44.6% PPL, 7.4% IFR). In total, ca. 35% of contributors were commercial pilots, flight instructors or airline transport pilots. These are regarded as the pilots whose profession is flying, or they earn at least an amount of money through aviation. Some 10% of the participants were student pilots and the final 5% were glider and sport pilots.

There was a large spread in how long participants had had their license for. 34.7% of the participants had had

their license for more than 10 years. The other data from this question can be found in Figure 9.1.

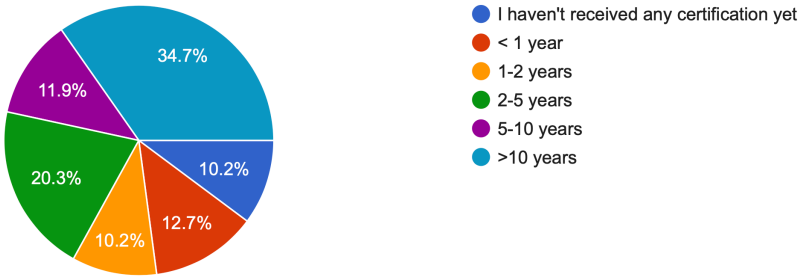

Figure 9.1: "How long has it been since you received your first flight certification?", 118 responses

The age distribution was very similar to the duration since first certification. For the categories of 16-21 years, 22-25 years, 26-20 years, 31-40 years, 41-50 years and >50 years, the results were as follows. Respectively, the percentages of age groups were: 11.9%, 11.9%, 11.9%, 11.9%, 16.1% and 37.3%.
The results of the question "How many hours do you fly per month?" can be seen in Figure 9.2

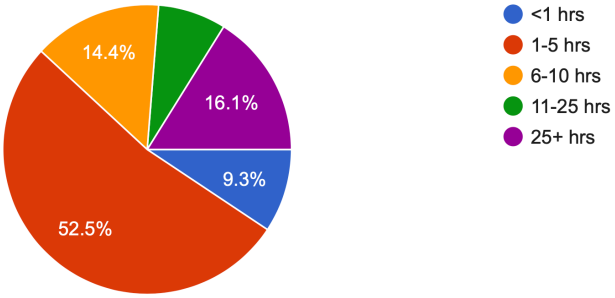

Figure 9.2: "How many hours do you fly per month?", 118 responses

Most people who have a PPL seem to fly just enough to stay current, which typically requires 12hrs/yr in the year before the license expires. Everyone who selected that they fly 25+ hours per month were flight instructors, commercial pilots or airline pilots.
The answers to the open question, as seen in Figure 9.3 regarding the improvement of flight training were very varied. There were however several topics which stood out as they were mentioned many times. Of the 118 responses, 82 people answered this question, as it was not a mandatory question. The most mentioned improvement - which was mentioned by 10 people - is a flight data, voice and video recorder, which can be used for debriefing, mentioned by 8 people. An increase in the use of simulators was mentioned by 9 people. Furthermore, 8 people mentioned an improved ground training, for example using videos, or by improved practice, for example the use of chair flying. Five more responses related to an improved (forgiving) handling of the aircraft. Several participants also mentioned the integration of upset prevention and recovery training.

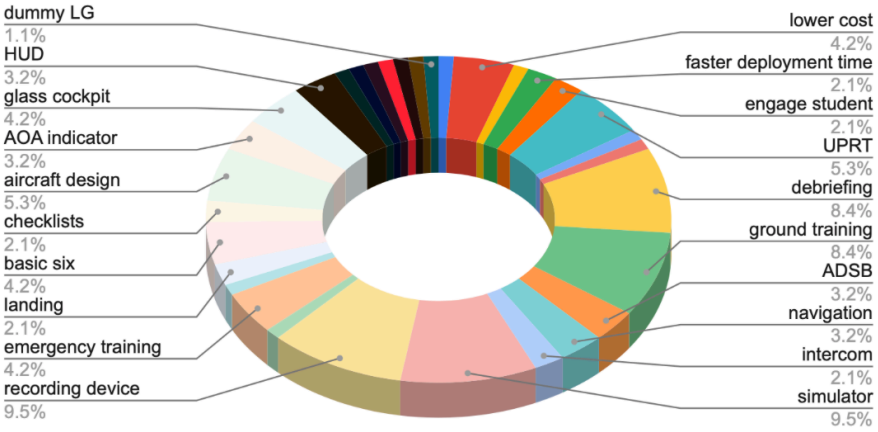

Figure 9.3: "How do you think flight training effectiveness can be improved? Think about certain items you may want to add to a trainer aircraft in order to make flight training more efficient", 82 responses

Following the open question, the participants were asked to share their opinion on several proposed TE items. The results of this are summarised in Table 9.1.

Table 9.1: Perceived usefulness of TE items on a scale of 1-5, 118 responses

Item	AR Glasses	Autpilot	Debrief Software	Ballistic Parachute	Fitness Band	Virtual CFI	Modular Cockpit	Flight Simulator
Mean	2.97	2.60	4.38	2.84	2.94	2.73	3.31	4.28
STDV	1.35	1.36	0.85	1.40	1.20	1.33	1.29	0.92

The items with by far the highest perceived usefulness, i.e. those with the highest average, were the debrief software and the simulator. They both received an average score of above 4, with the smallest standard deviation (STDV) of 0.85 and 0.92 respectively. The third best item according to potential customers is the modular cockpit, with an average of 3.31 and a STDV of 1.29. The item that was perceived as least useful was the autopilot, with an average score of 2.6. It should be noted however that the results for this item have a high STDV of 1.36, which shows that many people thought it was useful, but many thought it was not.

The question on the flight simulator and which one is perceived as most useful yielded an interesting result. Against the team's expectations, the three simulator types were considered best by an almost equal amount of people. The exact numbers can be seen in Figure 9.4. The green additional small pie slice comes from an error in the google form, it belongs with the blue virtual reality simulator slice.

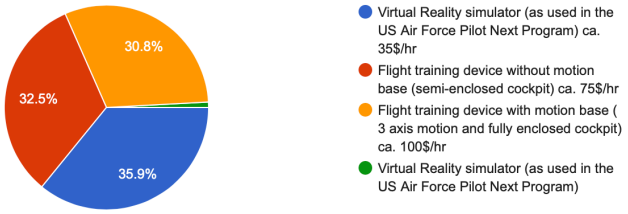

Figure 9.4: "Which type of flight simulator do you think is the best for initial flight training, while accounting for both the cost and added training effectiveness?", 118 responses

9.5. In-flight Segment

This section describes the steps taken during the design phase of the in-flight segment of the TE package. First an overview of the previous phase of the design is presented in Section 9.5.1. Then the detailed design phase is delved into in Section 9.5.2. Here the items included in the final proposed in-flight TE package will be discussed. It is important to note that the design on the Dragonfly is geared mostly towards larger flight schools who aim to educate pilots for flying careers and therefore include many items to prepare them for the operation of larger, more complex aircraft than the Dragonfly.

9.5.1. Midterm Phase

In the previous design phase five different concepts have been proposed for the in-flight training enhancement package. An overview of the items that are included in each concept, the estimated mass and cost of each individual item, as well as the total mass and cost of each concept may be found in Table 9.2. A 10% margin has been added to the total mass and cost of the five concepts for contingency management.

Table 9.2: Concepts for TE package.

Item	Weight (kg)	Cost (US$)	Conc. 1	Conc. 2	Conc. 3	Conc. 4	Conc. 5
AR Glasses [7]	0.14	1,140	X		X		
AR Glasses w/ eye tracker [8]	0.15	3,000		X			X
Autopilot [9]	4	2,500		X	X		
Ballistic Parachute [10] [11]	21.7	6,900			X		
Fitness Band [12]	0.05	100			X		
Glass Cockpit [13]	10	6,490	X	X	X	X	
Virtual CFI	N/A	500	X	X	X	X	
Removable Instructor Seat	1	500	X	X	X	X	X
Fly-by-wire	20	5,000		X			
Simulate Different Wind&Weather	N/A	N/A		X			
Simulate other aircraft	N/A	N/A		X			
Portable Instrument Panel	5	8,000		X			
Camera&Voice recording [14] [15]	0.4	300	X	X	X	X	X
Flight Data recording option (SD card) [16]	0.01	40	X	X	X	X	
iPad/Tablet [17]	0.5	330	X				X
Debrief software [18]	N/A	150	X	X	X	X	
Total Mass (kg)			*12.05*	*40.56*	*37.3*	*11.41*	*2.05*
Total Cost (US$)			*9,450*	*26,480*	*18,620*	*7,980*	*4,130*
Total Mass+10% (kg)			**13.26**	**44.62**	**41.03**	**12.55**	**2.26**
Total Cost+10% (US$)			**10,395**	**29,128**	**20,482**	**8,778**	**4,543**

The items that are displayed in Table 9.2 have been each selected in such a way as to fulfil at least one of the functions mentioned in Section 9.2. Having decided upon the combination of items that would be included in each concept, a trade-off between the five proposed TE packages could be performed, as seen in 9.3. The weight of each technical performance measurement has been obtained with the use of the Quality Function Deployment method. The customer demands for the in-flight TE package that have been included in the QFD are: that it shall increase the training effectiveness, that it shall be light-weight and cost-effective, and that it shall be safe to operate. The weight of each trade-off criterion has been calculated by assessing the correlation between the customer demands and the proposed technical performance measurements. The added training effectiveness had the highest weight, namely 40%, which was expected as this is the most important aspect of the TE package. The next highest weight, equal to 20%, was cost. This is also an important factor due to the aircraft cost being limited, with the goal of optimising this parameter to be as low as possible for the final aircraft. The safety and mass were the next most important criteria, with a weight of 15% each. Finally, technology readiness - which includes certifiability - had a weight of 10%. For more information on the QFD method applied for the in-flight TE package, please refer to [1].

[7] URL: https://www.vuzix.com/Products/AddToCart/163
[8] URL: https://www.tomsguide.com/us/lumus-dk-50-augmented-reality-glasses,news-22103.html
[9] URL: https://www.dynonavionics.com/downloads/order_form.pdf
[10] URL: https://www.galaxysky.cz/grs-6-800-990-sds-175m2-p43-en
[11] URL: https://www.aviationconsumer.com/safety/brs-parachute-retrofits-a-cost-benefit-analysis/
[12] URL: https://buy.garmin.com/en-US/US/p/605739
[13] URL: https://www.dynonavionics.com/skyview-hdx.php
[17] URL: https://www.apple.com/shop/buy-ipad/ipad-10-2
[18] URL: https://www.cloudahoy.com/product.php

Table 9.3: Trade-off for the Five TE Package Concepts

Design Option	Technical Performance Measurements	Added training effectiveness	Cost	Safety	Technology Readiness/ Certifiability	Mass	Score
	Weight	40%	20%	15%	10%	15%	100%
Concept 1		2	3	2	3	3	2.45
Concept 2		4	1	3	1	2	2.65
Concept 3		3	2	4	2	2	2.7
Concept 4		2	3	3	3	3	2.6
Concept 5		1	4	1	4	4	2.35

In terms of training effectiveness, concept 2 was awarded an excellent score as it implements the most TE features and is also the only concept that includes the option to simulate other aircraft. On the other hand concept 5 only implements the most basic training devices and not even a glass cockpit.

The cost and mass rankings quite simply come from the cost and mass estimates as seen at the bottom of Table 9.2. Whenever the cost or mass of two concepts were similar, they have been awarded the same score and were otherwise scaled according to their relative cost or mass.

The highest safety rating was achieved by concept 3 as it includes a ballistic parachute which can possibly save the life of a student pilot in an emergency situation when flying solo. Concepts 2 and 4 were assigned a score of 3, as they both include a virtual CFI and stress monitoring measures which may be used to determine when a student is overwhelmed.

For the certifiability and technology readiness the second concept scored the lowest as the possibility of simulating another aircraft while in-flight has not been certified yet and the technology needs extensive further development until it would be widely used in GA aircraft. Concept 5 is so simple, however, that it is not assumed to create any certification difficulties. Concept 1 and 4 both have a certifiability rating of 3. Concept 3 has a slightly lower certifiability, solely due to the implementation of the autopilot.

The final winner of this trade-off was concept 3. It should be noted, however, that the final score for concepts 2 and 3 are very similar. In order to obtain the best TE package, as previously stated in [1], certain characteristics of concept 2 may be added to concept 3. The most important characteristic that should be implemented is the possibility of simulating different aircraft with the Dragonfly. The way in which this will be implemented will be explained next.

9.5.2. Detailed Design

In this section, the items and technology considered to be included in the final concept of the in-flight TE package are going to be discussed and analysed. Furthermore, the functionality of each item will be addressed.

Mixed Reality Headset

The most unique aspect of the Dragonfly and probably the main selling point is represented by the fact that this aircraft will have the capability to transform into an in-flight simulator. Thus, it shall be able to simulate different aircraft, as well as provide the student pilots with the possibility of performing certain manoeuvres that are usually trained only in a flight simulator (such as a near-miss). The most common and affordable flight simulators that are currently used for training are fixed flight training devices (FTD). These do however not have the ability to simulate the motion of an actual aircraft. The certified and high fidelity full motion flight simulators that are available on the market are usually very expensive, the cost of some reaching $10 million[19]. The less expensive full motion FTDs that may be used for general aviation training, such as the Redbird MCX[20], are still not affordable for some flight schools and their visual and haptic quality cannot match what a pilot experiences during an actual flight scenario. By transforming the aircraft itself into a flight simulator, the flight schools would save a significant amount of money (not having to purchase highly expensive flight simulators with limited capabilities), while also offering their students a tremendously enhanced training experience.

The idea of blending reality and simulation for flight research and training was first implemented by Systems Technology Incorporated (STI) within the Small Business Innovative Research Phase II agreement with NASA's Dryden Flight Research Center[21]. The system that was developed by STI is called Fused Reality and it was used by the test pilots at NASA to successfully land on a simulated runway at an altitude of 5000 ft, perform formation flight, and aerial refuelling exercises with the help of simulated aircraft outside the window [57]. Fused Reality works in the following way: live video is captured from the pilot's perspective, sent to a processor that preserves the live image of the cockpit, while either converting the image of the outside of the cockpit into a completely

[19]URL: https://www.aviationtoday.com/2019/08/01/training-brain-mind/
[20]URL: https://simulators.redbirdflight.com/products/mcx#aircraft-configurations
[21]URL: https://www.nasa.gov/centers/dryden/Features/fused_reality.html

virtual environment (for example when performing a landing at a higher altitude), or blending certain virtual objects in the real environment (when training formation flight). The processed visual, which takes into account the head movement of the pilot, is shown on the their head mounted displayed (HMD) [58]. The main benefit of the Fused Reality technology, apart from the impressive level of immersiveness provided to the pilot, is the fact that it reduces the risk of accidents during flight testing/training. For example, if the pilot performs a landing at high altitude, they will be able to easily recover if they make a mistake. Furthermore, if they do not manage to correctly recover from a near-miss and they "collide" with the simulated aircraft, no one will get injured. In addition to this, Fused Reality allows for significantly less expensive training of manoeuvres which would usually require the operation of another aircraft. For these reasons, it is desirable to adapt this technology to general aviation training. In order to achieve this, the main item that shall be implemented in the in-flight TE package of the Dragonfly is a mixed reality (XR) or augmented reality (AR) headset.

A possible XR headset that may be used in order to implement the Fused Reality concept is the Varjo XR-1, shown in Figure 9.5a. This is the most advanced XR currently available for industrial use[22]. It has a very high image resolution, referred to as "human eye resolution", which is guaranteed to deliver a high degree of visual realism for the student pilot. Furthermore, it is equipped with highly accurate eye tracking technology, which would allow for a significant increase in the effectiveness of each training session, as the instructor would be able to closely monitor the progress and accuracy of the student's looking pattern e.g. if they look at the controls as well as outside in the optimum way and at the correct time during the training. In addition to this, this system has already been employed in on-ground flight training[23]. Another proposed design would be the headset used in the new generation of the Fused Reality system [59], namely the Oculus Rift[24], in combination with a ZED Mini Stereo Camera [25], shown in Figure 9.5b. However, the visual quality is not as sharp using this headset, when compared to the Varjo XR-1 and there are no eye tracking capabilities. Another possible headset that may be used is the Microsoft HoloLens 2, shown in Figure 9.5c, which is an augmented reality HMD, also equipped with eye tracking technology[26]. In contrast with the other two options, this HMD is not able to portray a (partly) virtual environment, but only to blend certain simulated objects within the reality or display text right in front of the user's eyes. The last option that would be considered for this application is the VIVE Pro Eye[27], shown in Figure 9.5d, in combination with a ZED Mini Stereo Camera. This option has advanced eye tracking and virtual world rendering capabilities provided by the VIVE Pro Eye, as well as mixed reality rendering capabilities provided by the ZED Mini.

Figure 9.5: AR/VR headsets.

(a) The Varjo XR-1 Mixed Reality Headset.

(b) ZED Mini mounted on Oculus Rift [59].

(c) The Microsoft HoloLens 2 headset.

(d) The Vive Pro Eye headset.

An overview of the cost, weight, resolution per eye, possibilities of eye tracking and rendering of AR and VR for each headset previously mentioned may be found in Table 9.4. The original Oculus Rift headset that has been used for the new generation of the Fused Reality system has been discontinued, thus, the relevant specifications of the Oculus Rift S have been summarised in the table. Observing Table 9.4, it is clear that the Varjo XR-1 has the best resolution and has both AR and Vr rendering possibilities, as well as eye tracking capabilities. However, it comes at a high cost and it is also considerably heavier than the other options. Due to the fact that eye tracking would be very beneficial in increasing the training effectiveness, as previously described, the combination of the VIVE Pro Eye headset with the ZED Mini camera is preferred over using the Oculus Rift S with the ZED Mini camera. This decision is also supported by the fact that their weight is very similar and the price difference may be accommodated by the budget. The Microsoft HoloLens is not capable of using chroma key composting technology (layering two video streams, for example to simulate a virtual background outside the window, as done in the Fused Reality concept), but it can display certain objects/pieces of text right in front of the student pilot's eyes. Thus, it might be used,

[22]URL: https://varjo.com/
[23]URL: https://bit.ly/3gRguHv
[24]URL: https://www.oculus.com/rift/
[25]URL: https://www.stereolabs.com/zed-mini/
[26]URL: https://www.microsoft.com/en-us/hololens/buy
[27]URL:https://www.vive.com/eu/product/vive-pro-eye/

for example, to efficiently display certain digital checklists or instructions, in order to decrease the pilot's reaction time and, thus, the efficiency of the training. An experiment proving a decrease in pilot's reaction time to certain instructions when using the Microsoft HoloLens has already been performed, as explained in [60]. Furthermore, this is the only option that does not fully obstruct the normal view of the student pilot, as its lenses are transparent.

Table 9.4: Overview of the specifications of the AR/VR headsets.

AR/VR Headset	Cost [€]	Weight [g]	Resolution (per eye)	Eye Tracking	AR	VR
Varjo XR-1[28]	9995	1300	"human eye resolution" 1920x1080 (central focal area) 1440x1600 (peripheral display)	X	X	X
Oculus Rift S[29] [30] **+ ZED Mini**	802	624	1920x1080 (30 fps)		X	X
Microsoft HoloLens 2[31]	3097	566	2048 x 1080	X	X	
VIVE Pro Eye[32] **+ ZED Mini**	1792	618	1920x1080 (30 fps)	X	X	X

It was decided that the VIVE Pro Eye headset with a mounted ZED mini camera will be used for the flights where the student is accompanied by the instructor, in order to ensure a sufficient level of safety. When using this set-up, it will be possible to simulate different weather conditions (such as rain)- **ELTA-TE-01-01**, different aircraft or flight situations-**ELTA-TE-01-03**, by making use of the chroma key composting (the windshield/instrument panel will be lined with coloured tape, which will enable simulating the cockpit of another aircraft or a different environment outside the windshield, such as a runway at a certain altitude). Furthermore, it will provide the possibility to safely train a near-miss-**ELTA-TE-08-03**. In addition to this, it may be efficiently used to improve checklist procedures-**ELTA-TE-03** and **ELTA-TE-03-01**, visualisation of instantaneous flight information- **ELTA-TE-09** and **ELTA-TE-09-01**, as well as manoeuvre training- **ELTA-TE-04**, **ELTA-TE-04-01** and **ELTA-TE-04-02**. It may also be used to guide the student using Highway-In-The-Sky technology.

AR Glasses

As opposed to the mixed reality headset, the Epson Moverio BT-300 AR glasses may be also used when the student is flying solo. These glasses will be mainly utilised as an HUD which will guide the student, using the Highway-In-The-Sky technology, displaying the flight path, the angle of attack, the airspeed etc. Furthermore, certain checklists and instructions may be displayed using these AR glasses. Thus, they may be used to improve checklist procedures-**ELTA-TE-03** and **ELTA-TE-03-01**, visualisation of instantaneous flight information- **ELTA-TE-09** and **ELTA-TE-09-01**, as well as manoeuvre training- **ELTA-TE-04**, **ELTA-TE-04-01** and **ELTA-TE-04-02**.

Simulated Gear Lever

After completing their PPL, many student pilots will presumably fly a more complex aircraft at a certain point in their career, one equipped with a retractable landing gear. As landing is one of the most critical flight phases, and lowering the landing gear is crucial for a successful, safe landing, it is very important to ensure that the students are taught how to correctly operate a retractable landing gear from the very beginning of their training. This may be achieved by installing a simulated landing gear lever inside the aircraft, as part of the in-flight TE package. The simulated lever will be equipped with a warning system that will be triggered if the student forgets to retract the landing gear after take-off or, more importantly, lower the landing gear before landing. In this way the student will be able to train their reflex of efficiently operate the retractable landing gear, while also benefiting from a high level of safety guaranteed by the fixed landing gear of the Dragonfly. Introducing the simulated gear lever will aid in fulfilling **ELTA-TE-01-03**, as this is a feature that simulates characteristics of another aircraft.

Simulated Engine Controls

The Dragonfly, being an electrical aircraft would only need one throttle in order to adjust the power output from the engine, and thus control the RPM level of the fixed propeller. The simplicity of having only one engine control knob would be welcomed in the early stages of flight training. However, one of the most often encountered reasons for not buying an electrical trainer aircraft, as resulting from the questionnaire and explained in Section 4.7.2, is that it would not prepare the student pilot to fly a combustion engine propeller aircraft. This problem would be tacked by including additional engine/propeller controls in the cockpit. Combustion engine trainer aircraft that are equipped with a fixed propeller have two knobs or levers: a black one- the throttle, which adjusts the amount of fuel going to the engines, and a red one- the mixture control which may be used to adjust the air/fuel ratio, process

[28] URL: https://store.varjo.com/varjo-xr-1
[29] URL: https://www.oculus.com/rift-s/?locale=en_US
[30] URL: https://www.stereolabs.com/zed-mini/
[31] URL: https://www.microsoft.com/en-us/hololens/hardware
[32] URL: https://www.vive.com/eu/product/vive-pro-eye/

also known as leaning. In the case of a variable pitch/constant speed propeller, an extra knob/lever is added: a blue one- the propeller control. This may be used in order to select the optimum RPM level for a specific flight phase, in order to maximise the efficiency of the propeller. It acts by adjusting the propeller pitch and regulating the engine load as needed in order to maintain the selected RPM constant. In order to obtain the highest increase in training effectiveness, both a simulated propeller control and a mixture control knob will be added to the cockpit of the aircraft. As the propeller used for the Dragonfly is fixed, the simulated propeller control knob will not have any direct effect on the performance of the aircraft, being used for instructive purposes only. In combustion engine fixed propeller aircraft, by pulling the mixture control knob towards you during flight, an increase in the RPM may be observed until a certain point. After reaching this optimum point, further pulling of the knob will result in a lower RPM. Complete pulling of the knob results in 0 fuel being fed to the engine, and, thus, an "engine failure". These characteristics may be emulated by the Dragonfly: when the student pulls the knob, an increase in RPM shall be registered (by possibly connecting the mixture knob to the throttle). If the student pulls the knob excessively, a warning will be triggered. Under close supervision of an instructor, by pulling the mixture knob all the way, an engine out emergency procedure may be initiated. Adding the two extra engine/propeller control knobs in the cockpit, the following functions will be fulfilled: **ELTA-TE-01-03**, as these items aid in simulating certain characteristics of another aircraft, and **ELTA-TE-08**, as it would aid in training emergency situations.

Simulated Carburettor Heat Control

Another characteristic of a normal combustion engine that could be implemented for the purpose of enhancing training effectiveness of the Dragonfly is a simulated carburettor heat control knob. The carburettor is usually implemented on internal combustion engine aircraft and it is used to mix the air and the fuel in the desired ratio for combustion. A dangerous phenomenon that might ultimately lead to engine failure is carburettor icing. This event might occur at any time during the year, but it is most commonly encountered during cool summer and early autumn days, when the humidity is high and phenomena such as rain or haze might take place. The carburettor icing occurs when the Venturi effect of air passing through the carburettor lowers the temperature inside the device significantly, causing water vapour to freeze. If the ice layer builds up and it is not eliminated, this might lead to engine failure. Thus, in order to combat carburettor icing, it is important even for beginner student to understand and gain experience operating the carburettor heat knob, which will allow heated air to flow from the exhaust into the carburettor and melt the ice. The simulated carburettor heat control will be equipped with the ability to trigger a warning if the student has not activated it for a certain amount of time, as in general this control shall be used regularly to prevent the formation of ice. However, as landing is one of the most crucial flight phases and the performance of the engine shall be optimal during this time, it is highly important that the student gets accustomed with using the carburettor heat control knob at least when preparing for landing procedures. Integrating this additional control knob inside the cockpit of the Dragonfly will serve in fulfilling once again **ELTA-TE-01-03**, as it would simulate a characteristic of another aircraft, and **ELTA-TE-08**, as it would aid in training (avoidance of) emergency situations.

Simulated Fuel Pump and Fuel Selector

Tying into the topic of equipping the student pilot with the necessary set of skills that would allow for optimal and efficient operation of the engine and, thus, of the fuel system of the aircraft that they might fly in the future, a simulated fuel pump switch and fuel selector instrument will be added to the cockpit. The fuel pump switch will serve in the process of priming the engine before take-off, which is important to ensure the optimal start of the engine, especially during cold days. When the pilot primes the engine excessively, it will lead to a flooded engine that is difficult to start and, eventually, due to fuel residue contamination, it may lead to expensive repairs of the fuel servo. Furthermore, overpriming is the most common cause of aircraft engine fires encountered on the ground [33]. Thus, it is important to train the students to properly prime the engine of the aircraft since the beginning. This process may be performed by using a combination of the fuel pump switch and the mixture control knob. A warning shall be triggered if the student has overprimed the engine.

Furthermore, it is important to teach the beginner student pilots how to operate the fuel selector. Thus, an instrument that will be equipped with four settings: right, left, both and off will be implemented in the cockpit of the Dragonfly. Most pilots usually use the "both" option. However, in some combustion engine aircraft, it is advised to only use one fuel tank at a time after reaching a certain altitude (5000 ft for the Cessna 172 [61]), as otherwise power irregularities, ultimately resulting in engine failure, may arise. These irregularities occur due to the accumulation of fuel vapours, as a result of high fuel temperature, operating altitude as well as low fuel rate in the tank [61]. Furthermore, by switching between the left and right fuel tank, pilots may balance the fuel load in such a way that the banking moment is reduced. In addition to this, the student pilots should form a reflex of immediately switching the fuel selector to the "off" position in case engine fire was detected. In order to train these skills, it is beneficial to implement the simulated fuel selector in the cockpit.

[33] URL: https://www.boldmethod.com/learn-to-fly/aircraft-systems/what-causes-engine-fires-during-start/, LA 09-06-2020

Both the simulated fuel pump and the simulated fuel selector will aid in emulating characteristics of a different aircraft and will serve in training certain emergency situations, thus they are shall fulfil **ELTA-TE-01-03** and **ELTA-TE-08**.

Sound System

In an effort to further enhance the training experience for the student pilots, a sound system designed to emulate the sounds usually encountered when on-board a combustion engine aircraft will be incorporated into the in-flight TE package. This kind of technology has not been implemented on-board any aircraft yet. However, the development of such a system shall be achievable, as a similar technology to that used for matching specific sound tracks to certain manoeuvres performed in the flight simulator training is expected to be used. In order to contribute towards noise minimisation, while also allowing students to experience- to a certain extent- the feel of flying a combustion engine aircraft, the sound will be transmitted directly to their headphones. In order to allow for efficient communication, the student and the instructor will be able to adjust the volume of the sound system, as well as to turn it off completely at any point during flight training. The software of the sound system will be incorporated in the flight computer and it will be controllable via the MFD. Including this system in the TE package will help fulfil **ELTA-TE-01-03**, as it will provide a mean of simulating the characteristic of another aircraft.

Ballistic Parachute

The integration of a (remotely deployable) ballistic parachute into the aircraft brings great safety benefits. It would - in combination with the stress level monitor - allow for safe landing in emergency situations where the student cannot land themselves. It will result in a total loss of the aircraft, but often saves lives. According to Alaziz et al. [62], 72% of accidents in their study on Cirrus aircraft were caused by human error, and 71% of errors were made by student or private pilots. The results of this study also showed a "13-fold reduction in the odds of a fatal accident with the use of CAPS" [62]. For this device, a parachute from the company Galaxy GRS has been chosen, and will cost around $5 000 excluding installation [34]. The system weights around 21.7kg[35]. The addition of a ballistic parachute to the Dragonfly aids in fulfilling requirement **ELTA-TE-01**.

Stress Monitor

A stress level monitor in the form of a fitness wristband or smart watch can be used to determine the students heart rate and blood oxygen levels in order to determined how stressed a student is. This technology can be useful especially when the student is flying solo, so that the flight instructor who is positioned on the ground can respond to an emergency situation or lower the level of training if a student is too unconfident with the tasks they are performing. While any wearable device with stress measuring capability could be used for this puprose, the Garmin vivosmart is recommended [36]. The FAA conducted a study in 1967 [63] in which eight participant's heart rates were monitored during their PPL lessons. The data of heart rates from this study can be implemented into the TE package of the Dragonfly. If the heart rate of a student pilot exceeds those recorded in this study, the flight instructor can decide to lower the amount of stress on the student. Factors that cause stress include engine and system noise [37], which are simulated in the Dragonfly. Turning these off would result in lowered stress levels and more efficient learning for the student [64]. The addition of this item aids in fulfilling requirements **ELTA-TE-01-02**, **ELTA-TE-01-02-A** and **ELTA-01-02-B**.

Glass Cockpit

A glass cockpit typically consists of a PFD and an MFD (primary- and multi-function display). For the Dragonfly, a PFD from the company Dynon has been chosen. This company provides affordable avionics solutions for GA aircraft, and provide all the necessary avionics to equip the Dragonfly. The system will cost around $25 000 [38] and include all necessary sensors, a PFD and MFD, engine monitoring and the structural attachments and wiring. The screens will be either 10 inches or 7 inches in diagonal length, depending on the dimensions of the cockpit. The altitude indicator will indicate the ground level, while the airspeed indicator will show the approach, stall and other speeds so they are easily accessible to the pilot. Furthermore, it will teach the student the layout of the cockpit of aircraft they will likely fly in the The addition of these items aids in fulfilling requirements **ELTA-TE-08** and **ELTA-TE-09**.

Flight Data Recorder

For efficient debrief procedures, it is important to be able to access the flight data. As the most important flight data is processed and displayed by the PFD of the glass cockpit, this device may also be used for flight data recording purposes. This will be done by making use of the PFD's USB port: an USB stick will be inserted into

[34] URL: https://www.aviationconsumer.com/safety/brs-parachute-retrofits-a-cost-benefit-analysis/, LA 09-06-2020
[35] URL: https://www.galaxysky.cz/grs-6-800-990-sds-175m2-p43-en, LA 09-06-2020
[36] URL: https://buy.garmin.com/en-US/US/p/605739, LA 09-06-2020
[37] URL: https://www.skybrary.aero/index.php/Stress_and_Stress_Management_(OGHFA_BN), LA 16-06-2020
[38] URL: https://www.dynoncertified.com, LA 08-06-2020

the port at the beginning of the lesson and it will store the data from that specific flight. The information may then be fed into a software that will animate the flight for the student to process their mistakes. Furthermore, this information on altitude, velocity, pitch, yaw, roll, pitch rate, yaw rate, roll rate, temperature, and air density can be inputted into the flight simulator so that the student can truly relive their flight and learn how to possibly act or react differently in a situation encountered in a flight lesson. This feature aids in fulfilling requirements **ELTA-TE-06-01-D**, **ELTA-TE-06-01-E** and **ELTA-TE-06-01-F**.

Collision Avoidance System

According to AOPA, "collision avoidance is one of the most basic responsibilities of a pilot flying in visual conditions" [39]. Therefore, it is critical for pilots to have an overview of traffic and terrain. The performed questionnaire (Section 9.4) showed that many pilots wish that some sort of traffic avoidance system was installed in a trainer aircraft, in order to aid the student. For this, several types of avoidance systems are available. US aircraft flying in airspace where transponders are mandatory require an ADS-B (Automatic Dependent Surveillance Broadcast) out starting January 2020. The chosen Dynon glass cockpit includes an ADS-B out transponder. In order to not overwhelm the student in the first stages of flight training, there will be a possibility to shut off this system so that the student can focus on learning the proper scanning method, especially in the traffic pattern, as this is where most mid air collisions (MACo) happen [39]. TCAS is deemed too sophisticated for many GA aircraft, and has therefore not been considered for the Dragonfly. The addition of the ADS-B transponder related to the requirement **ELTA-TE-01**.

Autopilot

The addition of the autopilot to the aircraft will assist student pilots in getting used to the autopilot feature, as they will also use these in further stages of training in larger aircraft. The Dragonfly will contain a 2-axis autopilot for pitch and roll motion. It can also assist the student in recovering from many situations by setting the autopilot to straight and level in case the student panics. It will aid in fulfilling requirement **ELTA-TE-04**.

Virtual Certified Flight Instructor

The glass cockpit will include a virtual CFI. It is a piece of software which can be used by the student while flying solo. The virtual CFI could give audio cues when the student is not performing a manoeuvre how they should be. Some manoeuvres that could be trained using the virtual CFI include stalls, steep turns, navigation (cross-country) flight and more. It could also utilise the AR glasses in order to augment gates into the student pilot's vision through which they have to fly, in order to visualise the target goals for altitude for example. It will also warn the student when they are making a mistake using audio and/or haptic feedback, and announce and guide the student through the next manoeuvre. The implementation of a virtual CFI aids in fulfilling requirement **ELTA-TE-01**, **ELTA-TE-04**, **ELTA-TE-04-01**, **ELTA-TE-04-02**, **ELTA-TE-04-03**, **ELTA-TE-04-03-A** and **ELTA-TE-04-03-B**.

Voice Recorder

Connected to the intercom, the voice recorder uses an inserted SD card to save all the communication in the cockpit. This can aid the pilot during debriefing as they can re-listen to the ATC commands. The voice recordings also bring benefits during at home flying practice, for example chair flying, as the student can practice to keep focus on radio communications and learn to filter out the important parts of ATC. Its implementation aids in fulfilling requirements **ELTA-TE-06-01-C** and **ELTA-TE-06-01-F**. It was also one of the answers that stood out in the questionnaire, as many participants wished for a voice recording method.

Video Recorder/Camera

The added camera in the cockpit will allow for improved debriefing procedure, as explained in the next section. It was also a highly requested item in the questionnaire. Camera recordings are not only useful to impress family and friends, but can also act as a useful learning tool. To fulfil this purpose, the GoPro Hero 7 has been chosen, which can record video at 4k resolution and 60 frames per second [40], however, only HD (1080p) resolution will be used for the TE package. The camera addition aids in fulfilling requirements **ELTA-TE-06-01-A**, **ELTA-TE-06-01-B** and **ELTA-TE-06-01-F**. In order to fully fulfil **ELTA-TE-06-01-A**, an SD card of at least 32GB must be added.

Debrief Software

In order to enhance learning and aid the student pilot in retaining information, it is vital to include a debrief software in the TE package. The debrief software is also a highly requested item, as determined by the performed questionnaire. Several people mentioned it in the open question and the vast majority of participants deemed it "very useful". Even though many pilots already use some form of debrief software, the TE package will include CloudAhoy. It is a yearly subscription service for 65$ or 150$ per year, depending on whether the standard or pro version is chosen [41]. The pro version offers 2D and 3D flight animation, wind data, cockpit view animation, video

[39] URL: `https://www.aopa.org/training-and-safety/online-learning/safety-advisors-and-safety-briefs/collision-avoidance`, LA 08-06-2020
[40] URL: `https://www.mediamarkt.de/de/product/_gopro-hero7-black-2464536.html`, LA 08-06-2020
[41] URL: `https://www.cloudahoy.com/product.php`, LA 08-06-2020

integration and more, as well as a CFI assistant which scores the student on how well they performed certain tasks. With all this information, the student can truly relive their flight and learn from it in the future. The addition of CloudAhoy to the TE package will fulfil requirement **ELTA-TE-06**.

Electronic Flight Bag

The electronic flight bag (EFB) is the device which replaces all the paper checklists and paper charts within the cockpit. Furthermore it runs the debrief software, mentioned previously. It was also mentioned by the participants of the questionnaire. It may come in the form of an iPad as suggested in the midterm report [1], for around 500 euros [42]. Furthermore, the EasyVFR 4 application will be used on the iPad for flight planning. This is done as the membership can be combined with updating the Dynon database used for the PFD/MFD [43]

Removable Instructor Seat

With a removable instructor seat, the Dragonfly has the possibility of providing more range and endurance, as the lack of seat and instructor weight will allow for the insertion of more batteries. The front seats of a Cessna 172 weigh 23lbs, or 10.4kg [44]. In total, the elimination of the passenger seat will allow for up to 80kg extra of battery space. The addition of a removable instructor seat aids in fulfilling requirement **ELTA-TE-01**.

9.5.3. Mass and Cost Budget Breakdown

An overview of the mass and cost budget breakdown for the in-flight TE package may be found in Table 9.5. In this table the estimated cost in [€] and mass in [kg] is listed for each item that will be included in the TE package. Furthermore, the total cost and mass are displayed, each including a margin of 5% added for contingency management.

In order to emulate a real fuel pump, a simple metal switch may be added to the cockpit. The proposed sound system has not been previously implemented on any GA aircraft. However, as explained in Section 9.5.2, the software that will be developed to fulfil this function is expected to be similar to the one found in a flight simulator. Thus, as a first estimate, the price of a realistic sound system extension package for a flight simulator has been selected for this item. For the PFD and MFD, the screens themselves, as well as the batteries needed for their operation have been accounted for in the mass and price estimates. Similar to the sound system, the virtual CFI has not been implemented on any GA aircraft yet, as it has not been developed until now. As an estimation for the price of including this type of software on-board the Dragonfly, the cost of a virtual flight instructor software that may be used for at-home simulator training purposes was used. Furthermore, for the flight data recorder, the item that is considered is actually an SD card, which is added to store the flight data that is displayed on the PFD. Regarding the removable instructor seat, only estimates of the mass and cost of the hardware that ensures that the seat is removable is considered in this table. The cost of the actual seat will be stated when discussing the design of the aircraft's interior.

Table 9.5: Mass and cost budget breakdown for the in-flight TE package.

Item	Cost [€]	Mass[kg]
HTC VIVE Pro Eye + ZED Mini Stereo Camera	1792	0.62
Epson BT-300	669	0.069
Simulated Gear Lever [45]	77	0.05
Simulated Engine Controls (Propeller and Mixture Control) [46]	164	0.91
Simulated Carburettor Heat Control [47]	109	0.45
Simulated Fuel Pump [48]	5	0.05
Simulated Fuel Selector [49]	64	0.10
Sound System (Software) [50]	31	N/A
Ballistic Parachute [51] [52]	4450	21.70
Stress Monitor (Fitness Wristband) [53]	114	0.02

[42] URL: https://www.apple.com/de/shop/buy-ipad/ipad-10-2/32gb-space-grau-wifi-cellular, LA 08-06-2020
[43] https://easyvfr4.aero/efis-datasets/dynon-avionics-data/ accessed on 20-6-2020
[44] URL: http://www.cessna172club.com/forum/ubbthreads.php?ubb=showflat&Number=198883, LA 08-06-2020
[45] URL: https://www.aircraftspruce.com/catalog/elpages/racbezelswitches.php?clickkey=28056, LA 10-06-2020
[46] URL: https://www.aircraftspruce.com/catalog/appages/a750.php, LA 10-06-2020
[47] URL: https://www.aircraftspruce.com/catalog/eppages/carbheatcontrols2.php?clickkey=12010, LA 10-06-2020
[48] URL: https://www.aircraftspruce.com/catalog/elpages/metlevswitch.php?clickkey=28056, LA 10-06-2020
[49] URL: https://www.aircraftspruce.com/catalog/appages/fuelselcessna.php?clickkey=9216, LA 10-06-2020
[50] URL: http://www.flight1.com/products.asp?product=audenvga, LA 10-06-2020
[51] URL: https://www.aviationconsumer.com/safety/brs-parachute-retrofits-a-cost-benefit-analysis/, LA 10-06-2020
[52] URL: https://www.galaxysky.cz/grs-6-800-990-sds-175m2-p43-en, LA 10-06-2020
[53] URL: https://buy.garmin.com/en-US/US/p/605739, LA 10-06-2020

PFD [54 55]	8700	2.47
MFD [54 55]	3150	1.46
Collision avoidance system [54 56 57]	2763	0.52
Autopilot [54 58]	1900	1.80
Virtual CFI (Software) [59]	53	N/A
Voice Recorder [60]	32	0.07
Video Recorder [61]	300	0.11
Debrief Software [62]	150	N/A
EFB + ForeFlight software [63 64]	614	0.49
Removable Instructor Seat (Hardware)	100	1.00
Total	***25,237.56***	***31.89***
Total + 5%	**26,499.44**	**33.48**

9.6. Ground Segment

In addition to the TE items that will be included inside the aircraft, an optional ground segment of the TE package will be offered to the flight schools in order to further increase the training effectiveness. The flight simulator is one of the items with the highest perceived usefulness by the participants in the questionnaire, as mentioned in Section 9.4.2. Thus, the main component of the ground segment will be a flight simulator. Three types of flight simulators have been included in the questionnaire, as explained in Section 9.4.2. The perceived usefulness of each of the three types of flight simulators was almost equal, thus, a trade-off between the three design options needed to be performed. In order to identify which are the most important criteria to evaluate each proposed design option for the flight simulator, the quality function deployment method has been used, as shown in Table 9.6.

Table 9.6: Quality Function Deployment for the ground segment of the TE package.

Customer importance rating	Customer Requirements/ Customer Demands (What)	Functional Requirements/ Technical Performance Measurements (How)	Added Training Effectiveness (Including Realism)	Cost	Risk	Technology Readiness	Size	Total
5	The ground segment of the TE package shall **increase the training effectiveness** of the system in comparison to existing training solutions.		9	3	3	3		90
1	The ground segment of the TE package shall **occupy the least amount of space** possible.			1		1	9	11
4	The ground segment of the TE package shall **be cost-effective**.		3	9	1	3	1	68
2	The ground segment of the TE package shall **be safe to operate**.		3		9	1		26
	Technical Importance Score		63	52	37	30	13	195
	Criteria Importance		32.31%	26.67%	18.97%	15.38%	6.67%	100.00%
	Criteria Weight		**35%**	**25%**	**20%**	**15%**	**5%**	**100%**

Several customer demands have been considered when generating the QFD in Table 9.6. It was deemed that the most important one was that the chosen ground segment shall increase the training effectiveness in comparison

[54] URL: https://www.dynoncertified.com/pdfs/Certified-Price-Sheet-032020.pdf, LA 10-06-2020
[55] URL: https://www.dynonavionics.com/skyview-specifications.php, LA 10-06-2020
[56] URL: https://www.dynonavionics.com/mode-s-transponders.php, LA 10-06-2020
[57] URL: https://www.dynonavionics.com/adsb-dual-band-receiver-472.php
[58] URL: https://dynonavionics.com/public_html/yabbfiles/Attachments/Catalog-Dynon-web.pdf, LA 10-06-2020
[59] URL: https://store.takeflightinteractive.com/, LA 10-06-2020
[60] URL: https://amzn.to/2XPPS1T, LA 10-06-2020
[61] URL: https://www.mediamarkt.de/de/product/_gopro-hero7-black-2464536.html, LA 10-06-2020
[62] URL: https://www.cloudahoy.com/product.php, LA 10-06-2020
[63] URL: https://www.apple.com/de/shop/buy-ipad/ipad-10-2/32gb-space-grau-wifi-cellular, LA 10-06-2020
[64] URL: https://foreflight.com/pricing, LA 17-06-2020

to existing training solutions. Furthermore, it is important that the flight simulator will be profitable for the flight school in order to enhance the business case, thus, it shall be cost-effective. The customer demands that have been awarded a lower importance score are the fact that the flight simulator shall be safe to operate and occupy the least amount of space possible.

The technical performance measurements of the flight simulator that have been included in the QFD are the added training effectiveness, where the level of realism provided by the device will be accounted for, cost, risk, technology readiness and size. The scores that have been used in order to asses the correlation between the customer demands and the technical performance measurements in this QFD are: 1- low/weak correlation, 3- moderate correlation, 9- very strong correlation.

There is a moderate correlation between the increase in training effectiveness and the cost, risk and technology readiness of the simulator. This is due to the fact that the more costly a simulator is, the more complex this usually is, meaning that it may have the ability to more efficiently mimic real flight situations, leading to a higher increase in training effectiveness. Furthermore, the risk of an error occurring when operating a simulator increases with its level of complexity, and, consequently, with its ability of providing an increase in training effectiveness. In addition to this, the faster a certain simulator technology is fully developed and available to the flight schools, the faster an increase in the training effectiveness may be observed. Additionally, there is a moderate correlation between the desired cost-effectiveness and the technology readiness of the simulator. This is due to the fact that if a certain simulator has yet to be fully developed and certified before it may be used by the flight school, this process might be costly.

The result was that the most important criterion in the trade-off, with a weight of 35% shall be the added training effectiveness, which is reasonable. The cost is also an important criterion, having a weight of 25%, as well as the risk, with a weight of 20%.

The design options that are considered in this trade-off are: a VR simulator, such as the one used by the U.S. Air Force in the Pilot Training Next program [54], presented in Figure 9.6a, a flight training device (FTD) without a motion base, such as the Redbird LD [65] displayed in Figure 9.6b- "FTD- no motion" and an FTD with full motion capabilities, such as the Redbird MCX [66] shown in Figure 9.6c- "FTD- full motion".

Figure 9.6: Types of simulator considered in the trade-off.

(a) VR simulator used in the Pilot Training Next US Air Force Program.

(b) The Redbird LD, an FTD with no motion base.

(c) Redbird MCX, an FTD with full motion base.

An overview of the trade-off that was performed for the three types of simulator may be found in Table 9.7. In terms of added training effectiveness, it was considered that the VR unit and the FTD-full motion deserve an excellent score of 4. This is due to the fact that the VR unit delivers a high degree of visual realism, while the FTD-full motion delivers a high degree of haptic/movement realism, thus increasing the training effectiveness by closely emulating a real flight experience. The FTD- no motion is usually the one used in most flight schools at the moment, as resulted from research as well as interviews with the Head of Training of the KLM Flight Academy and of Vliegschool Rotterdam. Thus, even though this device is not equipped with a motion base and the same visual realism a VR unit may provide, it has proven to add a significant amount of training effectiveness.

[65] URL: https://simulators.redbirdflight.com/products/ld#aircraft-configurations
[66] URL: https://simulators.redbirdflight.com/products/mcx#aircraft-configurations

Table 9.7: Trade-off for the Ground Segment/Simulator.

Design Option	Technical Performance Measurements	Added training effectiveness	Cost	Risk	Technology Readiness	Size	Score
	Weight	35%	25%	20%	15%	5%	100%
VR unit		4	4	3	3	4	3.65
FTD- no motion		3	2	3	4	3	2.90
FTD- full motion		4	1	2	4	2	2.75

Regarding the cost of the flight simulators, the VR unit has been awarded an excellent score. This unit is built using off the shelf products. The exact cost is not known, but research has shown that the total cost of such a VR unit is approximately 8000-10000 [67] [55], which is considerably lower than the price of the various FTDs available on the market. The cost of the considered FTD-no motion, the Redbird LD, is approximately 33000$, which is more than 3 times the cost of the VR unit, thus being awarded the neutral score 2. The FTD-full motion that was considered in this trade-off, the Redbird MCX, is approximately 90000$, which may already be considered too costly by the flight schools, thus being awarded a score of 1.

In terms of risk, due to the motion base of the FTD-full motion, this device is considered complex and, thus, it may present more operational risks. The VR unit and the FTD-no motion are less complex when compared to the FTD-full motion, and thus scored better in the risk category.

Regarding technology readiness, both the FTD-no motion and the FTD-full motion scored excellently, as these devices are readily available on the market and they may be immediately purchased. The VR unit scored lower for this criterion, as it is not widely used in flight training at the moment and it requires collecting several off-the-shelf products before the flight schools may be able to use it. Furthermore, it is more difficult to certify than the other two types of flight simulators, as the technology is newer.

The VR unit would occupy the least amount of space, thus being awarded a score of 4 in this category. The FTD full-motion would occupy more space than the FTD-no motion, due to its motion base.

As can be seen on the last column of Table 9.7, the VR unit received the overall highest score, meaning that it is the winner of the trade-off, and, thus, the chosen design option for the flight simulator. Only if the weight of technology readiness would be increased to 50%, while decreasing the weight of the added training effectiveness and cost accordingly, the VR unit would not be the winner anymore, which indicates that the trade-off is robust.

The VR unit that will be used for ground training purposes will fulfil requirements **ELTA-TE-08, ELTA-TE-08-01, ELTA-07, ELTA-07-01, ELTA-07-01-A, ELTA-07-01-B** and **ELTA-TE-06**. Furthermore, as previously stated, this VR unit is composed of off-the-shelf products which will be discussed next. The main component will be a VR headset. The pilots in the PTN program are reported to be using the HTC Vive Pro VR headsets[68]. As an HTC Vive Pro Eye headset is already included in the in-flight TE package, this could be potentially taken out from the aircraft and directly used for ground training purposes as well, when needed. The great advantage of using this headset is the fact that it is equipped with eye tracking capabilities, which allows the instructor to closely monitor the student's learning process, by knowing exactly the student's scanning method. Furthermore, the student may use the footage that was displayed and recorded on the VR headset during the flight and review any desired situation in the on-ground simulator, for an efficient debriefing process. According to [65], the other components of the VR unit are:

- A dual screen desktop computer powered by Intel Core i7 6-core processor;
- An NVIDIA GeForce CTX 1080 8GB graphics card;
- A Thrustmaster Warthog Hands on Throttle and Stick and rudder pedals;
- Guitammer Buttkicker 2 haptic feedback seat attachments.

The complete set-up of the VR unit may be observed in Figure 9.7.

[67] URL: https://www.airforcemag.com/usaf-brings-pilot-training-next-to-regular-training-in-experimental-curriculum LA 11-06-2020

[68] URL: https://www.airforcemag.com/article/The-Future-of-Pilot-Training/, LA 11-06-2020

Figure 9.7: Complete set-up of the VR unit.

This flight simulator may also be used to efficiently train the student on multiple aircraft models, as switching between different cockpit configurations takes less than 10 seconds [66], which further increases the training effectiveness. In addition to this, it is reported that 13 out of the 30 students participating in the PTN graduated in 67% less time than using usual training procedures, and this successful outcome was mainly due to efficient use of the VR unit [66]. In addition to this, the VR unit used in the PTN enabled one instructor to supervise the performance of multiple student pilots at the same time, and it replaced up to 80 flight hours in a T-6 aircraft[68], significantly reducing the costs by eliminating the need of extra resources.

In order to increase the training effectiveness and to decrease the overall costs of the flight training, one of the goals of the TE package is to minimise the amount of time required for the instructor to be on-board of the aircraft in order to guide the student. It was reported by the Head of Training of the KLM Flight Academy that in their flight program, the student usually spends 10h flying with the instructor until they gain the necessary set of skills to fly solo. After that, 20 more hours of combined solo and dual flight are required to complete the second phase of the training. By limiting the amount of dual flight hours in this phase, the flight school could save a significant amount of money. In order to achieve this, a system capable of displaying real time flight information collected from the aircraft in which the students will be flying solo at that specific moment, may be made available to the instructors, as part of the ground segment of the TE package. In this way, the instructor may monitor the performance of multiple students at the same time. In order to collect flight data and display it in front of the flight instructor, on the ground, in real time, as well as provide the flight instructor with the option of remotely deploying the ballistic parachute if the student is in an overwhelmingly dangerous situation, technology used for operating Unmanned Aerial Vehicles (UAVs). According to the principles of operating UAVs [67], the Dragonfly and the ground station- the flight school- are both equipped with antennas that facilitate communication using radio waves. Keeping in mind that the maximum range of the Dragonfly is around 250 km and that usually flight training is performed in the proximity of the flight school, it is safe to assume that direct, Line-of-sight (LOS) radio wave transmission of flight data is possible, at least during take-off and landing, which represent the most critical phases of flight. In this way, especially during landing, the instructor may observe the student's flight data and even vocally guide them through the landing procedure, which would provide the student with an enhanced level of safety.

9.7. Cockpit Layout Design

This section presents the cockpit layout design. First, the items that will be implemented in the cockpit are explained in Section 9.7.1. The mass and cost breakdown of the cockpit items may also be found in Section 9.7.1. The cockpit layout may be visualised in Section 9.7.2.

9.7.1. Cockpit Items Mass and Cost Breakdown

This section explains all the cockpit items that are included within the cockpit. Table 9.8 shows each cockpit item which is not part of the TE package, as these have been explained in detail in Section 9.5. The TE items row is the total cost of all items explained in the aforementioned section.

Table 9.8: Mass and cost of cockpit items, including 5% contingency.

Item	Cost [€]	Mass[kg]
TE Items	25237	31.89
Pitot tube/AOA indicator [69]	175	0.15
Flap Switch [70]	80	0.01
Flap Computer [71]	210	0.10

[69]URL: https://www.dynonavionics.com/aoa-pitot-probes.php, LA 11-06-2020
[70]URL: https://www.aircraftspruce.com/pages/el/switches_flaps/flaphandlecombo.php, LA 11-06-2020
[71]URL: https://www.aircraftspruce.com/catalog/avpages/tcw11-13462.php?clickkey=33888, LA 11-06-2020

Annunciator Panel [72]	147	0.28
Backup instruments [73]	2050	0.66
Radio antenna [74]	215	0.10
Audio control panel [75]	260	0.20
Tachometer [76]	215	0.37
Cabin Air Vent [77]	98	0.05
Switch & Circuit Breaker Panel [78]	570	1.15
Control Stick (including trim) [79]	155	0.15
Instrument Panel Lights [80]	125	0.20
Ignition Switch [81]	195	0.15
Parking Brake Cable [82]	65	0.20
Parking Brake Sticker [83]	0.40	0.00
Cabin Heat Valve [84]	65	0.20
Seats [85]	1580	21.0
Seat Belts [86]	430	3.00
Installation Hardware (cable&harnesses)	500	5.00
Static Port [87]	15	0.15
Throttle [88]	82	0.46
COM Radio Panel [89]	1155	0.509
Total	***33,624.96***	***65.98***
Total + 5%	**35,306.21**	**69.28**

The items that make the cockpit a glass cockpit take up the largest part when one looks at the cost of the PFD/MFD. While the TE benefits of the glass cockpit have been explained in Section 9.5, this section aims to further discuss the non-training enhancement related functions of the PFD and MFD.

The SkyView HDX by Dynon has been chosen as the PFD and MFD. It is a 10 inch screen which contains most information which is relevant for the (student) pilot during flight. The SkyView HDX has a 10 inch touchscreen which features good readability with wide viewing angles and simple screen navigation [90]. Furthermore, the PFD system is equipped with ADAHRS, a remote magentometer, a GPS receiver, a backup battery and a USB port, which will allow the transfer of flight data to be used for debriefing, as mentioned in Section 9.5.2.

The PFD - which is capable of IFR navigation in combination with an IFR navigator - displays all information from the basic six instruments and more on one screen, which will assist the student pilot in keeping an overview of the aircraft attitude and plan this attitude ahead in time. [90]. It also allows for the display of the basic six without synthetic view being activated, which is very useful for initial pilot training in order to not overwhelm the student and allowing them to feel the aircraft.

[72] URL: https://www.aircraftspruce.com/catalog/inpages/ap_7h.php?clickkey=3600, LA 11-06-2020
[73] URL: https://www.dynonavionics.com/efis-d10a.php, LA 11-06-2020
[74] URL: https://www.air-store.eu/epages/AIRStore-LuftfahrtbedarfundAvionik.sf/en_GB/?ObjectPath=/Shops/AIRStore-LuftfahrtbedarfundAvionik/Products/AV-10, LA 11-06-2020
[75] URL: https://www.dynonavionics.com/includes/guides/SV-INTERCOM-2S_Installation_and_Pilots_User_Guide-Rev_A.pdf, LA 11-06-2020
[76] URL: https://www.aircraftspruce.com/pages/in/tachometers_0browse/mech_tachs.php, LA 11-06-2020
[77] URL: https://www.aircraftspruce.com/catalog/appages/cabinvent.php, LA 11-06-2020
[78] URL: https://www.aircraftspruce.com/catalog/elpages/lsapowerpanel.php, LA 11-06-2020
[79] URL: https://www.aircraftspruce.com/catalog/elpages/g305.php, LA 11-06-2020
[80] URL: https://www.aircraftspruce.com/catalog/pspages/sptlightstrip.php?clickkey=3047345, LA 11-06-2020
[81] URL: https://www.aircraftspruce.com/catalog/elpages/igswitches2.php, LA 11-06-2020
[82] URL: https://www.aircraftspruce.com/catalog/appages/a700.php?clickkey=8314, LA 11-06-2020
[83] URL: https://www.aircraftspruce.com/catalog/appages/buttoninsters3.php?clickkey=8314, LA 11-06-2020
[84] URL: https://www.aircraftspruce.com/catalog/appages/a700.php?clickkey=8314, LA 11-06-2020
[85] URL: https://www.texasairsalvage.com/main_view.php?editid1=215342, LA 11-06-2020
[86] URL: https://www.aircraftspruce.com/catalog/appages/hooker2.php, LA 11-06-2020
[87] URL: https://www.aircraftspruce.com/pages/in/staticports/alumstaticports.php, LA 11-06-2020
[88] URL: https://www.aircraftspruce.com/catalog/appages/a750.php, LA 11-06-2020
[89] URL: https://www.dynonavionics.com/vhf-com-radio-controls.php, LA 11-06-2020
[90] URL: https://www.dynoncertified.com/pdfs/Certified-brochure-032020.pdf, LA 12-06-2020

Figure 9.8: Main view of the PFD

Furthermore, the SkyView HDX includes engine monitoring - currently only for traditional combustion engine aircraft[90] - but with a little modification and changed sensors, it is expected that it will be able to display the engine parameters of the Dragonfly. It provides "helpful verbal and visual alarms" that "grab your attention when required"[90].

Since January 2020, most aircraft flying in the US are required to be equipped with at least ADS-B out. In order to be prepared to enter the US market, the PFD also includes ADS-B out with a mode S transponder. In addition to this, it includes an ADS-B receiver to collect and show data on traffic and weather. This aids the student in gaining situational awareness[90].

The PFD also includes flight planning and mapping with the included maps, and optional "charts, airports diagrams, and procedures."[90]. In order for it to be fully IFR approach capable, it is advised to include an IFR navigator such as the Garmin aera 760[91]. However, this item is not included as a standard cockpit item, as the SkyView HDX has basic VNAV approach capabilities which can be used for initial IFR training. The included IFR connectivity kit enables connectivity with certified GPS/NAV devices, for example those made by Garming or Avidyne [90], and allows this information to be displayed on the PFD too.

While the SkyView HDX's touch screen can also control the two-axis autopilot, which has been certified for many other trainer aircraft such as most versions of the Cessna 172[90], it has been decided to integrate a separate autopilot panel in order to limit the necessity of navigating menus on the touch screen.

An additional separate panel mount has been introduced with the COM radio. It has "dedicated buttons for tuning Tower/CTAF, ATIS/WX, ATC and ground frequencies" [90]. It will be used for all communication occurring on board the aircraft and allow for example the flight instructor to assist the student from the ground once they are soloing. Furthermore, the COM system requires a separate radio antenna, which is also included in the cockpit items.

In order to be IFR capable, the aircraft requires backup instruments. For this purpose, the Dynon D10 EFIS was chosen[92]. It is less costly than a separate set of traditional instruments, which would also require the installation of a vacuum pump, which is prone to failing, with a failure occurring roughly every 500 hours[93].

Further items that are included in the cockpit, or which are required for its components, include the pitot tube and angle of attack (AOA) sensor. An AOA sensor was requested by many in the performed questionnaire as it gives enhanced information on the aircraft's stall. In order to electrically operate the flaps, a flap computer and a flap switch are required. The position of the flaps can be indicated on the PFD. In order for the aircraft to calculate its velocity a static port has also been included.

To control the audio inside the plane, an audio control panel has been added, which also adds stereo functionality. It connects to the headsets and allows for implementation of the pilot's own music. The cockpit also includes a tachometer in order to determine the flown hours. The tachometer is often used by flying clubs and flight schools to determine how much the student owes them.

In order to warn the pilot of a low voltage of the battery, a low voltage warning light has been implemented.

[91] URL: https://buy.garmin.com/en-US/US/p/681883, LA 12-06-2020
[92] URL: https://www.dynonavionics.com/efis-d10a.php, LA 12-06-2020
[93] URL: https://www.aopa.org/training-and-safety/students/flighttestprep/skills/vacuum-system-failure, LA 20-06-2020

Furthermore, a switch and circuit breaker panel is implemented as it is in most general aviation cockpits. It allows the pilot to check that all circuits are functioning and contains the master switch for the avionics. The fuel pump simulated switch is also included in this panel. In addition to this, the ignition switch is located at the side of the control switch panel.

For the pilot's and passenger's comfort, a cabin air vent and heat valve have been installed. The air vent can distribute both warm and cold air in the cockpit and will help with fogging up of the windshield.

The aircraft will be controlled using a stick on both sides of the cockpit in stead of a yoke to give the cockpit a cleaner look and to not block the view of any instruments/ The electrical trim in both directions is integrated on this stick. To anticipate on the allowance for the aircraft to be certified at night, instrument panel lights are already included.

The cockpit also contains a parking brake cable, which will be equipped with the parking brake sticker. The throttle - which uses the same components as the simulated mixture and propeller controls - will be used to control the amount of power the engines deliver.

Finally, the interior of the cockpit requires seats and seat belts. The chosen seats are examples of the possible seats that could be used, and come from a Cessna 172. The seat belts are four-point seat belt systems which are configurable in fabric and trim colour. For the installation of all avionics devices, 500€ and 5kg have been added for wiring and harnesses within the cockpit.

9.7.2. Cockpit Layout

This subsection shows the final cockpit layout. It also lists all items which can be seen in Figure 9.9.

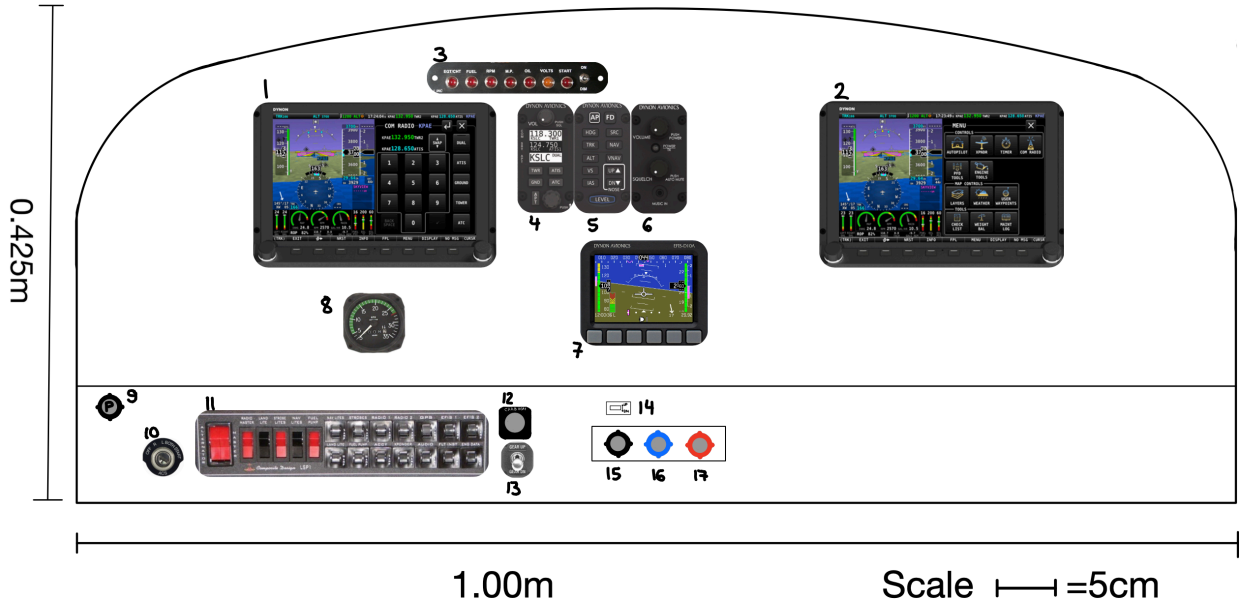

Figure 9.9: The final cockpit layout of the ELTA.

The items listed in Figure 9.9 are as follows:

1. Primary Flight Display
2. Multi-functional Display
3. Annunciator Panel
4. COM Panel
5. Autopilot Panel
6. Audio Control Panel
7. Backup EFIS
8. RPM + Tachometer
9. Parking Brake
10. Ignition Switch
11. Switch and Circuit Breaker Panel
12. Simulated Carb Heat Control
13. Simulated Landing Gear Switch
14. Flap Switch
15. Throttle
16. Simulated Propeller Governor
17. Simulated Mixture Control

9.8. Risk Assessment

To have an indication of the possible risks for the TE-package all items will be analysed individually.

Mixed reality headset. The mixed reality headset could fail due to several things. It could be overheated or experience a software error for example. When this occurs the user can just take off the headset and resume normal flight operations. To prevent overheating the aircraft has a ventilation system within the cockpit which not only prevents overheating of the headset, but also of the pilot himself. Software errors can be mitigated by updating the software regularly.

Simulated levers. A failure of a simulated lever could be caused by an improper connection of the lever to the annunciator panel or engine computer. If the simulated levers fail this has no influence on the actual flight operation, and this may result in the risk of the student becoming incompetent on flying actual piston aircraft where improper usage of the levers will result is possibly fatal accidents. This can be mitigated by having a little light next to each lever which lights up only if the lever is properly connected.

Sound system. A risk could be that the sound system is set at the wrong volume. This could be mitigated by a knob where the sound can be manually adjusted. As the sounds mimic those experienced in a real piston engine aircraft, it is important for the student to know to regulate the volume so that they can be heard and audio cues can be picked up with regards to the engine noises. Another risk is that the sound system fails completely. This can easily be recognised by the pilot as the simulated piston engine noise will not be heard and therefore no mitigation method is required.

Ballistic Parachute. A failure within the ballistic parachute system will be fatal. For that reason, this risk should be mitigated by performing regular maintenance checks as well as 5-yearly repacking of the parachute.

Glass Cockpit. To mitigate the risk of a failure within the glass cockpit, the backup EFIS has been implemented. Furthermore, backup batteries are included with the PFD, MFD and backup EFIS to guarantee a minimum of one extra hour of life on these devices.

Collision Avoidance System. As the Dragonfly is used for VFR training, collision avoidance is the responsibility of the pilot himself. The collision avoidance system should never be blindly trusted as failures could occur and the system detects only aircraft. Birds and small drones are also a potential hazard, which can only be detected visually at this moment. To minimise the risk of not seeing an aircraft it could be mandatory to have ADS-B on each aircraft which is currently the case in the USA for most airspace.

Autopilot. To minimise the risk of an autopilot failure it should always be checked during maintenance. Furthermore, the autopilot should include a self-test on the ground which should run successfully in order for it to be turned on during flight. Finally, the autopilot can always simply be switched off using the autopilot-off switch.

Virtual CFI. If the virtual CFI should fail, the student can become stressed. To minimise this risk, the student should only be allowed to fly solo when he knows how to fly the aircraft without help from the instructor as is currently the case for PPL training. The goal of the virtual flight instructor is also not to teach new manoeuvres, but only to recapitulate what the student already knows.

EFB. To mitigate the risk of a failing EFB and not knowing where you are and who to contact there should be at least one back-up, as prescribed by regulations. This back-up can be another EFB or a paper chart. To minimise the risk of flying with an out-of-date EFB it should be updated before every flight. If this is not done, the pilot should get a message that he has to update the EFB before going to fly.

Voice Recorder. A risk can be that it is not allowed to record ATC as is the case in Germany for example. To mitigate the risk of getting sued the voice recorder should only record the intercom.

Other items. The other TE items will not affect the direct flight environment. They only have influence on the debriefing. For that reason no mitigation strategy is thought of other than repairing the systems whilst on the ground during regular maintenance intervals.

9.9. Verification and Validation

Some of the items that have been selected for the TE package need further verification and validation before they may be employed on-board the aircraft for training purposes.

One such item is represented by the selected AR glasses, the Epson Moverio BT-300. In order to ensure that their performance during flight is appropriate for the student, they will first be tested on the ground on the following criteria: accuracy of the displayed information, latency of data transfer, as well as level of visibility of the information in high brightness situations. Once the item has been tested and approved on the ground, the same series of tests will be performed during test flights. If all the tests are completed successfully, the instructors as well as the flight schools may introduce these AR glasses to the students during flight training.

Another item that shall be thoroughly verified and validated before being introduced in the cockpit is the mixed reality headset. Even though a similar headset has been validated by NASA, as they have proven that this concept aids in training certain manoeuvres, the item still needs to be verified and validated for general aviation training. The main aspects that need to be tested include: the quality/clarity of the displayed real image (the ZED

Table 9.9: Compliance Matrix of all TE functional and non-functional requirements

Identifier	Relevant Item Software	Req met?	Identifier	Relevant Item Software	Req met?
ELTA-TE-01	All	✓	**ELTA-TE-06-01-B**	Camera	✓
ELTA-TE-01-01	Mixed Reality Headset, Electrical Engine	✓	**ELTA-TE-06-01-C**	Camera, SD Card	✓
ELTA-TE-02	Fitness wristband, eye tracking	✓	**ELTA-TE-06-01-D**	Flight data recording, PFD	✓
ELTA-TE-01-02-A	Fitness wristband	✓	**ELTA-TE-06-01-E**	Flight data recording, PFD	✓
ELTA-01-02-B	Fitness wristband	✓	**ELTA-TE-06-01-F**	USB port in PFD	✓
ELTA-TE-01-03	Modular cockpit	✓	**ELTA-TE-07**	VR simulator	✓
ELTA-TE-01-04	All	✓	**ELTA-TE-07-01**	VR simulator	✓
ELTA-TE-02	PFD, EFB	✓	**ELTA-TE-07-01-A**	Flight data recording, VR simulator	✓
ELTA-TE-02-01	EFB	✓	**ELTA-TE-07-01-B**	VR simulator	✓
ELTA-TE-03	EFB, AR glasses	✓	**ELTA-TE-08**	Mixed reality headset	✓
ELTA-TE-03-01	EFB, AR glasses	✓	**ELTA-TE-08-01**	Aircraft, VR simulator	✓
ELTA-TE-04	Virtual CFI	*	**ELTA-TE-08-02**	Electrical engine	✓
ELTA-TE-04-01	Virtual CFI	*	**ELTA-TE-08-03**	Mixed reality headset	✓
ELTA-TE-04-02	Virtual CFI	*	**ELTA-TE-09**	PFD, MFD, AR glasses	✓
ELTA-TE-04-03	Virtual CFI	*	**ELTA-TE-09-01**	PFD, AR glasses	✓
ELTA-TE-04-03-A	Virtual CFI	*	**ELTA-TE-NF-01**	Test flying	✓
ELTA-TE-04-03-B	Virtual CFI	*	**ELTA-TE-NF-02**	Cockpit layout, CAD drawings	✓
ELTA-TE-05	Autopilot	✓	**ELTA-TE-NF-03**	USB port on PFD	✓
ELTA-TE-06	Voice, Video, Data recording, EFB, Debrief software	✓	**ELTA-TE-NF-04**	Battery	✓
ELTA-TE-06-01	Camera	✓	**ELTA-TE-NF-05**	DSE constraint	✓
ELTA-TE-06-01-A	Camera	✓			

mini camera shall record video with sufficient quality for the student to be able to read the flight data on their instruments and to be immersed in the experience), the quality/clarity/level of realism of the displayed virtual environment/simulations outside of the windshield, the chroma key composting accuracy, as well as the latency of data transfer. These shall all be tested on the ground first and then in a test flight.

A compliance matrix for the requirements stated in Section 9.3 may be found in Table 9.9. The requirements that are assumed to be fulfilled by the virtual CFI have been marked with "*" due to the fact that the actual software of the virtual CFI has not been developed or tested yet.

9.10. Training Effectiveness Provided by the Electric Propulsion

A unique aspect of the Dragonfly is represented by its electrical propulsion. This characteristic greatly contributes towards the increase in training effectiveness that is to be achieved with the aircraft. This section explains the added training benefits of the electric propulsion alone.

First, the implementation of the electric propulsion in combination with the light weight of the aircraft allows for reaching a significantly higher power to weight ratio compared to standard combustion engine aircraft. This means that the aircraft will be able to climb faster than usual trainer aircraft. This will provide the possibility of more effective training of manoeuvres by using the time within the training sessions more efficiently. Additionally, having an electric propulsion system allows for easily controllable power output from the engines. This aspect is highly important, as it would provide the students with the opportunity to safely recover from their mistakes by having the aircraft react quickly to their input. Moreover, the engines of the electrical trainer aircraft are more reliable than conventional propulsion alternatives, as they are less complex and, thus, present less operational risks. This feature makes training safer for the beginner students. Furthermore, the very low noise aspect and the fact there are no vibrations would help increase the level of concentration of the beginner student. This will help them learn the basics of flying more efficiently.

Another big advantage of the electric propulsion is the low operational cost associated with it. This will make the business case more profitable for the flight schools, as well as make flight training more accessible to potential students. With lower operational costs, the students will be able to train more and thus improve their skills. A cost analysis that determines the operational cost of the Dragonfly is presented in Section 11.4.1.

9.11. Quantifying the Training Effectiveness of the TE Package

Now that the benefits of training in an aircraft equipped with electric propulsion have been discussed in Section 9.10, it is time to dive deeper into the added training effectiveness of the items that will be included in the TE package. On average, it takes student pilots 55-60 hours to complete their PPL training [94]. The minimum number of hours to receive your PPL license varies between Europe, where it is 45 hours, and the USA, where it is 40 hrs under Part 61 and 35 hrs under Part 141. This means that the amount of training hours can be decreased by 25% to 42%, depending on location, while still fulfilling minimum requirements. This may be achieved by implementing certain TE items. In this section, typical ways of quantifying training effectiveness will be discussed first. Then, the added training effectiveness of multiple TE items will be assessed.

Typical ways of quantifying Training Effectiveness

One way to quantify training effectiveness is the so called Transfer Effectiveness Ratio (TER). An example of this is presented in a paper by J.M. Rolfe and P.W. Caro [68]. The TER is measured by applying Equation (9.1), where TE_{-sim} is the training effort required to learn the task on the job without a simulator, $TE+sim$ is the training effort required to learn the task on the job when some training is performed using the simulator and TE_{insim} is the time required to learn the task using just the simulator[68].

$$TER = \frac{TE_{-sim} - TE_{+sim}}{TE_{insim}} \tag{9.1}$$

This equation will "give a TER= $+1.0$ when the amount of training effort saved on the job is equalled by the amount of training effort expended in the simulator" [68]. The TER is > 1 if the training hours in the simulator are less than the time saved in an on-the job-situation. The TER is < 1 if the training time in the simulator is larger than the time saved on the job[68].

Furthermore, one may not only be interested in the TER, but also the cost effectiveness of their training. Therefore, Roscoe developed the Training to Cost Ratio (TCR), which is defined by Equation (9.2)[68]. The median TCR - taken from 33 different aircraft and simulator pairs - is 0.116, meaning that the cost of operating a simulator is roughly 10% of the cost of operating the real aircraft counterpart.

$$\text{TCR} = \frac{\text{cost of operating the simulator (\$/hr)}}{\text{cost of operating the actual equipment (\$/hr)}} \tag{9.2}$$

The resulting Cost Effectiveness Ratio (CER) is represented by Equation (9.3)[68]. If the CER > 1, cost effective training can be achieved.

$$CER = \frac{TER}{TCR} \tag{9.3}$$

A different way of quantifying training effectiveness is the incremental transfer effectiveness function (ITEF). In his 1971 paper, Roscoe explains the ITEF with the aid of an example [69]. The idea of ITEF is that one hour of training in a simulator can save more than one hour of pre-solo flight training, but with increasing simulator hours, the added effect becomes less [69].

In order to determine the ITEF, first, the basic transfer computation must be understood. This can be found in Equation (9.4)[69].

$$\frac{Y_o - Y_x}{Y_o} \tag{9.4}$$

Where Y_o is the time required in the aircraft for flight training without any training enhancement and Y_x is time required for flight training after the introduction of TE items [69]. $Y_o - Y - x$ represents the hours saved in flight training by the introduction of TE items. When dividing the saved hours by the initially required hours Y_o, the transfer percentage can be determined. The transfer percentage will be used throughout this section in order to account for the TE package's added training effectiveness. The CTEF is then defined as Equation (9.5). The X represents "the total time required by the experimental group to achieve a performance criterion".

$$CTEF = \frac{Y_o - Y_x}{X} \tag{9.5}$$

Y_o and Y_x are identical to those explained in Equation (9.4). Finally, the ITEF is defined as Equation (9.6).

$$ITEF = \frac{Y_{x-\Delta x} - Y_x}{\Delta X} \tag{9.6}$$

[94] URL: https://www.telegraph.co.uk/travel/comment/how-to-get-a-private-pilot-license/, LA 15-06-2020

The unknown ΔX represents the incremental unit in time, Y_x is identical to that described in Equation (9.4) and $Y_{x-\Delta x}$ is "the amount of time required by an experimental group to reach a performance criterion after $x - \Delta x$ training units" [69]. With increasing hours of ground training, the TER decreases. A different paper by Roscoe [70] led to the conclusion that 11 hours of ground training in a simulator are the optimum - on average - before the TER drops below 1[70].

AR Glasses- Epson Moverio BT-300

It was proven that when using AR glasses, pilots experience a significant decrease in their reaction time when faced with an emergency situation [60]. This has been demonstrated by testing two distinct groups of pilots in a fixed base Airbus A320 simulator. Group A would be wearing the Microsoft HoloLens AR headset which would display the instructions that needed to be followed, while group B simply received their instructions on the Electronic Centralised Aircraft Monitoring System (ECAM). After the instructor has initiated an engine fire during the descent, the time needed for each pilot to follow the instructions to handle this event was measured. The median time of group A was 29.5 seconds, while the median time of group B was 43 seconds. This means that using the Microsoft HoloLens headset increased the efficiency of completing the series of tasks by 31.4%. This proves that utilising AR glasses has great advantages when training emergency situations and also improves the overall training effectiveness by helping the student complete a series of tasks/checklist in significantly less time. In order to quantify the amount of time that would be overall saved by introducing this technology in the cockpit, the prediction made by Adventia European College of Aeronautics may be used: by employing Google Glass, a model comparable to the chosen Epson Moverio BT-300, they predict that the students will save 10% of their overall training time[95]. This time will be saved by providing the students with fast, easy access to information such as checklists, real time weather data as well as updates of notices to airmen (NOTAMs) etc. by displaying these in front of their eyes, rather than on paper. Furthermore, the added benefits of the Epson Moverio BT-300 are that it may act exactly as a HUD: it may display instantaneous flight data, such as the airspeed, angle of attack, flight path, as well as guide the student using Highway-In-The-Sky technology. Thus, it is safe to assume that these AR glasses will provide at least a 10% increase in training efficiency.

Debrief Software

In terms of the debrief procedure, there are clear links between thoroughly completing it using a debrief software and an increase in the efficiency of the training and performance. A meta-analysis concluded that a well performed debrief procedure may lead to a 20-25% improved individual performance[71]. Furthermore, it is estimated that the quality of the debrief procedure contributes towards 33% of the efficiency of training in a flight simulator[96]. If proper debriefing is performed, it is clear that the time spent during actual flight training will be used more efficiently[72]. However, no estimates for the exact time that would be saved by implementing a debrief software in the training procedure have been found. This is mainly due to the fact that it is necessary for the student pilot to also invest personal time in proper debriefing procedures: in addition to using the proposed debrief software, CloudAhoy, right after the flight, possibly together with the instructor, they are also advised to utilise it to review their flight at home, in preparation for the next flying lesson.

Mixed Reality Headset

According to [73], flight simulators that combine visual and motion simulation have a mean transfer ratio of 38%. By turning the aircraft itself into an actual flight simulator (by implementing the Fused Reality concept with the HTC VIVE Pro Eye headset and the ZED mini camera, as previously discussed), the motion will be significantly more realistic when performing certain manoeuvres than in any full motion based ground simulator. Thus, it will be assumed that the added training effectiveness provided by the mixed/fused reality unit is at least 38%. However, this does not mean that this estimate would lead to a 38% saving from the overall flight training time, as this mixed reality headset may only be utilised when an instructor is on-board and it will most probably be used only for a segment of the flight, when certain manoeuvres need to be trained. This aspect will be elaborated upon later in this section.

Electronic Flight Bag

Regarding the use of electronic flight bags on-board during flight training, it is apparent that this increases the performance of the student pilots in several areas, such as interpretation of charts, acquiring information from NOTAMs and weather products as well as the flight information/overall awareness by 15%-20% on average [74]. Furthermore, a lot of studies have been found that the electronic flight bags contribute towards an increase in the pilot efficiency [97], as a significantly reduced response time was registered when using the EFB as opposed to paper printed resources [75], leading to reduced overall flight time[98]. However, no actual quantification of

[95] URL: https://aeriaa.com/on-the-use-of-google-glass-in-pilot-training/, LA 12-02-2020
[96] URL: cefa-aviation.com/how-to-consequently-improve-the-quality-of-debriefing-digital-age-debriefing-2-0-2/, LA 15-06-2020
[97] URL: https://fluix.io/case-study-titan, LA 16-06-2020
[98] URL: https://www.bytron.aero/aviation-news/benefits-of-the-electronic-flight-bag, LA 16-06-2020

the amount of training time saved by using this technology was found. Thus, an estimation of the overall time saved by introducing the EFB on board of the Dragonfly shall be used. The EFB is used for displaying various flight information, in a similar way as the Google Glass. As previously stated, the predicted increase in efficiency provided by the Google Glass is 10%. The main difference between the Google Glass and the iPad that represents the EFB is the fact that the former displays flight information right in front of the pilot's eyes, while the latter implies that the pilot will be looking down. Even if the pilot needs to move their head in order to read the information on the EFB, it is safe to assume that using this technology on board will save at least 5% of the time of a normal flight lesson, where the student would need to search through heavy textbooks and large maps to obtain the desired information.

Glass Cockpit

The implementation of a glass cockpit is useful in enhancing training effectiveness. According to a study conducted by the FAA [76], in which two groups' flight training was investigated: one that trained using a traditional syllabus in an analogue aircraft and one in an aircraft with a glass cockpit. The implementation of a glass cockpit in flight training of the PPL and IFR saved 34% of training hours. The traditional group of flight training - consisting of 449 students - took 134.3 flight hours from zero experience to their IR license. For the same license, the glass cockpit group - consisting of 97 students - took 88.7 flight hours [76]. By interpolating the data presented in [76], it was found that the group training on the aircraft with a glass cockpit needed 14% less hours to complete their PPL level training when compared to the control group. Thus, it will be considered that the added effectiveness of introducing a glass cockpit is 14%.

Modular Cockpit

In 2017 the Swiss company AlpinAirPlanes in collaboration with the Slovenian company Pipistrel have designed an ab-initio flight training programme that mainly relied on the use of the all electric Pipistrel Alpha Electro aircraft. The aircraft was distributed to 10 different flight schools in Switzerland. It was reported that, in order to help the students familiarise with the combustion engine aircraft technology that they would most likely encounter in their future career, 10% of the total flight training time was required to be spent on-board the Alpha Trainer, the combustion engine version of the Alpha Electro [99]. By having a modular cockpit that can emulate diverse characteristics of a complex combustion engine aircraft (the simulated engine controls, the sound system, simulated gear lever, etc.), it may be assumed that the Dragonfly will thus provide an increase in training effectiveness of up to 10% when compared to its competitor, the Alpha Electro, as 10% of the overall flight training time might be saved.

Stress Level Monitor

While stress level monitoring can not directly increase training effectiveness, it can be used to track a student pilot's stress level in order to judge their confidence with certain situations and manoeuvres and possibly tailor their fight training accordingly. According to the US Air Force's human resources laboratory [64], flight students learn most efficiently at moderate stress levels. On the contrary, high levels of stress result in the increase in time required by the student to acquire a certain skill [64]. The performance increase under moderate stress levels is based on the levels of epinephrine and norepinephrine in the student's body. No exact data on quantifying the effectiveness of stress level monitoring during flight training was found.

VR Unit Simulator

Regarding the VR unit simulator that will be offered as part of the ground segment of the TE package, data on the added training effectiveness was collected from a study that was comparing two pilot training strategies for the US Air Force: the original Undergraduate Pilot Training (UPT) programme and the Pilot Training Next (PTN) programme [55]. The main difference between the two was the implementation of the VR unit simulator in the PTN programme. According to the study, the reduced number of aircraft and instructors required for training, due to the implementation of the VR simulators, represents the main advantage of the PTN programme. Thus, the added training effectiveness of the VR unit simulator may be quantified by comparing the amount of flight hours needed for the students to complete the training during the original UPT programme to the one needed to complete the PTN programme. Following from [55], UPT students needed on average 117 hours in a T-6 aircraft, while the PTN students only required 65 training hours in the same aircraft. Thus, it could be concluded that the training efficiency increased by 44.44%, and the main contributing factor to this result is the implementation of the VR unit simulator. However, taking into account that military training is usually more intensive than general aviation training, the usual PPL students will not use the VR unit simulator for the same amount of time as the student pilots being trained by the military. Thus, a more appropriate estimate for the increase in training effectiveness provided by the VR unit is 25%, which corresponds to the transfer percentage of a flight simulator with no motion base, according to [77].

Quantifying the Overall Training Effectiveness

In order to determine the overall increase in training effectiveness, the previously determined potential training effectiveness increases were multiplied by an "usage factor". The "usage factor" quantifies during how much of

[99] URL: `http://www.alpha-electro.ch/en/`, LA 16-06-2020

the training this TE item can be used. In order to determine this, a syllabus by the Vliegschool Hilversum was used [100] which splits the 45 minimum required hours into four phases. In total this syllabus consists of 10 hours of solo flight time and 35 hours of dual flight time. The usage factors are based on the assumption that student pilots will only require the prescribed 45 hours to complete their PPL training. The amount of hours that are stated to be saved by using each of the in-flight TE item is calculated based on the 60 hours average needed by usual student pilots to finish their PPL training.

The usage factor for the AR glasses was deemed to be 33.3%, as it is considered useful for 15 of the required 45 hours. It is expected that the student will not use if for the very first flight hours, but that it will be useful in many flights in which the VR/mixed reality headset cannot be used, which includes many of the solo hours. The AR glasses can show the flight student data similar to that of a HUD, for example airspeed, angle of attack, pitch and Highway-In-The-Sky. The total amount of time saved for the student pilot is therefore 2 hours in total.

For the mixed reality/VR headset, the usage factor was set at 15%. As it cannot be used when flying solo, and it is not useful for some of the dual lessons as the student cannot become too reliant on it, it will be used for 6.75 hours of flight training. Mostly, it will be used for stall training in order to simulate that the ground is closer than it really is, it will be used to train near misses, approaches towards a simulated runway at altitude, and also worse weather conditions. It may also be used in certain segments of the cross-country flight lessons, in order to simulate a different terrain, such as mountains, in front of the student and perhaps certain obstacles like birds. It therefore saves the student around 3.4 hours of flight training in total.

The EFB, which comes in the form of an iPad with EasyVFR 4 installed, will be used in every single lesson and for solo flight, as well as beyond the PPL training. It will be used in order to plan flights and display checklists. Therefore, its usage factor is 100% and it saves the student up to 3 hours in flight training.

As glass cockpits are becoming standard equipment on more and more GA aircraft, it is likely that it will not greatly increase the training efficiency when compared to a modern standard trainer aircraft. In comparison to the training performed solely on an aircraft with a traditional steam gauge cockpit, however, it is expected to save 8.4 hours of flight time. Furthermore, many pilots will proceed to train for their IFR license, in which the glass cockpit has an even higher training efficiency than for the PPL [76], and can save 34% of flight time.

The modular cockpit, used to train students how to fly a complex combustion engine aircraft, will also be used in 100% of the flight lessons. It saves 10% of training time, as no additional lessons are hence required to change from the electrical to a combustion engine aircraft. In total, this therefore saves an estimated 6 hours of training. Furthermore, it allows for relatively cheap training time on a complex aircraft for the commercial pilot's license.

The VR simulator has a training efficiency of 25%. This means that every hour flown in the simulator is equal to 1.25 hours in the real aircraft. Most flight schools do not heavily utilise simulators for basic PPL training, but with a very low operating cost and a high profit margin, it is deemed a useful added training item. It is expected that five hours in PPL training will be flown on the VR simulator, resulting in 1.25 hours of total saved time in the air.

An overview of the increase in training effectiveness provided by each item, their usage factor, weighted training effectiveness and amount of hours saved from the average 60 hours may be found in Table 9.10.

Table 9.10: Overview of the training effectiveness of each item and the amount of flight hours it would save.

Item	Increase in Training Effectiveness	Usage Factor	Weighted Increase in Training Effectiveness	Amount of Hours Saved
AR Glasses	10%	33.33%	3.33%	2
Mixed Reality Headset	38%	15%	5.7%	3.4
EFB	5%	100%	5%	3
Glass Cockpit	14%	100%	14%	8.4
Modular Cockpit	10%	100%	10%	6
VR Unit Simulator (assuming 5 hours of use)	25%	8.33%	2.08%	1.25

By using the data in Table 9.10, it may be estimated that, without accounting for the interaction between the different TE items, the overall increase in training effectiveness of the Dragonfly, provided by the TE package, will be:

- **30%** when compared to a normal combustion engine trainer aircraft that is not equipped with a glass cockpit (the percentage accounts for all items apart from the modular cockpit, as the normal combustion engine trainer would not need this extra feature);
- **16%** when compared to a normal combustion engine trainer aircraft that is equipped with a glass cockpit (the percentage accounts for all items apart from the glass cockpit and the modular cockpit);

[100] URL: https://www.vliegschool-hilversum.nl/en/flight-training/, LA 17-06-2020

- **26%** when compared to competitive electrical trainer aircraft (the percentage accounts for all items apart from the glass cockpit, as electrical trainer aircraft are usually equipped with this type of cockpit).

9.12. Cost-Benefit Analysis of TE

In this section, the cost benefit of the items in the TE package will be analysed. Now that the amount of hours saved by each TE item has been established, this information may be used in order to estimate the amount of money that the student pilot may save by training in the Dragonfly and making use of its TE package. From Section 11.4.1, it follows that the direct costs of the aircraft are roughly 20€/hr. As it is difficult to give rental prices (depending on all the utility/standing prices) a rental price of 100€/hr is assumed. This is chosen conservatively so that the actual business case for the flight schools will be improved. By multiplying the amount of hours saved by using each TE item by the hourly rental cost of the aircraft, the total amount of money that may be potentially saved by the student is obtained. Thus, by choosing to train for their PPL in the Dragonfly, the student may save (excluding the additional amount that would be economised by not having to hire an instructor for the saved hours):

- **1806.8€** when compared to the total cost of PPL training in a normal combustion engine trainer aircraft that is not equipped with a glass cockpit (this amount accounts for the use of all items apart from the modular cockpit);
- **966.8€** when compared to the total cost of PPL training in a normal combustion engine trainer aircraft that is equipped with a glass cockpit (this amount accounts for the use of all items apart from the glass cockpit and the modular cockpit);
- **1566.8€** when compared to the total cost of PPL training in a competitive electrical trainer aircraft ((this amount accounts for the use of all items apart from the glass cockpit).

Thus, from the student pilot's perspective, adding the TE items would be highly favourable as it would lead to considerable cost reductions. In addition to this, at this moment, only 22.22% of the flight hours in the 45 hours PPL training syllabus used by the Vliegschool Hilversum[101] are performed solo. By having a removable instructor seat, as well as "remote control" capabilities (providing the on-ground instructor with real time flight data and ensuring communication between them and the student pilots, at least during the most critical phases of the flight, such that assistance and guidance may be provided to the students), the percentage of solo-flight may be significantly increased. Thus, by having multiple students sharing one instructor for the duration of a flight lesson, even more money may be saved by the student during training. If, for example, the percentage of solo flight hours is extended to 50%, assuming that the cost of hiring the instructor for one flight lesson is 75€, and that by employing the new "remote control" technology an instructor may supervise 4 students at the same time, each student will save an additional $\frac{3}{4} \cdot \frac{50-22.22}{100} \cdot 45hrs \cdot 75€/lesson =$ **703.2€**.

However, when considering the cost benefit from a flight school's perspective, it becomes more clear why such training enhancement items haven't been implemented on training aircraft so far: by having the students finish their training faster, the flight schools will not make as much profit, as they won't be able to charge students for as many flight hours. Furthermore, flight schools may be concerned that if the students finish their training faster, they will leave the school earlier and that at some point in time there will be a shortage of students, potentially even leading to putting the flight school out of business. In order for the flight schools to profit from purchasing/leasing an aircraft with training enhancement items, a high inflow of new people interested in acquiring a PPL needs to be ensured. Even though the flight schools may be sceptical of purchasing an electrical aircraft (35.8% of the participants in the previously discussed questionnaire admitted that they were not interested in buying an electrical aircraft), it is clear that the trend of the new technology is to be as sustainable and as eco-friendly as possible, thus opting for electrical alternatives. Flying may nowadays be considered as old-school sometimes, as well as extremely expensive and highly polluting. By offering this new electrical trainer aircraft, which has significantly more affordable rental prices, has exciting new technology implemented on-board (such as the Fused Reality concept which can actually turn the aircraft into an in-flight simulator, the use of AR glasses, etc.), the ability of preparing the students even for flying in a complex combustion engine aircraft, negligible noise emissions and zero tailpipe emissions, as well as enough endurance for efficient flight training, the team is confident that more and more people will become interested in flying. Thus, even if the implementation of the TE items may not be desired as of now by most flight schools, it is predicted that this will become profitable for them at some point in the not so distant future.

9.13. Further Recommendations

In this section some further recommendations with regards to the TE package will be discussed.

Experiment to Quantify Added Training Effectiveness of the Dragonfly

In Section 9.11, it became clear that for some TE items, no conclusive studies have been performed in order to assess just how many hours can be saved during PPL training by using them. In order to quantify the added

[101] URL: https://www.vliegschool-hilversum.nl/en/flight-training/, LA 18-06-2020

training effectiveness of the TE package of the Dragonfly as a whole, an experiment is proposed.

The experiment will take two groups of at least 10 people with no prior flying experience who wish to complete their PPL. The control group will be completing their PPL training according to a standard flight school syllabus, on a standard trainer aircraft such as the Cessna 172 Skyhawk or the Diamond DA40, that is not equipped with any training enhancement items. Whether the control group aircraft should have a glass cockpit or not will be based on the definition of a "standard" trainer aircraft at the time of performing the experiment. The control group will also use a syllabus which is determined as "standard" at the time of performing the experiment.

The experimental group will perform all of their training with the Dragonfly and its TE items, as well as the simulator, and the possible changes in ground training which were deemed out of the scope of this research. The experiment will record how many setbacks per lesson on average students experience when comparing the Dragonfly method to the standard method. A setback is defined as a lesson which needs to be retaken because the student did not satisfy the performance requirements of this lesson [76]. The use of this setback method will show in what phases of PPL training which one of the training methods is more effective. The final average total number of hours the students need in order to receive their PPL in each of the aircraft will then be evaluated and compared. The expected percentage of savings in flight hours can be found in Section 9.11. If the average flight hours taken to achieve the PPL drops to less than the required number of hours, the difference between these can be used in order to re-train manoeuvres and can aid the pilot in becoming more proficient at flying. Furthermore, the pilot could already get more familiar with the basics of instrument flying before commencing training for their IFR license.

Portable Instrument Panel

In order to be able to simulate another aircraft while in-flight, and to make the situation as realistic as possible for the student pilot, a separate instrument panel may be inserted in the cockpit, in front of the original instrument panel. This additional panel will occupy roughly half of the cockpit's space. A camera will be installed, facing the half of the cockpit where the original instruments may be seen. The true flight data registered by the camera will be displayed on the instruments of the additional panel. This extra-panel will be used in combination with the AR/VR headset, the VIVE Pro Eye with mounted ZED mini camera, in the following way: the added panel and the original panel will be lined with coloured tape, to enable chroma key composting. The live video of the section of the cockpit occupied only by the additional panel will be left unaltered, while its surroundings will be transformed in order to emulate the cockpit of a different aircraft. In this way, the student may benefit from an immersive experience piloting, for example, the Cessna Citation II, while still on board of the Dragonfly. Adding to this, as the aircraft will be equipped with electrical propulsion, the power output from the engines may be easily altered in such a way as to emulate the performance of a different aircraft and to further increase the training effectiveness. The addition of the extra instrument panel will improve the business case for the flight schools, as it would enable the students to train for multiple, potentially bigger, aircraft models using only the Dragonfly. Thus, the flight school will benefit immensely by not having to purchase additional aircraft in order to allow students to train for more advanced pilot licenses.

Virtual CFI

By implementing a reliable virtual CFI, the percentage of dual flights will be lowered significantly, meaning that both the students as well as the flight schools would benefit from saving the cost associated with hiring an instructor. As the time allocated for completing the present project was limited, no software was developed for the virtual CFI as of now. However, if the time resources would be extended, the team plans on developing a software that would allow the student to be guided during their entire training and that would help them build healthy habits by pointing out their mistakes as soon as possible in the process.

10
Final Design

This chapter will summarise the final design which is created by integration of the subsystem designs, and it discusses the future of this project. Section 10.1 shows the communication diagram of this aircraft, which shows air-to-air, air-to-ground and air-to-satellite communications. In Section 10.2, the integration of the subsystems is explained. Section 10.3 shows a summarising table with all the final design parameters, along with drawings. In Section 10.4, the sustainability aspect of the Dragonfly is explored. Section 10.5 explains the verification and validation strategies for the entire aircraft, Section 10.6 explains possible certifiability issues and finally, Section 10.7 contains the technical sensitivity analysis of this project.

10.1. Aircraft Communication

This section describes the aircraft's communication with the ground, other aircraft and satellites. The communication diagram of the Dragonfly can be seen in Figure 10.1.

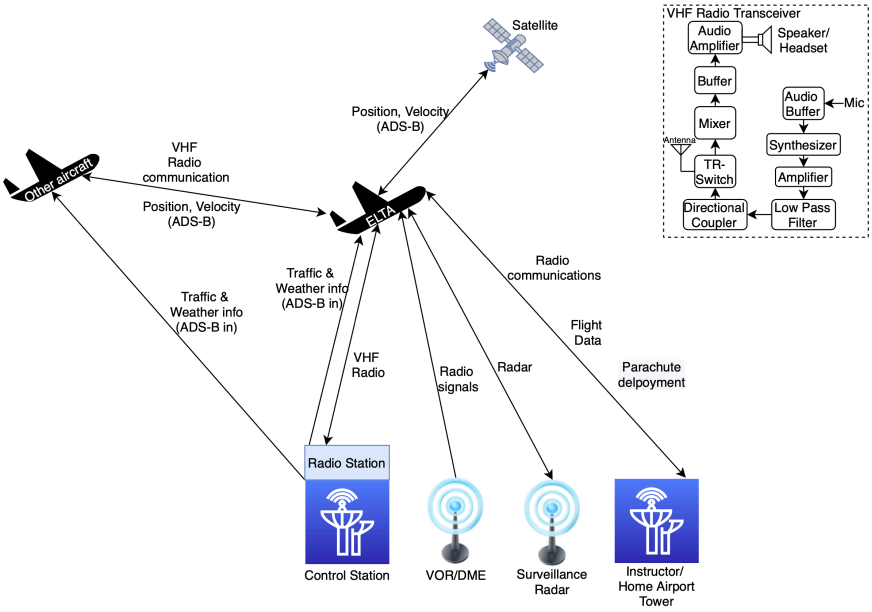

Figure 10.1: Communication Diagram of the Dragonfly.

There are three main communication types in which the pilot and the aircraft engage; the air-to-air communication, air-to-ground-communication and the aircraft-satellite communications.

The air-to-air communication between the Dragonfly and other aircraft works by VHF radio, in which pilots can talk to each other as long as they are on the same frequency and within a certain radius. Furthermore, the ADS-B out system installed on most modern aircraft transmits its location and speed data with at least $1Hz$, so that it can be seen on other aircraft's traffic screens.

The aircraft satellite communications are very simple. The ADS-B system fetches its position and velocity data at a frequency of at least $1Hz$ from the satellite. ADS-B is commonly used and unlike radar also functions when no direct line of sight is present [1]. Its ground stations are also cheaper to maintain than those required for radar.

The most complex form of communication occurs in the air-to-ground communication. The pilot communicates with the tower, during most of the performed training this will be the tower at the location of the flight school. As discussed in Section 9.12, the flight instructor will not always be in the aircraft's passenger seat. When supervising students from the ground, their flight data will be transferred in real time to a computer on which the flight instructor can see the instruments and talk the student out of a dangerous situation using the on-board VHF radio. Furthermore, the air traffic control station and the accompanying radio station transfer ADS-B in data to the aircraft in the vicinity, which most often include traffic data of aircraft without an ADS-B out transponder as well as weather information. For navigation purposes the aircraft communicates with VOR/DMEs which help it determine its location.

[1] URL: `https://www.faa.gov/nextgen/equipadsb/capabilities/ins_outs/`, LA 19-06-2020

10.2. Integration of the Subsystems

The following section describes how the aircraft systems are integrated. First, the design iteration process is explained in Section 10.2.1. In order to show how the cockpit items interact with the main hardware components of the aircraft's subsystems, a hardware diagram has been generated and may be found in Section 10.2.2. Furthermore, to show the integration of the main software components within the aircraft, a software block diagram is provided in Section 10.2.4.

10.2.1. Subsystem integration & design iteration

After the preparation of all subsystem designs & analyses in the previous chapters, the subsystems were integrated by integrating all tools into a single python program and subsequently iterating this until the take-off weight converged. For the initial input parameters, where necessary, the inputs from the midterm design or class II estimates were used [1]. First, the design point from the midterm design phase was calculated one-off. Then the iteration loop was initiated with the sizing of the wing and the calculation of aerodynamic properties of the airplane, as described in Chapter 6. This is followed up by the sizing of the battery and power group from Chapter 8. A subloop was then initialised to calculate the centre of gravity and do the tail sizing from Chapter 7 until the tail size converged. Next, a structural weight estimate is obtained using the structural analysis tools from Chapter 5. This is finalised by the calculation of remaining airplane systems (such as control surfaces and landing gear) and a new take-off weight estimate is made by combining all the obtained weights (including cockpit items & other electronics). This is then fed back into the design point, and the design is iterated until the take-off weight converges. The results of this are shown in Table 10.1.

10.2.2. Hardware Diagram

The hardware block diagram of the Dragonfly is presented on Page 119. This diagram explains the interaction between the different items included in the cockpit (including items found in the TE package, such as the simulated gear lever and propeller/mixture controls) and the control surfaces, the engine, multiple sensors placed on the fuselage used for acquiring flight information, as well as the lighting system. The type of connection between two elements- wire, actuator, type of cable/line- is specified on the arrow linking them.

10.2.3. Data Handling Diagram

Figure 10.2 shows the data handling diagram of the Dragonfly. It shows how data flows between the different hardware points. The blocks represent the hardware items and the arrows show the data that flows between them.

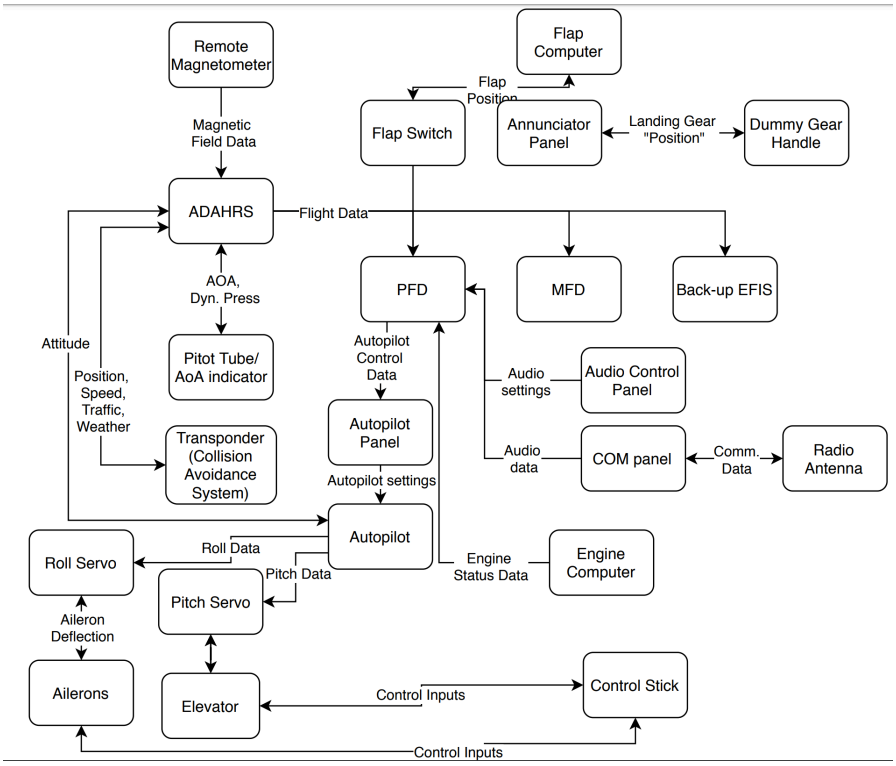

Figure 10.2: Data Handling Diagram of the Dragonfly.

10.2.4. Software Diagram

The software block diagram of the aircraft may be found in Figure 10.3. This diagram showcases the main software/data processing components of the aircraft. The arrows going into a certain block represent the input received by the component while the arrows coming out of the block represent the output produced by the component.

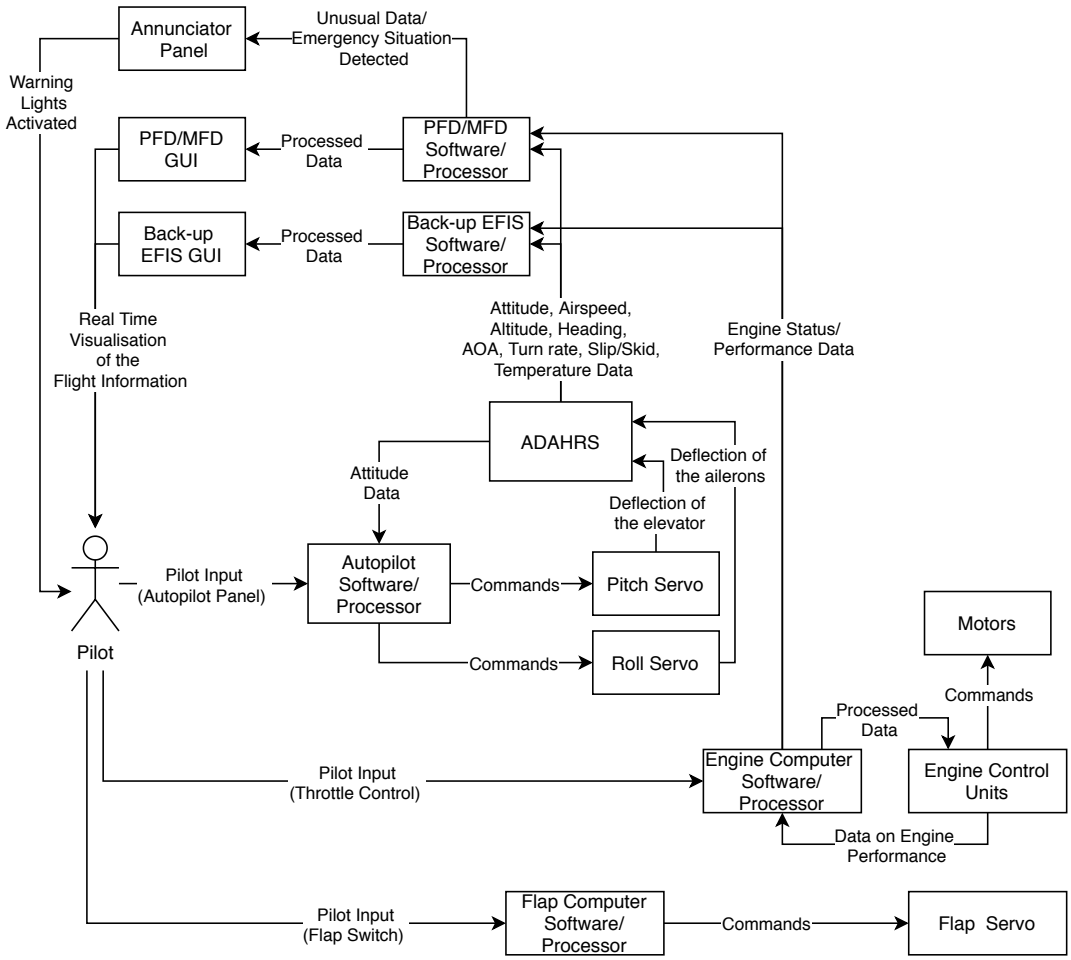

Figure 10.3: Software Block Diagram of the Dragonfly.

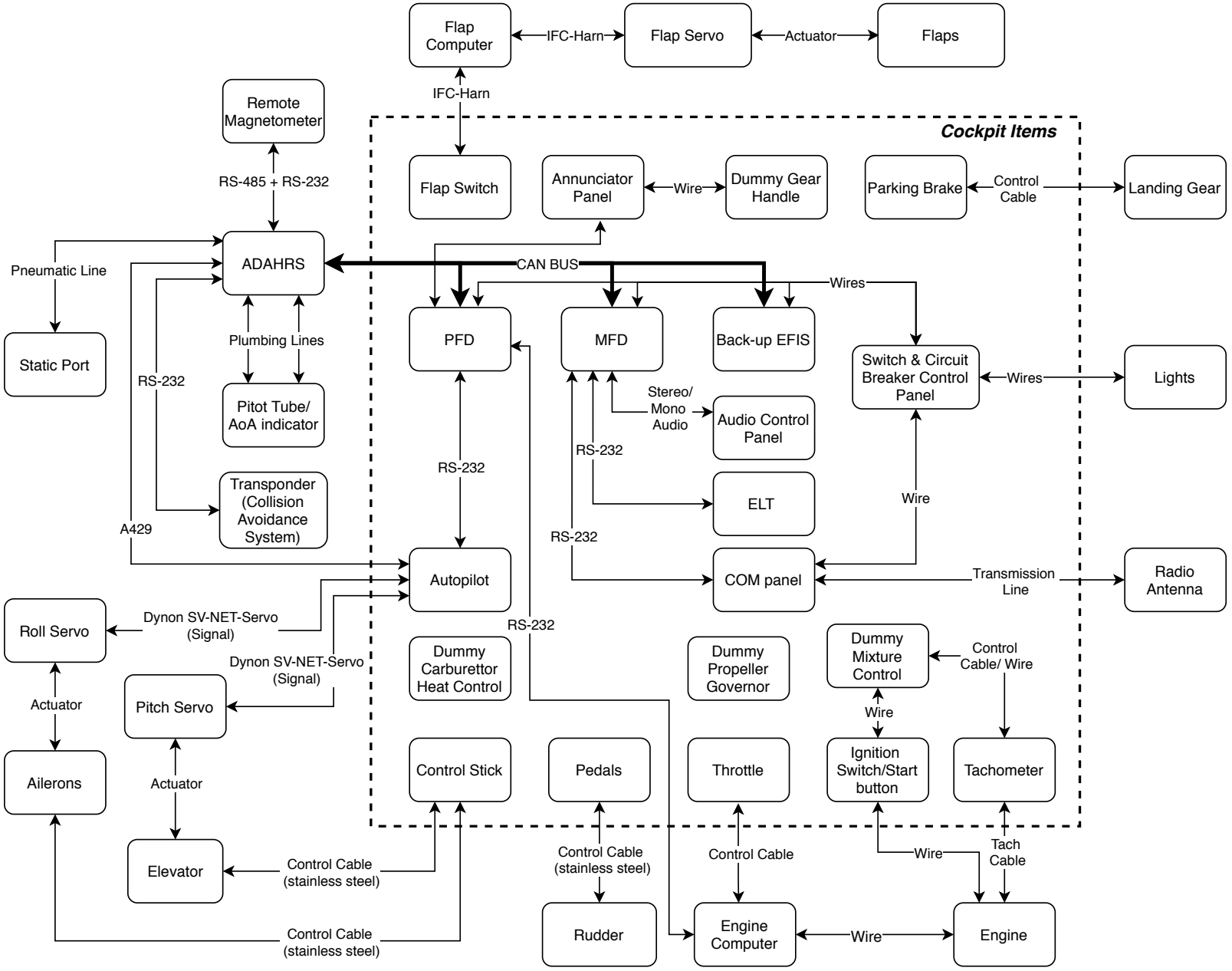
Flap Computer
IFC-Harn
Flap Servo
Actuator
Flaps
IFC-Harn
Remote Magnetometer
Cockpit Items
RS-485 + RS-232
Flap Switch
Annunciator Panel
Wire
Dummy Gear Handle
Parking Brake
Control Cable
Landing Gear
ADAHRS
CAN BUS
Wires
Pneumatic Line
Static Port
Plumbing Lines
RS-232
Pitot Tube/ AoA indicator
PFD
MFD
Back-up EFIS
Switch & Circuit Breaker Control Panel
Wires
Lights
Stereo/ Mono Audio
Audio Control Panel
RS-232
RS-232
Transponder (Collision Avoidance System)
ELT
Wire
A429
RS-232
Autopilot
COM panel
Transmission Line
Radio Antenna
Roll Servo
Dynon SV-NET-Servo (Signal)
RS-232
Dummy Carburettor Heat Control
Dummy Propeller Governor
Dummy Mixture Control
Control Cable/ Wire
Dynon SV-NET-Servo (Signal)
Actuator
Pitch Servo
Wire
Ailerons
Actuator
Control Stick
Pedals
Throttle
Ignition Switch/Start button
Tachometer
Elevator
Control Cable (stainless steel)
Control Cable (stainless steel)
Control Cable
Wire
Tach Cable
Control Cable (stainless steel)
Rudder
Engine Computer
Wire
Engine

10.3. Aircraft Parameters & Design

After integration and iteration of the design, the final specifications of the aircraft are listed in Table 10.1. This results in the aircraft design as visualised in Figure 10.4.

Table 10.1: Final design parameters of the aircraft

Parameter	Value	Unit
Maximum take-off weight	883.9	kg
Battery weight	291.9	kg
Maximum payload weight	200	kg
Stall speed	23.15	m/s
Max speed	61.7	m/s
Take-off speed	26.46	m/s
Maximum range	310	km
Maximum endurance + reserve (max passengers)	2.5	h
Take-off distance (including 50ft climb)	500	m
Glide ratio	19.33	$-$
Aircraft length	9.5	m
Centre of gravity range	2.44 - 2.86	m
Weight-to-power ratio	12.33	kg/kW
Maximum power	71.68	kW
Propeller diameter	1.8	m
Wing surface area	14.65	m^2
Wing aspect ratio	10.1	$-$
Wingspan	12.16	m
Mean aerodynamic chord	1.262	m
Airfoil type	NACA 4415	$-$
Horizontal tail surface	3.27	m^2
Vertical tail surface	1.22	m^2

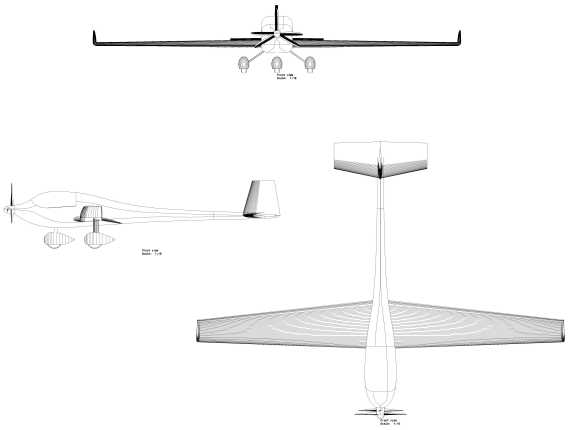

(a) Drawing of the final aircraft design

(b) Rendering of the final aircraft design

Figure 10.4: Visualisation of the aircraft design

10.4. Sustainability

In Chapter 3 is mentioned what steps should be taken to ensure sustainability throughout this project. The first requirement was that the aircraft should fill a sustainability gap in the market of current trainer aircraft. This is requirement is met as there is not an electric trainer aircraft that is adopted on large scale by flight schools. The second requirement was about the sustainability of the materials, due to the cost constraints of this project it was decided in a trade-off that not the finest materials will be used. The lean manufacturing that was mentioned in requirement three will be implemented in the production plan. Regarding the operational life of the aircraft it is expected that the lifetime can be stretched the same way as for conventional trainers as all the aircraft components can be replaced. Only the tail shoul be handled carefully as composite thermoset materials are difficult to replace. This means that if the tail is damaged, probably the whole tail needs to be replaced. The last requirement was about the end-of-life plan, it is briefly touched upon in Section 13.1.3 what the possibilities are.

10.4.1. Compliance matrix

In Table 10.2 the compliance matrix of the sustainability development strategy can be seen.

Table 10.2: Compliance matrix for the sustainability development strategy

Identifier	Requirement	Obtained value	Requirement met?
ELTA-SUS-01	The aircraft concept shall fill a sustainability gap in the market of current trainer aircraft for initial pilot's training.	*	✓
ELTA-SUS-02	The materials used for the aircraft concept shall be selected based on a trade-off between material performance, cost and environmental impact.	*	✗
ELTA-SUS-03	Lean manufacturing shall be applied during the production of the aircraft concept.	*	≈ ✓
ELTA-SUS-04	The aircraft concept lifetime shall be at least the same as current trainer aircraft.	*	✓
ELTA-SUS-05	An end-of-life plan shall be made for the aircraft concept.	*	✓

10.5. Verification and Validation

Before the Dragonfly may enter the mass production phase, a prototype of the aircraft shall be built in order to be tested. The methods of verifying and validating the individual subsystems of the aircraft have been previously discussed. After the subsystems have been tested individually, it will be time to verify their integration in the form of system tests of the whole aircraft. Thus, the built prototype will undergo a series of ground tests first, before being cleared for flight testing. If the two testing phases are successfully completed, the Dragonfly may be considered for certification and, ultimately, production and market deployment. The two testing phases will be discussed into further detail.

Ground Testing. An important part of the ground testing process is represented by structural static tests. These typically include a Flight Test Installation (FTI) calibration test and maximum wing bending at limit load [2]. Furthermore, it will be assessed whether the ailerons function correctly under maximum wing bending. Other tests that may be conducted on the ground include flight cycle simulation, as well as fatigue testing. Although these last two types of tests are mostly encountered in the context of large aircraft, as the Dragonfly is a trainer aircraft and thus the safety aspect is highly important and a reliable aircraft is desired, these tests shall be conducted too. Furthermore, the functioning and the calibration of the avionics/cockpit instruments shall be verified first on the ground. In addition to this, in order to verify the fulfilment of the MTOW requirement, as well as other requirements related to this, weight and balance testing will be carried out. During these tests, the weight of the aircraft will be assessed, as well as its c.g. excursion.

Flight Testing. Once all the ground tests have been successful, it is time to test the prototype of the Dragonfly in the air. The flight testing phase will be comprised mainly of flight performance testing and stability and controls testing. For the first category, flight performance parameters, such as endurance, rate of climb and range will be assessed. The obtained values will be then be used to evaluate whether the previously imposed requirements are truly fulfilled. These tests will be highly important as they serve in assessing some of the driving requirements of the project. Furthermore, for stability and control testing, parameters such as the stall speed, encountered wing flutter, the functionality of the control surfaces during flight as well as the responsiveness of the aircraft to the pilot's input will be verified and validated. Furthermore, certain emergency scenarios, such as the engine out, will be initiated and evaluated. Also some extreme weather/temperature testing shall be performed. As the aircraft is equipped with electric propulsion and thus the risk of fire hazard due to the batteries may be considered higher than for normal combustion engine trainer aircraft, it is important to perform a flight test in hot weather conditions.

10.6. Certifiability Issues

Certification is one of the most important aspects during the design of the Dragonfly as it is a costly process and because it determines under what conditions the aircraft will be allowed to fly (day VFR. night VFR, IFR, etc.)

The ultimate goal is to certify the aircraft under CS-23 which is applicable to normal, utility, aerobatic, and commuter aeroplanes [78]. To cut the costs on certification it was decided in [2] to initially certify the aircraft under CS-VLA which is applicable to aircraft weighing not more than 750 kg, have a single spark or compression ignition engine, have not more than two seats, have a stalling speed in landing configuration not exceeding 45 kts CAS and are approved for day-VFR only.

Issues that will arise during the certification process of the Dragonfly are the following:

MTOW. From the performed iteration it became clear not all requirements could be met. The combination of endurance and MTOW was not achievable. Due to the higher certification costs of going to CS-23 (40% more

[2] URL: https://www.airbus.com/aircraft/how-is-an-aircraft-built/test-programme-and-certification.html, LA 21-06-2020

costs according to DAPCA-IV) where the take-off weight can be increased to 5700kg it was decided to stick to the 750kg and downgrade the endurance of the aircraft. As the density of batteries keeps on increasing it is just a matter of time before the endurance will meet the required 2.5 hours.

Single Spark or Compression Ignition Engine. The Dragonfly will have two engines while for CS-VLA only one engine is allowed. Besides, the engine is electric, hence no spark or compression ignition engines. The latter is no issue as recently, the first fully electric aircraft (Velis Electro) has been certified under CS-LSA [3]. Although VLA is another category it is assumed the knowledge of the certification process of the Velis Electro can be used. The only issue that remains is the fact the Dragonfly has two engines which will be controlled by a single lever in the cockpit. For conventional combustion aircraft this would be nearly impossible to certify due to the high complexity. For the Dragonfly however just one signal goes to the engine from the inverters which tell what power is needed. As there are several back ups, which can be seen in Figure 8.8, it is assumed not much extra costs will go into the certification.

Batteries. For the batteries no issues will be expected as recently the first electric aircraft with batteries is certified (see previous item). This has opened the gate for other manufactures to also design electric aircraft with batteries and certify those.

Contra-rotating propeller. Probably the largest issue during the certification is the fact the Dragonfly has a contra-rotating propeller system. In CS-VLA no such aircraft exist. Within CS-23 there exist aircraft that use a counter rotating propeller system (pull - push) such as the Cessna Skymaster, however there are no CS-23 aircraft that use the contra-rotating propeller system. Due to the combination with electric engines it is expected that the certification process will be easier. The interaction between the propellers will be thoroughly investigated using the test plan written in Section 8.5.6.

Training enhancement. As long as an instructor is sitting next to the student no certifiability issues are expected. Only when the student is allowed to go solo when he would not be ready for this without the TE issues could arise. If the student for example has to rely on the instructions how to land from the virtual instructor this would mean an enourmous amount of software testing and test flying. Only certifying an autopilot will take more than 100 hours of test flying according to Garmin [4].

Night flying. To be able to fly at night the aircraft needs to be certified under CS-23. This will be the ultimate goal. To anticipate on this cockpit lights are already included. Navigation lights, outside air temperature indicator and an alternate static source will need to be added to the aircraft [5]. An advantage of the Dragonfly is that it has two engines, so if one would fail, one can still continue to fly safely to the nearest airport.

IFR flying. IFR certification will not only result in higher certification costs, but also higher operational costs as maintenance will increase. Therefore, only simulated IFR practice will be done in the Dragonfly. Maybe it will be possible to certify it as an IFR simulator in which the AR-glasses will draw cloud layers for the student pilot.

10.7. Technical Sensitivity Analysis

After the iterations had been performed to come up with the final design parameters a sensitivity analysis needed to be performed. This can be seen in Figure 10.5. In the figure it can be seen that the range and winglet height are not a limiting factor as it has no influence on the maximum take-off weight. The other parameters do have an influence.

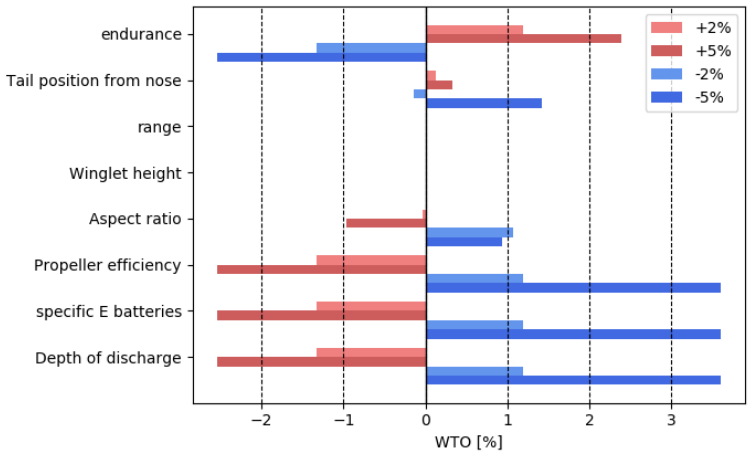

Figure 10.5: Sensitivity Analysis of the entire aircraft

[3] EASA Press release, June 10, 2020
[4] Flieger Magazine Podcast: 'Alles über Autopiloten'
[5] https://vfrg.casa.gov.au/operations/night-vfr/aircraft-equipment-for-night-vfr/ LA: 21-06-2020

11
Business Case

This chapter describes several business case scenarios based on the given requirements in Section 11.1. The primary focus within this chapter is on the ELTA company and flying schools, but there will also be looked into potential private owners. For analysis, all scenarios take place in the Netherlands. As the Netherlands is an expensive country for flying (high fuel prices and relative high landing fees [1]), the scenarios will be worst-case-scenarios. The future of this project will not be limited to the borders of the Netherlands.

11.1. Requirements

- **Dragonfly-USER-COST-01** - *The aircraft shall have a unit cost of no more than €150K;*
- **ELTA-MAR-01** - *The aircraft shall be refuellable/rechargable at 4-digit-ICAO-registered airports.* This requirement serves to comply with **ELTA-FUN-MAR-02**;
- **ELTA-MAR-02** - *The system shall be able to undergo maintenance at conventional maintenance facilities.* This requirement serves to comply with **ELTA-FUN-MAR-03**;
- **ELTA-MAR-15** - *The aircraft's periodic propulsion replacement cost shall have a maximum of €5,000 per 1,000 hours of flight.* This requirement serves to comply with **ELTA-FUN-MAR-03**;
- **ELTA-MAR-16** - *The peak aircraft operating cost shall be 50 €/hour.* This requirement serves to comply with **ELTA-FUN-MAR-04**.

11.2. Funding

To fund the Dragonfly project, two main ways of funding will be discussed, those being subsidies and partners. These will be discussed in Section 11.2.1 and Section 11.2.2 respectively.

11.2.1. Subsidies

Bringing a new aircraft to the market is a costly process, especially when new or unconventional concepts are introduced such as electric engines, contra-rotating propellers and a single lever in the cockpit for two engines. The Dutch government has set up an action program for hybrid electric aviation (AHEV) until the year 2070 together with 26 parties from the aviation sector including the TU Delft. The government has the ambition of reducing domestic GA emissions by 15% by 2030 with respect to 1990. In 2050, the goal is to have zero emissions in domestic aviation, and by 2070, no more emissions shall be created by commercial flights. Innovation will be performed by 2030 in a 'living lab', which will consist of a collaboration with the Dutch government, the business community and knowledge from research institutes like universities [79].

Currently, 376.5 M€ are put aside for the mentioned ambitions for the period 2020-2025 of which 45M€ are meant for the general aviation sector. According to Mark Rademaker, who is a member of the board within the AHEV, it is however too early to know how much of this money could be used for the Dragonfly project. He did say that currently, 170k€ are reserved for improving the infrastructure at Dutch airports. Therefore, is will be assumed that the ELTA company, as well as the buyers of the aircraft, will not have to invest in modifying existing infrastructure.

11.2.2. Partners

To fund large scale projects the design and production of an aircraft, there is a need to search for partners. This is done to have more money for the project and to reduce risks as it is spread out over multiple companies. The ELTA company should therefore look for partners. Following Section 11.2.1, the government could be a partner for the subsidies. Saluqi motors will build the engines for the Dragonfly and could, therefore, become a partner. More companies that provide parts for the Dragonfly could become potential partners, as long as they are willing to invest in the Dragonfly Project. To find partners or sponsors, the ELTA company may consider visiting fairs like the AERO in Friedrichshafen which is the largest show for general aviation [2].

11.3. ELTA Company

To come up with a cost estimate for the entire aircraft program, the DAPCA-IV method as described by Gudmundsson [14] is used. While this method was created in 1986, the formulae were updated in 2012. To account for inflation between 2012-2020, the consumer price index is used [3], which stated the inflation has been 1.13, or 13%.

[1] based on own experience of the author
[2] https://www.aero-expo.com/aero-en/ (LA 19-06-2020)
[3] https://www.bls.gov/data/inflation_calculator.htm (LA 19-06-2020)

11.3.1. Program Costs

First, research on comparable aircraft was performed, to determine how many aircraft GA manufacturers typically build per year. The results are shown in Table 11.1 [4] [5] [6] [7]. The number of aircraft built by Cessna significantly increase the average and are unrealistically high for the ELTA company. Based on the knowledge gained from Section 11.2.1, that electric flying should be the norm for all general aviation in the Netherlands by 2050, a production rate of 100 aircraft per year is assumed. In Table 11.2 the general input parameters for the DAPCA-IV method are presented.

Table 11.1: Number of aircraft built per year

Aircraft	# built per year
Alpha Electro	62.5
C150	1260
C152	948
DA20	71
Blackshape Prime	52

Table 11.2: DAPCA-IV method input parameters

Parameter	Value	Unit
Airframe Weight	392	kg
Max Airspeed	120	kts
Number of aircraft built over 5 years	500	-
Inflation (2012-2020)	1.13	-

In Table 11.3 the costs for the certification process are listed. One should note that the man-hours multiplied by the hour rate does not add up to the total cost value as the DAPCA method uses an additional factor to include overhead costs. If one is interested in this, please have a look at Gudmundsson [14]. The method is based on conventional aircraft. The Dragonfly is everything except conventional due to its contra-rotating propeller and the electric engines with only one lever to control both engines. It is assumed, however, that due to the number of subsidies provided by the Dutch government, the costs reduce to the certification costs only as if it were a conventional aircraft.

Table 11.3: Certification costs

Cost Item	Man hours	$ per hour	Total cost ($)
Engineering	26,220	90	4,948,300
Tooling	45,750	60	5,756,000
Development support			129,500
Flight test operations			43,400
Total			**10,877,200**

After the aircraft is certified, it should be produced. The costs that come into play are listed in Table 11.4. The DAPCA method incorporates the learning curve of the people working on the aircraft during production (Equation (11.1)). For this, the user has to define the experience effectiveness (F_{exp}). To be conservative the highest value was chosen and that was 95%. With N being 500 units built, the QDF factor is 0.63. However, during the production of the first couple of aircraft, this factor will be higher. The average factor that can be applied in the end is 0.68. This is found by calculating the QDF for every single aircraft and then taking the mean.

$$QDF = F_{exp}^{1.4427ln(N)} \tag{11.1}$$

In Table 11.4 all the costs that were originally in € (battery, engine, avionics, propellers) are converted to USD as these are the DAPCA method's units. The current exchange rate of EUR to USD is 1.12 [8]. An odd value is the landing gear discount; according to the method, you get this discount if the aircraft has fixed gear instead of retractable gear. Furthermore, it is not chosen to implement a quantity discount on the battery, engine, avionics, propeller and TE. This is done to be conservative and give a worst-case scenario. Besides, no suitable numbers could be found for bulk discounts, as these would have to be determined in a contract on a per-company basis.

[4] https://www.pipistrel-aircraft.com/aircraft/electric-flight/alpha-electro/ (LA 19-06-2020)
[5] https://cessna150152club.org/History (LA 19-06-2020)
[6] https://www.flightglobal.com/diamond-delivers-1000th-da20/82969.article (LA 19-06-2020)
[7] https://avia-dejavu.net/photo%20I-B953.htm (LA 19-06-2020)
[8] https://www.wisselkoers.nl/dollar-euro (LA 19-06-2020)

Table 11.4: Aircraft production costs

Item	Cost per aircraft ($)
Manufacturing labour	61,650
Quality Control	4,050
Materials/equipment	8,400
Battery	33,500
Engine	9,000
Avionics	9,950
Propellers	6,500
Landing gear discount	-5,115
Production Cost	127,935
Liability insurance	17,250
Min. Sales Price, no TE	145,185
TE Cost	28,265
Min Sales Price, with TE	173,450

11.3.2. Selling Aircraft

In the previous section, the costs for the production as well as the certification of the Dragonfly is discussed. Furthermore, requirement **ELTA-USER-COST-01** stated the aircraft unit cost shall not be more than €150,000m, which is currently equivalent to $168,880. Typically, the selling price of an aircraft is the minimum selling price. This will go up for all the extra features the customer wants. Applying this to the Dragonfly would imply that it is sold for $168,800 as a minimum price which excludes the training enhancement. In Table 11.5 one can see what the profit is for both options and after how many aircraft sold the certification/developing cost debts are gone. For this break-even point, it is assumed there was no interest on the total certification/developing costs by assuming the subsidies will cover these.

Table 11.5: Break-even calculation of the Dragonfly

	No TE	With TE
Unit Cost ($)	145,185	173,450
Selling Price ($)	168,800	168,800
Profit ($)	23,615	-4,650
Break-even	474 Planes	not possible

Based on the break-even points from Table 11.5 it is not feasible to have a selling price of $168,800, which includes the TE-package. The break-even point for the same selling price excluding the TE-package seems on the high side, but it is possible. In this scenario, the $168,800 is a 'starting at price', on which the customer can add the TE-package as an option.

11.3.3. Leasing

Besides selling the Dragonfly, another option could be to offer to lease it. For this, however, there should be a large reserve in the amount of money as it will take longer until you have earned the aircraft back. For that reason, it is assumed to be unfeasible before the break-even-point is reached by selling aircraft. When this is reached two options could be offered, namely financial lease and operational lease. For financial leasing, $4,000 per month could be taken for a lease duration of 4 years. The ELTA company has then earned $46,815 after 4 years from the aircraft which is $23,200 more in the case the customer would have bought the aircraft. For operational leasing, this project is in a too preliminary stage as it is not yet known into what detail maintenance intervals should be performed and what their costs would be.

Another option would be to only offer leasing regarding the training enhancement package. In this scenario, the customer will buy the aircraft without TE. In this case, the package should be updated to keep it attractive to flight schools. A scenario could be to offer a leasing contract for 4 years and then again give the option for financial lease and operational lease. For the first option, $700 per month could be chosen. In the end the ELTA company will have earned $5,335. For operational lease, the same holds for leasing the aircraft. Besides, the customer could choose to select which TE item he would want. It may be that the modular cockpit is not that suitable, but a simulated gear lever is for example.

11.4. Customer

When this project started the customers were set to be flight schools as they would be interested in the added training effectiveness. After doing a market analysis (Chapter 4) it turned out that the target group would be large flight schools which train pilots for the airline market. However, to improve the business case, private owners were also included by making the TE package optional.

11.4.1. Operational Costs

It is difficult to quantify the operational costs per flying hour that include everything from a flight school as there are too many variables like, did the flight school take a loan for the aircraft, what is the cost for staff, are they an approved training organisation or a declared training organisation, etc. Therefore, this section is about the operational savings with respect to conventional SEP aircraft. Furthermore, all the costs described in this section will be in euros in contrary to the previous sections. The data mentioned in this section is from own experience of flying in the Netherlands as a private pilot.

First, there is the propulsion aspect. Normal conventional SEP aircraft usually have a time between overhaul of 1500-2100 hours. After these 1500 hours a new engine is needed which will cost around 35 000 euros. Furthermore, fuel costs can easily add up to 50 euros per hour. Per flight hour the SEP propulsion costs will hence be roughly 75€ per hour when saving money for the engine overhaul.

The Dragonfly's engine is not comparable to piston engines. It only has one moving part, which is the shaft. After having contact with Maarten Klomp of Saluqi Motors it turned out electric cars have an engine overhaul after 20 000 driving hours. According to Maurice Fiechter who works for Special Air Services this should be reduced by a factor of 5 to give reliable data for aircraft. In this case, the overhaul is after 4000 hours which will cost 8000 €. The 'fuel' costs of the Dragonfly are 5.50 €per hour [9]. The only expensive part is the battery which is assumed to have an overhaul after 2,000 hours where 1000 cycles are used. The overhaul will cost 29,950€. Calculating the cost per hour it turns out to be 22.15€ per hour. This is a saving of more than 50€ compared to piston aircraft.

For the customer, endurance is important and this is one of the reasons the Alpha Electro is not popular amongst flight schools. Furthermore, the infrastructure should be ready at airports to accommodate electric flying. As mentioned in 11.2.1 it is assumed the infrastructure will be ready at Dutch airports when the Dragonfly will be ready for operation. Another aspect is maintenance, maintenance organisations will need to be educated on the Dragonfly which will take time as the concept is not comparable to conventional single-engine piston (SEP) aircraft due to the electric engine and the contra-rotating propeller. The maintenance companies will have to invest this time, in return they can perform maintenance, but this will be less compared to conventional aircraft, as more maintenance goes into checking the engine for piston aircraft. So it is debatable if maintenance companies want to invest the time. On the other hand, as mentioned in 11.2.1, all GA should be electric by 2050, so at some point, the maintenance companies will need to invest their time into transitioning.

11.5. Verification and Validation

In this chapter, the DAPCA-IV method is used. Originating in 1986, this method is known in the aerospace industry and has been updated in 2012 by Gudmundsson [14]. The method was inserted into Python. The verification is performed by inserting examples from [14] and comparing the results. Validation is difficult as companies don not mention what the certification, development and production costs are. The selling price is often the only thing known, and even for this, a quotation if often required. Based on experience in buying a Robin DR401 (IFR Certified, glass cockpit with Garmin avionics), this is used for validation purposes. The selling price is 250,000€, the OEW of this aircraft is roughly 660kg and the airframe weight is not known but assumed to be 550kg (OEW minus engine, avionics, seats). Based on Table 11.1 the aircraft produced over 5 years is taken to be 300. Lastly, the maximum airspeed is taken as 179 kts which is V_ne. As the selling price is the only known variable, only the final result can be validated. For avionics, $37 400 are taken based on the equipment of the aircraft that was bought. Furthermore, an average quantity discount factor of 0.7 is used. With this, the cost price according to the DAPCA-IV is $230,600. 250,000€ equated to $280,000 which would imply a profit of $49,400 per aircraft. According to Gudmundsson [14], a profit of around $50,000 is reasonable.

11.6. Risks

The risks in this chapter are all associated with finances. It could be the case that the developing or certification costs will be higher than expected. This risk could be mitigated by setting set-points during the certification process where at every set-point it is evaluated how much is deviated from the budget at that moment in time. If this deviation is too negative new investors could be found. Hanging onto that solution, it could be one of the investors gets bankrupted. Also in this case new investors will have to be found. One of these investors could be the Dutch government as it is their goal to realise electric flying for all general aviation by 2050.

It could also be the case the production costs turn out to be higher than expected. In this case, the selling price could go up, but the aircraft could also be sold as a kit-plane which would save all the manufacturing labour as the customer will build the aircraft by themselves. When this is done, the aircraft will belong to the experimental aircraft and not CS-23 or CS-VLA. In this case, it would not be of interest anymore for flight schools, but only for private customers who will not be interested in the TE-package.

[9] based on 29.5 kWh and 0.22€/kW in the Netherlands

Another risk could be that the budgeted 500 aircraft is too much. This risk is not likely to happen as the Dutch government is doing its best to promote electric flying in GA. Assuming other countries are doing or are planning on doing the same, this risk is mitigated.

11.7. Compliance Matrix

In Table 11.6 the compliance matrix for the business requirements is shown. The first requirement is partially met. This is because the unit price can easily be €150k, but only without the TE package to be profitable. Furthermore, **ELTA-MAR-15** is not met. This requirement was originally set-up only thinking of the engine being part of propulsion. However, the propulsion system from the Dragonfly also includes the battery pack which is the cause of not meeting this requirement. The operating costs are lower than conventional piston aircraft.

Table 11.6: Compliance matrix for the business cases

Identifier	Requirement	Obtained value	Req. met?
ELTA-USER-COST-01	The aircraft shall have a unit cost of not more than €150k.	from €150K	≈ ✓
ELTA-MAR-01	The aircraft shall be refuellable/rechargable at 4-digit-ICAO-registered airports.	*	✓
ELTA-MAR-02	The system shall be able to undergo maintenance at conventional maintenance facilities.	*	✓
ELTA-MAR-15	The aircraft's periodic propulsion replacement cost shall have a maximum of €5000 per 1000 hours of flight.	€15,000	✗
ELTA-MAR-16	The peak aircraft operating cost shall be 50 €/hour.	€22.15	✓

12
Risk Assessment

In this chapter one can find all significant risks, for a more detailed description one should refer to the relevant chapters. The general risk assessment will be presented, as well as the newly identified risks for each subsystem and their mitigation strategy.

12.1. Technical Risk Assessment

The most important general and previously identified risks [1] are presented in Table 12.1. Every risk is given a likelihood and an impact. The scale used is listed below.

Likelihood:

1. Small to zero chance of occurrence;
2. Marginal but notable chance of occurrence;
3. Reasonable chance of occurrence;
4. High chance of occurrence;
5. Almost guaranteed occurrence.

Impact:

1. Small to zero impact;
2. Marginal impact;
3. Moderate impact;
4. Significant impact;
5. Catastrophic impact.

After the general risk assessment, specific risks were identified per subsystem. The identification and a detailed description of the risks can be found in the corresponding chapters. Risks in power and propulsion (PP) are mainly related to the CRP as this is not a widely implemented system and therefore brings some uncertainties into the design. Next to that, risks regarding aerodynamics (AER) and structures (STR) are treated. Furthermore, some new business case (BC) and safety (SAF) risks were identified and finally risks for all training enhancement (TE) items were assessed. For these new risks mitigation strategies were made to deal with them.

Table 12.1: General risk assessment and mitigation strategy of the risks

No.	Risk	Likelihood (1-5)	Impact (1-5)	Mitigation strategy	Residual Likelihood (1-5)	Residual Impact (1-5)
RSK-DES-01	MTOW exceeds the limit	4	4	Add a margin, in the design aim for a lower weight	3	4
RSK-BC-01	Lack of recharge infrastructure at airports	4	4	Make use of current recharge technology	1	4
RSK-DES-04	Structure is not able to handle the loads	3	5	Apply a safety factor	2	5
RSK-DES-08	Tools used not accurate	3	5	Set up V&V plan	2	5
RSK-SAF-07	Batteries overheat/explode	3	5	Implement a battery thermal management system	2	5
RSK-DES-05	Noise pollution higher than expected	3	4	Apply a safety factor	2	4
RSK-DES-07	Bad trade-off performed	3	4	Set trade-off guidelines	2	4
RSK-BC-04	The system can not meet the required TE improvement	3	4	Provide the possibility to install different TE technologies	2	2
RSK-BC-02	After a few years product is not competitive anymore, due to technology improvement	4	3	Provide the possibility to replace the batteries with future state of the art batteries	4	2

For post-DSE the same strategy will be applied which was implemented during the final design phase during this DSE: Risks that will have to be mitigated post-DSE will be closely monitored by the systems engineer. The systems engineer together with the quality manager will go over the mitigation strategy checklist on a daily basis with all relevant departments, to check whether the strategies are applied in order to maintain the reduced risks [1].

Table 12.2: Subsystems risk assessment and mitigation strategy of the risks

No.	Risk	Likelihood (1-5)	Impact (1-5)	Mitigation strategy	Residual Likelihood (1-5)	Residual Impact (1-5)
RSK-PP-01	More propeller torque than expected	2	4	Design rudder with safety margin	2	2
RSK-PP-02	Propeller ground clearance smaller than expected	2	4	Add margin on vertical position propeller	1	4
RSK-PP-03	Suboptimal number of propeller blades selected	4	3	Perform detailed in-depth research and optimisation analysis	2	3
RSK-PP-04	Exceed maximum allowed rpm	4	3	Install FADEC system or reduce power	1	3
RSK-PP-05	Resonance between propellers occurs	2	3	Adjust power setting	1	3
RSK-PP-06	Propeller stall occurs	2	3	Install FADEC system or decrease rpm	1	3
RSK-PP-07	Testing becomes expensive because there is little known about CRPs	4	3	Analyse the best options only and prepare the tests in high detail	1	3
RSK-PP-08	Testing makes clear that a CRP is not the best option	2	4	Add the option of removing a propeller and fly with only one	2	1
RSK-PP-09	Battery energy and weight estimations not close to real numbers	3	4	Compare to values of general aviation aircraft	1	4
RSK-PP-10	Faulty battery cell	2	1	Add safety cells for failure	1	1
RSK-PP-11	Battery charging time estimations unrealistic	3	4	Design should feature option of swappable batteries	3	1
RSK-PP-12	Engine computer failure	1	5	Throttle lever position goes directly to ECU	1	1
RSK-PP-13	ECU failure	1	5	Install back-up (ECU and motor inverter)	1	1
RSK-PP-14	Total battery/engine failure	1	4	Brief pilot on battery/engine failure procedure	1	3
RSK-AER-01	Design does not meet performance requirements	2	4	Perform tests to validate requirements	1	4
RSK-AER-02	Aerodynamic design affects structure more than expected	2	4	Frequently evaluate with aerodynamics and structures	1	4
RSK-AER-03	Aerodynamic noise higher than expected	2	3	Perform component windtunnel tests	1	3
RSK-STR-01	Landing gear not properly positioned	2	3	Iterate position in stability and control analysis and/or add option to shift landing gear location once built	1	1
RSK-STR-02	Too much/not enough weight on front gear	2	3	Add option to shift landing gear location once built	1	3
RSK-STR-03	Gear suspensions not able to handle landing loads	2	4	Ensure that under critical loading the gear will not get closer to the fuselage than 20 cm	1	4
RSK-SAF-08	Aircraft not stable/controllable	3	5	Apply safety margin and set up V&V plan	1	5
RSK-BC-07	Development/certification costs higher than expected	4	3	Set evaluation moments for certification process	1	3
RSK-BC-08	Production costs higher than expected	1	3	Increase selling price	1	2
RSK-TE-01	Mixed reality headset overheats	2	1	Install aircraft ventilation	1	1
RSK-TE-02	Ballistic parachute failure	2	5	Perform regular maintenance checks	1	5
RSK-TE-03	Engine failure at low altitude (ballistic parachute is unusable)	2	5	Perform take-off failure briefing	2	4
RSK-TE-04	Glass cockpit failure	2	2	Install back-up instruments and back-up battery	2	1
RSK-TE-05	Autopilot failure	2	3	Perform maintenance checks and install self-test, use autopilot off-switch	1	3

12.2. Risk Map

The risk map for the initial risks is shown in Table 12.3. The further to the top right, the higher the risks. After mitigation, the risks will decrease. This means that in the risk map they will move towards the bottom left. The risk map with the final risks is shown in Table 12.4. It can be clearly concluded from these two figures that all risks in the region of likelihood 4 - 5 and impact 4 - 5 have been lowered to lower likelihood and impact regions.

Table 12.3: Initial Risk Map

Likelihood	1	2	3	4	5
5			RSK-BC-02, RSK-PP-03, RSK-PP-04, RSK-PP-07, RSK-BC-07	RSK-DES-01, RSK-BC-01	
4					
3				RSK-DES-05, RSK-DES-07, RSK-BC-04, RSK-PP-09, RSK-PP-11	RSK-DES-04, RSK-SAF-07, RSK-SAF-08
2	RSK-TE-01, RSK-PP-10	RSK-TE-04	RSK-PP-05, RSK-PP-06, RSK-TE-05, RSK-AER-03, RSK-STR-01, RSK-STR-02	RSK-PP-01, RSK-PP-02, RSK-PP-08, RSK-AER-01, RSK-AER-02, RSK-STR-03	RSK-TE-02, RSK-TE-03
1			RSK-BC-08	RSK-PP-14	RSK-PP-12, RSK-PP-13
	Impact				

Table 12.4: Final Risk Map

Likelihood	1	2	3	4	5
5		RSK-BC-02			
4					
3	RSK-PP-11			RSK-DES-01	
2	RSK-PP-08	RSK-BC-04, RSK-PP-01, RSK-TE-04	RSK-PP-03	RSK-DES-05, RSK-DES-07, RSK-TE-03	RSK-DES-04, RSK-DES-08, RSK-SAF-07
1	RSK-TE-01, RSK-PP-10, RSK-PP-12, RSK-PP-13, RSK-STR-01	RSK-BC-08	RSK-PP-04, RSK-PP-05, RSK-PP-06, RSK-PP-07, RSK-BC-07, RSK-TE-05, RSK-PP-14, RSK-AER-03, RSK-STR-02	RSK-BC-01, RSK-PP-02, RSK-PP-09, RSK-AER-01, RSK-AER-02, RSK-STR-03	RSK-TE-02, RSK-SAF-08
	Impact				

13
Operations, Logistics and Project Planning

This chapter discusses the operations (Section 13.1), flight envelope (Section 13.1.1), operational and logistics concept description (Section 13.1.2), the production plan (Section 13.2) and project planning for the future of the Dragonfly project (Section 13.3).

13.1. Operations

To give an indication on the operation of the Dragonfly, the flight envelope will be discussed in Section 13.1.1. Then the operation and logistics will be touched upon in Section 13.1.2.

13.1.1. Flight Envelope

As the Dragonfly will be certified initially under CS-VLA, the flight envelope criteria are taken from [80]. During operation the aircraft should always stay within this envelope. Three characteristic speeds are needed, namely the stall-, cruise- and dive speed. The input parameters for the envelope are listed in Table 13.1. The method is copied from [80]. To safe space in this report the method is therefore not be further discussed. In the end it turned out the maximum load factor encounterd during cruise will be 3.8 and the minimum -1.5 which can be seen in Figure 13.1.

Table 13.1: Flight Envelope Parameters

Parameter	Symbol	Value	Unit
Stall speed (EAS)	V_{stall}	23.15	m/s
Cruise speed (EAS)	V	50.00	m/s
Dive speed (EAS)	V_d	61.73	m/s
Max. maneuver load factor [80]	n	3.8	-
Min. maneuver load factor [80]	n	-1.5	-
Max. cruise gust speed [80]	U	15.24	m/s
Max. dive gust speed [80]	U	7.62	m/s
Wing lift curve slope	a	4.80	1/rad
Mass	M	864	kg
Wing area	S	14.34	m2
Mean aerodynamic chord	$\bar{C}$	1.25	m
Air density cruise	ρ	1.12	kg/m3
Air density sea level	ρ_0	1.225	kg/m3

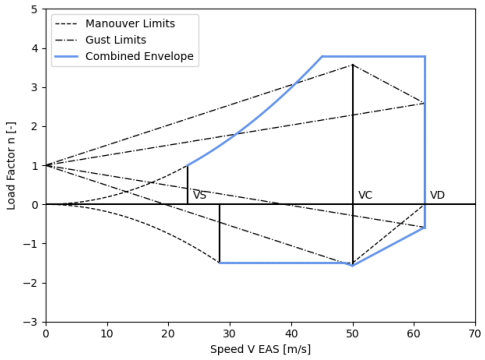

Figure 13.1: Flight Envelope

13.1.2. Operational and Logistic Concept Description

In Figure 13.2 the operational flow of the Dragonfly is shown.

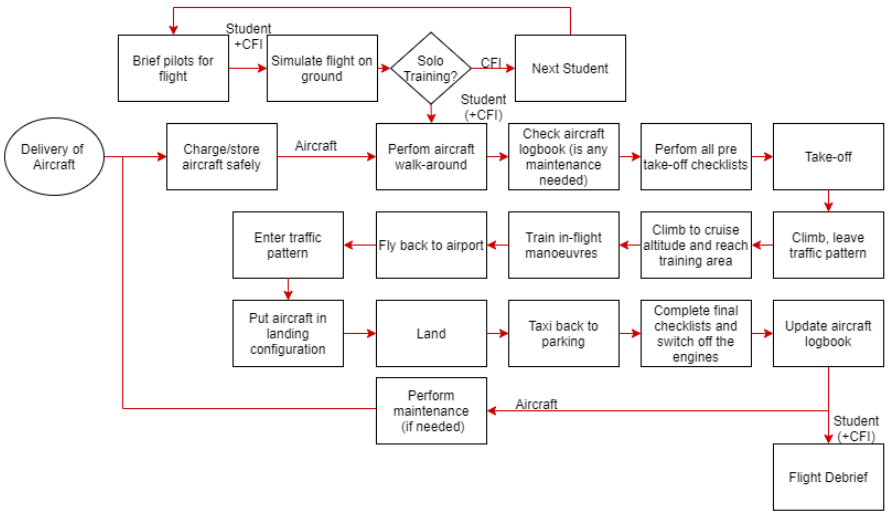

Figure 13.2: Operational flow diagram for the electrical light trainer aircraft. [1]

"Regarding the logistics aspect of the project, as of now two possible concepts have been proposed. The first one

involves a more widely used and straight-forward strategy for distributing the aircraft to the customers, namely: each flight school may place an order for the amount of electrical trainer aircraft that they wish to purchase. The aircraft will then be delivered as they are finished in the factory. The batteries of the aircraft will be charged at the airport that serves as the ground base of the specific flight school.

The second possible concept consists of consulting different flight schools in order to gather information about how many electrical trainer aircraft are desired by each of them. The required amount of aircraft will be produced and then leased by the ELTA-company to the flight schools. In this way, the flight schools will just need to pay the lease cost and the operational costs, which are low considering the aircraft's electrical propulsion. Furthermore, a suitable amount of interchangeable batteries (higher than the amount of aircraft) will be produced. The ELTA-company will ensure that each flight school has enough batteries and will be responsible for swapping them once they have reached the end of their life cycle. This however requires the possibility of regular battery swapping in the aircraft. Furthermore, the ELTA-company will ensure efficient use of resources. For example by transporting available batteries for a flight school that might not need them on a certain day to another flight school that is located relatively close by and is in need of extra batteries."[1] This second option however will only be possible after the break-even point has reached as mentioned in Chapter 11.

13.1.3. End-Of-Life-Plan

The Dragonfly has not a general end-of-life as its components have different end-of-life times. But when the items have reached their individual end-of lives something should happen. In aviation safety standards are high compared to other sectors like the automotive industry. When the engine and batteries have reached their end-of-life they could therefore get a second life in this industry. Another option would be that the batteries are sold to households where it is used to store an over production of power by solar panels which can not be put in the power net due to over capacity. The avionics and airframe could be used for flight simulators.

13.2. Production Plan

Before the aircraft can take to the skies, it has to be built. In order to achieve this, a production plan has been set up. This is visible in Figure 13.3.

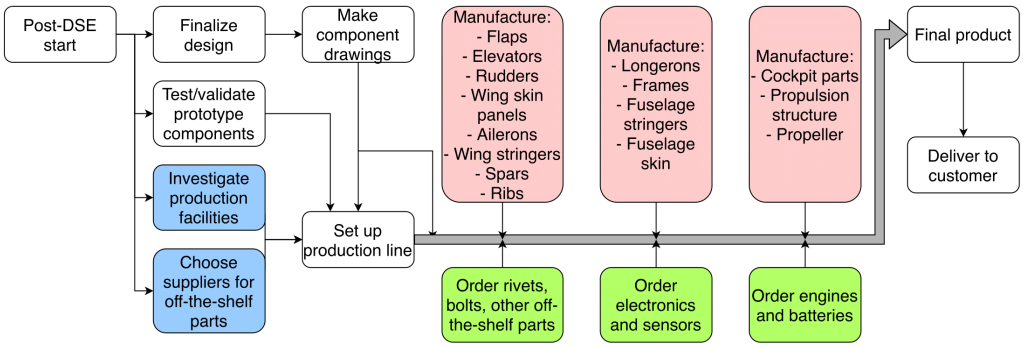

Figure 13.3: Production plan of the complete aircraft

In this figure, light blue boxes at the bottom left are the pre-production phase. Here, it is investigated which existing facilities and suppliers are best suitable for the parts and components that are needed, and which production facilities have to be developed. Simultaneously, prototyping of critical components that should still be tested can already begin, and the testing can be executed. After that, the production line is set up. This continues all the way until the final product. First, in-house manufactured parts are coloured red and are located at the top of the figure. Parts that will be ordered or come from other suppliers are coloured green and are located at the bottom-middle.

13.3. Project Planning- Future Steps

This section describes what the future plans are for the development of the aircraft proposed in this report. The future steps are displayed in Figure 13.4 in which the phases corresponding to the mission lifetime cycle phases of ESA[1]. Right now, the design is in phase C: the detailed definition. Once the detail design is finished, the system will flow into phase D in which the aircraft is qualified and produced, which basically means that the aircraft will be certified and produced in order to perform flights tests. After phase D the system will flow into phase E: utilisation, in which the aircraft will be mass produced and delivered to customers, which will then finally flow into phase F: disposal or end-of-life of the aircraft.

Phase C This pahse will take the aircraft to the detailed design phase. For this testing will start to take place.

[1] https://www.esa.int/Science_Exploration/Space_Science/How_a_mission_is_chosen, Last accessed: 21-06-2020

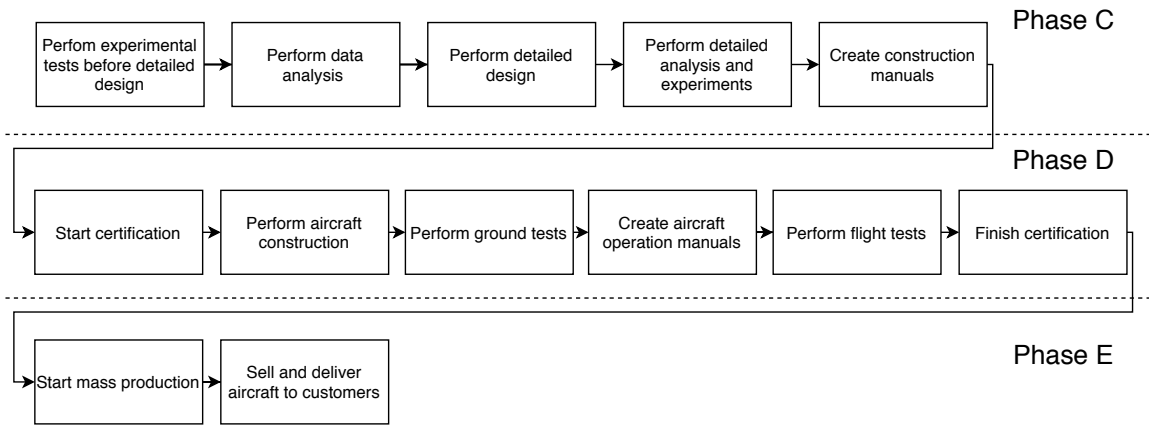

Figure 13.4: Future design steps.

Think of the wind tunnel tests for both the contra rotating propeller and the main wing or for example experiments on battery management and degradation, these future plans are specified in this report under future validation or test plans for each subsystem. Once these tests are performed, data analysis on the outcomes of the tests will be conducted in order to better understand the performance influence of certain design parameters and to increase the accuracy of the design methods which will then result in a full detailed aircraft design. The detailed design can then be used to perform detailed analysis and experiments. Think of control and stability simulations, computation fluid dynamic analysis on the complete aircraft shape, wind tunnel tests with a scaled version of the aircraft and/or propeller design, etc. The detailed design step and detailed analysis step will most likely be repeated several times as the outcomes of the detailed analysis and experiments are influenced by the detailed design and vice versa. Once the aircraft is fully designed into detail the construction manuals can be created, which may include high detailed CAD-drawings. These manuals are required in order to actually manufacture the aircraft.

Phase D. With the finished construction manuals, the certification process of the Dragonfly may begin, by first building a prototype of the aircraft. This prototype will then undergo a series of ground tests, as explained in Section 10.5. After the ground testing is completed successfully, operation manuals may be generated, in preparation for flight testing. Several proposed flight tests are mentioned in Section 10.5. Once this series of tests is complete, the aircraft will be eligible for full certification under VLA certification requirements.

Phase E. With the aircraft being fully VLA certified, the mass production of the Dragonfly can be started. With this, the first aircraft deliveries to customers can take place. This will result in the first profit, which is of course required to support the development/production of the aircraft and its subsystems.

Overall, the steps displayed in Figure 13.4 describe the future steps in the development of the proposed design in this report. However, it should be noted that these steps describe the global overview and that per mission phase more in depth work flow diagrams and work breakdown structures should be created in order to efficiently develop the aircraft.

13.3.1. Gantt Chart

The steps described above in Section 13.3 will result in a Gantt chart representing the phases past the completion of the DSE project. This Gantt chart can be observed in Figure 13.5.

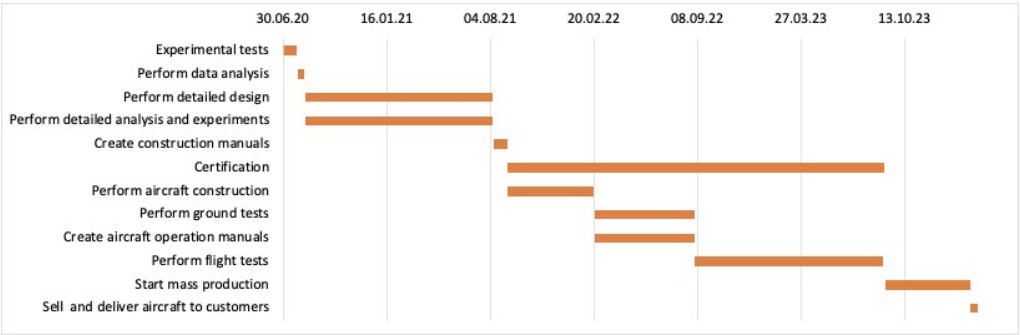

Figure 13.5: Gantt chart for the future of the project.

14
Conclusion and Recommendations

Ten weeks prior to this report, we set out to make emission-free flight more feasible for flight schools. After spending 4 000 hours on the design of the Dragonfly, it can be concluded that, although it is possible at this moment to have a feasible design for an electric aircraft for flight schools (and private owners) from a physics point of view, it is not financially viable. This chapter discusses several clear reasons as to why this is the case, and addresses what needs to happen to fulfill our mission.

The first reason is the cost of certification, which is heavily dependent on the MTOW. The MTOW for each considered category, in order of increasing certification cost, is: 600 kg for CS-LSA, 750 kg for CS-VLA and 5,670 kg for CS-23. If one wants to design and build an electric aircraft with competitive range and endurance characteristics, when compared to existing trainer aircraft, the weight of the batteries will influence the weight of the aircraft such that it is only possible to certify it under CS-23. This results in an increase of 40% for the certification costs, which can make the difference between a viable or non-viable business case for the aircraft manufacturer. Also, in order for the company to make profit and for the break-even point to be reduced, the unit cost of the aircraft will have to be more than €150 000, and from the conducted questionnaire, it resulted that 2 out of 3 potential customers are not interested in buying an aircraft that costs more than €150 000. However, the public may be swayed in the future when shown that the hourly operating costs of an electric vehicle are nearly €50 less compared to combustion engine aircraft. This will play a crucial part in creating a business case for electric flight in the near future.

Another reason is the batteries. Within this report, the time-between-overhaul (TBO) is calculated to be 2000h, after which the battery pack (weighing almost 300 kg and costing nearly €30 000) needs to be overhauled. Although electric power is generally far less CO_2-heavy than fossil fuel, one can argue that changing the batteries every 2000h is not more environmentally friendly than using fossil fuels. Currently research is being performed with regards to increasing the battery lifetime, which can make the difference in terms of environmental impact, and batteries are thus expected to become much more feasible in the near future.

In terms of training enhancement possibilities, implementing the TE package on board of the aircraft, as well as making use of the VR unit flight simulator is highly profitable for the student pilots. By increasing the effectiveness of their training by up to 30% they may save up to €1,800 in aircraft rental cost alone. However, as the students will require less flight hours, the flight schools will earn less money, given the same profit margin per rental hour when compared to a traditional combustion engine aircraft.

Another obstacle in the path of progress of this project is the mentality of flight schools with regards to training. From the questionnaire and interviews performed throughout this phase of the project, it has become clear that the vast majority of flight instructors as well as pilots believe that the best way of training is to simply use the basic six instruments. Currently, the most common approach to training is very conservative, using no training enhancement items. However, another portion of the interviewees did seem interested in the prospect of implementing modern technology into flight training to make it more contemporary. The implementation of training enhancement as explained in this report will pave the way towards revolutionising the way flight training is done and open up the path to a new era. Similarly to electrical cars, it is expected that the level of acceptance of both electrical and enhanced flight training will increase with time, and eventually become the norm.

At this point in time, the infrastructure for electric aircraft is also lacking, as there are no fast chargers at airports. If the aircraft manufacturer or the customers have to pay for this, it will negatively influence the transition to electric flying. Currently, sustainable aviation initiatives, such as the action plan Hybrid Electric Flying in the Netherlands, are working on making the infrastructure more present at airfields across the country.

Furthermore, more research should be performed on the contra-rotating propeller. The CRP has huge potential with its high efficiency and is therefore especially valuable when combined with electric flying. From a noise perspective, anti phasing the two propellers should be researched and tested to be able to implement the CRP in general aviation. As of right now, little research is performed on this implementation and researching this can make one a pioneer in improving propeller efficiency.

Having all of this in mind, the recommendations to make an affordable environmentally friendly electric trainer will be that EASA should change the way certification takes place. The current certification process is based on conventionally-powered aircraft, that will fly in the same configuration for decades. In this way, it is impossible to implement the ever improving technologies regarding batteries. Furthermore, the batteries need to improve with regards to two aspects: the power density and the amount of charging cycles. The current design of the Dragonfly

has shown that electricity is able to power a perfectly functional, usable airplane, and shows that electric flight is on the verge of taking off. Flight schools and everyone who reads this report should realise that training with electric aircraft is becoming reality and that other applications of electric flight may become possible in the very near future, with the help of further research and funding. A recommendation to investors is to allocate funds for electric flight now, as in the coming decades the battery technology will improve and the market will rise. Investing now will almost guarantee profit or a share in one of the fastest rising markets. Electric flight is not a dream; it is a matter of time.

Bibliography

[1] B. van Dillen, M. van Ede, N. Hogervorst, H. Hoogendoorn, M. Meijkamp, E. Overbosch, Y. Pejonn, F. Sîrghi, C. Teirlinck, and R. Warnat, *Midterm report electric light trainer aircraft,* (2020).

[2] B. van Dillen, M. van Ede, N. Hogervorst, H. Hoogendoorn, M. Meijkamp, E. Overbosch, Y. Pejonn, F. Sîrghi, C. Teirlinck, and R. Warnat, *Baseline report electric light trainer aircraft,* (2020).

[3] B. van Dillen, M. van Ede, N. Hogervorst, H. Hoogendoorn, M. Meijkamp, E. Overbosch, Y. Pejonn, F. Sîrghi, C. Teirlinck, and R. Warnat, *Project plan electric light trainer aircraft,* (2020).

[4] A. Olieman, *Ecodesign strategy wheel,* (2011).

[5] D. Rohacs, *Preliminary analysis of small aircraft traffic characteristics and its impact on european atm parameters – a small aircraft prediction model,* (2004).

[6] AOPA, *State of general aviation,* (2019).

[7] R. Bayerl, M. Berkemeier, and et al, *World Directory of Leisure Aviation 2011–12* (WDLA UK, Lancaster UK, 2011) p. 78 and 169.

[8] B. Z. R. Vos, J.A. Melkert, *Aerospace Design and Systems Engineering Elements I – AE1222-II,* (2018), TU Delft.

[9] M. Ashby, H. Shercliff, and D. Cerbon, *Materials: Engineering, Science, Processing and Design*, 4th ed. (Butterworth-Heinemann, 2018).

[10] M. F. Ashby, *Materials selection in mechanical design*, 4th ed. (Butterworth-Heinemann, 2017).

[11] T. H. Megson, *Introduction to aircraft structural analysis*, 2nd ed. (Butterworth-Heinemann, Elsevier, 2014).

[12] G. Gerard, *Handbook for structural stability, part v, compressive strength of flat stiffened panels,* (1957).

[13] Dr. C. Rans, Ir. J. Melkert, *AE2135-I Structural Analysis & Design,* (2018), TU Delft.

[14] S. Gudmundsson, *General Aviation Aircraft Design: Applied Methods and Procedures*, 1st ed., ISBN: 978-0-12-397308-5 (Elsevier, The Boulevard, Langford Lane, Kidlington, Oxford OX5 1GB, UK 225 Wyman Street, Waltham, MA 02451, USA, 2014).

[15] D. F. Oliviero, *Aerospace Design and Systems Engineering Elements II – AE2111-II,* (2018), TU Delft.

[16] M. Nita and D. Scholz, *Estimating the oswald factor from basic aircraft geometrical parameters,* (2012).

[17] D. Raymer, *Aircraft Design: A Conceptual Approach* (American Institute of Aeronautics and Astronautics, Inc., 1992).

[18] D. M. G. Dr.A. Sciacchitano, *Aerodynamics I – AE2130,* (2018), TU Delft.

[19] I. H. Abbot and A. E. von Doenhoff, *Theory of wing sections*, 1st ed., ISBN: 978-0-486-60586-9 (Dover Publications, 1959).

[20] M. Hoffmann, R. R. Ramsay, and G. Gregorek, *Effects of grit roughness and pitch oscillations on the naca 4415 airfoil,* (1996).

[21] E. Obert, *Aerodynamic Design of Transport Aircraft* (Delft University Press, 2009).

[22] P. M. Sforza, *Commercial Airplane Design Principles* (Butterworth-Heinemann, 2014).

[23] E. Torenbeek, *Synthesis of Subsonic Airplane Design* (Springer Science+Business Media, 1982).

[24] D. F. Oliviero, *Ae3211-i systems engineering and aerospace design lecture slides,* (2020), tU Delft.

[25] M. O. Courseware, *Wing taper considerations,* (2006).

[26] D. Raymer, *Aircraft Design: A Conceptual Approach, Sixth Edition* (American Institute of Aeronautics and Astronautics, Inc., 2018).

[27] M. Drela and H. Youngren, *XFOIL 6.9 User Primer* (MIT, 2001).

[28] I.H. Abbott, A.E. von Doenhoff, L.S. Stivers, Jr., *Summary of Airfoil Data,* (n.d.).

[29] S. Hoerner, *Fluid-Dynamic Lift* (L.A. Hoerner, 1985).

[30] M. H. Sadraey, *Aircraft design : a systems engineering approach* (John Wiley & Sons, Ltd, 2013).

[31] I. Bouton, *Airplane pitching moment of inertia,* Journal of the aeronauthical sciences (1950).

[32] C. Riboldi and F. Gualdoni, *An integrated approach to the preliminary weight sizing of small electric aircraft,* Aerospace Science and Technolgy **Vol. 58**, pg. 134 (2016).

[33] DR. A. Cervone and Ir. B.T.C. Zandbergen, *Electrical Power Systems for Aerospace Vehicles – AE2230-II: Propulsion & Power,* (2017), TU Delft.

[34] Pipistrel, *Aircraft Information Pipistrel ALPHA ELECTRO* (2017).

[35] L. Lam and P. Bauer, *Practical Capacity Fading Model for Li-Ion Battery Cells in Electric Vehicles,* IEEE Transactions On Power Electronics **Vol. 28, No. 12**, pg. 5910 (2013).

[36] G. Ning and B. N. Popov, *Cycle Life Modeling of Lithium-Ion Batteries,* Journal of The Electrochemical Society **Vol. 151, No. 10**, pg. A1584 (2004).

[37] H. Popp, N. Zhang, M. Jahn, M. Arrinda, S. Ritz, M. Faber, D. Sauer, P. Azais, and I. Cendoya, *Ante-mortem analysis, electrical, thermal, and ageing testing of state-of-the-art cylindrical lithium-ion cells,* (2020).

[38] A. Balitskii, *Assessment of the fatigue damage to the propeller shaft of a sea craft,* Materials Science **49** (2013), 10.1007/s11003-013-9592-4.

[39] T. Megson, *Aircraft Structures for Engineering Students* (Elsevier, 2017).

[40] F. B. Metzger, *An assessment of propeller aircraft noise reduction technology,* (1995).

[41] B. Chandrasekaran, *Method for the prediction of the installation aerodynamics of a propfan at subsonic speeds,* NASA (1985).

[42] P. Carter, *CROTOR v755-ES1.0,* (2011), `http://www.esotec.org/sw/crotor.html`.

[43] G. Ananda, *Uiuc propeller database - volume 1,* (2015), the Graupner CAM Prop 9x6.

[44] W. Choi, J.S. Choi, I.M. Jung, J.H. Kim, I.W. Lee, S.H. Han and Y.S. Won, *CFD analysis of aerodynamic characteristics of regional turboprop aircraft propeller,* KoreaScience (2011).

[45] M. Hepperle, *JavaFoil Version 2.28,* (2017), `https://www.mh-aerotools.de/airfoils/index.htm`.

[46] M. Drela and H. Youngren, *XROTOR v7.55,* (2003), `http://web.mit.edu/drela/Public/web/xrotor/`.

[47] M. Haddaoui, *Development of a Propeller Source Noise Model*, Master's thesis, Delft University of Technology (2019).

[48] J.S. Vanderover and K.D. Visser, *Analysis of a Contra-Rotating Propeller Driven Transport Aircraft,* American Institute of Aeronautics and Astronautics (n.d.).

[49] J. Zimmerman, *Pilot's discretion: Incorporating technology in flight training,* (2017).

[50] U. D. of Transportation, *Advanced avionics handbook,* (2009).

[51] *Notice of proposed amendment 2017-03. in-flight recording for light aircraft,* (2017).

[52] J. Gregoire, *Ann guest editorial: Flight training in the time of insecurity,* (2011).

[53] H. Slutsken, *Sims for schools: The value of flight simulators,* (2019).

[54] K. Prokopovic, *Vr simulators – the future of pilot training?* (2019).

[55] T. M. Pope, *A Cost-Benefit Analysis of Pilot Training Next,* (2019).

[56] D. Allerton, *The Case for Flight Simulation in General Aviation* (College of Aeronautics, Cranfield University, 2002).

[57] D. H. K. Ryan T. Olson and B. R. Cogan, *Flight testing of fused reality visual simulation system,* NASA (2015).

[58] E. Bachelder and D. Klyde, *Fused reality for enhanced flight test capabilities,* NASA Tech Briefs (September 2011), Dryden Flight Research Center, Edwards, California.

[59] J. R. G. David H. Klyde and G. Park, *A mixed reality simulation tool for in flight evaluations,* AIAA Scitech 2020 Forum (2020).

[60] N. F. A. A. Huy Tran, Ferdinand Behrend, *Single pilot operations with ar-glasses using microsoft hololens,* (2018).

[61] Cessna Aircraft Company, *Cessna 172 owners manual,* (1984).

[62] D. O. M. Alaziz, A. Stolfi, *Cirrus airframe parachute system and odds of a fatal accident in cirrus aircraft crashes,* Aerospace Medicine and Human Performance , 556 (2017).

[63] C.E. Melton, M. Wicks, *In-flight Physiological Monitoring of Student Pilots,* (1967).

[64] G.S. Krahenbuhl, J.R. Marett, *Stress and Simulation in Pilot Training,* (1979).

[65] Naval Air Warfare Centre Training Systems Division, *T-6B Pilot Training Next Virtual Reality Part-task Trainer (T-6B PTN VR-PTT),* (2019).

[66] C. Ellis, *Are VR flight simulators the future of pilot training?* (September, 2019).

[67] M. H. Sadraey, *Design of Unmanned Aerial Systems* (John Wiley & Sons, 2020).

[68] P. C. J.M. Rolfe, *Determining the training effectiveness of flight simulators:some basic issues and practical developments,* Applied Ergonomics , 243 (1982).

[69] S. Roscoe, *Incremental transfer effectiveness,* Human Factors , 561 (1971).

[70] S.N. Roscoe, H.K Povenmire, *An evaluation of ground based flight trainers in routine primary flight training,* Human Factors , 109 (1971).

[71] S. I. Tannenbaum and C. P. Cerasoli, *Do Team and Individual Debriefs Enhance Performance? A Meta-Analysis* (Human Factors and Ergonomics Society, 2012).

[72] G. M. S. R. Key Dismukes, *Facilitation and Debriefing in Aviation Training and Operations* (Ashgate Publishing, 2000).

[73] M.G. Pfeiffer, J.D. Horey, *Training effectiveness of Aviation Motion Simulation: A Review and Analysis of the Literature,* (1987).

[74] S. Misra, M. Halleran, *The Effect of Electronic Flight Bags in Flight Training on Preflight Skill Development and Aeronautical Decision Making,* (2019).

[75] M.N. Milner et. al, *The Effect of Chart Type on Pilots' Response Time,* (2017).

[76] P. A. Craig, J. E. Bertrand, W. Dornan, S. Gossett, K.K. Thorsby, *Ab initio Training in the Glass Cockpit Era: New Technology meets new Pilots,* (n.d.).

[77] D. D. Joost C. F. de Winter and M. Mulder, *Training Effectiveness of Whole Body Flight Simulator Motion: A Comprehensive Meta-Analysis,* (2012).

[78] EASA, *Certification specifications for normal-category aeroplanes cs-23 (amendment 5),* (2017).

[79] Rijksoverheid, *Draft action programme for hybrid electric aviation (ahev),* (2020).

[80] EASA, *Easy access rules for very light aeroplanes (cs-vla) (amendment 1),* (2018).

A
FFD and FBS

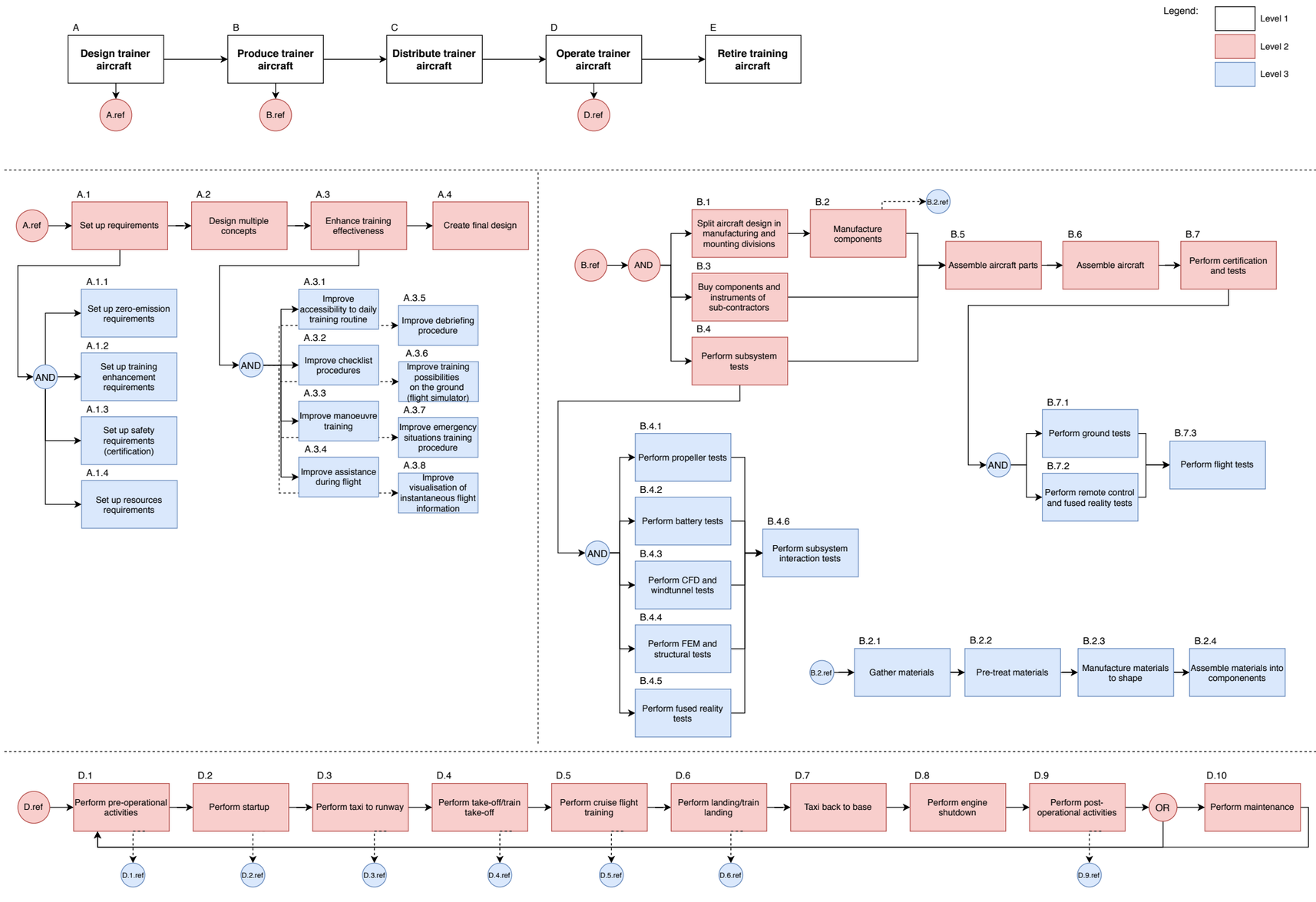

Figure A.1: Functional flow diagram

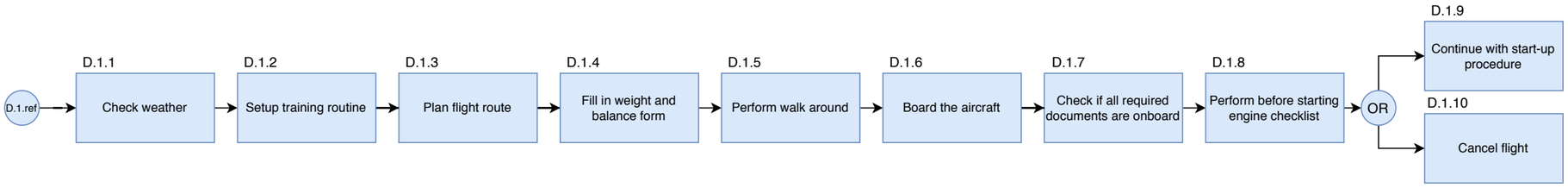
D.1.ref
D.1.1
Check weather
D.1.2
Setup training routine
D.1.3
Plan flight route
D.1.4
Fill in weight and balance form
D.1.5
Perform walk around
D.1.6
Board the aircraft
D.1.7
Check if all required documents are onboard
D.1.8
Perform before starting engine checklist
OR
D.1.9
Continue with start-up procedure
D.1.10
Cancel flight

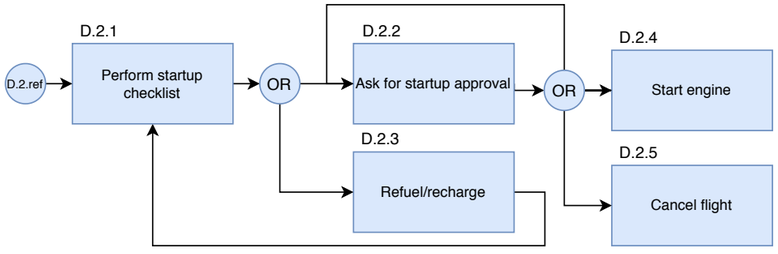
D.2.ref
D.2.1
Perform startup checklist
OR
D.2.2
Ask for startup approval
D.2.3
Refuel/recharge
OR
D.2.4
Start engine
D.2.5
Cancel flight

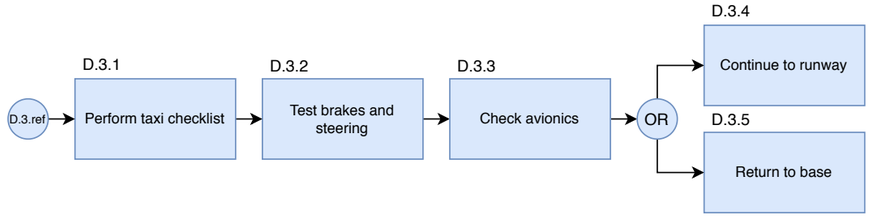
D.3.ref
D.3.1
Perform taxi checklist
D.3.2
Test brakes and steering
D.3.3
Check avionics
OR
D.3.4
Continue to runway
D.3.5
Return to base

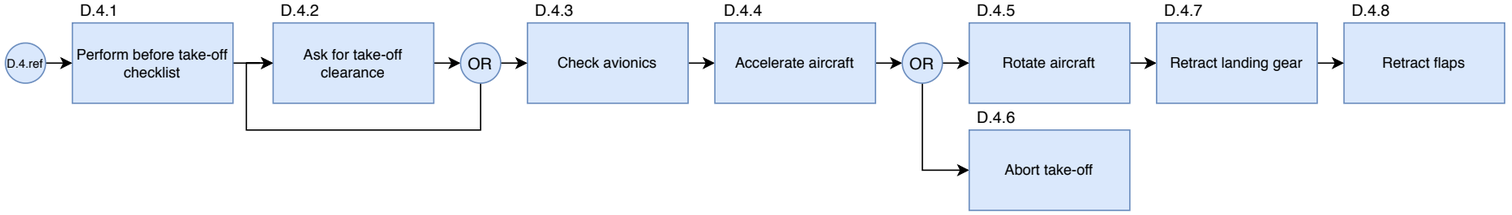
D.4.ref
D.4.1
Perform before take-off checklist
D.4.2
Ask for take-off clearance
OR
D.4.3
Check avionics
D.4.4
Accelerate aircraft
D.4.5
OR
D.4.7
Rotate aircraft
Retract landing gear
D.4.8
Retract flaps
D.4.6
Abort take-off

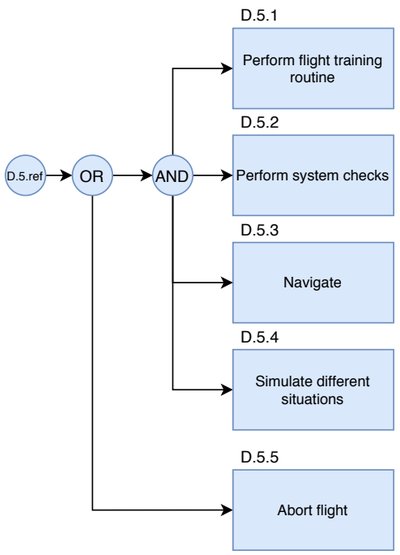
D.5.ref
OR
AND
D.5.1
Perform flight training routine
D.5.2
Perform system checks
D.5.3
Navigate
D.5.4
Simulate different situations
D.5.5
Abort flight

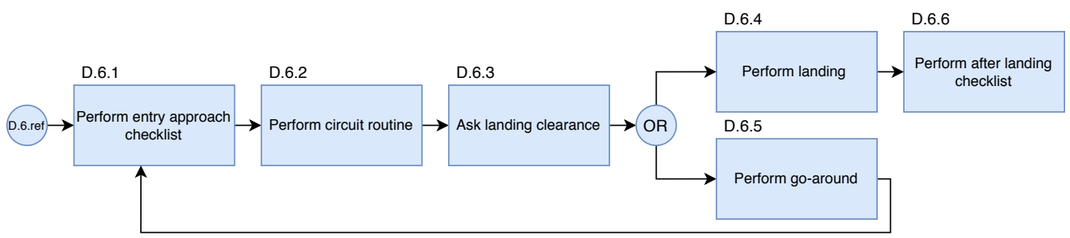
D.6.ref
D.6.1
Perform entry approach checklist
D.6.2
Perform circuit routine
D.6.3
Ask landing clearance
OR
D.6.4
Perform landing
D.6.6
Perform after landing checklist
D.6.5
Perform go-around

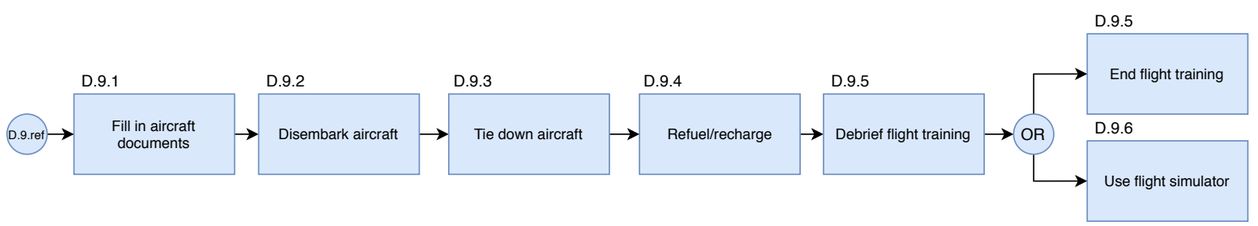
D.9.ref
D.9.1
Fill in aircraft documents
D.9.2
Disembark aircraft
D.9.3
Tie down aircraft
D.9.4
Refuel/recharge
D.9.5
Debrief flight training
OR
D.9.5
End flight training
D.9.6
Use flight simulator

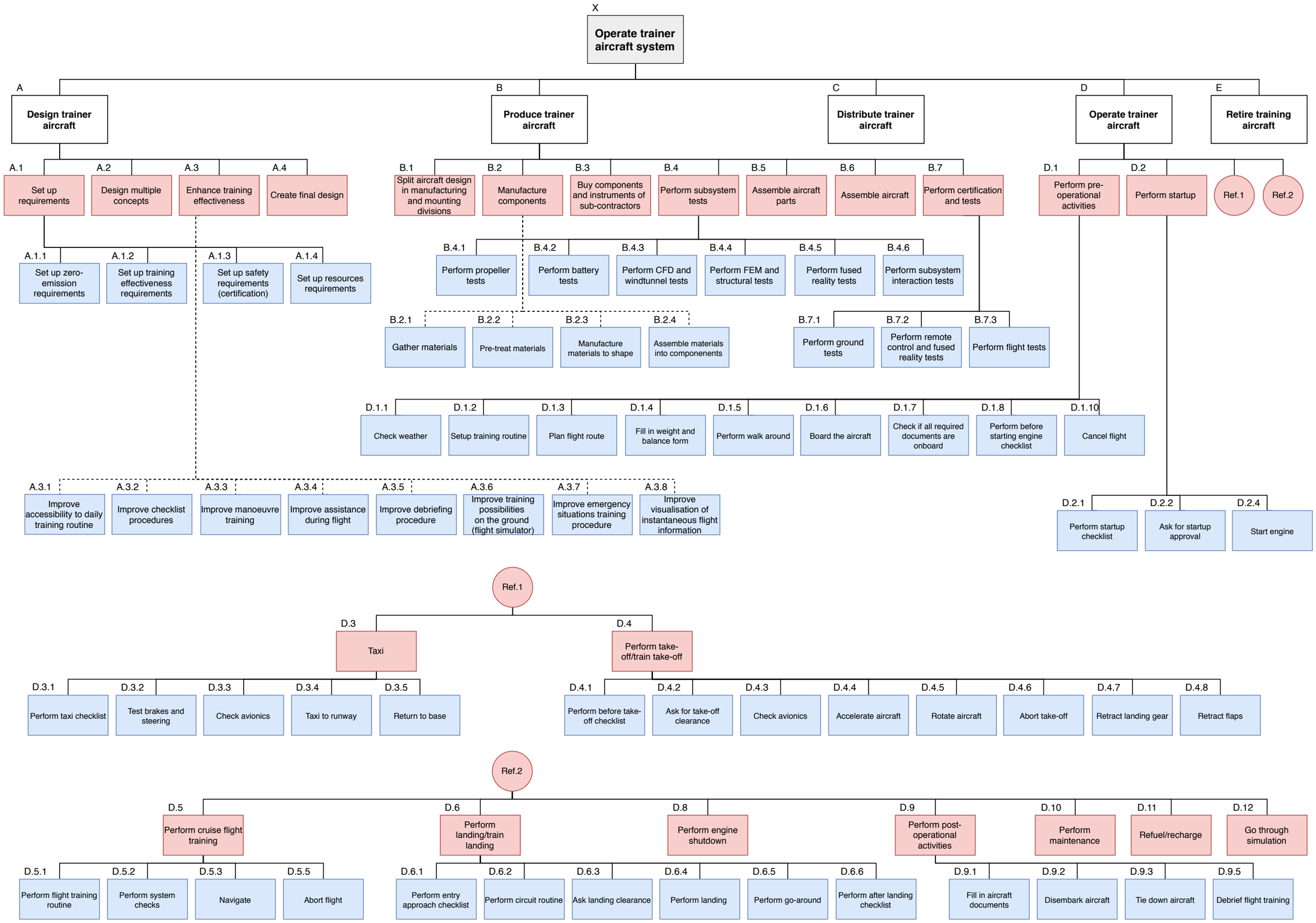
X
Operate trainer aircraft system
A
Design trainer aircraft
B
Produce trainer aircraft
C
Distribute trainer aircraft
D
Operate trainer aircraft
E
Retire training aircraft
A.1
Set up requirements
A.2
Design multiple concepts
A.3
Enhance training effectiveness
A.4
Create final design
A.1.1
Set up zero-emission requirements
A.1.2
Set up training effectiveness requirements
A.1.3
Set up safety requirements (certification)
A.1.4
Set up resources requirements
B.1
Split aircraft design in manufacturing and mounting divisions
B.2
Manufacture components
B.3
Buy components and instruments of sub-contractors
B.4
Perform subsystem tests
B.5
Assemble aircraft parts
B.6
Assemble aircraft
B.7
Perform certification and tests
B.4.1
Perform propeller tests
B.4.2
Perform battery tests
B.4.3
Perform CFD and windtunnel tests
B.4.4
Perform FEM and structural tests
B.4.5
Perform fused reality tests
B.4.6
Perform subsystem interaction tests
B.2.1
Gather materials
B.2.2
Pre-treat materials
B.2.3
Manufacture materials to shape
B.2.4
Assemble materials into componenents
B.7.1
Perform ground tests
B.7.2
Perform remote control and fused reality tests
B.7.3
Perform flight tests
D.1
Perform pre-operational activities
D.2
Perform startup
Ref.1
Ref.2
D.1.1
Check weather
D.1.2
Setup training routine
D.1.3
Plan flight route
D.1.4
Fill in weight and balance form
D.1.5
Perform walk around
D.1.6
Board the aircraft
D.1.7
Check if all required documents are onboard
D.1.8
Perform before starting engine checklist
D.1.10
Cancel flight
A.3.1
Improve accessibility to daily training routine
A.3.2
Improve checklist procedures
A.3.3
Improve manoeuvre training
A.3.4
Improve assistance during flight
A.3.5
Improve debriefing procedure
A.3.6
Improve training possibilities on the ground (flight simulator)
A.3.7
Improve emergency situations training procedure
A.3.8
Improve visualisation of instantaneous flight information
D.2.1
Perform startup checklist
D.2.2
Ask for startup approval
D.2.4
Start engine
Ref.1
D.3
Taxi
D.4
Perform take-off/train take-off
D.3.1
Perform taxi checklist
D.3.2
Test brakes and steering
D.3.3
Check avionics
D.3.4
Taxi to runway
D.3.5
Return to base
D.4.1
Perform before take-off checklist
D.4.2
Ask for take-off clearance
D.4.3
Check avionics
D.4.4
Accelerate aircraft
D.4.5
Rotate aircraft
D.4.6
Abort take-off
D.4.7
Retract landing gear
D.4.8
Retract flaps
Ref.2
D.5
Perform cruise flight training
D.6
Perform landing/train landing
D.8
Perform engine shutdown
D.9
Perform post-operational activities
D.10
Perform maintenance
D.11
Refuel/recharge
D.12
Go through simulation
D.5.1
Perform flight training routine
D.5.2
Perform system checks
D.5.3
Navigate
D.5.5
Abort flight
D.6.1
Perform entry approach checklist
D.6.2
Perform circuit routine
D.6.3
Ask landing clearance
D.6.4
Perform landing
D.6.5
Perform go-around
D.6.6
Perform after landing checklist
D.9.1
Fill in aircraft documents
D.9.2
Disembark aircraft
D.9.3
Tie down aircraft
D.9.5
Debrief flight training